

Includes Papers Presented in the  
National Conference on Synthetic Membranes

Indian J Chem  
JUNE 1992

CODEN: IJOCAP 31A(6) 291-392 (1992)  
ISSN: 0376-4710

# INDIAN JOURNAL OF

# CHEMISTRY

## SECTION A

(Inorganic, Bio-inorganic, Physical, Theoretical &  
Analytical Chemistry)



Published by

PUBLICATIONS & INFORMATION DIRECTORATE, CSIR, NEW DELHI

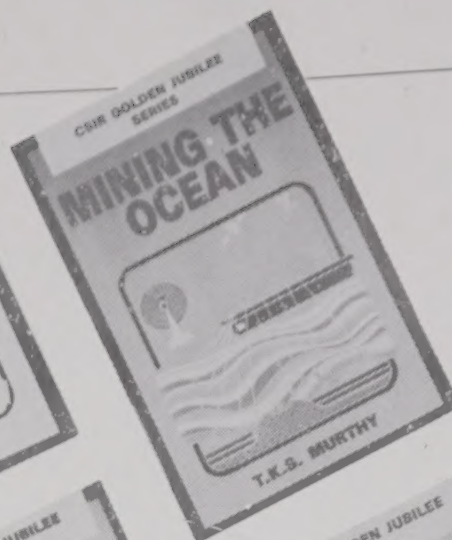
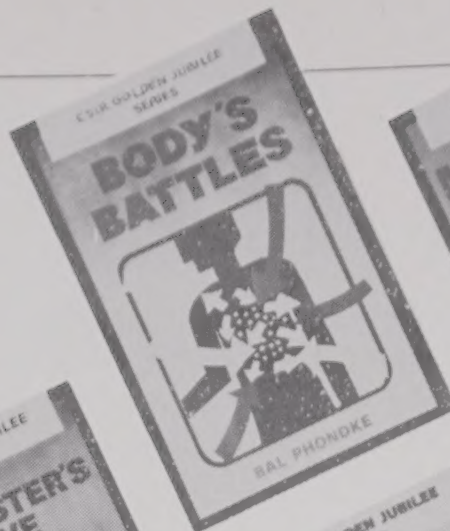
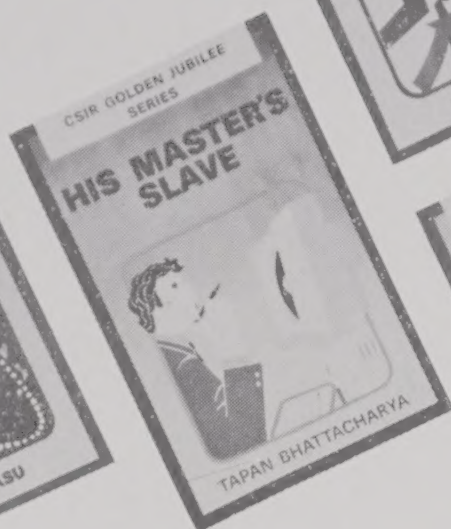
in association with

THE INDIAN NATIONAL SCIENCE ACADEMY, NEW DELHI

Prof. Lib  
10/6/92

183  
10/6/92

**FREE  
GIFT  
WITH  
COMPLETE SET**



# GOLDEN OFFER

You can now book your copies of the attractive, lavishly illustrated popular science titles under  
**CSIR GOLDEN JUBILEE SERIES**  
in advance and also get a  
**FREE GIFT**

## Titles in print

### **BODY'S BATTLES**

By **Bal Phondke**

Unfolds the story of the inner defence organisation of the body, the diversity and specificity of its armament and its round the clock vigil that meets every threat to it.

84 pages;

Price: Rs. 9 (Paperback), Rs. 18 (Hardcover)

### **MINING THE OCEAN**

By **T K S Murthy**

Reveals, the timeless secrets of the seas and the secret bounty that they hold in reserve

106 pages;

Price: Rs. 12 (Paperback), Rs. 20 (Hardcover)

### **HIS MASTER'S SLAVE**

By **Tapan Bhattacharya**

Tells the non-specialist the riveting story of the modern day genie of the bottle, the PC.

88 pages;

Price: Rs. 10 (Paperback), Rs. 18 (Hardcover)

### **INSIDE STARS**

By **Biman Basu**

Provides a privileged glimpse into star nurseries, tracking the luminescent trail to fiery senescence and death of stars to reveal the mysteries and marvels of cosmic drama.

90 pages;

Price: Rs. 10 (Paperback), Rs. 18 (Hardcover)

### **PLASTIC FEAST**

By **Subodh Jawadekar**

Celebrates the dawn of the plastics era and elaborates the myriad ways in which plastics touch our lives. A veritable feast of plastics, very palatable to the readers.

96 pages;

Price: Rs. 12 (Paperback) Rs. 20 (Hardcover)

### **CERAMICS ARE FOREVER**

By **B C Sharma**

Highlights the fascinating versatility of ceramics and provides an excellent close-up of the symbiotic relationship between man and materials.

84 pages;

Price: Rs. 11 (Paperback), Rs. 20 (Hardcover)

## Forthcoming Titles

**ARTIFICIAL INTELLIGENCE**

**HARDY COMPOSITES**

**MAN IN SPACE**

**MIND MASTER**

You may place an order for all 10 titles by sending Rs. 120.00 (for paperback) or Rs. 200.00 (for Hard-cover) including postage by Demand Draft/M.O. payable to "Publications and Information Directorate". The titles already published will be sent to you as soon as the payment is received and the forthcoming titles will be sent by post as soon as they are published, one every month. With every order you will receive a free gift.

For further information write to:  
Sales and Distribution Officer  
Publications and Information Directorate  
(CSIR)  
Dr. K S Krishnan Marg, New Delhi 110 012

# INDIAN JOURNAL OF CHEMISTRY

## Section A: Inorganic, Bio-inorganic, Physical, Theoretical & Analytical Chemistry

### Editorial Board

Prof. R C Mehrotra  
Vice-Chancellor  
Allahabad University  
Allahabad 211 002

Prof. D V S Jain  
Chemistry Department  
Panjab University  
Chandigarh 160 014

Prof. A Chakravorty  
Department of Inorganic Chemistry  
Indian Association for the  
Cultivation of Science  
Calcutta 700 032

Prof. V Krishnan  
Department of Inorganic  
& Physical Chemistry  
Indian Institute of Science  
Bangalore 560 012

Prof. K K Rohatgi Mukherjee  
Department of Chemistry  
Jadavpur University  
Calcutta 700 032

Dr J P Mittal  
Chemistry Division  
Bhabha Atomic Research Centre  
Bombay 400 085

Prof. S K Rangarajan  
Director  
Central Electrochemical Research Institute  
Karaikudi 623 006

Prof. R C Srivastava  
Department of Chemistry  
Banaras Hindu University  
Varanasi 221 005

Prof. E D Jemmis  
Department of Chemistry  
University of Hyderabad  
Hyderabad 500 134

Dr S K Date  
Physical Chemistry Division  
National Chemical Laboratory  
Pune 411 008

Prof. I Gutman  
Faculty of Science  
Yu. 34000, Kragujevac  
Radoja Domanovica  
Yugoslavia

Prof. A B Sannigrahi  
Department of Chemistry  
IIT, Kharagpur 721 302

Dr D Papousek  
J. Heyrovsky Institute  
of Physical Chemistry  
Prague  
Czechoslovakia

Prof. P P Singh  
Department of Chemistry  
M.D. University  
Rohtak 124 001

Dr Pradip K Mascharak  
Department of Chemistry  
University of California  
Santa Cruz  
California 95064  
USA

Dr G P Phondke Director, PID

---

**Editors :** Dr B.C. Sharma, Dr S. Sivakamasundari and Dr S.K. Bhasin

**Sr. Scientific Assistant :** Geeta Mahadevan

---

**Published by the Publications & Information Directorate (CSIR), Hillside Road, New Delhi 110-012**

**Director: Dr G P Phondke**

---

Copyright, 1992, by the Council of Scientific & Industrial Research, New Delhi 110 012

The Indian Journal of Chemistry is issued monthly in two sections: A and B. Communications regarding contributions for publication in the journal should be addressed to the Editor, Indian Journal of Chemistry, Publications & Information Directorate, Hillside Road, New Delhi 110 012.

Correspondence regarding subscriptions and advertisements should be addressed to the Sales & Distribution Officer, Publications & Information Directorate, Hillside Road, New Delhi 110 012.

The Publications & Information Directorate (CSIR) assumes no responsibility for the statements and opinions advanced by contributors. The Editorial Board in its work of examining papers received for publication is assisted, in an honorary capacity by a large number of distinguished scientists, working in various parts of India.

Annual Subscription: Rs. 400.00 £ 100.00 \$ 150.00; 50% discount admissible to research workers and students and 25% discount to non-research individuals on annual subscription.

Single Copy: Rs. 40.00 £ 10.00 \$ 15.00

Payments in respect of subscriptions and advertisements may be sent by cheque, bank draft, money order or postal order marked payable to Publications & Information Directorate, Hillside Road, New Delhi 110 012.

**Claims for missing numbers of the journal will be allowed only if received within 3 months of the date of issue of the journal plus the time normally required for postal delivery of the journals and the claim.**

# AUTHOR INDEX

Aminabhavi T M	328	Nair M K T	373
Anil Kumar	373	Paci S	355
Audinos R	348,355	Parmar Jayant S	386
Bajaj H C	303	Patel Chetan G	386
Bajpai D D	373	Patel Dinesh K	386
Bakhshi A K	291	Polishchuk A Ya	366
Balundgi R H	328	Prasad Rao M	309
Datta Nivedita	342	Ramachandhran V	376
Deoki Nandan	317	Ramani M P S	376,391
Ghosh Soumyadeb	338	Razumovskii L P	366
Goswami A N	361	Sarangi K	379
Guha B K	342	Sarma P V R B	389
Gupta T C S M	361	Sarma P V R Bhaskar	379
Harogoppad S B	328	Sethuram B	309
Iordanskii A L	366	Shah P R	369
Iyer R M	317	Sharma Anshu	361
Iyer Sita T	317	Sharma S K	361
Kalpagam V	334,338	Sharma Uma	383
Kanungo S B	389	Shririn Zahida	303
Khan A A	369	Shukla J P	323,373
Khan G Y	369	Singh Kehar	313
Mahadevan Neena	383	Singh R K	373
Misra B M	376	Taqui Khan M M	303
Misra S K	323	Thomas K C	376
Mohapatra R	389	Tiwari A K	313
		Venkata Lalitha T	309
		Venkatasubramanian K	303
		Vishalakshi B	334

# Indian Journal of Chemistry

Sect. A: Inorganic, Bio-inorganic, Physical, Theoretical & Analytical

VOLUME 31A

NUMBER 6

JUNE 1992

## CONTENTS

### Advances in Contemporary Research

- Tailoring electrically conducting polymers: An overview . . . . . 291  
A K Bakhshi

### Papers

- Crystal and molecular structure of aquoethylenediaminetetraacetatoruthenium(III) and its extraordinary lability towards substitution . . . . . 303  
M M Taqui Khan\*, K Venkatasubramanian, H C Bajaj & Zahida Shririn

- Sodium ruthenate catalysis in the oxidation of substituted benzyl alcohols by hexacyano-ferrate(III) . . . . . 309  
T Venkata Lalitha, M Prasad Rao & B Sethuram\*

### Papers presented at the National Conference on Synthetic Membranes

- Electrochemical characterization of membranes . . . . . 313  
Kehar Singh\* & A K Tiwari

- Thermodynamic equilibrium constants of alkali metal ion-hydrogen ion exchanges and related swelling free energies in perfluorosulphonate ionomer membrane (Nafion-117) in aqueous medium . . . . . 317  
Sita T Iyer, Deoki Nandan & R M Iyer\*

- Studies on the selective carrier-mediated transport of plutonium(IV) ions through tributyl phosphate/dodecane liquid membranes . . . . . 323  
J P Shukla\* & S K Misra

- Molecular transport of binary liquid mixtures into EPDM and NBR membranes at 25°C. 328  
S B Harogoppad, T M Aminabhavi\* & R H Balundgi

- Permeability properties of polyelectrolyte complexes from carboxymethylcellulose and poly(2-vinyl-N-methylpyridinium iodide) . . . . . 334  
B Vishalakshi & V Kalpagam\*

- Electromembrane from polyelectrolyte complex of polyaniline and carboxymethylcellulose . . . . . 338  
Soumyadeb Ghosh & V Kalpagam\*

- Studies on concentration polarisation in a membrane module . . . . . 342  
Nivedita Datta & B K Guha\*

- Electric power produced from two solutions of unequal salinity by reverse electrodialysis 348  
R Audinos

- Direct production of pure concentrated tartaric acid from its salts by electromembrane processes . . . . . 355  
R Audinos\* & S Paci

Contd

## CONTENTS

Removal of phenol from refinery waste waters using liquid surfactant membranes in a continuous column contactor . . . . .	361
A N Goswami*, S K Sharma, Anshu Sharma & T C S M Gupta	
<b>Notes</b>	
Transport of water through cellulose derivatives used as the cover of osmotic systems for drug release . . . . .	366
A L Iordanskii, A Ya Polishchuk & L P Razumovskii	
Permselectivity of acetate ion to nitrate ion in electrodialysis of aqueous solutions . . . . .	369
P R Shah, G Y Khan & A A Khan*	
Macrocycle-facilitated transport of uranyl ions across supported liquid membranes using dicyclohexano-18-Crown-6 as mobile carrier. . . . .	373
Anil Kumar*, R K Singh, J P Shukla, D D Bajpai & M K T Nair	
Studies on ultrafiltration membrane systems based on cellulosic and polysulfone polymers . . . . .	376
K C Thomas, V Ramachandhran, B M Misra & M P S Ramani*	
Pertraction of copper(II) in the presence of cobalt(II), nickel(II), manganese(II) and iron(II) using supported liquid membrane . . . . .	379
K Sarangi* & P V R Bhaskar Sarma	
Transport of alkali metal cations through liquid membrane using non-cyclic synthetic ionophores . . . . .	383
Neena Mahadevan & Uma Sharma*	
New cation exchanger of poly(N-substituted phenylmaleimide) type . . . . .	386
Chetan G Patel, Dinesh K Patel & Jayant S Parmar*	
Separation of Co(II)-Zn(II), Co(II)-Mn(II) and Zn(II)-Mn(II) systems from their binary solutions through supported liquid membrane containing organophosphorus acid as extractant . . . . .	389
R Mohapatra, S B Kanungo* & P V R B Sarma	
<b>Book Review</b>	
Basic principles of membrane technology (Author: M Mulder) . . . . .	391
M P S Ramani	
<b>Errata</b> . . . . .	392

Authors for correspondence are indicated by (\*)

## Tailoring electrically conducting polymers: An overview

A K Bakhshi

Department of Chemistry, Panjab University, Chandigarh 160 014

Received 3 December 1991; revised and accepted 5 March 1992

Current efforts to design novel conducting polymers with desired conduction properties are reviewed. The strategy and the methodology used to achieve this tailoring are discussed. Some recent results on the electronic structure and conduction properties of tailored conducting polymers and their superlattices are briefly discussed. It is found that quasi-one-dimensional polymeric superlattices of conducting polymers are promising candidates for tailoring copolymers with conduction properties intermediate between those of its components. Finally, the future possibilities in this direction are briefly outlined.

### 1. Introduction

During the last ten years, few other areas in polymer research have generated as much interest among a wide variety of disciplines, as that of conducting polymers. These new materials, also called synthetic metals, combine the electrical properties of metals with the advantages of polymers such as lighter weight, greater workability and lower cost. The first and the stimulating development in this field occurred in 1977 when it was discovered<sup>1-3</sup> that the electrical conductivity of polyacetylene (PA) (which is an insulator like all other pure polymers) increases manifold from that of an insulator ( $10^{-9} \Omega^{-1} \text{ cm}^{-1}$ ) on doping with oxidising agents (p-doping) or reducing agents (n-doping). This discovery of highly conducting PA led to a sudden spurt in research activity directed towards the study and discovery of new conducting polymeric systems.

The instability of PA in air<sup>4</sup> further intensified this search (on exposure to air covalent bonds are formed between oxygen and carbon atoms and these bonds lower the conductivity of PA because of their interruption of conjugated double bonds). At present many new conducting polymers with properties similar to those of PA have been synthesized and studied. Such systems include poly(*p*-phenylene) (PPP), poly(*p*-phenylene) sulphide (PPS), polythiophene (PTP), polypyrrole (PPY), polyfuran (PFU) and their derivatives. These polymers, though they share many structural similarities (Fig. 1), have wide range of conductivity values depending upon the doping per cent, the alignment of the polymer chains and the purity of the sample. Light weight and rechargeable batteries, solar batteries, electrochromic display devices, permanent information storage devices and sensors are

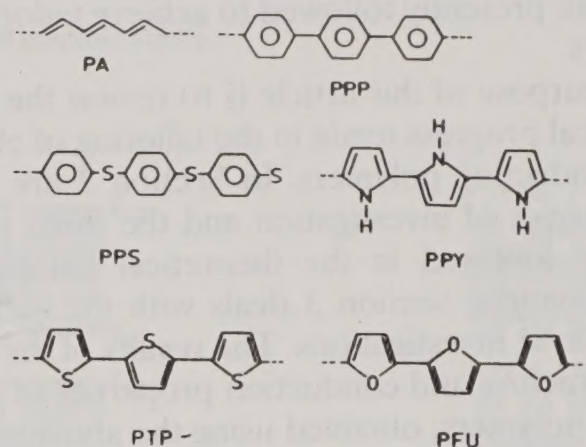


Fig. 1—Structures for *trans*-polyacetylene (PA), poly(*p*-phenylene) (PPP), poly(*p*-phenylene)sulphide (PPS), polypyrrole (PPY), polythiophene (PTP) and polyfuran (PFU).

some of the proposed applications<sup>5</sup> of these polymers.

Currently, major efforts in the field of conducting polymers focus on the molecular engineering of novel polymers with tailor-made conduction properties. This implies even looking for the polymers that are intrinsically good electrical conductors without the need of doping. To achieve this tailoring of conducting polymers, one needs to have a complete understanding of the relationship between the chemical structure of the polymer and its electronic and conduction properties. With such an insight, desired electronic properties could be obtained by specific synthesis after molecular design.

The conduction properties of an undoped polymer, in terms of the band theory of solids, are known to be related to its electronic properties such as band gap ( $E_g$ ), ionization potential (IP), electron affinity (EA) and band widths. Band gap of a polymer is a measure of its ability to show intrinsic conductivity while ionization potential and the electron af-

finity values of a polymer determine its ability to form conducting polymer through oxidative and reductive doping respectively. Band widths are a measure of the extent of delocalisation in the system and can be qualitatively correlated with the mobilities of charge carriers in the band. The relationship between these electronic properties of a polymer and its chemical structure is, however, not completely understood. Some understanding of this relationship has been achieved through an insight gained into the ground state properties of the undoped polymeric systems by quantum chemical calculations. These calculations have been found to be an efficient tool not only for the interpretation of the experimental results but also for the investigation of the finer details of the electronic structure which would be barely accessible by experiments. Based on this existing knowledge of structure-property relationship in these conducting polymers, three routes are presently followed to achieve tailoring of polymers.

The purpose of this article is to review the latest theoretical progress made in the tailoring of electrically conducting polymers. In Section 2 are given the strategies of investigation and the three routes generally followed in the theoretical tailoring of novel polymers. Section 3 deals with the methods used in these investigations. The results of the electronic structure and conduction properties of some selected polymers, obtained using the above strategy and methodology are briefly discussed in Section 4.

## 2. Strategy of the Investigation

### 2.1. Through Substitution

In this route one starts with polymers with very small band gap values and then tries to modify their electronic properties by incorporating substituents, provided the polymers can undergo substitution reactions. Among the known conducting polymers, *trans*-PA with a band gap of 1.5 eV<sup>1</sup> and polythiophene (PTP) with a band gap of 2.1 eV<sup>6</sup> appear to be the ideal starting materials for substitutions. A priori, one can qualitatively predict the effect of substituents on the electronic properties of the polymers with the help of substituent constants. For conjugated polymers such as PA and PTP, Hammett substituent constants<sup>7</sup> are appropriate. They include contributions from both inductive (via  $\sigma$  bonds) and resonance (via  $\pi$  bonds) effects. In the case of some conjugated systems, Hammett constants are shown to be direct measures of ionization potentials<sup>8</sup> and electron affinities<sup>9</sup>. While studying the effect of substituents on polymers, one also needs to take into

consideration the steric effects of substituents which are very important and in fact very predominant in most cases. The substituted groups should not be bulky enough to introduce large non-bonded interactions between these groups and thus twist the polymer backbone. Such a twist may lead to non-coplanarity and thus a decrease in the  $\pi$  orbital overlap and effective conjugation length, thereby resulting in diminished carrier mobilities and lower conductivities.

### 2.2. One-Dimensional Graphite Family

An exciting possibility in the search for novel conducting polymers is provided by the hydrocarbon polymers with fused aromatic rings. This new class of polymers, frequently referred to as one-dimensional graphite family, has been theoretically predicted<sup>10</sup> to have, in addition to stability in air, unusual electronic properties ranging from metallic conductivity to high temperature superconductivity and ferromagnetism. This family includes members such as polyacene (PAC), polyacenacene (PACa), polyphenanthrene (PPh), polyphenanthrophenanthrene (PPhP) and polyperinaphthalene (PPN). The structures of these systems are shown in Fig. 2. Except PPN, these members can be considered to form two series of polymers derived from *trans*-PA and *cis*-PA respectively. PAC and PACa can be considered to be the ladder versions of two and three chains of *trans*-PA respectively while PPh and PPhP those of the corresponding *cis*-PA chains. One may continue building these series further: every higher member in a series has a larger carbon content ultimately leading to 1-D graphite. PPN, on the other hand, can be considered to be a fused version of planar poly(*p*-phenylene) and *cis*-PA skeletons as shown in Fig. 2. Another fusion of *cis*-PA to PPN will lead to poly(peri-anthracene) and so on.

### 2.3. Polymeric Superlattices

The third possible route to obtain novel conducting polymers is through the technique of growing quasi one-dimensional superlattices (copolymers) of conducting polymers. Semiconductor superlattices or quantum well structures are the artificial periodic one-dimensional structures of thin layers of two semiconductors, these were first proposed by Esaki and Tsu<sup>11</sup>. The thickness of the individual layers varies from a few angstroms to a few hundred angstroms but is always shorter than the electron mean path and longer than the lattice spacing. The periodic potential in such superlattices modifies considerably the band structure of two host semiconductors dividing the brillouin zone into a series of mini-zones, thus giving rise to narrow bands separated by

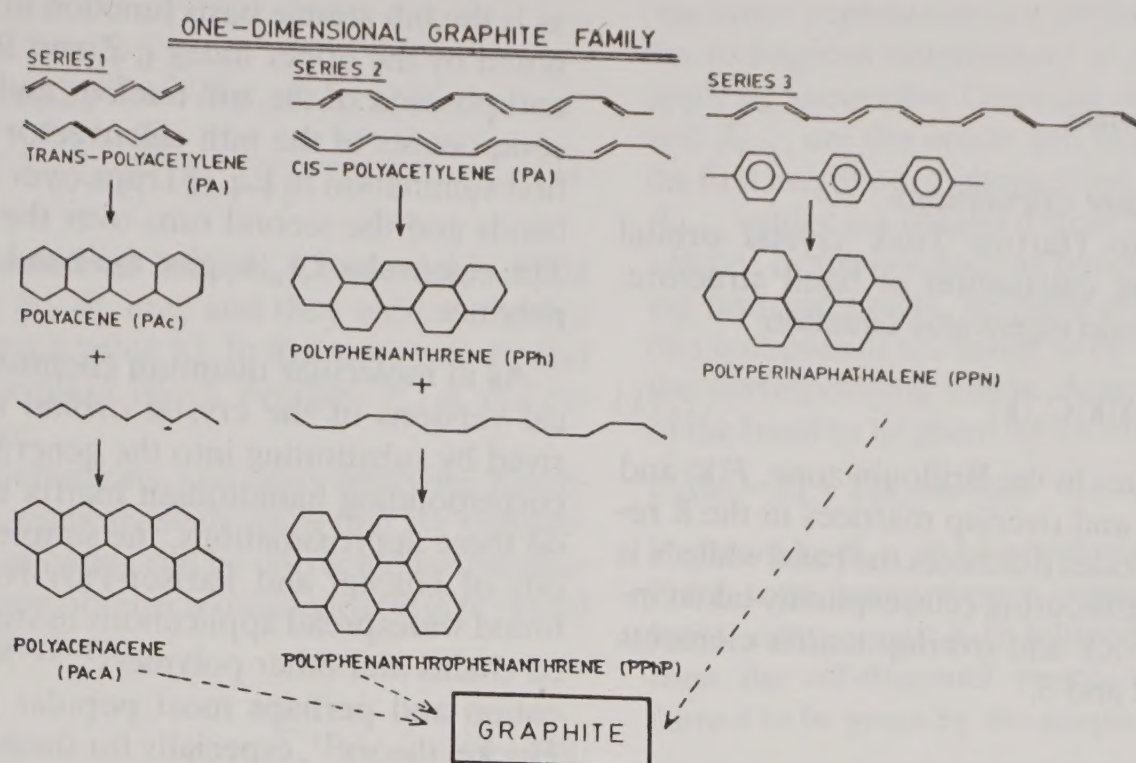


Fig. 2—Members of the one-dimensional graphite family.

forbidden regions. Such structures are found to possess unusual electronic properties<sup>12</sup> and are currently of great technological interest<sup>13</sup> with possible applications as semiconductor diode lasers, electro-optical modulators and non-linear optical devices.

It is also possible to conceive of polymeric quasi one-dimensional superlattices (or copolymers) with tailor made properties through the choice of two semiconducting components, their relative amounts and their arrangement in the polymer chain. It is already well known that copolymerisation<sup>14-17</sup> (periodic or random) considerably influences the electronic properties which, however, always remain intermediate between those of the constituent homopolymers. Depending upon the band alignment of the two constituent polymers, polymeric superlattices, like the inorganic superlattices, may be divided into four types<sup>13</sup>, viz., Type I, Type II—staggered, Type II—misaligned and Type III (Fig. 3). Type I comprises systems where the band gap of one component is contained entirely within the band gap of the other component. Systems in which the top of the valence band of one component lies within the band gap of the other and the bottom of the conduction band of the second lies in the band gap of the first belong to Type II—staggered. In Type II—misaligned superlattices, the band match up is such that the conduction band minimum of one is below the valence band maximum of the second component. In Type III polymeric superlattices, one component is semi-metallic while the other is a normal semiconductor.

The electronic properties of a superlattice are controlled by two fundamental parameters—the

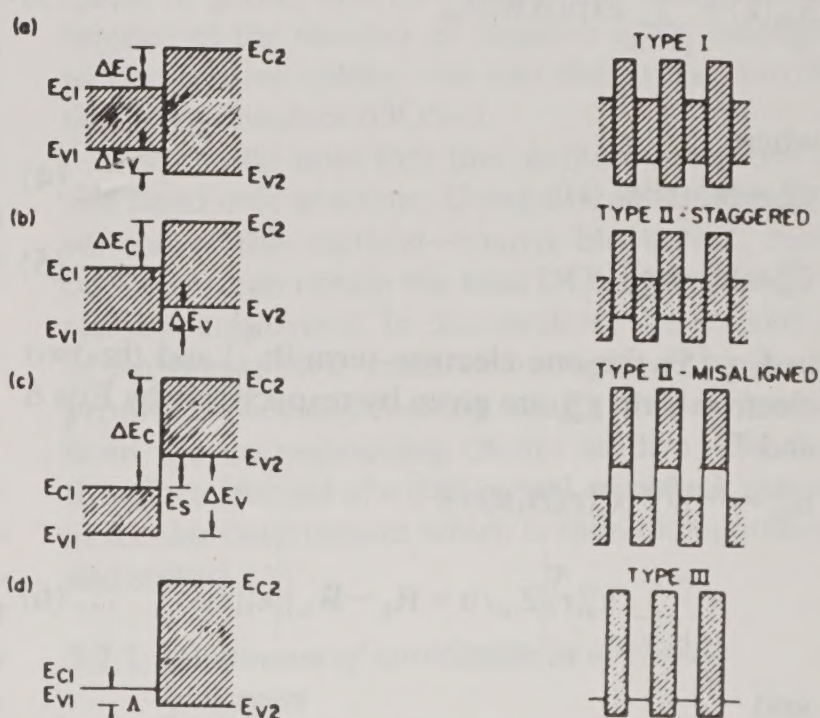


Fig. 3—Various types of polymeric superlattices classified on the basis of the band alignments of the two components A and B.

conduction band discontinuity ( $\Delta E_c$ ) and the valence band discontinuity ( $\Delta E_v$ ).  $\Delta E_c$  is defined as the difference in the electron affinities of the two components while  $\Delta E_v$  equals the corresponding difference in the ionisation potentials. These parameters have the opposite signs for Type I superlattices but the same sign for Type II superlattices. The electronic density of states (DOS) of the quasi-one-dimensional superlattices can be determined using the negative factor counting (simple or matrix block) based on Dean's negative eigen value theorem.

### 3. Methodology

#### 3.1. Periodic Polymers

##### 3.1.1. Band structure calculations

In the *ab initio* Hartree Fock crystal orbital method<sup>18,19</sup> for the calculation of band structure, one solves the pseudo eigenvalue equation,

$$F(k)C_n(k) = \varepsilon_n(k)S(k)C_n(k) \quad \dots (1)$$

for different  $k$  values in the Brillouin zone.  $F(k)$  and  $S(k)$  are the Fock and overlap matrices in the  $k$  representation. The index  $n$  denotes the band while  $N$  is the number of neighbouring cells explicitly taken into account. The Fock and overlap matrix elements are given by Eqs 2 and 3,

$$F_{ab}(k) = \sum_{j=-N}^N \exp(ikR_j) f_{ab}^{oj} \quad \dots (2)$$

$$S_{ab}(k) = \sum_{j=-N}^N \exp(ikR_j) s_{ab}^{oj} \quad \dots (3)$$

where

$$s_{ab}^{oj} = \langle x_a^o(r) | x_b^j(r) \rangle \quad \dots (4)$$

$$f_{ab}^{oj} = h_{ab}^{oj} + g_{ab}^{oj} \quad \dots (5)$$

In Eq. (5), the one electron term ( $h_{ab}^{oj}$ ) and the two electron term  $g_{ab}^{oj}$  are given by respectively by Eqs 6 and 7,

$$h_{ab}^{oj} = -1/2 \langle x_a^o(r) | \Delta | x_b^j(r) \rangle + \sum_h \sum_\alpha \langle x_a^o(r) | Z_\alpha / |r - R_h - R_\alpha| | x_b^j(r) \rangle \quad \dots (6)$$

and

$$g_{ab}^{oj} = \sum_{h,j=-N}^N \sum_{c,d} p_{cd}^{hl} \left[ 2 \begin{pmatrix} o & j & h & l \\ a & b & c & d \end{pmatrix} - \begin{pmatrix} o & h & j & l \\ a & c & b & d \end{pmatrix} \right] \quad \dots (7)$$

where

$$p_{cd}^{hl} = \sum_m \sum_k \exp\{-ik(R_h - R_l)\} C_{c,m}^* C_{d,m} \quad \dots (8)$$

and the two electron integral is given by

$$\begin{pmatrix} o & j & h & l \\ a & b & c & d \end{pmatrix} = \int dr_1 \int dr_2 x_a^o(r_1) x_b^j(r_1) \frac{1}{|r_1 - r_2|} \times x_c^h(r_2) x_d^l(r_2) \quad \dots (9)$$

$x_b^j$  is the  $b$ th atomic basis function in the unit cell denoted by the upper index  $j$ ;  $Z$  and  $R$  are the charge and position of the  $\alpha$ th nucleus and  $C_{d,m}(k)$  are the components of the  $m$ th eigenvector of Eq. (1). The first summation in Eq. (8) runs over all doubly filled bands and the second runs over the Brillouin zone. The eigenvalues  $\varepsilon_n(k)$  give the band structure of the polymer.

As in molecular quantum chemistry, semiempirical versions of the crystal orbital method are derived by substituting into the general formalism the corresponding hamiltonian matrix elements. Based on these approximations, the simple electron methods of Hückel and Pariser-Parr-Pople (PPP) have found widespread applications in studying conjugated chains and other polymers<sup>20-22</sup>. Next in sophistication and perhaps most popular is the extended Hückel theory<sup>23</sup>, especially for the band structure itself because unlike other HF methods, it does not predict too large band gaps. Self consistent field methods such as the different variations of neglect of the differential overlap (NDO) have also been used for polymers<sup>24</sup>. Some other techniques, e.g., the simulated *ab initio* method<sup>25,26</sup> and the non-empirical effective potential approach of Nicholas *et al.*<sup>27,28</sup> and the polynomial matrix method<sup>29,30</sup> are also used to investigate polymers.

##### 3.1.2. Correlation correction to band structure results

One of the principal deficiencies of the Hartree Fock crystal orbital method is the neglect of the correlation between motions of electrons with opposite spins. The result is that the Hartree Fock method overestimates the fundamental energy gap. The treatment of correlation in polymers is necessary for a more exact determination of their electronic properties. Only the size consistent methods such as Moeller-Plesset (MP) many body perturbation theory<sup>31</sup> and the coupled cluster theory<sup>32,33</sup> can be used for this treatment (a method which is not size consistent such as that of configuration interaction (CI) gives less and less correlation energy per electron as the number of electrons increases and hence cannot be used).

If the MP perturbation theory is used in second order (MP/2)<sup>34</sup>, it can be shown that the total second order perturbation contribution can be easily partitioned into a double sum of pair correlation energies.

$$E_2 = \sum_{i,j} \varepsilon_{i,j} \quad \dots (10)$$

where

$$\varepsilon_{IJ} = \sum_{A,B} \frac{\left| \langle \phi_I(1) \phi_J(2) | \frac{(1 - P_{12})}{r_{12}} | \phi_A(1) \phi_B(2) \rangle \right|^2}{\varepsilon_I + \varepsilon_J - \varepsilon_A - \varepsilon_B} \quad \dots (11)$$

Here the combined indices I, J stand for filled Bloch orbitals  $\phi_I$ ,  $\phi_J$ , etc., and they indicate both a band index  $i$  and  $k$  value  $K_i$ . In the same way  $\phi_A$  and  $\phi_B$  stand for unfilled Bloch orbitals.  $P_{12}$  is the exchange operator.

Using the definitions and also applying Koopmans theorem, one can easily show that HF conduction and valence bands can be corrected for correlation and that one obtains a quasiparticle (QP) band structure<sup>35</sup> of the form,

$$\varepsilon_C(\text{QP}) = \varepsilon_C(\text{HF}) + \sum_C^{(N+1)} (e) + \sum_C^{(N+1)} (h) \quad \dots (12)$$

$$\varepsilon_V(\text{QP}) = \varepsilon_V(\text{HF}) + \sum_V^{(N)} (e) + \sum_V^{(N)} (h) \quad \dots (13)$$

where  $\Sigma(e)$  and  $\Sigma(h)$  are the electron and hole self-energies which arise if one puts an extra electron into the conduction band (indicated by the composite index C) or creates a hole in the valence band (denoted by index V). These corrections have been shown to lead to a decrease in the band gap and in the band widths.

## 3.2. Aperiodic Polymers

### 3.2.1. Density of states (DOS) calculations

In the general case of a disordered system, the coherent potential approximation (CPA) with an energy and  $K$ -dependent self-energy seems to be the relatively most accurate method<sup>36</sup> to obtain the DOS of the system. On the other hand, if one has a quasi 1-D system, one can obtain the DOS of the periodic or random copolymer much more easily and accurately using the negative factor counting (NFC) technique<sup>37</sup> based on Dean's negative eigenvalue theorem<sup>38</sup>. In this method, the number of eigenvalues of a tridiagonal tight binding (Huckel) secular determinant of a polymer chain which are smaller than a given trial energy equals the number of negative factors  $\varepsilon_i(\lambda)$  obtained by the recursion relations,

$$\prod_i (\lambda_i - \lambda) = \prod_i \varepsilon_i(\lambda) \quad \dots (14)$$

$$\varepsilon_1(\lambda) = \alpha_1 - \lambda \quad \dots (15a)$$

$$\varepsilon_i(\lambda) = \alpha_i - \lambda - \frac{\beta_{i-1,i}}{\varepsilon_{i-1}(\lambda)} \quad \dots (15b)$$

(the latter expressions are obtained by transforming the tridiagonal determinant to a didiagonal one by applying successive Gaussian elimination). Here  $\alpha_i$  and  $\beta_{i-1,i}$  are the onsite and hopping parameters in the first neighbours' interactions approximation. The  $\beta_{i-1,i}$  values are obtained from the dispersion of the valence or the conduction bands of the corresponding homopolymers, respectively, and the  $\alpha_i$ -values of a component are taken to be the middle points of the corresponding bands. Assuming the dispersion of the band to be given by the simple relation,

$$\varepsilon_A(k) = \varepsilon_A^0 + 2\beta_{i,i} \cos(ka) \quad \dots (16)$$

we can take  $\beta_{A,A}$  to be one-fourth of the band width if the same component is repeated. If on the other hand, component A is followed by component B, then the off-diagonal matrix element  $\beta_{A,B}$  is assumed to be given by the simple relation,

$$\beta_{A,B} = \frac{1}{2}(\beta_{A,A} + \beta_{B,B}) \quad \dots (17)$$

Thus, by giving different values and taking the difference of the number of negative  $\varepsilon_i(\lambda)$ s belonging to consecutive values, one can obtain the distribution of eigenvalues (DOS-s).

One should note that this method works out for one band only at a time. Using a more sophisticated version of this method—matrix block NFC method<sup>39</sup>—one can obtain the total DOS of a periodic or random copolymer. In this method, the  $\alpha$ 's and  $\beta$ 's of the simple NFC method are replaced by the appropriate Fock and overlap matrix blocks obtained from the corresponding cluster studies. One has, therefore, instead of a tridiagonal, a triblock diagonal secular determinant which is then didiagonalised and solved.

### 3.2.2. Treatment of correlation in aperiodic polymers

Generally two methods are used for treating correlation effects in aperiodic polymers. Firstly, the correlated quasi-particle bands are calculated using the MP perturbation theory for the periodic polymers constituting the aperiodic chain. The correlated quasi-particle band structure data of the components of an aperiodic polymer are then used in the NFC method in tight binding approximation to calculate the DOS of that aperiodic system<sup>39</sup>. The second method, which has been recently<sup>40</sup> developed, consists of determining the quasi-particle shifts of valence and conduction bands of the corresponding periodic polymers constituting the aperiodic chain and then employing these shifts in the matrix block NFC calculations of the corresponding

aperiodic polymers. The shifts, which are added to the diagonal blocks of the Fock matrix, are the blocks

$$\Delta_{HH} = S_{HH} \left( \frac{1}{2\pi} \int_{-\pi}^{\pi} dK U(K) M(K) U^*(K) \right) S_{HH} \dots (18)$$

where  $S_{HH}$  are the blocks of the overlap matrix,  $U(K)$  the  $K$ -dependent eigenvector matrix of the single component periodic polymer crystal-orbital calculation corresponding to cell  $H$  and  $M(K)$  the matrix containing the quasi-particle shifts.

## 4. Some Selected Results

### 4.1. Polyacetylene and Its Derivatives

Among the conducting polymers, PA is unique in the sense that its ground state is degenerate (the two states related to each other by the interchange of single and double bonds) (Fig. 4). In such compounds the energy gap ( $E_g$ ) is usually defined in the following way<sup>41</sup>,

$$E_g = 2E_o = 2(\epsilon_e + \epsilon_i) \dots (19)$$

where  $\epsilon_e$  is a fixed "external" contribution to the  $E_g$  due to the  $\sigma$  skeleton and  $\epsilon_i$  refers to the internal contribution from the  $\pi$  electron framework. In the case of PA, it is now fairly well established that the internal contribution to the gap increases as a function of increasing bond length alternation along the chains.

PA with a very small band gap of  $\sim 1.5$  eV and with capability to undergo substitution reactions is a very promising candidate for designing novel conducting polymers. At present more than 95 substituted polyacetylenes<sup>42</sup> (including both mono- and di-substituted) have been reported, but only 14 of these substituted polyacetylenes have been doped. Steric effects of substituents in polyacetylenes are found to play a very important and predominant role in most cases. Poly(methylacetylene)<sup>43</sup>, for example, in contrast to polyacetylene is soluble, has limited visible absorption and dopes to only  $10^{-3} \Omega^{-1} \text{ cm}^{-1}$  with iodine. These diminished properties in relation to PA, may be ascribed to non-coplanarity as a result of the methyl substituents. This non-coplanarity is also believed to reduce considerably the band widths, thereby leading to diminished carrier mobilities and lower conductivities. Similar behaviour is observed in the case of most of the other substituted polyacetylenes.

The effects of the substituents on the band structure of PA have been investigated in quite a few cases<sup>42</sup>. Such studies are necessary to determine the nature of the dopant (whether electron acceptor or

donor) and the strength required. One such interesting study<sup>44</sup> has been in the case of mono- and di-fluoro derivatives (Fig. 5) (not yet synthesized). *Ab initio* calculations (Table 1) of these system predict (i) the *trans* form to be more stable for both polymonofluoroacetylene (PMFA) and polydifluoroacetylene (PDFA) and (ii) both PMFA and PDFA to be better intrinsic conductors and better candidates for *n*-doping than *trans*-PA. Poly(methylacetylene)<sup>42</sup>, assuming a planar backbone, has been predicted to have a slightly decreased ionization potential and narrower bandwidths, compared to polyacetylene. Likewise poly(1,6-heptadyne)<sup>42</sup> is predicted to possess a lower ionization potential and narrower bandwidths than polyacetylene.

### 4.2. Nitrogen Containing Analogues

The isoelectronic analogues of PA obtained by the replacement of methine groups (CH) with azo nitrogen have also been proposed and studied<sup>45,46</sup> (Fig. 6). These are polyazoethene (PAE), polyazine (PAZ) and polymethineimine (PMI). Among these polymers, PMI and PAZ have already been synthesized. Euler and Hauer, on the basis of their extended Huckel calculations<sup>46</sup> of these systems, have predicted that PAE shall be a better semiconductor than PA and PAZ. The predicted order of decreasing band gap is  $\text{PMI} > \text{PAZ} > \text{PA} > \text{PAE}$ . On the other hand, the *ab initio* band structure calculations<sup>45</sup> (Table 2) of these systems predict the order of decreasing band gap as  $\text{PAE} > \text{PAZ} > \text{PMI} > \text{PA}$ .



Fig. 4—Degenerate ground state of *trans*-polyacetylene.

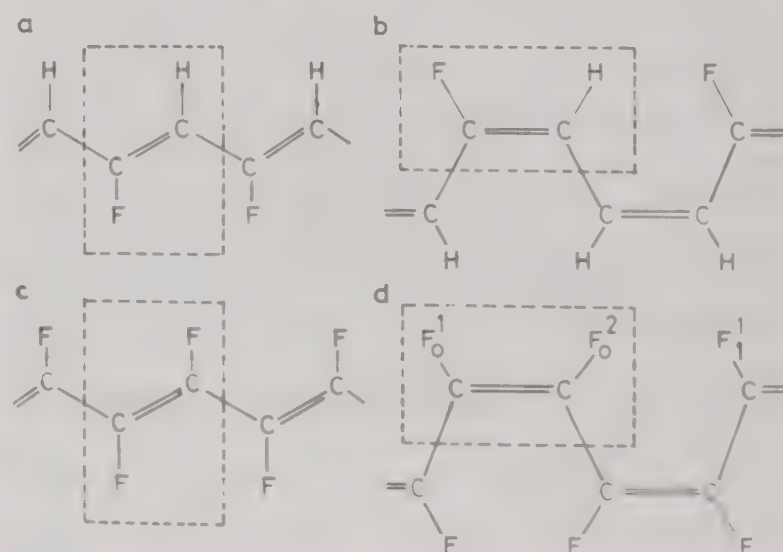


Fig. 5—Structures of (a) *trans*-polydifluoroacetylene (b) *cis*-polydifluoroacetylene; (c) *trans*-polymonofluoroacetylene and (d) *cis*-polymonofluoroacetylene (unit cells are surrounded by broken lines).

Table 1—Calculated electronic properties (in eV) of polyacetylene and fluorinated polyacetylenes  
[in both *cis* and *trans* configurations] (Fig. 5)]

	<i>cis</i> -PA	<i>trans</i> -PA	<i>cis</i> -PMFA	<i>trans</i> -PMFA	<i>cis</i> -PDFA	<i>trans</i> -PDFA
Valence band width	7.370	7.479	6.780	6.815	6.412	5.919
Conduction band width	9.580	9.330	9.918	9.697	9.410	9.701
Ionisation potential	8.666	8.347	8.625	8.977	8.230	9.725
Electron affinity	0.975	1.878	2.226	2.895	1.901	3.706
Band gap	7.692	6.469	6.401	6.082	6.328	6.019
Total energy per unit cell (in a.u.)	-76.58261	-76.58628	-175.15820	-175.1706	-273.57358	-273.74391

Table 2—Calculated electronic properties (in eV) for polyacetylene (PA), polymethineimine (PMI), polyazoethene (PAE) and polyazine (PAZ) (Fig. 6)

	PA	PMI	PAE	PAZ
Valence band width	7.479	7.707	3.329	3.773
Conduction band width	8.330	9.439	4.822	4.994
Ionization potential (top of valence band)	8.347	11.238	11.304	11.315
Electron affinity (negative of bottom of conduction band)	1.878	2.755	1.685	1.753
Band gap	6.469	8.483	9.619	9.562
Total energy per unit cell (in a.u.)	-76.58628	-92.52548	-185.04221	-185.05543

The predicted order of electron affinity values is  $\text{PMI} > \text{PA} > \text{PAZ} > \text{PAE}$ . Therefore, PMI is expected to have the greatest capability to undergo reductive doping and PAE the least. Similar conclusions about PMI have been obtained using VEH method<sup>47</sup> and the *ab initio* method using extended basis sets<sup>48</sup>.

#### 4.3. Aromatic Polymers

Among this class of polymers, poly(*p*-phenylene) (PPP), polypyrrole (PPY), polythiophene (PTP) and polyfuran (PFU) have been the focus of enormous interest, both theoretically<sup>49,50</sup> and experimentally. These polymers differ from PA in the sense that they do not have a degenerate ground state (Fig. 7) and hence Eq. (19) is no longer valid. Theoretical calculations on such polymers have shown<sup>51</sup> that their band gap ( $E_g$ ) does not decrease as a function of decreasing bond length alternation as is known in polyacetylene-like compounds, but rather as a function of increasing quinoid character of the polymer backbone. What then one needs is a compound in which some quinoid contributions are stabilized in the ground state. The decrease in band gap, for example, when going from polythiophene ( $E_g \approx 2.1$  eV) to polyisothianaphthene<sup>52</sup> ( $E_g \approx 1.0$  eV) can, therefore, be rationalized on the basis that the fusion of a benzene ring onto the thiophene ring effectively increases the quinoid contributions to the electronic structure<sup>53</sup>. The increased quinoid contribution to the electronic structure cuts the band gap into half

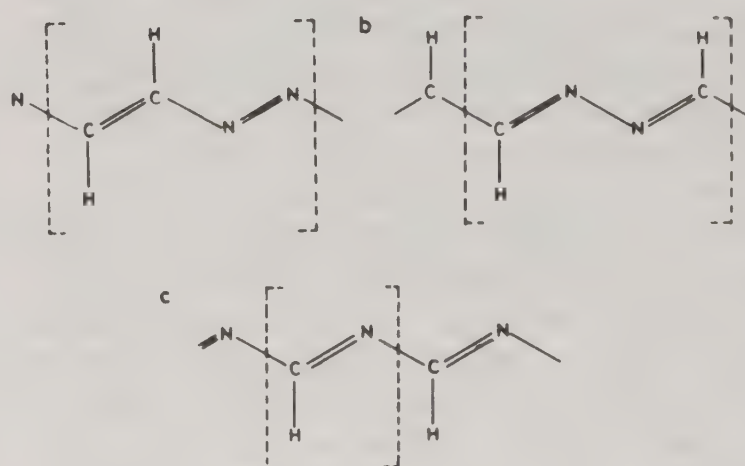


Fig. 6—Structures of (a) polyazoethene (PAE); (b) polyazine (PAZ); and (c) polymethineimine (PMI) (unit cells are surrounded by broken lines).

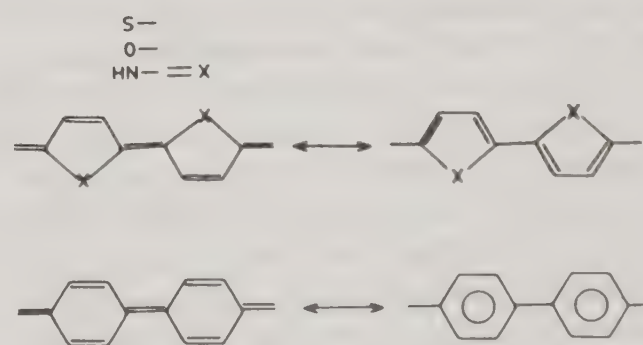


Fig. 7—Resonance structures for (a) poly(*p*-phenylene); (b) heterocyclic polymers (X = -NH (polypyrrole); X = -O (polyfuran) and X = -S (polythiophene)). The aromatic ground state structures are shown on the left hand side and the quinoid structures of higher energy on the right hand side.

with respect to that of the parent polymer, polythiophene.

For designing compounds with band gap even smaller than that of PITN, one would have to have compounds in which the effective quinoid contributions to the electronic structure would be slightly larger than that in PITN. However, this task is quite difficult as the quinoid form of aromatic polymers, associated with a smaller band gap, is energetically predicted to be less stable than the corresponding aromatic form. The study of the energy gaps and stability of various derivatives of PTP has shown<sup>54</sup> that  $E_g$  of aromatic and quinoid forms of PTP decreases and increases, respectively, as the number of six-membered ring fused to PTP increases.

As far as energetics is concerned, the quinoid form is more stable than the aromatic one when rings are attached to PTP. Therefore, according to these calculations, one has to stabilise the aromatic form in comparison to the quinoid form if the number of six-membered rings fused to PTP is more than one, in order to reduce  $E_g$  further. Similar trends are expected for polypyrrole and polyfuran. In the light of above results, there has been an attempt to incorporate quinoid character into the skeleton by a regular insertion of a methine group<sup>55</sup> between thiophene rings, resulting in the reduction of the band gap value to as small as 0.75 eV.

From an analysis<sup>50</sup> of the Bloch wave-functions of the highest occupied and the lowest unoccupied bands of the  $\alpha,\alpha'$ -linked PPY, PTP and PFU, it is found that the substitution on backbone ( $\beta$ -carbon atoms) influences both IP and EA values while the choice of the heteroatom affects EA more than IP. With these results as guidelines, there have been studies<sup>56-65</sup> of the various derivatives of these systems. While preparing derivatives, highly polarisable substituents (such as benzene in PITN) are always preferred. High polarisability of the substituents tends to reduce the electron-electron interactions between the two  $\pi$  electrons on the same ring or on the neighbouring carbons along the backbone, an effect which would lead to smaller band gap.

The aromatic polymers discussed above are similar in that they become conducting through oxidation (removal of electrons from the polymers'  $\pi$  electron structure). An alternative type of conducting polymer which has found immense use as electrode material<sup>66</sup> in conducting polymer batteries, is polyaniline. At least four possible forms of polyaniline have been proposed and largely identified by various experiments. These different forms of polyaniline can be reversibly converted by oxidation/reduction and alkali/acid treatment<sup>67</sup>. The structure of the emeraldine base (EB) form of polyaniline is il-

lustrated in Fig. 8a. This polymer consists of equal numbers of oxidised (Fig. 8c) and reduced (Fig. 8d) units. The relative ratio of the oxidised (concentration  $y$ ) and the reduced (concentration  $1 - y$ ) units can be controlled from the completely oxidised to the completely reduced through electrochemical modification. The EB form ( $y = 0.5$ ) (Fig. 8a) has a room temperature conductivity of  $\sim 10^{-10} \Omega^{-1} \text{ cm}^{-1}$  and upon treatment with aqueous HCl of pH 0.0 yields the highly conducting ( $\sim 5 \Omega^{-1} \text{ cm}^{-1}$ ) completely protonated state (emeraldine salt (ES)) (Fig. 8b)).<sup>68,69</sup> In contrast to the polymers discussed earlier, in this polymer on oxidation the number of electrons on the polymer backbone remains constant while the number of protons changes. Another conducting form of polyaniline can also be synthesized through the electrochemical oxidation of the leucoemeraldine form of the polymer which, before oxidation, is composed of the reduced repeat units (Fig. 8d) and is insulating with a large band gap (3.1 eV).

There have been many theoretical studies<sup>70-74</sup> on the electronic structure and conduction properties of the different redox forms of polyaniline. *Ab initio* calculations on both the *cis*- and *trans*-configurations of the oxidised form of polyaniline with alternating benzoid-quinoid structure have been reported by Otto and Dupuis<sup>74</sup>. For both the configurations, the optimisation of the twist angle between the nearest neighbours shows the *cis*-configuration with rings perpendicular to each other as the most stable structure in agreement with the  $C^{13}$ -NMR spectroscopic data<sup>75</sup>. Analogous investigations on the salt formed between polyaniline and HCl reveal again the *cis*-configuration with perpendicular conformation of adjacent rings as the energetically preferred geometry. The band gap in the

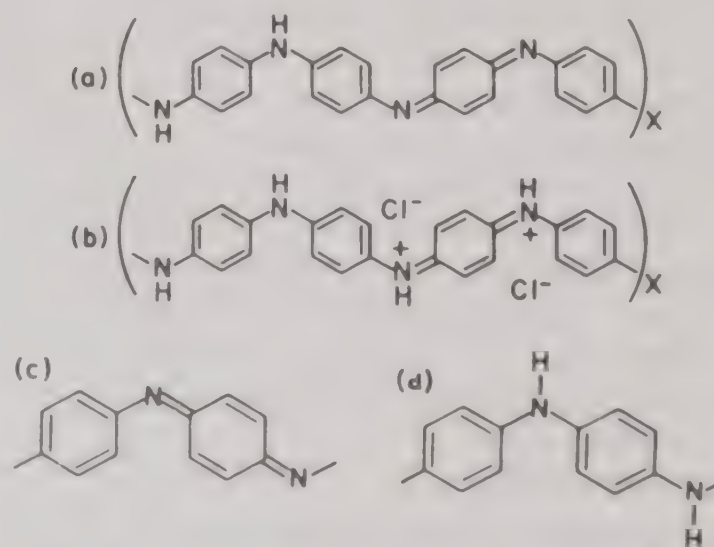


Fig. 8—(a) The emeraldine base (EB) and (b) emeraldine salt (ES) forms of polyaniline. (c) Oxidised and (d) reduced repeat units for polyaniline.

protonated polyaniline is found to be smaller than that for the neutral form and may, therefore, be responsible for the conductive properties of the salt form.

#### 4.4. One Dimensional Graphite Family

There have been many theoretical investigations<sup>76-80</sup> of the electronic structure and conduction properties of the members of 1-D graphite family. PAc is the most studied polymer of this family followed by PPN, PPh and PPhP. The band structure calculations<sup>80</sup> of PPN show that due to its internal symmetry, its band structure can be considered to be derived from the interaction of two *cis*-polyacetylene (PA) chains. This interaction splits the original *cis*-PA highest occupied crystal orbital (HOCO) and the lowest unoccupied crystal orbital (LUCO) resulting in a much smaller band gap than in *cis*-PA.

In the case of polyacene, three isomers are possible (Fig. 9) and the question of its most stable polymer is still unresolved. The predicted order of stability among the three isomers, on the basis of *ab initio* calculations<sup>81</sup>, is PAc1 > PAc2 > PAc3 (Table 3) implying thereby that the aromatic skeleton is the most stable structure. It, therefore, means that Pierls transition does not take place in PAc, as also claimed by Baldo *et al.*<sup>82</sup>. Tanaka *et al.*<sup>76</sup>, on the other hand, predict PAc3 to be the most stable isomer of PAc. Our preliminary investigations<sup>83</sup>, using the same methodology, in the case of PAcA show that PAcA has still smaller band gap than PAc implying thereby that the system tends to become more and more intrinsically conducting along this series of polymers. The predicted order of conductivities along this series is PAcA > PAc > *trans*-PA. Our results<sup>83</sup> show that the band gap of PPh, however, decreases by about 0.5 eV in contrast to that of *cis*-PA chain. These results are interesting in the sense that though PAc and PPh differ from each other only in the mode of growth of condensed aromatic rings,

the band gap of PAc is very small as compared to that of PPh. However, as one goes from PhP to PPhP, the band gap is found to decrease considerably.

There have been several attempts to actually synthesize members of 1-D graphite family. The synthesis of conducting films of PPN has been reported by Kaplan *et al.*<sup>84</sup> by the pyrolysis of 3,4,9,10-perylene tetracarboxylic dianhydride at temperatures between 700° and 900°C. Similar films have also been obtained by Schmidt *et al.*<sup>85</sup> and Forest *et al.*<sup>86</sup> by electron and argon ion beam bombardment respectively of PTCDA. No other member of this family has so far been prepared. The synthesis of PAc has been attempted by Ozaki *et al.*<sup>87</sup> via its prepolymer poly(ethynyl acetylene) (PEA) which was obtained by the desilylation of poly(trimethylsilyl ethynyl acetylene) (PTMSEA). Recently, Tanaka *et al.*<sup>88</sup> have studied theoretically the cyclisation reactions of polybutadiyne and polyhexatriyne to PAc and PAcA respectively and have concluded that these reactions are favourable from energetics point of view.

#### 4.5. DOS of Polymeric Superlattices

The electronic DOS of the various periodic and random quasi-one-dimensional superlattices (copo-

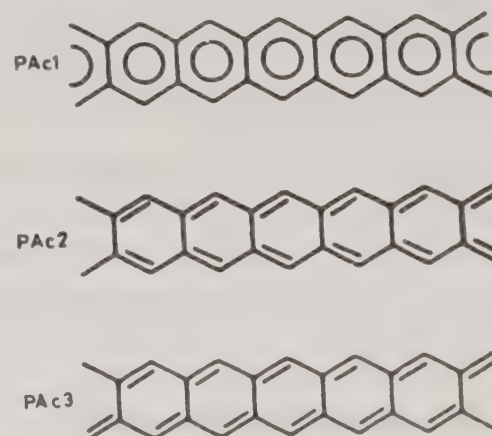


Fig. 9—Structural isomers of polyacene (PAc).

Table 3—Calculated electronic properties (in eV) of polyacene (Fig. 9)

	PAc1	PAc2	PAc3
Ionisation potential	7.650	7.590	7.451
Electron affinity	4.921	4.887	4.793
Valence band width	7.961	7.983	8.054
Conduction band width	8.375	8.542	8.533
Band gap	2.728	2.704	2.658
Electronic energy (in a.u.)	-514.860084	-514.863599	-514.719508
Nuclear repulsion energy (in a.u.)	362.759092	362.762731	362.618665
Total Energy (in a.u.)	-152.100992	-152.100868	-152.100843

lymers) of the type  $(A_m B_n)_x$  of the heterocyclic polymers have been calculated. Two types of superlattices have been extensively studied<sup>89,90</sup>: Type I (where A=furan and B=thiophene) and Type II-staggered (where A=pyrrole and B=thiophene). For each of these two types of superlattices, the trends in their electronic structure and conduction properties as a function of (i) composition ( $m/n$ ), (ii) block sizes  $m$  and  $n$  and (iii) arrangement of blocks in the copolymer chain have been investigated. It has been found that besides some trends characteristic of each type of superlattice, for both tuning of the electronic properties intermediate between those of their components is easier by synthesizing periodic copolymers. Random copolymers, on the other hand, lead relatively faster to the saturated electronic properties, characteristic of the lower band gap component (thiophene in both cases) and largely independent of the larger gap component.

Figs 10 and 11 show the DOS curves of both periodic and random copolymers of type  $(A_m B_n)_x$  belonging to Type I superlattice. The DOS curves of periodic copolymers, consist of relatively narrower and well separated peaks while the random systems consist of relatively broader regions of allowed energy states with fewer gaps in between. Such a feature was also observed by us in the case of aperiodic proteins and DNA-B and is due to the lifting of degeneracies at the edges of the reduced Brillouin zone of the periodic chains. Random copolymers, in general, are found to be less insulating than the corresponding periodic copolymers.

It should be noted that the controlled synthesis of the copolymers according to the desired sequence and block sizes has not been achieved yet but it is perhaps possible by using the Langmuir Blodgett<sup>91</sup> or the Merrifield synthetic technique<sup>92</sup>.

## 5. Conclusions and Future Possibilities

In this paper, the various theoretical approaches presently pursued to tailor novel conducting polymers have been discussed. A common feature of all these approaches has been to draw qualitative conclusions regarding conduction properties of the undoped polymers or copolymers on the basis of their electronic properties obtained from either their band structure calculations or their electronic DOS calculations. The results obtained through such calculations undoubtedly provide important guidelines for designing novel conducting polymers and their superlattices. Since most of these conducting polymers are extrinsic conductors of electricity, it would be worthwhile as a next step to investigate their electronic structure and conduction properties in the doped state. These investigations have not so

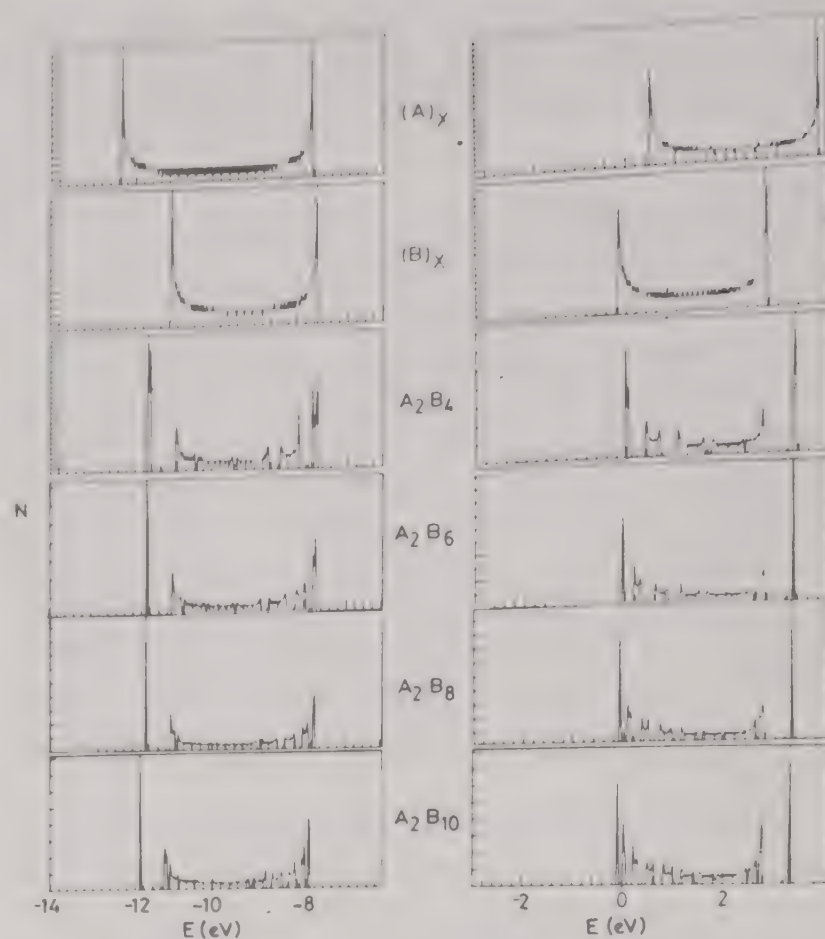


Fig. 10—DOS curves for  $(A)_x$ ,  $(B)_x$  and periodic block copolymers of type  $(A_m B_n)_x$  (A=furan; B=thiophene) (energy in eV, number of states  $N$  in relative units).

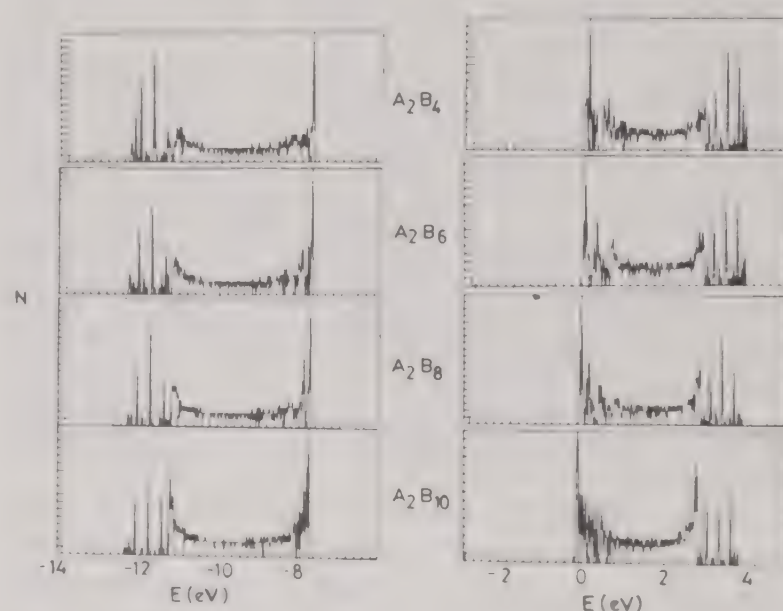


Fig. 11—DOS curves for random copolymers of type  $(A_m B_n)_x$  (A=furan; B=thiophene) (energy in eV, number of states  $N$  in relative units).

far been carried out because the doped organic polymers are very complicated systems with properties sensitive to factors such as disorder, low dimensionality of electronic motion and strong electron-phonon coupling. The doping process in these conducting polymers is basically a redox process accompanied by the modification of their geometry. This local modification of the geometry affects the electronic structure by inducing localised electronic states in the band gap corresponding to the forma-

tion of elementary excitations such as charged soliton, polaron and bipolaron. The calculations of the electronic structure of the doped systems, particularly at *ab initio* level with better basis set and with consideration of electronic correlation effects, would also help in firmly establishing the nature of charge carriers in these systems. One may then, while tailoring electrically conducting polymers, look for the systems which can support such carriers. One may also perform similar calculations on the doped quasi-one-dimensional superlattices and thus obtain important guidelines for designing doping polymeric superlattices in contrast to the compositional superlattices presently being studied.

### Acknowledgement

The author is grateful to the Indian National Science Academy (INSA) for the award of INSA Research Fellowship and to the CSIR for the financial support.

### References

- Shirakawa H, Louis E J, MacDiarmid A G, Chiang C K & Heeger A J, *J chem Soc, Chem Commun*, (1977) 578.
- Chiang C K, Fincher (Jr) C R, Park Y W, Heeger A J, Shirakawa H, Louis E J, Gan S C & MacDiarmid A G, *Phys Rev Lett*, 39 (1977) 1098.
- Chiang C K, Druy M A, Gan S C, Heeger A J, Louis E J, MacDiarmid A G, Park Y W & Shirakawa H, *J Am chem Soc*, 100 (1978) 1013.
- Shirakawa H, Ito T & Ikeda S, *J polym Sci, Polym Chem Ed*, 12 (1974) 11.
- See for example: *Handbook of conducting polymers*, Vols 1 and 2, edited by T A Skotheim (Marcel Dekker, New York) 1986.
- Kobayashi M, Chen J, Chung T C, Moraes F, Heeger A J & Wudl F, *Synth Met*, 9 (1984) 77.
- Advances in linear free energy relationships*, edited by N B Chapman & J Shorter (Plenum Press, New York) 1972.
- Gibson H W, *Can J Chem*, 51 (1973) 3065.
- Zuman P, *Substituent effects in organic polarography*, (Plenum Press, New York) 1967; Peover M E, *Trans Faraday Soc*, 58 (1962) 1656, 2370; Kuder J E, Gibson H W & Wyckick D, *J org Chem*, 40 (1975) 875.
- Kivelson S & Chapman O L, *Phys Rev(B)*, 28 (1983) 7236.
- Esaki L & Tsu R, *IBM J Res Develop*, 14 (1970) 61.
- For a review see Smith D L & Maithio C, *Rev Mod Phys*, 62 (1990) 173.
- Esaki L, *IEEE J Quant Electron*, 22 (1986) 1611.
- Bakhshi A K & Ladik J, *Chem Phys Lett*, 129 (1986) 269.
- Bakhshi A K, Otto P, Ladik J & Seel M, *Chem Phys*, 108 (1986) 215.
- Bakhshi A K, Ladik J, Seel M & Otto P, *Chem Phys*, 108 (1986) 233.
- Ladik J, Otto P, Bakhshi A K & Seel M, *Int J quantum Chem*, 29 (1986) 597.
- Del Re G, Ladik J & Biczio G, *Phys Rev*, B155 (1967) 997.
- Andre J M, Gouverneur L & Leroy G, *Int J quantum Chem*, 1 (1967) 427, 451.
- Ladik J, in *Advances in quantum chemistry*, edited by P O Lowdin (Academic Press, New York, London) 7 (1973), 397.
- Wilson E G, *J Phys C*, 8 (1975) 727.
- Balasubramanian K & Yarkony D R, *Chem Phys Lett*, 70 (1980) 374.
- Hoffmann R, *J chem Phys*, 39 (1963) 1397.
- Andre J M, *Adv quantum Chem*, 12 (1980) 65.
- Duke B J & O'Leary B, *Chem Phys Lett*, 20 (1973) 459.
- Delhalle J, Andre J M, Demanet C & Bredas J L, *Theoret chim Acta*, 43 (1977) 215.
- Nicholas G, Durand P O & Burke L A, *Lect Notes Phys*, 113 (1980) 201.
- Nicholas G & Durand P, *J chem Phys*, 70 (1979) 2020; 72 (1980) 453.
- Kaulgud M V & Chitgopkar V H, *J C S Farad Trans II*, (1977) 1385.
- Kaulgud M V & Chitgopkar V H, *J C S Farad Trans II*, (1978) 951.
- Moeller C & Plesset M S, *Phys Rev*, 46 (1934) 618.
- Cizek J, *J chem Phys*, 45 (1966) 4256; *Adv quantum Chem*, 3 (1969) 35.
- Cizek J & Paldus J, *Int J quantum Chem*, 5 (1971) 359.
- Meyer W, *J chem Phys*, 58 (1973) 1017.
- Suhai S, *Phys Rev*, B27 (1983) 3506.
- Elliott A J, Krumhansl J A & Leath P, *Rev Mod Phys*, 46 (1974) 465.
- Seel M, *Chem Phys*, 43 (1979) 103.
- Dean P, *Proc R Soc London*, A254 (1960) 507; 260 (1961) 263; *Rev Mod Phys*, 44 (1972) 127.
- Ladik J, Steel M, Otto P & Bakhshi A K, *Chem Phys*, 108 (1986) 203.
- Liegner C M, *Chem Phys*, 133 (1989) 173.
- Mintmire J W, White C T & Elert M L, *Synth Met*, 16 (1986) 235.
- Gibson H W in *Handbook of conducting polymers*, Vol. 1, edited by T A Skotheim (Marcel Dekker, New York) 1986.
- Chien J C W, Wnek G E, Karasz F E & Hirsch J A, *Macromolecules*, 14 (1981) 479.
- Bakhshi A K, Ladik J & Liegner C M, *Synth Met*, 20 (1987) 43.
- Bakhshi A K & Ladik J, *Solid State Commun*, 60 (1986) 361.
- Euler E B & Hauer C R, *Solid State Commun*, 51 (1974) 473.
- Bredas J L, Themans B & Andre J M, *J chem Phys*, 78 (1983) 6137.
- Karpfen A, *Chem Phys Lett*, 64 (1979) 299.
- Tourillon G & Garnier F, *J Electroanal Chem Interfacial Electrochem*, 135 (1982) 173.
- Bakhshi A K, Ladik J & Seel M, *Phys Rev*, B35 (1987) 704.
- Bredas J L, *J chem Phys*, 82 (1985) 3808.
- Wudl F, Kobayashi M & Heeger A J, *J org Chem*, 49 (1984) 3382.
- Bakhshi A K & Ladik J, *Solid State Commun*, 61 (1987) 71.
- Lee Y S & Kertesz M, *Int J quantum Chem*, 21 (1987) 163.
- Jenekhe S A, *Nature*, 322 (1986) 345.
- Tanaka S, Wang S & Yamabe T, *Synth Met*, 30 (1989) 57.
- Toussaint J M, Themans B, Andre J M & Bredas J L, *Synth Met*, 28 (1989) C205.
- Riga J, Snauwaert Ph, Pryck A De, Lazzaroni R, Boutique J P, Verbist J J, Bredas J L, Andre J M & Talianai C, *Synth Met*, 21 (1987) 223.
- Montheard J P, Biotenx G, Themans B, Bredas J L, Parcal T & Froyer G, *Synth Met*, 36 (1990) 195.
- Bakhshi A K & Ladik J, *Solid State Commun*, 63 (1987) 1157.

- 61 Lazzaroni R, Taliani C, Zamboni R, Danieb R, Ostoja P, Lamer I, Porzio W & Bredas J L, *Synth Met*, 28 (1989) C515.
- 62 Kertesz M & Lee Y S, *Synth Met*, 28 (1989) C545.
- 63 Bakhshi A K & Ladik J, *Solid State Commun*, 65 (1988) 1203.
- 64 Bakhshi A K, *J molec Struct (Theochem)*, 209 (1990) 193.
- 65 Colaneri N, Kobayashi M, Heeger A J & Wudl F, *Synth Met*, 14 (1986) 46.
- 66 MacDiarmid A G, Chiang J C, Halpren M, Hwang W S, Mu S L, Somasiri N L D, Wu W & Yaniger S I, *Mol Cryst Liq Cryst*, 121 (1985) 173.
- 67 Chiang J C & MacDiarmid A G, *Synth Met*, 13 (1986) 195.
- 68 Epstein A J, Ginder J M, Richter A F & MacDiarmid A G, in *Conducting Polymers* edited by L Alcacer (D Reidel, Amsterdam), 1987, 121.
- 69 Genies E M, Boyle A, Lapkowski M & Tsintavis C, *Synth Met*, 36 (1990) 139.
- 70 Bredas J L, Themans B, Andre J M, Silbey R, Boudreaux D S & Chance R R, *Bull Soc Chim Belg*, 95 (1986) 511.
- 71 Euler W B, *Solid State Commun*, 57 (1986) 857.
- 72 Chance R R & Boudreaux D S, *Synth Met*, 18 (1987) 329.
- 73 Hjertberg T, Sandberg M, Wennerstrom O & Iangerstedt I, *Synth Met*, 21 (1987) 31.
- 74 Otto P & Dupuis M, *J chem Phys*, 86 (1987) 6309.
- 75 Hjertberg T, Salaneck W R, Lundstrom I, Somasiri N L D & MacDiarmid A G, *J Polym Sci Polym Lett Edn*, 23 (1985) 503.
- 76 Tanaka K, Ohzeki K, Nankai S & Yamabe T, *J phys Chem Solids*, 44 (1983) 1069.
- 77 Bredas J L, Chance P R, Baughman R H & Silbey R, *J chem Phys*, 76 (1982) 3673.
- 78 Bozovic I, *Phys Rev (B)*, 32 (1985) 8136.
- 79 Kertesz M, Lee Y S & Stewart James J P, *Int J quant Chem*, 35 (1989) 305.
- 80 Bakhshi A K & Ladik J, *Synth Met*, 30 (1989) 115.
- 81 Bakhshi A K in *Frontiers of polymer research* (Plenum Press, New York), 1992, 425-429.
- 82 Baldo M, Piccoto G, Pucci R & Tomasello R, *Phys Lett*, 95A (1985) 201.
- 83 Bakhshi A K (to be published).
- 84 Kaplan M L, Schmidt P H, Chen C H & Walsh W M, *Appl Phys Lett*, 36 (1980) 867.
- 85 Schmidt P H, Joy D C, Kaplan M L & Fieldmann W L, *Appl Phys Lett*, 40 (1982) 93.
- 86 Forrest S R, Kaplan M L, Schmidt P H, Venkatesan T & Lovinger A J, *Appl Phys Lett*, 41 (1982) 485.
- 87 Ozaki M, Ikeda Y & Nagoya I, *Synth Met*, 18 (1987) 485.
- 88 Tanaka K, Yamashita S, Koike T K & Yamabe T, *Synth Met*, 31 (1989) 1.
- 89 Bakhshi A K & Ladik J, *Int J Quant Chem* (in press).
- 90 Bakhshi A K, *J chem Phys*, 96 (1992) 2339.
- 91 Langmuir I, *Trans Farad Soc*, 15 (1920) 62; Blodgett K B, *J Am chem Soc*, 57 (1935) 1007.
- 92 Cartier F L, *NRL Mem Report No. 4335*, (1980) (unpublished); *Physica*, 10D (1984) 175.

## Crystal and molecular structure of aquoethylenediaminetetraacetatoruthenium (III) and its extraordinary lability towards substitution

M M Taqui Khan\*, K Venkatasubramanian, H C Bajaj & Zahida Shririn

Discipline of Coordination Chemistry & Homogeneous Catalysis, Central Salt & Marine Chemicals Research Institute, Bhavnagar 364 002

Received 27 May 1991; revised and accepted 18 November 1991

The crystal and molecular structure of  $[\text{Ru}(\text{HEDTA})(\text{H}_2\text{O})]$  (**2**), was determined using single crystal X-ray diffraction techniques. The complex crystallizes with 4 molecules in the space group  $P2_1/c$  with the unit cell dimensions  $a = 8.414(1) \text{ \AA}$ ,  $b = 8.835(1) \text{ \AA}$ ,  $c = 17.610(4) \text{ \AA}$ ,  $\beta = 99.64(1)^\circ$ . The structure has been solved taking advantage of the fact that the complex is isomorphous with the analogous Rh(III) complex. The structure is refined to an R value of 0.033 ( $R_w = 0.043$ ) for 5983 observed reflections. Ru occurs as a distorted octahedron. Ethylenediaminetetraacetic acid is a pentadentate ligand, with one free carboxylate group. Water approaches the coordination sphere *trans* to one of the nitrogens of the ethylenediamine moiety. Ring  $R_2$  is planar, while rings  $R_1$  and G are envelopes. Ring E occurs as a half-chair. The structure is held in three-dimensional space by an elaborate network of hydrogen bonds. Water exchange rate constants show that the complex is labile. An attempt is made to rationalize the unusual lability of the complex.

The EDTA complexes with Ru are important not only from the structural view point but also because of the roles these complexes play in various homogeneous catalytic reactions<sup>1-4</sup>. In most of the cases,  $[\text{Ru}(\text{HEDTA})(\text{H}_2\text{O})]$  is an active intermediate. The extreme lability of  $[\text{Ru}(\text{HEDTA})(\text{H}_2\text{O})]$  in comparison to other nonchelated complexes<sup>5,6</sup> of Ru has attracted attention in recent years<sup>7-9</sup>. It is generally accepted that the EDTA is coordinated as a pentadentate ligand with sixth coordination site being occupied by a water molecule. It has been reported<sup>7-9</sup>, in previous studies, that the H-bonding between the free carboxylate oxygen and the coordinated water molecule must account for the high lability of water molecule. In order to know the reason for high lability, we have presently studied the crystal and molecular structure of  $[\text{Ru}(\text{HEDTA})(\text{H}_2\text{O})]$  (**2**).

### Materials and Methods

$\text{K}[\text{Ru}(\text{HEDTA})\text{Cl}]\cdot 2\text{H}_2\text{O}$  (**1**) was prepared from  $\text{K}_2[\text{RuCl}_5(\text{H}_2\text{O})]$  as described in literature<sup>10</sup>. The complex was characterised by spectroscopic (IR) and analytical techniques<sup>11</sup>. In aqueous solution, complex (**1**) rapidly hydrolyses to  $[\text{Ru}(\text{HEDTA})(\text{H}_2\text{O})]$  (**2**). The aquo complex **2** was isolated from solution by removal of  $\text{Cl}^-$  ion with  $\text{Ag}_2\text{CO}_3$ . The white precipitate of  $\text{AgCl}$  was filtered by millipore filtration. The yellow coloured solution was concentrated to a small volume, treated with acetone and the resultant yellow precipitate filtered, washed

with acetone and dried *in vacuo*. Complex **2** was characterised<sup>12</sup> by spectroscopic (IR and UV-vis) techniques and elemental analysis.

Yellowish orange prismatic crystals of **2** were obtained by slow evaporation of an aqueous solution at room temperature. One such crystal ( $0.12 \times 0.15 \times 0.13 \text{ mm}$ ) was used for crystal structure study. Accurate cell dimensions were obtained by using 25 arbitrarily chosen higher order reflections between  $2\theta$  of  $31^\circ$  and  $33^\circ$  Mo- $K_\alpha$ . Intensity data were collected using graphite monochromatized Mo- $K_\alpha$  radiation ( $\lambda = 0.71068 \text{ \AA}$ ) upto  $2\theta$  value of  $80^\circ$ . Three reflections were used for orientation control and another three for intensity control to check alignment and decay during the process of data collection. The data were corrected for Lorentz-polarization factors as well as for absorption effects using the empirical correction method<sup>13</sup> and three reflections near  $\chi$   $90^\circ$ .

The structure was solved taking advantage of the fact that it is isomorphous with that of the rhodium complex<sup>14</sup>. Hydrogen atoms could be located after a complete convergence of anisotropic refinement of non-hydrogen atoms and were included with a B factor 1.3 times that of the atoms to which they were attached. Four cycles of anisotropic refinement of the non-hydrogen atoms with a Dunitz-Seiler weighting scheme<sup>15</sup> while keeping the hydrogens fixed resulted in convergence (shift/error = 0.0028) at an R of 0.033 ( $R_w = 0.043$ ). Atomic scattering factors of Ru, O, N and C were from Volume IV of the International

Table 1—Crystallographic data

Formula	= RuC <sub>10</sub> H <sub>15</sub> N <sub>2</sub> O <sub>9</sub>	temp. = 20 ± 1°C
fw	= 408.26	2θ limit = 2°–80° (Mo – K <sub>α</sub> )
Space group	= P2 <sub>1</sub> /c	λ = 0.71069 Å
a	= 8.414(4) Å	Data collected + h, +k, ±l
b	= 8.835(4) Å	No. of reflections collected = 7969
c	= 17.610(1) Å	No. of reflections observed = 5989
β	= 99.64(1)°	[1 ≤ 3σ(1)]
V	= 1290.5(4) Å <sup>3</sup>	No. of parameters refined = 235
Z	= 4	Transmission coefficient:
d <sub>calc</sub>	= 2.101 g cm <sup>-3</sup>	Min = 92.69%
Crystal size	= 0.12 × 0.15 × 0.13 mm	Max = 99.99%
F(000)	= 820	Av = 97.13%
μ (Mo – K <sub>α</sub> )	= 12.421 cm <sup>-1</sup>	R = 0.033
		R <sub>w</sub> = 0.043

Tables for Crystallography<sup>16</sup>, while those of hydrogens were from Stewart *et al.*<sup>17</sup>. The final difference map contained peaks of density of 0.8 eÅ<sup>-3</sup> near the heavy atom positions. All the computations were done using the SDP set of programs available for the PDP-11/73 system<sup>18</sup>. The relevant data collection and structure solution parameters are listed in Table 1.

## Results and Discussion

### Molecular structure of complex (2)

The final positional and equivalent isotropic thermal parameters of the non-hydrogen atoms are listed in Table 2, while Table 3 gives the bond lengths and angles in complex **2**. Because of the use of block-diagonal L.S. methods, the standard deviation quoted are underestimates.

Figure 1 shows an ORTEP<sup>19</sup> view of **2** along with the numbering scheme adopted. In **2**, ethylenediaminetetraacetic acid is pentadentate with a free carboxylic arm. Such pentadentate behaviour for the EDTA has been found in [Rh(HEDTA)(H<sub>2</sub>O)]<sup>14</sup>, K[Ru(HEDTA)Cl]·2H<sub>2</sub>O<sup>20</sup>, Ru(HEDTA)(PPh<sub>3</sub>)<sub>2</sub>·3H<sub>2</sub>O<sup>21</sup>, K[Ru<sup>III</sup>(EDTA)(CO)]<sup>22</sup> and [Ru(EDTA)(NO)]<sup>23</sup>. The sixth position of the Ru(III) octahedron is occupied by a water molecule. The distortion of Ru(III) octahedron is reflected in the lengths of the twelve edges of the octahedron, which range from 2.649(5) Å to 3.199(5) Å (av = 2.924(5) Å and in root mean square deviations of the least squares planes Ru-N4-O17-O13-O15 (0.131 Å), Ru-N1-N4-O15-O21 (0.127 Å) and Ru-N1-O13-O17-O21 (0.074 Å).

Two distinct sets of Ru–N distances (2.035(2) Å and 2.129(2) Å and of Ru–O distances (1.986(2) Å and 2.006(2) Å, and 2.062(2) Å) exist, depending on whether two or one acetate group(s) are attached to the nitrogen atom. Coordinated C–O bonds are

Table 2—Positional and equivalent isotropic thermal parameters of non-hydrogen atoms and their estimated standard deviations

Atom	x	y	z	B(A <sup>2</sup> )
Ru	0.19710(2)	0.82478(2)	0.14317(1)	1.10(2)
O13	0.3595(3)	0.8424(2)	0.2306(1)	1.89(3)
O14	0.4797(3)	0.7089(3)	0.3397(1)	2.78(5)
O15	−0.0004(3)	0.8531(2)	0.1914(1)	1.85(4)
O16	−0.2036(3)	0.7217(3)	0.2257(2)	2.79(5)
O17	0.0508(2)	0.8089(2)	0.0372(1)	1.57(3)
O18	0.0459(3)	−0.7731(3)	−0.0883(1)	2.31(4)
O19	0.6689(3)	0.6640(3)	0.257(2)	2.72(5)
O20	0.7504(3)	0.9041(3)	0.0502(2)	2.30(4)
O21	0.2238(3)	1.0577(2)	0.1174(1)	1.96(4)
N1	0.1727(3)	0.6073(2)	0.1774(1)	1.35(3)
N4	0.3675(2)	0.7375(2)	0.0777(1)	1.25(3)
C2	0.2502(3)	0.5069(3)	0.1252(2)	1.83(5)
C3	0.4054(3)	0.5807(3)	0.1120(2)	1.64(4)
C5	0.2567(4)	0.5949(4)	0.2593(2)	2.11(5)
C6	0.3766(3)	0.7206(4)	0.2020(2)	1.80(4)
C7	−0.0042(3)	0.5833(3)	0.1719(2)	1.71(4)
C8	−0.0776(3)	0.7262(4)	0.2003(2)	1.80(4)
C9	0.2932(3)	0.7288(4)	−0.0053(2)	1.71(4)
C10	0.1168(3)	0.7731(3)	−0.0214(1)	1.41(4)
C11	0.5105(3)	0.8378(3)	0.0891(2)	1.67(4)
C12	0.6496(3)	0.7890(3)	0.0504(2)	1.67(4)

Anisotropically refined atoms are given in the form of the isotropic equivalent displacement parameter defined as:  $\langle u^2 \rangle = [a^2 B(1,1) + b^2 B(2,2) + c^2 B(3,3) + ab(\cos \gamma) B(1,2) + ac(\cos \beta) B(1,3) + bc(\cos \alpha) B(2,3)]$

elongated over the non-coordinated ones by ~0.08 Å. N–C bond lengths averages to 1.494(4) Å and C–C bond lengths to 1.514(4) Å. The distribution of the angles in the carbonyl group differ depending on whether or not this occurs in the deprotonated or protonated form. In the former, the widened O–C–O angle is compensated by a more or less equal contraction of the C–C–O angles.

Table 3—Bond lengths (Angstroms) and bond angles (degrees) for the complex

Atom 1	Atom 2	Distance Å	Atom 1	Atom 2	Atom 3	Angle	Atom 1	Atom 2	Atom 3	Angle
Ru	O13	1.986(2)	O13	Ru	O15	97.62(9)	Ru	N4	C3	103.3(2)
Ru	O15	2.004(2)	O13	Ru	O17	173.36(8)	Ru	N4	C9	109.8(1)
Ru	O17	2.062(2)	O13	Ru	O21	91.29(8)	Ru	N4	C11	108.4(2)
Ru	O21	2.127(3)	O13	Ru	N1	84.95(8)	C3	N4	C9	111.5(3)
Ru	N1	2.035(2)	O13	Ru	N4	93.27(8)	C3	N4	C11	112.3(2)
Ru	N4	2.129(2)	O15	Ru	O17	88.86(8)	C9	N4	C11	111.1(3)
O13	C6	1.313(4)	O15	Ru	O21	95.40(9)	N1	C2	C3	108.3(3)
O14	C6	1.225(3)	O15	Ru	N1	81.95(9)	N4	C3	C2	108.9(2)
O15	C8	1.318(4)	O15	Ru	N4	162.91(8)	N1	C5	C6	112.7(2)
O16	C8	1.219(4)	O17	Ru	O21	86.64(8)	O13	C6	O14	123.1(3)
O17	C10	1.290(3)	O17	Ru	N1	97.46(9)	O13	C6	C5	116.4(2)
O18	C10	1.228(4)	O17	Ru	N4	80.76(7)	O14	C6	C5	120.4(3)
O19	C12	1.207(4)	O21	Ru	N1	175.06(9)	N1	C7	C8	108.4(2)
O20	C12	1.324(4)	O21	Ru	N4	97.48(9)	O15	C8	O16	123.3(3)
N1	C2	1.503(4)	N1	Ru	N4	85.95(9)	O15	C8	C7	115.4(2)
N1	C5	1.500(3)	Ru	O13	C6	114.9(2)	O16	C8	C7	121.3(3)
N1	C7	1.490(3)	Ru	O15	C8	113.9(2)	N4	C9	C10	114.0(2)
N4	C3	1.523(3)	Ru	O17	C10	118.0(1)	O17	C10	O18	124.2(2)
N4	C9	1.493(3)	Ru	N1	C2	107.4(2)	O17	C10	C9	117.0(3)
N4	C11	1.480(3)	Ru	N1	C5	107.4(2)	O18	C10	C9	118.9(2)
C2	C3	1.512(4)	Ru	N1	C7	105.3(2)	N4	C11	C12	116.2(2)
C5	C6	1.510(4)	C2	N1	C5	111.2(3)	O19	C12	O20	125.3(3)
C7	C8	1.527(4)	C2	N1	C7	114.0(2)	O19	C12	C11	125.6(3)
C9	C10	1.515(3)	C5	N1	C7	111.0(2)	O20	C12	C11	109.0(2)
C11	C12	1.513(4)								

Numbers in parentheses are estimated standard deviations in the least significant digits

while in the latter the contraction is unequal and large for one carrying the hydroxyl group. This may be due to the involvement of the free hydroxyl group in H-bonding. The uncoordinated acetate group exists in the non-protonated form and has two distinct values for the C—O bonds, —C=O (1.207(4) Å) and —C—OH (1.312(4) Å). While two of the glycinate rings (R<sub>1</sub>) Ru-N1-C5-C6-O13 (r.m.s. = 0.119 Å) and (R<sub>2</sub>) Ru-N4-C9-C10-O17 (r.m.s. = 0.036 Å) are less strained, the other ring (G) Ru-N1-C7-C8-O15 is more strained (r.m.s. = 0.189 Å). Ring R<sub>2</sub> is planar within experimental errors and rings R<sub>1</sub> and G are envelopes. This pattern follows the predictions made by Weakleim and Hoard<sup>24</sup> on the basis of cumulative strain calculations. Ring (E) comprising the ethylenediamine chain has a halfchair conformation and atoms C2 and C3 are displaced more or less equally from 0.340(3) Å and 0.398(3) Å and are situated on the opposite sides of Ru-N1-N4 plane. The torsion angle N1-C2-C3-N4 of -57.7 (3) Å lies within the values found for the ethylenediamine group in other EDTA complexes<sup>14,20,25-28</sup>. The

acetate groups C5-C6-O13-O14, C7-C8-O15-O16, C9-C10-O17-O18 and C11-C12-O19-O20 are planar with the maximum deviations of 0.014(3) Å, 0.019(3) Å, 0.001(3) Å and 0.012(3) Å, respectively.

The Ru-O21 distance of 2.127(3) Å is distinctly longer than those of Ru-O13, Ru-O15 and Ru-O17 ( $\approx 30\sigma$ ) and this shows that the Ru-OH<sub>2</sub> bond is quite labile. Elongation of this bond can be attributed to an elaborate inter-molecular H-bonding scheme. The ruthenium and rhodium complexes are isomorphous with those of iron, chromium and gallium<sup>25</sup>. However, a comparison of our results with those of the above systems is not possible, as detailed structure of these on the basis of refined structures are not available. At high pH, the iron complex becomes heptadentate, with EDTA acting as a hexadentate ligand while the seventh position is occupied by water<sup>29</sup>.

#### Hydrogen bonding and crystal packing

A view of the molecular packing is shown in Figure 2. Table 4 lists the short intermolecular contacts below 3.4 Å. The hydroxyl oxygen O20 donates its

hydrogen H201 to atom O17 to form a strong inter-molecular O20-H201-O17 H-bond. The carboxyl oxygen O18 accepts the hydrogen H211 of water inter-molecularly in the formation of strong O21-H211-O18 H-bond. Both O20-H201-O17 and O21-H211-O18 bonds run parallel to the a-axis. Water molecule O21 donates its hydrogen H212 to O16 to form a weak inter-molecular H-bond. Though there are short intramolecular contacts between O21 and O13 (2.943 Å) and O21 and O14 (2.819 Å), these are not considered as H-bonds because of the small values associated with H-bonding angle (O21-H212-O13 = 106.4°, O21-H212-O14 = 112.1°). The structure is held in three-dimensional space by these hydrogen bonds.

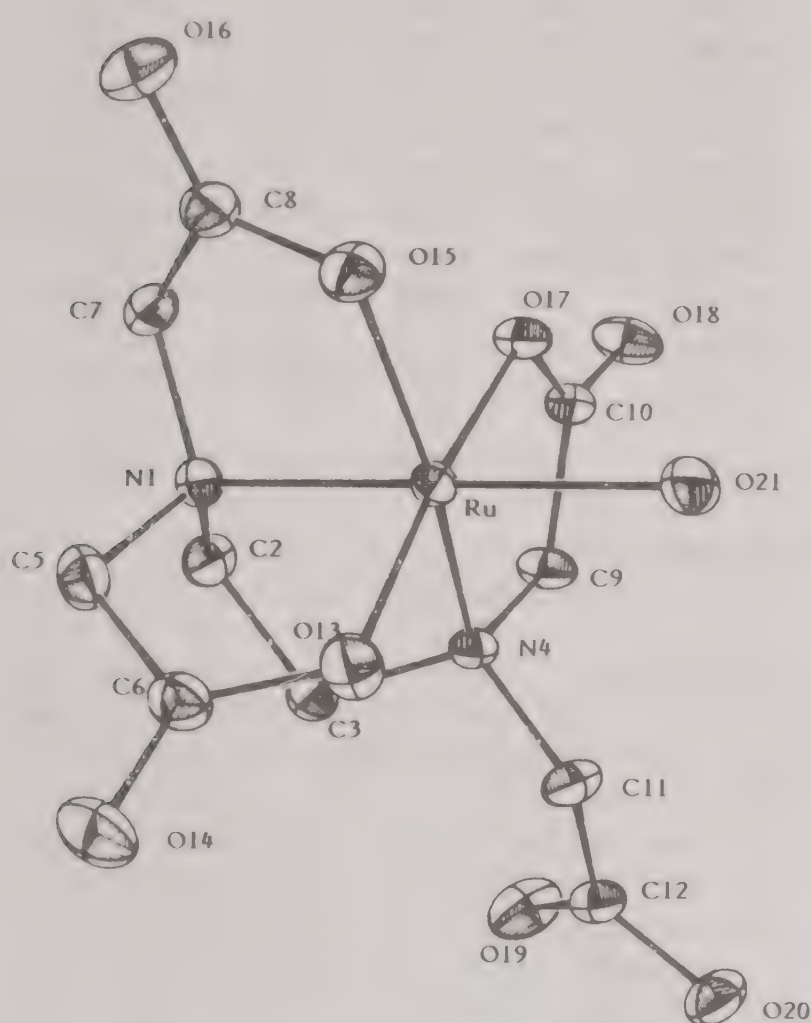


Fig. 1—The perspective view of complex [Ru(edta-H)H<sub>2</sub>O] with the numbering of atoms

An important structural feature of this complex is the marked difference in the Ru—OH<sub>2</sub> bond distance which reflects its extraordinary lability towards sub-

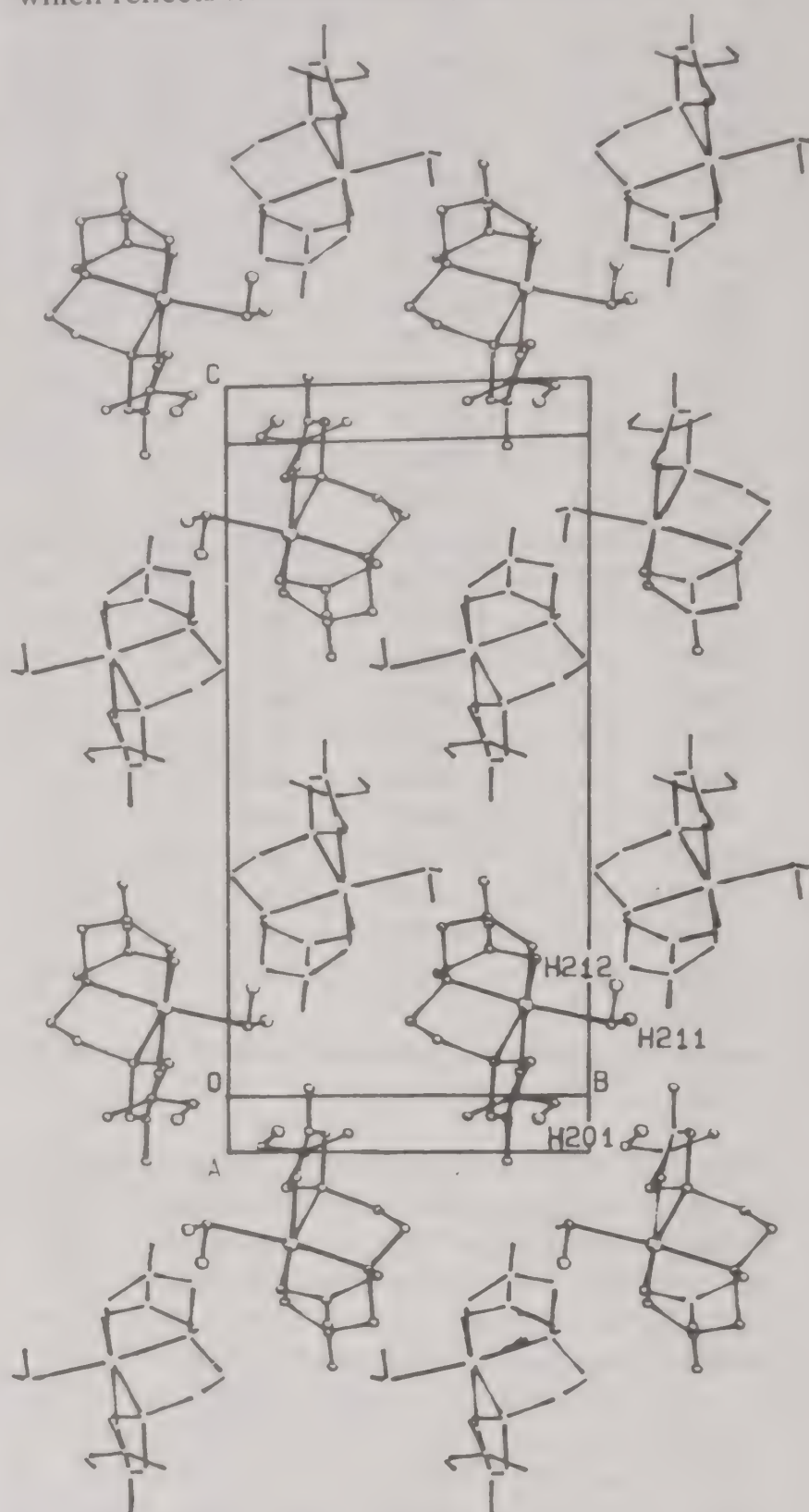


Fig. 2—Packing of molecules in the complex [Ru(edta-H)H<sub>2</sub>O]

Table 4—Geometry of hydrogen bonding in complex 1

Atom 1	Atom 2	Atom 3	1-3	1-2	2-3	1-2-3	Symmetry of 1	Symmetry of 2
O20	H201	O17	2.708	0.877	1.877	157.92	x,y,z	1+x,y,z
O21	H211	O18	2.693	0.920	1.802	162.59	x,y,z	-x, 1/2+y, 1/2-z
O21	H212	O16	3.149	1.152	2.329	121.28	x,y,z	-x, 2-y, -z

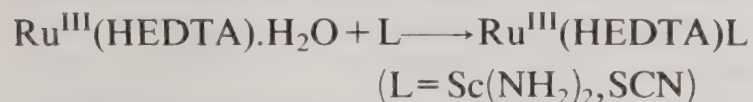
Bond lengths in angstroms and bond angles in degrees

Table 5—Summary of rate constants for the reaction  
[Ru<sup>III</sup>Y.H<sub>2</sub>O] + L → Ru<sup>III</sup>YL + H<sub>2</sub>O

L	Complex	M <sup>-1</sup> s <sup>-1</sup>	Ref.
SC(NH <sub>2</sub> ) <sub>2</sub>	Ru(edta)H <sub>2</sub> O <sup>a</sup>	2970 ± 50	7
	Ru(hedtra)H <sub>2</sub> O <sup>b</sup>	22.6 ± 1.0	36
	Ru(Medtra)H <sub>2</sub> O <sup>c</sup>	2.34 ± 0.1	37
SCN <sup>-</sup>	Ru(edta)H <sub>2</sub> O <sup>a</sup>	270 ± 27	7
	Ru(hedtra)H <sub>2</sub> O <sup>b</sup>	6.8 ± 0.3	36
	Ru(Medtra)H <sub>2</sub> O <sup>c</sup>	0.28 ± 0.02	37

<sup>a</sup>pH = 5 ± 0.1; <sup>b</sup>pH = 3 ± 0.1; <sup>c</sup>pH = 2.5 ± 0.1

stitution. The measured Ru—OH<sub>2</sub> distance of 2.127(3) Å is a normal Ru—OH<sub>2</sub> bond, which is close to the value reported<sup>30</sup> in Ru(bis(2-(2-pyridyl)ethyl (2-hydroxy-2-(pyridyl) ethylamine).H<sub>2</sub>O (2.115(3) Å) and in [H<sub>2</sub>O(bipy)<sub>2</sub>Ru<sup>III</sup>].H<sub>2</sub>O (2.136 Å)<sup>31</sup>, but significantly larger than distances observed in [Ru(H<sub>2</sub>O)<sub>6</sub>]<sup>3+</sup> (2.016 Å–2.037 Å) and in *trans*-[Ru<sup>III</sup>(bipy)<sub>2</sub>(OH)(H<sub>2</sub>O)]<sup>2+</sup> (2.007 Å)<sup>33</sup>. Table 5 lists the substitution rate constants for the reaction:



The water exchange rate constant<sup>6</sup> for [Ru(H<sub>2</sub>O)<sub>6</sub>]<sup>3+</sup> is  $3.5 \pm 3 \times 10^{-6} \text{ sec}^{-1}$ , whereas the substitution rate<sup>7–9</sup> for [Ru(HEDTA)(H<sub>2</sub>O)] lies in the range  $10 < k < 10^{-4} \text{ M}^{-1} \text{ sec}^{-1}$ , about 5 to 7 order of magnitude higher than the water exchange rate constant. Similarly substitution rate constant of  $5 \times 10^{-5} \text{ M}^{-1} \text{ sec}^{-1}$  was estimated<sup>34</sup> for the formation of [Ru(H<sub>2</sub>O)<sub>5</sub>Cl]<sup>2+</sup> from [Ru(H<sub>2</sub>O)<sub>6</sub>]<sup>3+</sup> and Cl<sup>-</sup> ion at 25°, which is close to the water exchange rate of [Ru(H<sub>2</sub>O)<sub>6</sub>]<sup>3+</sup>, but much lower than the substitution rate of [Ru(HEDTA)(H<sub>2</sub>O)]. A rate constant of  $4.7 \times 10^{-4} \text{ M}^{-1} \text{ sec}^{-1}$  at 35° has been reported<sup>35</sup> for the Cl<sup>-</sup> anation of [Ru(NH<sub>3</sub>)<sub>5</sub>(H<sub>2</sub>O)]<sup>3+</sup>, while that for reaction with pyrazine is  $4 \times 10^{-6} \text{ M}^{-1} \text{ sec}^{-1}$  at 25°.

On comparing the substitution rate constants for other aminopolycarboxylic complexes of Ru(III) with the same incoming ligands (Table 5), one can see that [Ru(HEDTA)(H<sub>2</sub>O)] is at least 1 to 2 order of magnitude more than the other complexes of similar structure. An inspection of the molecular structure of the aquo complex may provide a clue to its extraordinary lability. The water molecule, which is associated with the elongated Ru—O21 bond lies *trans* to N1 and the geometry of the EDTA moiety around Ru (Fig. 1) is such that it lies in an exposed position, which makes the accessibility of the incoming ligands easy. The *cis* angles involving O21 have a range of

86.64° to 97.74° with an average of 92.70°. It is, therefore, reasonable to assume that in [Ru(HEDTA)(H<sub>2</sub>O)] the coordinated water molecules is in an exposed position and makes inter-molecular H—bond contacts with O17 and O18 of the coordinated carboxylate group. This facilitates the approach of the incoming ligands by an associative manner and the extreme lability of the coordinated water molecule.

## References

- 1 Taqui Khan M M, Siddiqui M R H, Hussain A & Moiz M A, *Inorg Chem*, 25 (1986) 2760.
- 2 Taqui Khan M M, Samad S A, Siddiqui M R H & Shririn Z, *J mol Cat*, 54 (1990) 81.
- 3 Taqui Khan M M, Halligudi S B & Abdi S H R, *J mol Cat*, 44 (1989) 179.
- 4 Taqui Khan M M, Halligudi S B & Abdi S H R, *J mol Cat*, 45 (1989) 215.
- 5 Taube H, *Comments Inorg Chem*, 1 (1981) 17 and references cited therein.
- 6 Rapaport I, Helm L, Merback A E, Bernhard P & Ludi A, *Inorg Chem*, 27 (1988) 873.
- 7 Bajaj H C & Van Eldik R, *Inorg Chem*, 27 (1988) 4052.
- 8 Taqui Khan M M & Naik R M, *Polyhedron*, 8 (1989) 463.
- 9 Matsubara T & Creutz C, *Inorg Chem*, 18 (1979) 1956.
- 10 Diamantis A A & Dubrawski J V, *Inorg Chem*, 20 (1981) 1142.
- 11 Anal: Found (Calc): C, 24.50 (23.96); H, 3.43 (3.79); N, 5.96 (5.75). IR: νCOOH = 1730 cm<sup>-1</sup>, νCOO = 1642 cm<sup>-1</sup>.
- 12 Anal: Found (Calc): C, 29.41 (29.39); H, 3.59 (3.67); N, 6.75 (6.86). IR: νCOOH = 1730 cm<sup>-1</sup>, νCOO = 1650 b cm<sup>-1</sup>, UV-vis = λ<sub>max</sub> (εM<sup>-1</sup>cm<sup>-1</sup>) = 350 (sh) (680 ± 30), 280 (2800 ± 70).
- 13 North A C T, Phillips D C & Mathews F S, *Acta Crystallogr*, A24 (1968) 351.
- 14 Lin G H Y, Liggett J D & Wing R M, *Acta Crystallogr*, B29 (1973) 1023.
- 15 Dunitz J D & Seiler P, *Acta Crystallogr*, B29 (1973) 589.
- 16 *International tables for crystallography*, Vol 4 (D. Leidel, Dordrecht, Holland), 1983.
- 17 Stewart R F, Davidson E R & Simpson W T, *J chem Phys*, 42 (1965) 3175.
- 18 *SDP structure determination package* (Enraf Nonius Ltd, Delft, Holland) 1986.
- 19 Johnson C K (1976), *ORTEP II*, Oak Ridge National Laboratories, Tennessee, USA.
- 20 Taqui Khan M M, Chatterjee D, Merchant R R, Paul P, Abdi S H R, Srinivas D, Moiz M A, Siddiqui M R H, Bhadbhade M M & Venkatasubramanian K, *Inorg Chem* (accepted).
- 21 Taqui Khan M M, Chatterjee D, Siddiqui M R H, Bajaj H C, Bhatt S D & Venkatasubramanian K, *Inorg Chem* (communicated).
- 22 Taqui Khan M M, Venkatasubramanian K & Hussain A, *Acta Crystallogr*, (communicated).
- 23 Taqui Khan M M, Venkatasubramanian K, Shririn Z & Bhadbhade M M, *J chem Soc Dalton Trans* (accepted).
- 24 Weakleim H A & Hoard J L, *J Am chem Soc*, 81 (1959) 549.
- 25 Hoard J L, Kennard C H L & Smith G S, *Inorg Chem*, 2 (1963) 1316.

- 26 Stephens F S, *J chem Soc (A)*, (1969) 1723.  
27 Smith G S & Hoard J L, *J Am chem Soc*, 81 (1959) 556.  
28 Sergienkos V S, Dikareva L N, Porai Koshits H A, Sadikov G G K, Cheltsov P A, *Koord Khim*, 5 (1979) 920.  
29 (a) Hamor M J, Hamor T A & Hoard J L, *Inorg Chem*, 3 (1964) 34.  
(b) Mizuta T, Yamamoto T, Miyoshi K & Kushi Y, *Inorg chim Acta*, 175 (1990) 121.  
30 Che C M, Yam V W W & Mak T C W, *J Am chem Soc*, 112 (1990) 2284.  
31 Gilbert J A, Eggleston D S, Murphy W R Jr, Gesolonitz D A, Gersten S W, Hodgson D J & Meyer T J, *J Am chem Soc*, 107 (1985) 3885.  
32 Bernhard P, Burgi H B, Slauser J, Lehmann H & Ludi A, *Inorg Chem*, 21 (1982) 3936.  
33 Durham W, Wilson S R, Hodgson D J & Meyer T J, *J Am chem Soc*, 102 (1980) 660.  
34 Kallen T W & Earley J E, *Inorg Chem*, 10 (1971) 1149.  
35 Broomhead J A, Bosolo F & Pearson R G, *Inorg Chem*, 3 (1964) 826.  
36 Bajaj H C & Van Eldik R, *Inorg Chem*, 28 (1989) 1980.  
37 Bajaj H C & Van Eldik R, *Inorg Chem*, 29 (1990) 2855.

## Sodium ruthenate catalysis in the oxidation of substituted benzyl alcohols by hexacyanoferrate(III)

T Venkata Lalitha, M Prasad Rao & B Sethuram\*

Department of Chemistry, Osmania University, Hyderabad 500 007

Received 5 September 1991; revised and accepted 5 February 1992

Ru(VI) catalysis in the oxidation of benzyl alcohol and its monosubstituted analogues by hexacyanoferrate(III) [Fe(III)] in *t*-butanol (25%, v/v) in alkaline medium has been studied. The reaction is first order in [Ru(VI)], fractional order in [alcohol] and zero order each in [Fe(III)], [base] and [*t*-butanol]. The primary kinetic isotopic effect ( $k_H/k_D$ ) is 4.12 at 298 K. The solvent isotopic effect ( $k_{H_2O}/k_{D_2O}$ ) is 0.948 at 298 K. The reaction exhibits a reaction constant  $\rho$  of  $-0.540$  at 298 K. A mechanism involving the transfer of a hydride ion to the oxidant is suggested. The activation enthalpies and entropies are linearly related.

It is now recognised that sodium ruthenate catalysed oxidation of primary and secondary alcohols in aqueous alkaline media proceeds via the formation of a 1:1 Ru(VI)-substrate complex<sup>1</sup>, which unimolecularly dissociates in the rate determining step to give the corresponding acids or ketones. The role of oxidant appears to be one of regenerating the catalyst in the fast step.

Lee *et al.*<sup>2</sup> and Schroder *et al.*<sup>3</sup> have observed in their direct oxidation studies that Ru(VI) oxidises various organic substrates to give products in quantitative yields. But, so far no systematic study has been made to establish the nature of Ru(VI) when used directly as an oxidant or as a catalyst and the mode of electron transfer during the oxidation process. This paper reports a detailed study of the kinetics of oxidation of mono substituted benzyl alcohols by Fe(III) in aqueous alkaline medium in the presence of trace amounts of Ru(VI).

### Materials and Methods

All the benzyl alcohols (BA) were purified either by recrystallization or distillation. Sodium ruthenate was prepared by the reported procedure<sup>4</sup>. Iron(III) (Loba chemical) *t*-butanol (Baker-analytical) and all the other chemicals were of A.R. grade. Water used for reactions was doubly distilled.  $\alpha$ ,  $\alpha'$ -Dideuterobenzyl alcohol was prepared by the standard method<sup>5</sup> and its purity was checked by PMR. Aqueous solutions of benzyl alcohols were prepared in *t*-butanol (25%, v/v) due

to solubility problems. Deuterium oxide was obtained from BARC, Bombay, India.

The reaction was initiated by the addition of requisite quantities of sodium ruthenate to a mixture containing substrate, *t*-butanol and sodium hydroxide after thermally equilibrating the two solutions separately at the desired temperature ( $\pm 0.1^\circ\text{C}$ ) for atleast 30 min. The reaction was followed by noting the absorbance of Fe(III) at 420 nm at regular intervals of time using a Hitachi UV 1000 spectrophotometer. For studying the solvent isotope effect, 96% deuterium oxide was used.

Under the conditions of [oxidant]  $\gg$  [substrate] in 25% *t*-butanol, the amount of oxidant consumed per mole of the substrate was determined by estimating the unreacted oxidant after the reaction was allowed to go to completion. The values of  $\Delta[\text{Fe(III)}]/\Delta[\text{S}]$  under different concentration ranges revealed a 2:1 stoichiometry (oxidant:substrate).

Benzoic acid was identified as the product of oxidation of benzyl alcohol from its m.p. ( $120^\circ\text{C}$ ). Its derivative benzamide was prepared and confirmed by comparison with authentic sample by GC analysis using a Datacat instrument (conditions for GC being Apizon-KOH ( $6'' \times 1/8''$ ) column, column temperature =  $200^\circ\text{C}$ , injection and detection temperature  $\approx 175^\circ$ , detector -TCD, carrier gas-nitrogen, pressure -  $2.5 \text{ kg cm}^{-2}$ , flow rate  $40 \text{ CC min}^{-1}$ ). Similar procedure was adopted for various substituted benzyl alcohols.

Table 1 – Effect of varying  $[\text{Fe(III)}]$ ,  $[\text{Ru(VI)}]$  and  $[\text{BA}]$  in Ru(VI) catalysed oxidation of benzyl alcohol by Fe(III) $t$ -butanol = 25% (v/v);  $[\text{HO}^-] = 5.00 \times 10^{-2} \text{ mol dm}^{-3}$ ; temp. = 298 K

$10^3 [\text{Fe(III)}]$ ( $\text{mol dm}^{-3}$ )	$10^6 [\text{Ru(VI)}]$ ( $\text{mol dm}^{-3}$ )	$10^3 [\text{BA}]$ ( $\text{mol dm}^{-3}$ )	$10^7 k_0$ ( $\text{mol dm}^{-3} \text{ s}^{-1}$ )	$k_0/[\text{Ru(VI)}]$ ( $\text{s}^{-1}$ )
0.200	4.35	1.33	5.52	—
0.400	4.35	1.33	5.73	—
0.938	4.35	1.33	5.89	—
2.00	4.35	1.33	6.02	—
1.00	0.272	1.33	0.392	0.144
1.00	0.543	1.33	0.691	0.127
1.00	1.09	1.33	1.42	0.130
1.00	2.17	1.33	2.86	0.132
1.00	4.35	1.33	5.52	0.127
1.00	1.09	0.366	0.523	—
1.00	1.09	0.733	0.857	—
1.00	1.09	1.33	1.40	—
1.00	1.09	2.50	2.30	—
1.00	1.09	5.00	3.78	—

## Results and Discussion

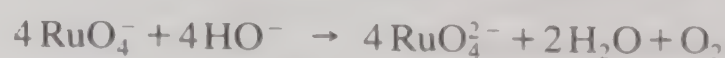
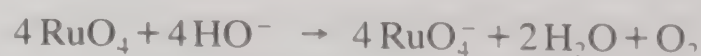
Tertiary alcohols and compounds with double bonds were found to be unreactive towards Ru(VI) under the experimental conditions employed. The trends in the results were same for all the substituted benzyl alcohols and hence only those of benzyl alcohol are being reported here as a representative example.

Concentration versus time plots were linear indicating zero order dependence of rate on  $[\text{Fe(III)}]$ . The zero order rate constants ( $k_0$ ), for different  $[\text{Fe(III)}]$ ,  $[\text{Ru(VI)}]$  and  $[\text{benzyl alcohol}]$  are listed in Table 1. The results show that the order in  $[\text{Ru(VI)}]$  is one and that in  $[\text{benzyl alcohol}]$  is less than one. The effect of  $[\text{HO}^-]$  and neutral salts like  $\text{NaClO}_4$  was negligible and the variation in dielectric constant (which was changed by varying the percentage of  $t$ -butanol) had no effect on the rate of the reaction.

The rate of oxidation of  $\alpha$ ,  $\alpha'$ -dideutero benzyl alcohol and benzyl alcohol at 303 K were  $1.27 \times 10^{-7}$  and  $5.23 \times 10^{-7} \text{ mol dm}^{-3} \text{ s}^{-1}$  respectively. The kinetic isotopic effect  $k_H/k_D$  was thus 4.12. The solvent isotopic effect was observed to be 0.948.

The oxidation of benzyl alcohol under nitrogen atmosphere failed to induce polymerization of acrylonitrile (AN). Also the rate of oxidation did not change in the presence of AN.

It is well known that tetraoxy anions  $\text{MO}_4^{x-}$  of 3d row elements do not expand their coordination shell in alkaline solutions. However, such expansions do occur to some extent with 4d and 5d elements<sup>6,7</sup>. Osmium being a 5d element,  $\text{OsO}_4$  solution in alkaline medium has been shown to contain mono and dihydroxy species viz.,  $[\text{OsO}_4(\text{OH})\text{H}_2\text{O}]^-$  and  $[\text{OsO}_4(\text{OH})_2]^{2-}$ . In the case of ruthenium, only the lower oxidation states have been shown to form complexes and exist in hydrated form<sup>8</sup>. On the other hand, the higher oxidation states have shown no tendency to form complexes and are also not solvated<sup>9</sup>. Infrared and Raman spectral studies<sup>10</sup> also support this view.  $\text{RuO}_4$  in alkaline solutions is reduced by hydroxide first to perruthenate ion, which later gets further reduced to ruthenate ion at higher concentrations of  $\text{HO}^-$  as shown below.



The UV-vis spectrum of Ru(VI) showed no appreciable change at different  $[\text{HO}^-]$  and also variation in  $[\text{HO}^-]$  had negligible effect on the reaction rate. Hence, under the kinetic conditions employed Ru(VI) appears to exist as tetrahedral  $\text{RuO}_4^{2-}$  ion.

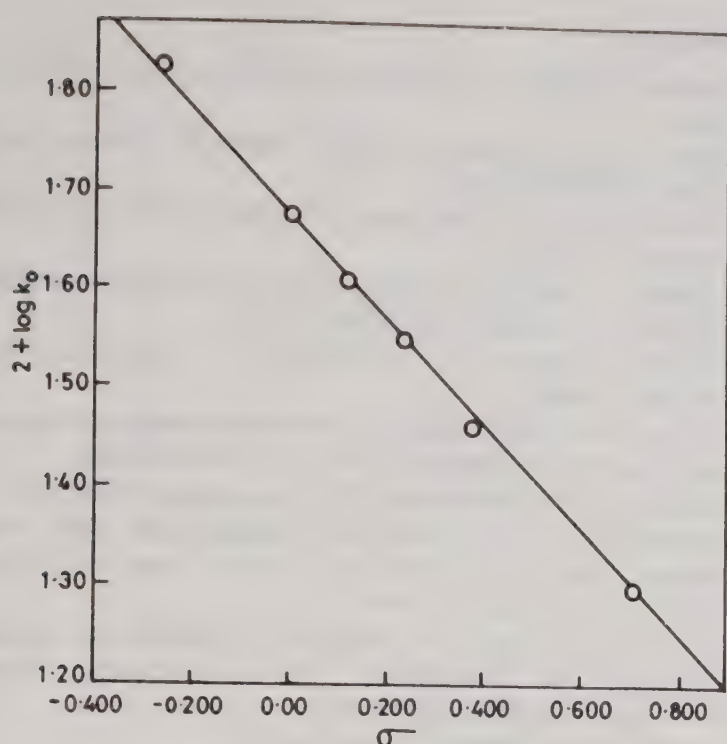


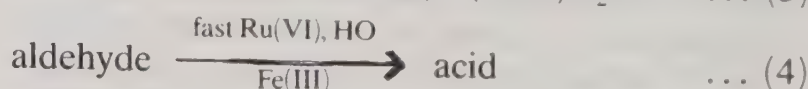
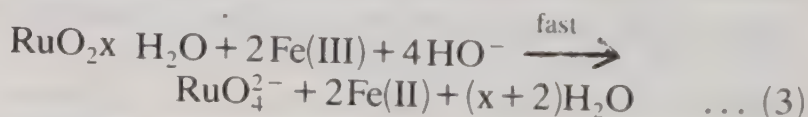
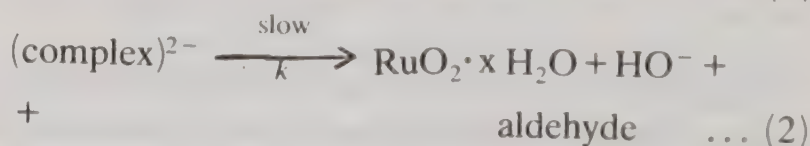
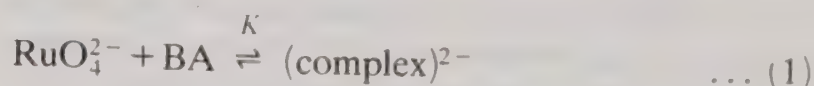
Fig. 1 – Plot of  $\log k$  versus  $\sigma$   $\{[\text{Ru(VI)}] = 1.086 \times 10^{-6} \text{ mol dm}^{-3}$ ;  $[\text{Fe(III)}] = 1.00 \times 10^{-3} \text{ mol dm}^{-3}$ ;  $[\text{NaOH}] = 5.00 \times 10^{-2} \text{ mol dm}^{-3}$ ; *t*-butanol = 25%; temp. = 298 K}

Table 2 – Thermodynamic and activation parameters for Ru(VI) catalysed oxidation of benzyl alcohols by Fe(III) at 298 K.

Compound	$E_a$ (kJ mol <sup>-1</sup> )	$\Delta G^\ddagger$ (kJ mol <sup>-1</sup> )	$\Delta H^\ddagger$ (kJ mol <sup>-1</sup> )	$-\Delta S^\ddagger$ (J mol <sup>-1</sup> )
<i>p</i> -OMe	44.3	74.0	41.8	108.0
H	49.9	74.8	47.4	91.9
<i>m</i> -OMe	52.9	75.2	50.4	83.3
<i>p</i> -Cl	55.4	75.6	53.0	75.9
<i>p</i> -Br	59.3	75.6	56.8	63.2
<i>m</i> -Cl	60.3	76.0	57.8	61.3
<i>m</i> -NO <sub>2</sub>	64.8	76.9	62.3	49.3

Benzyl alcohols under these conditions might be assumed to exist predominantly in neutral form. From fractional order dependence of rate on [BA] and also from the linear double reciprocal plot of  $k_0$  versus [BA], one can say a 1:1 complex between Ru(VI) and BA (ion-neutral type) is formed in the pre-equilibrium step. The complex so formed in the first step is assumed to undergo slow disproportionation giving the reduced form of ruthenium i.e., Ru(IV) as hydrated ruthenium dioxide (hydrated since, ruthenate cannot be regenerated from anhydrous ruthenium dioxide<sup>11,12</sup>) and the corresponding aldehyde. Hydrated ruthenium dioxide thus produced is assumed to get oxidised back to Ru(VI) by alkaline Fe(III) in a fast step since the order in [Fe(III)] is zero. Independent experiments show that the oxidation of aldehyde is very fast under experimental conditions.

Therefore, aldehyde thus produced (step-2 of Scheme-1), probably gets oxidised immediately to its corresponding acid (step-4). Product analysis also confirms the production of acid.



Scheme 1

Rate law (5) obtained from Scheme 1

$$-\frac{d[\text{Fe(III)}]}{dt} = k_0 = \frac{kK[\text{Ru(VI)}][\text{BA}]}{1 + K[\text{BA}]} \quad \dots (5)$$

which explains well all the observed results. The reciprocal of Eq. (5) gives Eq. (6)

$$1/k_0 = \frac{1}{Kk[\text{Ru(VI)}][\text{BA}]} + \frac{1}{k[\text{Ru(VI)}]} \quad \dots (6)$$

which suggests that a plot of  $1/k_0$  versus  $1/[\text{BA}]$  should be linear with an intercept on Y-axis, from the slope and intercept of which  $K$  and  $k$  can be calculated.

The rates of oxidation of various substituted benzyl alcohols are well correlated by a Hammett's plot with a reaction constant  $\rho = -0.540$  ( $\gamma = 0.999$ ) at 25°C (Fig. 1). The negative value points to an electron deficient carbon centre in the transition state. The magnitude of the reaction constant was found to decrease with temperature. For example, under the conditions  $[\text{Ru(IV)}] = 1.080 \times 10^{-6} \text{ mol dm}^{-3}$ ,  $[\text{BA}] = 5.0 \times 10^{-3} \text{ mol dm}^{-3}$ ,  $[\text{OH}^-] = 5.0 \times 10^{-2} \text{ mol dm}^{-3}$ ,  $[\text{Fe(III)}] = 1.0 \times 10^{-3} \text{ mol dm}^{-3}$ ,  $-\rho$  values are 0.540, 0.460, 0.409 and 0.356 at 298, 303, 308 and 313 K respectively.

The primary kinetic isotopic effect ( $k_H/k_D$ ) indicates the cleavage of the  $\alpha\text{-C-H}$  bond in the alcohol.

In order to establish the mechanism of the reaction, the manner of electron transfer has to be considered. In view of the failure to induce polymerization of acrylonitrile in nitrogen atmosphere, a hydrogen abstraction mechanism is considered unlikely. The negative value for the Hammett's reaction constant although not very high, is con-

sidered sufficient to suggest a hydride ion transfer mechanism especially in view of the fact that there is no reaction with *t*-butanol and the kinetic isotope effect is sufficiently high.

It is unlikely that the removal of the hydroxylic proton is synchronous with the hydride ion transfer in view of the absence of solvent isotopic effect and the finite value of the reaction constant.

From the slope and intercept values, the formation constant  $K$  and disproportionation constant  $k$  values have been determined at different temperatures. The activation parameters  $E_a$ ,  $\Delta H^\ddagger$ ,  $\Delta S^\ddagger$  and  $\Delta G^\ddagger$  calculated using  $k$  values at different temperatures are listed in Table 2. The constancy in  $\Delta G^\ddagger$  values suggest that a similar mechanism is operative with all the substrates studied. The activation enthalpies and entropies studied are linearly related ( $\gamma=0.998$ ). The correlation was tested and found valid by applying Exner's criterion<sup>13,14</sup> also. The isokinetic temperature thus computed was 350 K which is well above the experimental range of temperature suggesting that the reaction is enthalpy-controlled.

## References

- 1 Venkata Lalitha T & Sethuram B, *Trans metal Chem*, (in press).
- 2 Donald G Lee, David T Hall & James H Cleland; *Can J Chem*, 50 (1972) 3741.
- 3 Martin Schroder & William P Griffith, *J chem Soc Chem Comm* (1979) 58.
- 4 Donald G Lee, Udo A Spitzer, James Cleland & Merele E Olson, *Can J Chem*, 54 (1986) 2124.
- 5 Tamida H, Davies G T & Bunnett J F, *J Am chem Soc*, 84 (1962) 1606.
- 6 Cotton F A & Wilikinson G, *Advanced inorganic chemistry*, John Wiley & Sons N Y, 5th edn (1988) 880-882.
- 7 Carrington A & Symons M C R, *J chem Soc*, (1960) 284.
- 8 Sidwick N V, *The chemical elements and their compounds*, Vol. II (Oxford Univ. Press, London & New York), (1950) pp. 1455-1489.
- 9 Lee D G & Van Den Engh M, 'Oxidation in organic chemistry', in Trahanovsky Edition, (Academic Press, New York) Vol. 5B (1973) 180.
- 10 Griffith W P, *J chem Soc*, (1966) 1467.
- 11 Beynon P J, Collins P M & Overend W G, *Carbohydr Res*, 6 (1968) 431.
- 12 Parikh V M & Jones J K N, *Can J Chem*, 43 (1965) 3452.
- 13 Peterson R C, *J org Chem*, 29 (1964) 3133.
- 14 Exner O, *Coll Czech Chem Comm*, 29 (1964) 1094.

**Papers presented in the National Conference on  
Synthetic Membranes & Their Applications  
held during 29-31 November 1991  
at CSMCRI, Bhavnagar**



## Electrochemical characterization of membranes

Kehar Singh\* & A K Tiwari

Chemistry Department, Gorakhpur University, Gorakhpur 273 009

The determination of electrochemical characteristics of membranes on the basis of membrane potential measurements and electrochemical impedance studies has been described. Cellulose acetate membrane has been used alongwith sodium chloride and magnesium chloride solutions to investigate variation of transport number, permselectivity and fixed charge density with concentration and pH. Alteration in these membrane characteristics in the presence of lecithin has also been investigated. Dependence of impedance of Dowex-50 membrane with frequency has been studied over a wide range using solution of sodium chloride with and without cholesterol with the object of estimation of membrane conductance and capacitance; and to examine their variation with surfactant concentration. The results indicate progressive accumulation of surfactant molecules in the membrane solution interfacial region which is significantly altered with the electrical potential to which the membrane is subjected.

Cellulose acetate membranes exhibit weak cation selectivity in aqueous electrolyte solutions<sup>1</sup> because of dissociation of carboxyl groups<sup>2</sup> and become almost passive at higher concentrations and lower pH due to the suppression of this dissociation<sup>3,4</sup>. Present investigation shows that cellulose acetate membrane behaves as anion selective membrane when in contact with magnesium chloride solution because of  $Mg^{++}$  ion absorption. Alterations in the characteristics of the membrane when it supports lecithin liquid membrane have also been investigated. Lecithin liquid membrane formation was detected by membrane resistivity measurements<sup>5</sup>.

Electrochemical impedance spectroscopy is emerging as an attractive technique for *in situ* characterization of membranes. During impedance measurements the system is subjected to minimal perturbation. We have studied variation of impedance of Dowex-50 membrane with frequency over a wide range using solution of sodium chloride with and without cholesterol. The data have been used to estimate membrane conductance and capacitance; and to examine their variation with surfactant concentration.

### Materials and Methods

The preparation of the Dowex-50 and cellulose acetate membranes were carried out as follows:

For the formation of Dowex-50 membrane, a desired quantity of a Dowex-50 (J.T. Baker, Phillipsburg, N.J.) was dispersed in 20% solution of Kynar (polyvinylidene fluoride) in N,N-dimethyl acetamide (Riedel) by constant stirring for 3 to 4

hr until a thick slurry was obtained. It was spread on a clean, dried glass plate. The glass plate was kept in an electric oven at 80-90°C for about half an hour to remove the solvent. The plate was then immersed in distilled water to detach the membrane. Thereafter, the membrane was kept pressed between the folds of a filter paper to avoid wrinkles.

A similar method was used for the formation of the cellulose acetate membrane. A binary casting solution prepared by dissolving 2 gm cellulose acetate (BDH) in acetone (10 ml) was spread on a glass plate and allowed to dry at about 30°C. It was then immersed in distilled water to detach the membrane.

A piece of the membrane under investigation was fixed in a glass cell. The membrane was equilibrated with 1 mol dm<sup>-3</sup> solution of magnesium chloride and kept overnight in the experimental solution.

Lecithin (L- $\alpha$ -phosphatidyl choline, Sigma) was used in the present investigation without further purification. It was dispersed in water in the usual manner. For the determination of critical micelle concentration, the surface tension of lecithin solutions of different concentration was determined using the drop weight method. The critical micelle concentration was found to be  $25 \times 10^{-5}$  mol dm<sup>-3</sup>.

Liquid membrane formation detected by resistivity measurements was found to occur at about  $30 \times 10^{-5}$  mol dm<sup>-3</sup> of lecithin. Liquid membrane formation for cholesterol was found to occur at about  $15 \times 10^{-9}$  mol dm<sup>-3</sup>.

Membrane potential measurements using magnesium chloride solutions of known unequal concentrations containing lecithin were measured as reported elsewhere<sup>8</sup>.

For adsorption studies, a known amount of cellulose acetate (0.5 gm) was kept in magnesium chloride solution (0.05 mol dm<sup>-3</sup>). The system was kept stirred, and the change in conductance of the magnesium chloride solution with time was followed, the conductance attained a time-invariant limiting value. Change in concentration due to Mg<sup>++</sup> ion adsorption was estimated using previously obtained calibration curves. The Mg<sup>++</sup> ion adsorption was found to be 20.0 meq/g of dry cellulose acetate.

Experimental set up used for the purpose of impedance measurements already reported<sup>9</sup> is shown in Fig. 1. The model 378 Electrochemical impedance measurement system (EG & G Princeton Applied Research U.S.A.) consists of a potentiostat (Model 273 with a Model 276 Interface) and a lock-in-amplifier (Model 5208). It allows automatic data acquisition in the 10 hertz to 100 kilo hertz range when used in combination with IBM Personal Computer XT.

## Results and Discussion

When a completely non-selective membrane

separates aqueous magnesium chloride solutions of unequal concentration, it may be shown using thermodynamics principles that the liquid junction potential is given by

$$[(\Delta\phi)_{I=0}]_L = \left(\frac{3}{2}t_- - 0.5\right) \frac{RT}{F} \ln \frac{a_1}{a_2} \quad \dots (1)$$

Where  $a_1$  and  $a_2$  denote the activities of the magnesium chloride solutions, and  $t_-$  denotes the transport number of the anion. If the membrane is ideally selective then

$$[(\Delta\phi)_{I=0}]_{\text{ideal}} = 2.303 \frac{RT}{F} \log \frac{a_1}{a_2} \quad \dots (2)$$

Experimentally measured values of the membrane potential  $(\Delta\phi)_{I=0}$  are compared with theoretically estimated values obtained using Eqs (1) and (2) in Table 1. Mean activity coefficients needed for the purpose of computation of activities were obtained using ionic activity coefficients<sup>10</sup>.

The results presented in Table 1 clearly show that the cellulose acetate membrane is endowed with some selectivity. The membrane is anion selective, since the membrane potential is positive with respect to the higher concentration side which is taken as positive. Furthermore,  $(\Delta\phi)_{I=0}$  is always greater than  $[(\Delta\phi)_{I=0}]_L$  even when cellulose acetate supports the lecithin liquid membrane. This is possible only if the anion is accelerated, since  $t_- > t_+$  in the case of magnesium chloride. For a partially anion selective membrane, using the TMS approach<sup>11</sup>,  $(\Delta\phi)_{I=0}$  in the present case may be expressed as

$$(\Delta\phi)_{I=0} = \left(\frac{3}{2}\bar{t}_- - 0.5\right) \frac{RT}{F} \ln \frac{a_1}{a_2} \quad \dots (3)$$

$\bar{t}_-$  denotes transport number of the anion in the membrane phase.

The electrochemical characteristics of an ion exchange membrane may vary with concentration. The experimental data presented in Table 1 were

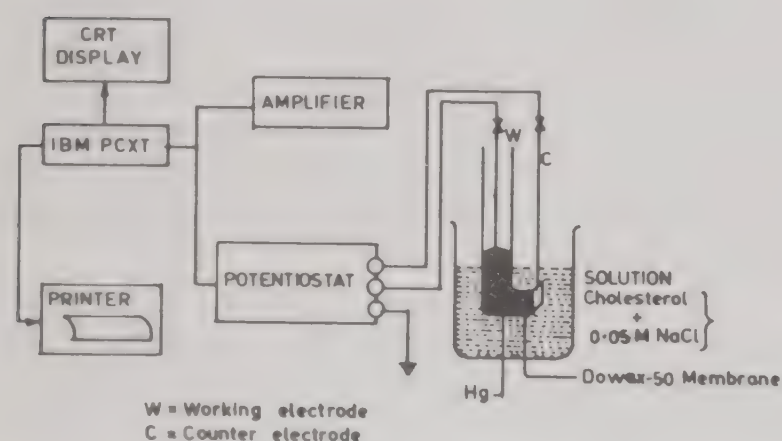


Fig. 1—Experimental set up for impedance spectroscopic studies

Table 1—Comparison of  $[(\Delta\phi)_{I=0}]_L$ ,  $[(\Delta\phi)_{I=0}]_{\text{ideal}}$  and  $(\Delta\phi)_{I=0}$  at constant mean concentration of MgCl<sub>2</sub> solution = 0.05 mol dm<sup>-3</sup> with and without lecithin

$C_1$ (mol dm <sup>-3</sup> )	$C_2$ (mol dm <sup>-3</sup> )	$[(\Delta\phi)_{I=0}]_{\text{ideal}}$ (mV)	$[(\Delta\phi)_{I=0}]_L$ (mV)	$(\Delta\phi)_{I=0}$	
				without lecithin	with lecithin
0.09	0.01	51.0	22.3	39.4	34.5
0.08	0.02	31.0	13.6	23.2	20.1
0.07	0.03	18.2	8.0	14.4	12.2
0.06	0.04	8.4	3.7	6.3	5.1
0.05	0.05	—	—	0.4	0.2

obtained at a constant mean concentration to obviate this alteration.

The results presented in Table 2 clearly show a significant variation in membrane potential with mean concentration when a cellulose acetate membrane is used alone or in conjunction with a lecithin liquid membrane. The membrane potential is lowered in both the cases when mean concentration is increased. This variation may be attributed to (i) increased adsorbability of  $Mg^{++}$  ion, (ii) reduction in swelling of the membrane matrix with increase in concentration and (iii) increase in membrane conductivity at higher mean concentration. Factor (i) is expected to enhance membrane selectivity, as a result of which observed membrane potential should increase with concentration; factor (ii) on the other hand will result in increasing membrane void volume due to lowering of matrix swelling at higher concentration. Increased membrane conductance will also contribute towards lowering of membrane potential. It appears that factor (ii) and (iii) together predominate, since a substantial decrease in membrane potential with increase in mean concentration has been observed. The  $\bar{t}$  values derived using Eq. (3) are presented in Table 2.

An examination of the results presented in Tables 1 and 2 shows that accumulation of lecithin molecules in the membrane solution interfacial region results in lowering of the membrane potential. Furthermore, the accumulated lecithin molecules interact with ions of magnesium chloride so as to make their migration less unequal.

A membrane in contact with and in a state of equilibration with an electrolyte may be described by an equivalent circuit analogous to that for a Randell cell. The resistance and capacitance combined in parallel provide alternative paths for the passage of current through the membrane. For this ideal circuit, frequency dependence of impedance,  $Z$ <sup>12,13</sup>,

$$Z = R_s + \frac{R_p - j(\omega R_p^2 C)}{1 + (\omega R_p C)^2} \quad \dots (4)$$

where

$R_s$  = Solution resistance;

$R_p$  = interfacial resistance

$\omega$  = angular frequency,  $j = \sqrt{-1}$

According to Eq. (4) at low frequency limit

$$Z = R_s + R_p \quad \dots (5)$$

and at high frequency limit

Table 2—Membrane potential data and  $\bar{t}_-$  values at different mean concentration,  $C$ , of  $MgCl_2$  without and with lecithin  $\Delta C = 0.04 \text{ mol dm}^{-3}$

$C$ ( $\text{mol dm}^{-3}$ )	$(\Delta\phi)_{t=0}$ (mV)		$\bar{t}_-$	
	without lecithin	with lecithin	without lecithin	with lecithin
0.04	19.4	16.5	0.859	0.780
0.06	11.2	9.3	0.835	0.750
0.08	9.1	7.2	0.822	0.733
0.01	6.7	5.1	0.813	0.699
0.12	4.6	3.5	0.742	0.644
0.14	3.0	2.9	0.652	0.640

Table 3—The parameters of the equivalent circuit

Concentration $\times 10^9$ ( $\text{mol dm}^{-3}$ )	$R_p$ ( $K\Omega$ )	$R_s$ ( $\Omega$ )	$C_{obs}$ (nF)	$C_{DL}$ (nF)	$C_{CHL}$ (nF)
0	1.65	51.00	1823	1823	0
10	4.77	51.00	209	1823	236
15	9.17	51.00	93	1823	97
20	10.18	51.00	87	1823	91
25	10.13	51.00	91	1823	97

Table 4— $R_p$  and  $C$  values obtained from Impedance Spectroscopic data obtained using different externally applied potentials. Solution composition = 0.05 mol  $\text{dm}^{-3}$  NaCl +  $25 \times 10^{-9}$  mol  $\text{dm}^{-3}$  cholesterol

Potential (volt)	$R_p$ ( $K\Omega$ )	$C^*$ (nF)
-1.0	6.82	95
-0.5	3.23	301
0	12.30	86
+0.5	4.73	230
1.0	3.10	397

\*estimated at  $\log \omega = 3.98 \text{ s}^{-1}$

$$Z = R_s \quad \dots (6)$$

The values of  $R_s$  and  $R_p$  can thus be obtained from the limiting value of impedance at high and low frequency limits.  $R_p$  and  $R_s$  values obtained using 0.05 mol  $\text{dm}^{-3}$  sodium chloride solution containing different concentrations of cholesterol are summarized in Table 3.

In the high frequency range, we get

$$Z_1 = \frac{1}{\omega C} \quad \dots (7)$$

Capacitance values derived using Eq. (7) at  $\log \omega = 3.98 \text{ s}^{-1}$  are also included in Table 4. The variation of  $R_p$  with cholesterol concentration in the solution shows progressive accumulation of cholesterol molecules in the membrane solution

interfacial region. It increases with cholesterol concentration and tends to become independent of concentration beyond  $20 \times 10^{-9} \text{ mol dm}^{-3}$ . This concentration is comparable with critical micelle concentration of cholesterol obtained on the basis of surface tension data. The impedance studies support the contention that for complete liquid membrane formation to take place, the concentration of amphiphilic molecules such as cholesterol should exceed its critical micelle concentration. The results given in Table 3 also reveal that the presence of cholesterol in sodium chloride solution results in substantial lowering of capacitance which tends to invariance when its concentration approaches  $\approx 20 \times 10^{-9} \text{ mol dm}^{-3}$ . The cholesterol molecules present in the interfacial region are preferentially oriented with their hydrophilic portion towards the bulk of the solution. The overall capacitance may thus be considered to be made up of two contributions (i) because of the electrical double layer while (ii) due to oriented cholesterol molecules. The capacitance of the composite system may thus be written in terms of these contribution as<sup>14</sup>

$$\frac{1}{C} = \frac{1}{C_{DL}} + \frac{1}{C_{CHL}} \quad \dots (8)$$

where

$C$  = observed capacitance,

$C_{DL}$  = double layer capacitance and

$C_{CHL}$  = capacitance due to cholesterol molecules.

Assuming that the electrical double layer contribution is not affected with progressive accumulation of cholesterol molecules,  $C_{CHL}$  may be estimated using Eq. (8). The values thus estimated are also included in Table 3 alongwith  $C_{DL}$  obtained in the absence of cholesterol. Impedance spectroscopic studies were also carried out by subjecting the membrane system to different initial electrical potential so as to investigate its effect on  $R_p$  and  $C$  values preferentially oriented

immobilized cholesterol molecule. The results are summarized in Table 3.  $R_p$  is seen to be maximum in the absence of applied potential while capacitance approaches its lowest value. It appears that application of externally applied electrical potential adversely affects immobilised cholesterol molecules irrespective of whether it is positive or negative in sign. This behaviour is consistent with the amphiphilic nature of cholesterol molecules.

### Acknowledgement

The authors are grateful to the Head, Chemistry Department for providing facilities under UGC, COSIST Programme. A.K. Tiwari thanks CSIR, New Delhi for financial assistance.

### References

- 1 Mears P & Chaudhary M A, in *Synthetic Membranes, Vol. 1 Desalination* edited by Turbak A F, ACS Symp, Ser No. 153 (American Chemical Society, Washington), 1981, p. 101.
- 2 Jensen J B Sorensen T S Malmgren Hansen J B & Sloth P, *J Colloid interface Sci* 108 (1981).
- 3 Lonsdale H K, in *Desalination by reverse osmosis*, edited by U Merten, (MIT Press, Cambridge) 1966, p 93.
- 4 Guyton A C, *Text book of medical physiology*, (W.B. Saunders, London) 1981, p 856.
- 5 Singh K & Tiwari A K, *J Colloid interface Sci*, 116 (1987) 42.
- 6 Singh K & Tiwari A K, *J membrane Sci*, 34 (1987) 55.
- 7 Srivastava R C, Sharma R K Tondon A & Bhise S E, *J Colloid interface Sci*, 249 (1985) 108.
- 8 Singh K, Tiwari A K & Rai J P, *Indian J Chem*, 24 (1985) 825.
- 9 Singh K & Tiwari A K, *Indian J Chem*, 30 (1991) 1010.
- 10 Lange N A, *Hand book of chemistry* (Mc Graw Hill, New York) 1967, p. 1216.
- 11 Lakshminaryanaiah N, *Membrane electrodes* (Academio Press, New York) 1976, p 64.
- 12 Bard A J & Faulkner L R, *Electrochemical methods, fundamentals and applications*, (John Wiley, New York) (1980), Ch 9.
- 13 Tian Z W, *Study methods of electrochemistry* (Scientific Publication, China) (1984) p. 274.
- 14 Gerasimov Ya, General Editor, *Physical Chemistry*, Vol 2, (Mir Publishers, Moscow) 1974.

## Thermodynamic equilibrium constants of alkali metal ion-hydrogen ion exchanges and related swelling free energies in perfluorosulphonate ionomer membrane (Nafion-117) in aqueous medium

Sita T Iyer, Deoki Nandan & R M Iyer\*

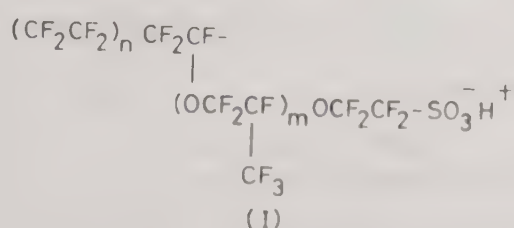
Chemistry Division, Bhabha Atomic Research Centre, Trombay, Bombay 400 085

$\text{Li}^+/\text{H}^+$ ,  $\text{Na}^+/\text{H}^+$ ,  $\text{K}^+/\text{H}^+$ ,  $\text{Rb}^+/\text{H}^+$  and  $\text{Cs}^+/\text{H}^+$  exchange equilibria on a perfluorosulphonate exchanger (Nafion-117) have been investigated at 0.1 *M* ionic strength in aqueous medium and thermodynamic equilibrium constants of 0.78 to 12.6 ( $\text{Li}^+/\text{H}^+$  to  $\text{Cs}^+/\text{H}^+$ ) have been evaluated and the alkali metal selectivity sequence has been found to be  $\text{Cs}^+ > \text{Rb}^+ > \text{K}^+ > \text{Na}^+ > \text{Li}^+$ . The various ionic forms of Nafion-117 involved have also been subjected to isopiestic water vapour sorption investigations and the hydration numbers and swelling free energies determined. The exchange selectivities have been found to be consistent with the sequence of ionic hydration and swelling free energies, the exchange free energies showing a linear relationship with the difference in free energies of hydration of the exchanging ions as per Eisenman's model. The expanded selectivity as well as swelling free energy ranges observed in Nafion-117 compared to Dowex 50W type of resins have been interpreted in terms of hydrative and osmotic swelling behaviours of the two exchangers. Existence of a solvent shared ion pair in Nafion-117, i.e.  $-\text{SO}_3^-(\text{H}_2\text{O})\text{Cs}^+$  observed in an earlier study has been supported by present selectivity data.

Due to its exceptional chemical inertness and favourable electrical properties, Nafion<sup>1-4</sup> (a novel perfluorinated ion exchanger) membrane has been exploited for a number of chemical and electrochemical applications<sup>4</sup> including its use as a separator in chlor-alkali cells. This ionomer of fluorocarbon backbone (structure I) has pendant side chains terminating with  $-\text{SO}_3^-\text{H}^+$  exchange groups (*m* is nearly unity and *n* varies between 5 to 11 thus generating an equivalent weight EW of 1000-1500). Although, conventional polystyrene-DVB sulphonate (PSS-DVB) exchangers<sup>3,5</sup> such as Dowex 50, Amberlite IR-120 etc., too possess the same exchange group and have been thoroughly studied for their ionic selectivity behaviour in aqueous medium, there is only one study reported<sup>2</sup> (on the alkali metal and alkaline earth ions versus  $\text{H}^+$ ) for Nafion-120 (EW ~ 1200) and even this study reports selectivity coefficients (*K<sub>c</sub>*) at 50% exchanger loading (also no attempt was made to incorporate solution phase activity coefficients to obtain equilibrium constants which represent the true selectivity). The authors<sup>2</sup>

have, however, emphasized that compared to PSS-DVB exchangers, Nafion-120 exhibits greater selectivity spread for alkali metal ions which could be attributed to the cluster morphology of Nafion and the lower charge density on  $-\text{SO}_3^-$  compared to that in PSS-DVB. The authors supported these observations through satisfactory column chromatographic separation of alkali metals using powdered Nafion-120.

In the recent past, a study from this laboratory<sup>3</sup> on the isopiestic water sorption isotherms of  $\text{H}^+$ ,  $\text{Li}^+$  and  $\text{Cs}^+$  forms of Nafion-117 (EW ~ 1100) membrane has revealed larger swelling free energy changes and swelling pressures generated from Nafion-117-water interactions involving  $\text{H}^+$  and  $\text{Li}^+$  forms. The hydration numbers (*n<sub>h</sub>*) for  $\text{H}^+$ ,  $\text{Li}^+$  were also deduced to be larger (6.0, 5.5 respectively) compared to 3.8 and 3.0 for PSS-DVB resins (hydration number for  $-\text{SO}_3^-$  group was considered to be same, 1.0)<sup>3</sup>. Again, contrary to PSS-DVB ( $\text{Cs}^+$ ), Nafion-117 ( $\text{Cs}^+$ ) revealed the presence of solvent shared ion pair [ $-\text{SO}_3^-(\text{H}_2\text{O})\text{Cs}^+$ ]. Another investigation relating to deuterium/hydrogen fractionation effects<sup>6</sup> revealed lesser hydrogen bonded structure of water in Nafion-117. These data relating to Nafion-117 membrane may indeed support the possibility of larger selectivity spread for alkali metals (and particularly high selectivity for  $\text{Cs}^+$  in Nafion-117 which can be a very useful consideration)



but suffer from the following (i) no water sorption isotherms are available for  $\text{Na}^+$ ,  $\text{K}^+$  and  $\text{Rb}^+$  forms (ii) no selectivity data are available concerning alkali metal –  $\text{H}^+$  exchanges on Nafion-117. As the total water sorption data set obtained for  $\text{H}^+$  and alkali ion forms of Nafion-117 is apparently different from that for Nafion-120, the ionic selectivities in the two ionomers are also likely to be different. Whether a greater spread of selectivity also exists for Nafion-117 thus remains to be explored.

In view of above, ion exchange equilibria in aqueous medium involving  $\text{Li}^+/\text{H}^+$ ,  $\text{Na}^+/\text{H}^+$ ,  $\text{K}^+/\text{H}^+$ ,  $\text{Rb}^+/\text{H}^+$  and  $\text{Cs}^+/\text{H}^+$  exchanges on Nafion-117 have been investigated in the present work. With the objective of getting a deeper insight into selectivities, isopiestic water sorption isotherms have also been determined for  $\text{Na}^+$ ,  $\text{K}^+$  and  $\text{Rb}^+$  forms while similar isotherms for  $\text{H}^+$ ,  $\text{Li}^+$  and  $\text{Cs}^+$  forms have been reobtained under identical conditions, extending them to lower water activity ( $a_w$ ) regions.

### Materials and Methods

**Membranes**— $\text{H}^+$ ,  $\text{Li}^+$  and  $\text{Cs}^+$  forms were generated as described earlier<sup>3</sup>.  $\text{Na}^+$ ,  $\text{K}^+$  and  $\text{Rb}^+$  forms of Nafion-117 were generated from the  $\text{H}^+$  form using 0.5 M solutions (aq) of NaOH, KOH and RbCl following standard procedures. The membranes were stored in air dried (AD) forms. Ion exchange capacities obtained on the totally dry basis are:  $\text{H}^+$  (0.94);  $\text{Li}^+$  (0.937);  $\text{Na}^+$  (0.915);  $\text{K}^+$  (0.900);  $\text{Rb}^+$  (0.870);  $\text{Cs}^+$  (0.845) meq/g.

**Isopiestic studies**—Water sorption as a function of water activity was investigated using two similar isopiestic units fabricated earlier<sup>3,7</sup> and aqueous electrolyte solutions<sup>7</sup> of LiCl and  $\text{H}_2\text{SO}_4$ . Sorption isotherms of various ionic forms of Nafion-117 were obtained as  $n_w$  (moles of water/equiv) versus  $a_w$  curves. Dry weights of the AD membranes for obtaining  $n_w$  were computed using another set of various ionic forms which were heated in a vacuum oven at 413 K and the moisture contents determined.

**Ion exchange equilibria**—Nearly 0.1 M solutions of HCl, LiCl, NaCl, KCl, RbCl and CsCl were employed. Batch method was used to investigate alkali metal –  $\text{H}^+$  exchange equilibria using approximately 0.5 g each of membrane pieces (AD) and a total of 25 ml solution ( $\text{HCl} + \text{MCl}$ ,  $\text{M} = \text{alkali metal}$ ) in each erlenmeyer allowing 48 hrs for equilibrium attainment. Equilibrium concentrations of  $\text{H}^+$  and  $\text{M}^+$  ions in the outer solution were determined titrimetrically (NaOH, 0.05 M), and flame photometrically using Varian Techtron AA6 model (Li, 670.8 nm; Na, 589.0 nm; K, 766.5 nm; Rb, 780.0 nm and Cs, 852.1 nm) respectively. Quantities of  $\text{H}^+$  and

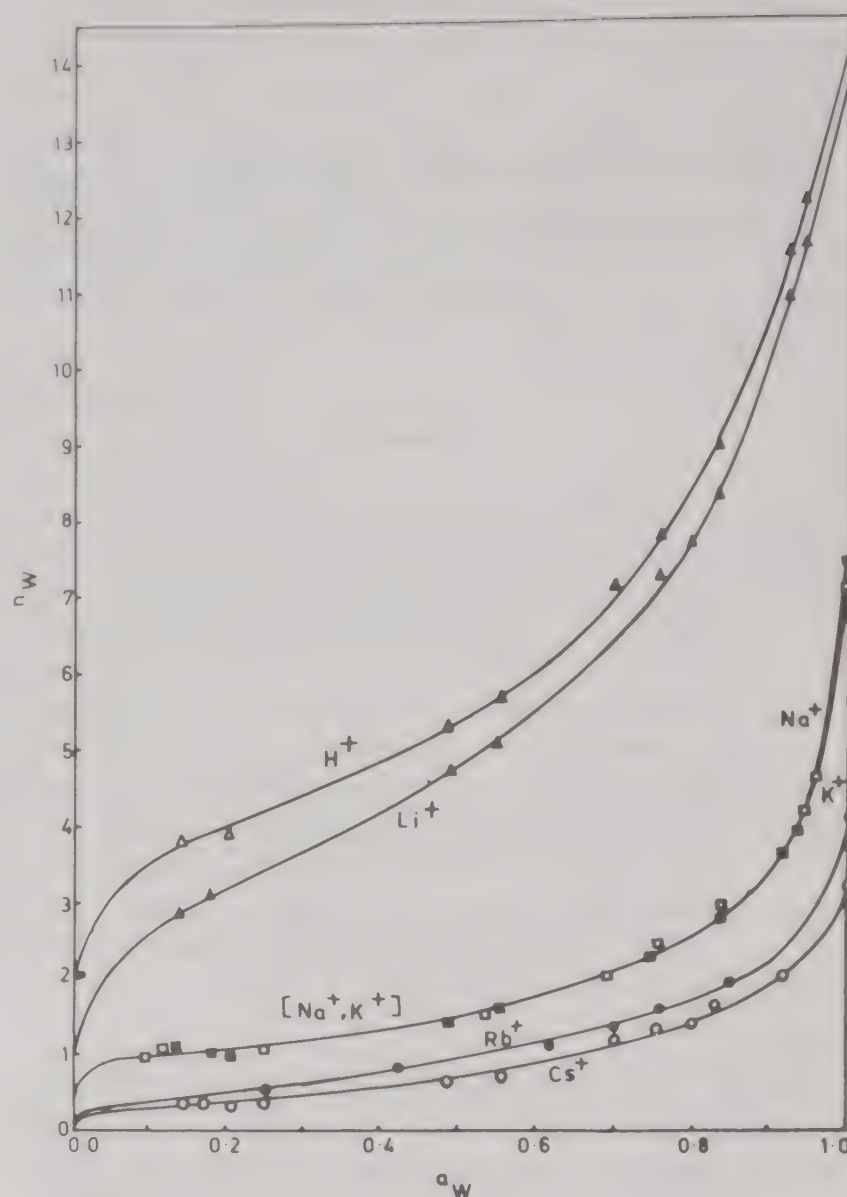


Fig. 1—Isopiestic water sorption isotherms for various ionic forms of Nafion-117 membrane (298 K)

Table 1—Ionic hydration and swelling free energy data for Nafion-117 membranes (298 K)

Ionic form	$n_w$ (at $a_w = 1$ )	$n_T$	$n_+$	$-\Delta G_{sw}$ (integral) kJ/mol
$\text{H}^+$	14.2	7.0	6.0 (3.8)*	45.0
$\text{Li}^+$	13.6	6.5	5.5 (3.0)*	36.1
$\text{Na}^+$	7.4	2.5	1.5 (2.5)*	14.4
$\text{K}^+$	7.1	2.5	1.5 (2.3)*	14.0
$\text{Rb}^+$	4.1	1.3	0.3	7.3
$\text{Cs}^+$	3.2	1.0	0.0 (2.0)*	6.1

\*Values are for Dowex 50 resins (ref. 3,9).

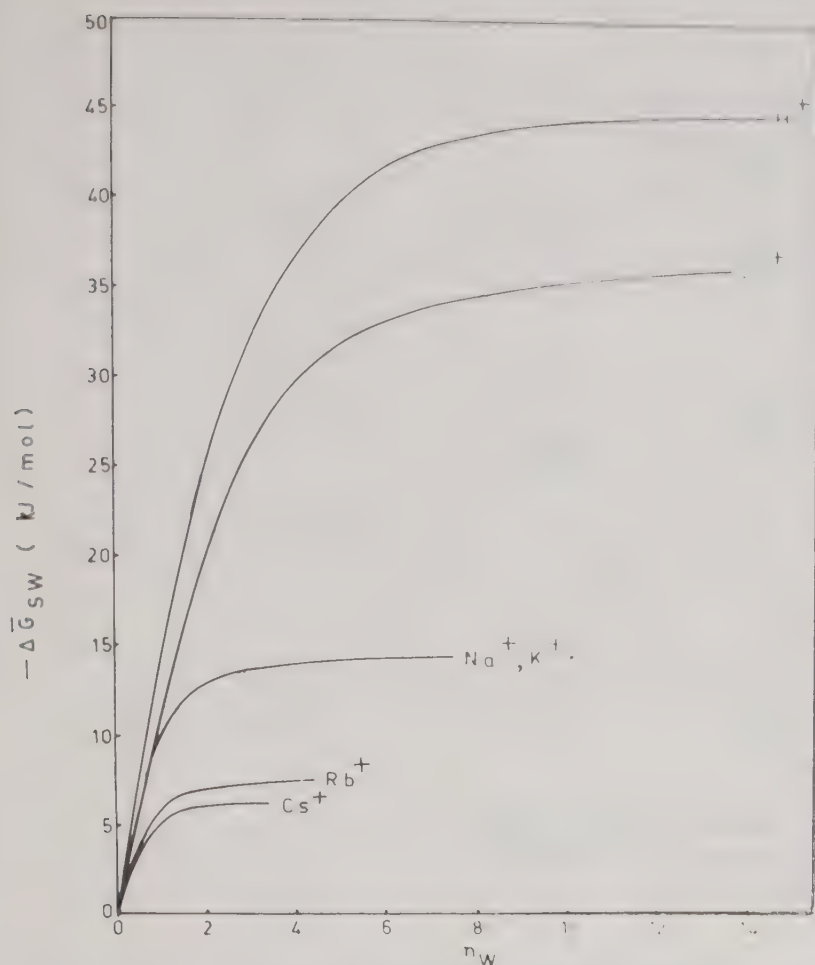
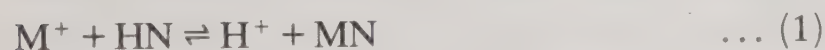


Fig. 2—Differential swelling free energy ( $\Delta \bar{G}_{sw}$ ) versus  $n_w$  plots for various ionic forms of Nafion-117 (298 K)

$M^+$  in the membrane phase at equilibrium were then obtained from the total quantities added in the erlenmeyer solution and the ion exchange capacities of membrane pieces. Selectivity coefficients ( $K_c$ ) for the exchange reaction ( $M^+$  stands for alkali metal ion):



(HN and MN represent  $H^+$  and  $M^+$  forms of Nafion) were computed using Eq. 2 (ref. 2) ( $X$  represents ionic fraction while  $m$  represents molality).

$$K_c = \frac{m_{H^+}}{m_{M^+}} \cdot \frac{X_{MN}}{X_{HN}} \quad \dots (2)$$

Equilibrium constants ( $K$ ) were computed using the relationship<sup>8</sup>,

$$\log K = \int_{X_{MN=0}}^{X_{MN=1}} \log K_c + \log \frac{\gamma_{\pm HCl}}{\gamma_{\pm MCl}} \quad \dots (3)$$

$\gamma_{\pm}$  being the mean molal activity coefficients of pure electrolytes in their aqueous solutions of 0.1  $M$  each. The ratio of molalities and molarities have been treated to be the same in the present study involving dilute aqueous solutions (Eqs 2 and 3) of ionic strength 0.1.

## Results

Water sorption isotherms for  $H^+$  and alkali metal ionic forms of Nafion-117 are shown in Fig. 1. As can be seen, the ionic sequence of water sorption at any water activity is  $H^+ > Li^+ > Na^+ > K^+ > Rb^+ > Cs^+$  ( $Na^+$  and  $K^+$  forms isotherms are identical upto  $a_w \sim 0.9$ ). Slight differences in the isotherms of  $H^+$ ,  $Li^+$  and  $Cs^+$  can also be observed on comparison with those reported earlier<sup>3</sup> though their shapes remain essentially same. Differential swelling free energy ( $\Delta \bar{G}_{sw}$ ) plots constructed from the data are shown in Fig. 2, as computed using the relationship<sup>3</sup>.

$$\Delta \bar{G}_{sw} = -RT \int_{a_w=0}^{a_w} n_w d \ln a_w + n_w RT \ln a_w \quad \dots (4)$$

Following the arguments and methodology advanced earlier<sup>3</sup>, total hydration numbers,  $n_T$  (Table 1) derived from Fig. 2 yielded cationic hydration numbers (assuming hydration number for  $-SO_3^-$  group as 1.0)<sup>3</sup> of 6.0, 5.5, 1.5, 1.5, 0.3 and 0.0 respectively for  $H^+$ ,  $Li^+$ ,  $Na^+$ ,  $K^+$ ,  $Rb^+$  and  $Cs^+$  ions. A comparison with literature values of similar hydration numbers in PSS-DVB exchangers<sup>3,9</sup> shows (i) larger hydration of  $H^+$  and  $Li^+$  in Nafion-117 (ii) lower hydration for remaining alkali metal ions in Nafion-117. Thus, compared to a narrow range of  $n_+$  (3.8-2.0) for  $H^+$  to  $Cs^+$  in PSS-DVB, a much larger range of 6.0-0.0 is obtained in Nafion-117. Also as can be seen,  $Cs^+$  form exhibits  $n_T$  value of unity thereby confirming the presence of solvent separated ion pairs in  $Cs^+$ -membrane. The integral free energies of swelling ( $\Delta G_{sw}$ ) for various ionic membranes, also summarized in Table 1 are consistent with the above ionic sequence for water sorption. They range from about  $-6$  kJ/mol to  $-45$  kJ/mol while similar range for a typical PSS-DVB (Dowex 50w, 4-8% crosslinking) resin is nearly  $-15$  to  $-30$  kJ/mol. Thus  $\Delta G_{sw}$  support the above observation of larger range of ionic hydration in Nafion-117 as is actually expected owing to the fact that generally larger hydration effects also lead to larger osmotic (and thus total swelling) effects in ion exchanger phase.

Alkali metal ion- $H^+$  exchange selectivity coefficients obtained as a function of exchanger loading ( $X_{MN}$ ) have been shown in Fig. 3. At any exchanger loading, the  $K_c$  increases from  $Li^+/H^+$  to  $Cs^+/H^+$ . Also  $K_c$  increases for most exchanges as  $X_{MN}$  decreases (a comparison of present plots with those of Nafion-120 reveals some significant differences which may be due to use of different EW exchangers as well as ionic strengths). However, integral va-

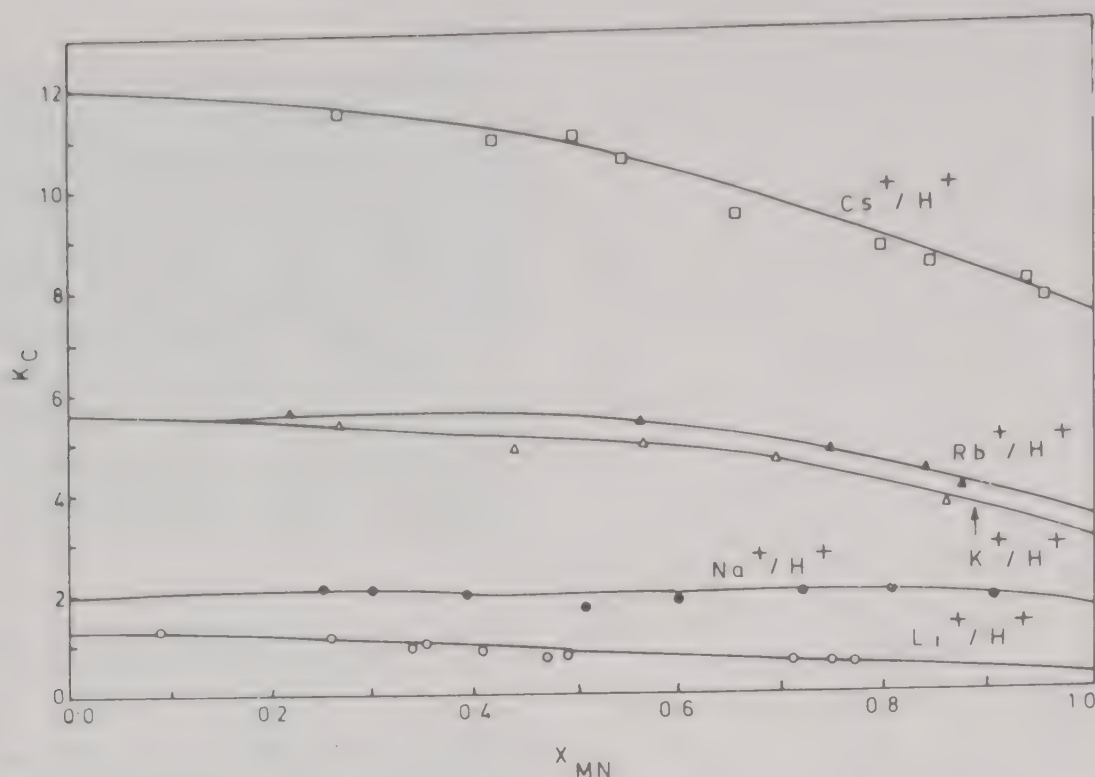


Fig. 3—Selectivity coefficient ( $K_c$ ) versus exchanger loading plots for alkali metal ion -  $H^+$  exchanges on Nafion-117 at 0.1 M ionic strength (298 K)

lues are of greater relevance (first term in Eq. 3; not available for Nafion-120) which are summarized in Table 2 for present exchanges. After incorporating activity coefficient corrections (second term in Eq. 3), thermodynamic equilibrium constants ( $K$ ) are found to range from 0.78 ( $Li^+/H^+$ ) to 12.6 ( $Cs^+/H^+$ ) yielding free energies of exchange ( $\Delta G_{ex}$ ) from +0.617 ( $Li^+/H^+$ ) to -6.29 ( $Cs^+/H^+$ ) kJ/mol (Table 2). These data clearly show that compared to  $H^+$ , all alkali ions exhibit greater selectivity excepting  $Li^+$ , the overall selectivity sequence being  $Cs^+ > Rb^+ > K^+ > Na^+ > Li^+$  which is exactly opposite to the sequence observed for ionic hydration as well as swelling free energies, as expected based on Eisenman's model, as well as Gregor's mechanistical model of ion exchangers (although the latter model is evolved for crosslinked resins such as PSS-DVB but is applicable to other exchangers). However, it is clear that present selectivity range is much larger than that of PSS-DVB resin such as Dowex 50WX8 (included in Table 2, 0.79-2.31), which should lead to better resolution in the alkali metal-ion separation as observed by Yeager *et al*<sup>2</sup>.

### Discussion

Compared to a three dimensional crosslinked and somewhat rigid and heterogenous hydrocarbon structure of PSS-DVB exchangers<sup>10</sup>, Nafion is considered to be a dynamic type of polymer of high molecular weight with a cluster morphology<sup>2,3,6</sup>. Owing to differences in the backbone material, ionic concentration (capacity) and morphology, the state of

water around fixed charges and counterions is expected to lead to important variation<sup>11</sup> in the overall swelling (hydration + osmotic) behaviour as well ion exchange selectivity in the two types of exchangers as is actually witnessed above in terms of expanded ranges for hydration numbers, integral swelling free energies and ion exchange equilibrium constants for Nafion-117 compared to Dowex 50 type of exchanger (8% DVB is taken as an example). It is recognised that due to the presence of fluorine in the Nafion backbone, the electric field strength on the sulphonate fixed group is lowered<sup>2</sup> thereby reducing its interaction with water (IR studies<sup>12</sup>, however, confirm that it does interact with water though the hydration number could not be determined and therefore is assumed to be unity<sup>3</sup> as is the case with PSS-DVB exchangers). This lowered hydration apparently promotes greater hydration of counterions with high charge density ( $H^+$ ,  $Li^+$ ) due to lesser competition for the available water while ions of lower charge density ( $Na^+$ ,  $K^+$ ,  $Rb^+$ ) are hydrated to a lesser extent. The cluster morphology of Nafion-117 must also be responsible. The presence of solvent separated ion pair in Nafion-117 ( $Cs^+$ ) has been reconfirmed in the present study. As integral free energies are mainly derived from free energies of hydration of ions, a larger range of  $\Delta G_{sw}$  is also observed for Nafion-117 compared to PSS-DVB resins.

The interrelationship between the swelling behaviour and the ionic selectivity is well recognised<sup>5,13</sup> and reflected in several theoretical models of ion ex-

Table 2—Selectivity coefficients, equilibrium constants ( $K$ ) and free energies of ion exchange ( $\Delta G_{ex}$ ) for alkali metal ion –  $H^+$  exchanges

Exchange system	$\int_{X_{MN(O)}}^{\infty} \log K_c$	$\log \frac{\gamma_{\pm HCl}}{\gamma_{\pm MCl}}$	$\log K$	$K$	$-\Delta G_{ex}$ (kJ/mol)
$Li^+/H^+$	-0.111	0.003	-0.108	0.78 (0.79)*	-0.617
$Na^+/H^+$	+0.295	0.010	0.305	2.02 (1.49)*	1.74
$K^+/H^+$	+0.636	0.014	0.650	4.47 (2.09)*	3.71
$Rb^+/H^+$	+0.708	0.018	0.726	5.32 (2.29)*	4.15
$Cs^+/H^+$	+0.979	0.022	1.101	12.6 (2.31)*	6.29

\*Values are for Dowex 50WX8 exchanger (ref. 2, 8).

changers<sup>5,14</sup>. Thus Gregor's theory<sup>5,14</sup> considers the difference between the partial hydrated volumes of the exchanging ions as the origin of selectivity while that of Eisenmann<sup>5,14,15</sup> considered to be a superior theory explains selectivity in terms of free energies of hydration of ions and the coulombic interactions using the relationship

$$\ln K = \frac{1}{RT} \left[ \left( \frac{e^2}{r_A + r_1} \right) - \left( \frac{e^2}{r_A + r_2} \right) + \Delta G_2 - \Delta G_1 \right] \dots (5)$$

where  $r_A$ ,  $r_1$ ,  $r_2$  are radii of anion and cations (for a cation exchanger), and  $\Delta G_2$ ,  $\Delta G_1$  are hydration free energies of exchanging ions. In the case of a cation exchanger with a larger size fixed grouping of low field strength (such as Nafion-117), the only term which will mainly contribute to  $\ln K$  will be  $(\Delta G_2 - \Delta G_1)$ . In the present work, the swelling free energies of Nafion-117 exhibit the same sequence as the hydration free energies of the ions reported<sup>16,17</sup>. Also excepting the special case of  $Cs^+$  form of Nafion-117, the hydration number sequence of ions also is consistent with the swelling free energies. Thus, it could be expected that  $\log K$  values in the present work should exhibit a linear relationship with  $[\Delta G_{(M^+)} - \Delta G_{(H^+)}]$  excepting probably the case of  $Cs^+/H^+$  exchange which is likely to show unusually high selectivity ( $K$ ) due to solvent shared ion pair formation. This expectation is clearly borne out (Fig. 4) from the plot of  $\log K$  versus  $[\Delta G_{hydration}(M^+) - \Delta G_{hydration}(H^+)]$ . It should be emphasized

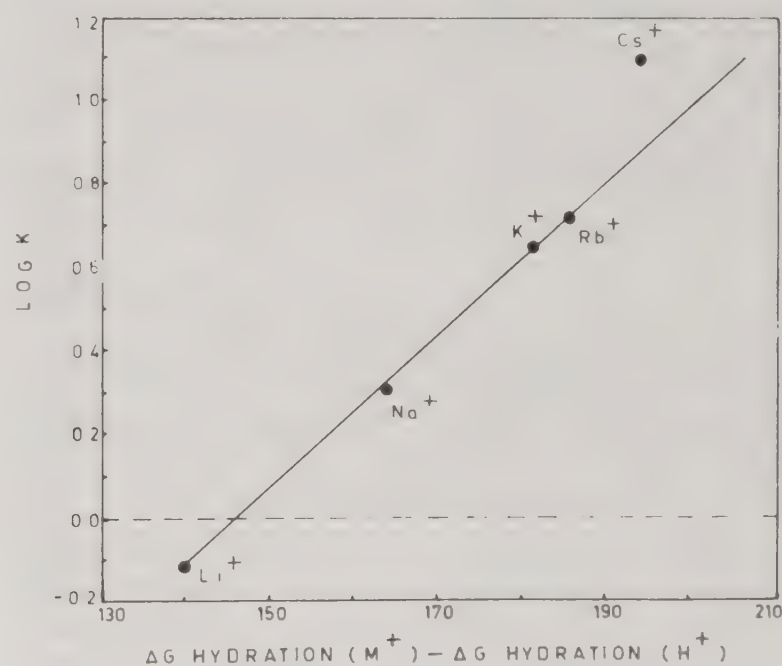


Fig. 4—Plot of  $\log K$  versus difference of hydration free energies for the exchanging ions for Nafion-117 (298 K)

here that observations of linear variation of ion exchange free energies (or  $\log K$ ) with water contents [e.g.  $n_w$  or  $n_w(\text{exchange})$ <sup>3,5</sup>] is mere coincidental and has no theoretical basis. Thus, the parameters of importance are free energies of hydration<sup>5,15</sup>, swelling free energies or the volume swellability<sup>5,14</sup>. The analysis of water sorption isotherms in terms of hydration numbers etc works as an aid to visualize any deviations from theory ( $Cs^+/H^+$ ) and to understand higher selectivities and the expanded ranges (while  $Li^+/H^+$  exchange selectivity is same in Nafion-117 and Dowex 50W×8,  $Na^+/H^+$ ,  $K^+/H^+$  and  $Rb^+/H^+$  selectivities are higher in Nafion-117 due to low-

er hydration numbers of  $\text{Na}^+$ ,  $\text{K}^+$ ,  $\text{Rb}^+$ ). The present data (Fig. 4) also emphasize that in the selectivity, inclusion of solution phase activity coefficients is essential.

### Acknowledgement

The authors thank Dr S. Ganapathy and his colleagues for making the flame photometer arrangement available and for all cooperation. STI and DN also thank Dr J.P. Mittal, Associate Director, Chemistry Group for all encouragement during the present investigations.

### References

- 1 Yeager H L & Eisenberg A, ACS Symp. Ser. No. 180; Perfluorinated ionomer membranes, edited by A Eisenberg and H L Yeager, (Am chem Soc, Washington DC, 1982), p. 1.
- 2 Yeager H L & Steck A, *Anal Chem*, 51 (1979) 862.
- 3 Pushpa K K, Nandan D & Iyer R M, *J chem Soc, Faraday Trans, I*, 84 (1988) 2047.
- 4 Sondheimer S J, Bunce N J & Fyfe C A, *JMS-REV, Macromol chem Phys*, C26(3) (1986) 353.
- 5 Helfferich F, *Ion exchange* (McGraw Hill, New York) 1962.
- 6 Pushpa K K, Nandan D & Iyer R M, *J chem Soc, Faraday Trans*, 86 (1990) 409.
- 7 Nandan D & Gupta A R, *J phys Chem*, 81 (1977) 1174.
- 8 Nandan D & Gupta A R, *J phys Chem*, 79 (1975) 180.
- 9 Nandan D & Gupta A R, *Indian J Chem*, 12 (1974) 808.
- 10 Goldring L S, in "*Ion exchange* (Vol. I)", edited by J A Marinsky (Marcel Dekker, New York) (1966) p. 205.
- 11 Tasaka M, Suzuki S, Ogawa Y & Kamaya M, *J memb Sci*, 38 (1988) 175.
- 12 Nandan D, Pushpa K K, Kartha V B, Wahi P K & Iyer R M, [Communicated].
- 13 Braud C & Selegny E, *Sep Sci*, 9 (1974) 13; 9 (1974) 21.
- 14 Reichenberg D, Ref. 10, p-227.
- 15 Eisenman G, in *Membrane transport and metabolism* (edited by A Kleinzeller and A Kotyk), (Academic Press, New York) 1961, pp 163-179; *Biophys J*, 2, part 2 (1962) 259.
- 16 Franks F, *Water, A comprehensive treatise*, (Plenum, New York) (1973) Vol. 3, Chapter 1.
- 17 Jain D V S, *Indian J Chem*, 3 (1965) 466.

## Studies on the selective carrier - mediated transport of plutonium(IV) ions through tributyl phosphate/dodecane liquid membranes

J P Shukla\* & S K Misra

Radiochemistry Division, Bhabha Atomic Research Centre, Trombay, Bombay 400 085

Highly selective transport of  $\text{Pu}^{4+}$  over several other long-lived fission product contaminants has been achieved through the organic bulk liquid membrane (BLM) and flat-sheet immobilized liquid membranes (ILM) employing tributyl phosphate (TBP) as the mobile carrier and dodecane as the membrane solvent. Extremely dilute plutonium nitrate solutions ( $\mu\text{g/ml}$ ) in about  $2 \text{ mol dm}^{-3} \text{ HNO}_3$  generally constitutes the source phase. Ascorbic acid serves most efficiently as the stripping agent.

Metal cation separations based on liquid-liquid extraction have been fully in vogue on industrial scale for many decades<sup>1,2</sup>. Of them, separations based on liquid membranes have attracted maximum attention. The membrane separation effectiveness is assessed by both the flux and selectivity of the transported species. Polymeric membranes have the disadvantages of usually low transmembrane fluxes in the condensed phase and also poor selectivities. On the other hand, liquid membranes generally afford relatively higher fluxes and much improved selectivities. Prompted by these considerations, we have recently initiated a comprehensive programme to explore varied analytical applications of liquid membranes employing commercially available carriers in the treatment of dilute actinide liquid nuclear wastes. As an example, tributyl phosphate (TBP) has been commercially exploited as the extractant in PUREX process<sup>3-5</sup> for the recovery and purification of U(VI) and Pu(IV) from various matrices in acidic solutions. In the present study, TBP dissolved in dodecane was selected as the mobile ion carrier in the facilitated transport of Pu(IV) across an organic bulk liquid membrane (BLM) as well as an immobilized liquid membrane (ILM). The bulk membrane system uses small quantities of carrier and, hence, is a good system for screening complexation agent properties. Effects of important parameters that affect cation flux in liquid membranes, such as the activity of the permeant salt, feed acidity and carrier concentration in the organic membrane phase were investigated. Dodecane was selected for use throughout this study because it has low volatility and negligible aqueous solubility<sup>6</sup> besides the traditional advantage of its inertness towards the polymeric support. Similarly, suitability of aliphatic hydrocarbons of high boiling point such as dodecane (b.p.  $216^\circ\text{C}$ ) as solvents has also been suggested<sup>7</sup>.

### Materials and Methods

All the reagents were analytical grade products. Pu-239 tracer ( $1 \mu\text{g/ml}$ ) purified by the usual ion exchange method was used throughout. Tetraavalency of plutonium in the feed was adjusted with sodium nitrite ( $\sim 0.05 \text{ mol dm}^{-3}$ ). Permeation of fission products was checked with an unpurified plutonium nitrate solution of the following composition received from reprocessing operations: Pu:  $2.64 \text{ mg dm}^{-3}$ , Ce-144:  $6.3 \text{ mCi dm}^{-3}$ , Ru-106:  $1.37 \text{ mCi dm}^{-3}$  and Cs-137:  $2.5 \text{ mCi dm}^{-3}$ . Dodecane procured from Aldrich, USA was of high purity grade.

### Liquid membrane cells

Details of glass BLM and ILM transport cells are described elsewhere<sup>9</sup>. The BLM cell (Shulman bridge type) consisted of a bulk TBP/dodecane phase separating the aqueous source phase ( $12.5 \text{ cm}^3$ ) and the aqueous receiving phase ( $2.2 \text{ cm}^3$ ). Single-stage ILM measurements were carried out with a two compartment permeation cell in which a source aqueous solution ( $12.0 \text{ cm}^3$ ) was separated from the aqueous receiving solution ( $2.0 \text{ cm}^3$ ) by a liquid membrane with an effective membrane area of  $1.13 \text{ cm}^2$ . The feed and product solutions were mechanically stirred at room temperature to avoid concentration polarization conditions at the membrane interface and in the bulk solutions. Membrane permeabilities were determined by monitoring the plutonium concentration radiometrically, primarily in the receiving phase, as a function of time. All the experiments were performed in triplicate and the deviation from the averages was found to be less than 10%. The plutonium flux,  $J_M$ , was computed with the equation:

$$J_M = C_{\text{Pu}}(\text{receiving}) \times V/A \times t$$

where  $C_{\text{Pu}}(\text{receiving})$ ,  $V$ ,  $A$  and  $t$  denote the Pu concentration in the receiving phase (M), volume of the receiving phase ( $\text{dm}^3$ ), effective area of the

membrane ( $\text{m}^2$ ) and time elapsed (seconds), respectively.

### Membrane supports

Throughout this study, 'Enka' Accurel polypropylene flat-sheet type hydrophobic microporous polymeric membranes, coded as 2E HF-PP (high flow type), used was 130 - 180  $\mu\text{m}$  thick and had a nominal porosity of about 70% with an average pore diameter of the order of 0.2  $\mu\text{m}$ . Filling the pores of this dry support polymer with the carrier solution was accomplished by soaking a circular sheet of the membrane in the liquid membrane solution for at least 6-8 h before use. Membranes prepared with different portions of the support polymer sample gave permeation results reproducible to approximately  $\pm 10\%$ .

## Results and Discussion

### Carrier-mediated membrane permeation

TBP dissolved in dodecane served as the organic membrane in both BLM and ILM permeability measurements. Plutonium (IV) is highly extractable by TBP from  $\text{HNO}_3$  media and therefore it permeated easily across these liquid membranes. Under similar conditions, transport of both  $\text{Pu(III)}$  and  $\text{Pu(VI)}$  was almost negligible. The transport of  $\text{Pu}^{4+}$  with TBP occurs by a neutral transport mechanism (neutral carrier and co-transport of an anion). Carrying out control experiments with no TBP in the membrane solvent showed that plutonium flux through such membranes was negligible ruling out any possibility of leakage or transport by the membrane solvent itself. About 70% of the plutonium was recovered in single run with ascorbic acid ( $0.5 \text{ mol dm}^{-3}$ ) as the receiving phase allowing a concentration of nearly six times.

### Effect of source phase acidity

Results for the single-ion transport of nearly  $3.98 \mu\text{g/ml}$  Pu from an aqueous feed adjusted to different  $\text{HNO}_3$  molarities through a TBP/dodecane BLM membrane into  $0.5 \text{ mol dm}^{-3}$  ascorbic acid strip solution are summarized in Table 1. Maximum plutonium permeation of over 70% and mean value of the maximum flux reaching  $2.8 \times 10^{-8} \text{ mol/m}^2/\text{s}$  after about 7h of transport process took place from the relatively lower feed acidity of  $\text{HNO}_3$  ( $2 \text{ mol dm}^{-3}$ ), while enhanced acidity of above  $2 \text{ mol dm}^{-3}$  adversely affected the plutonium transport which plummeted to 30% and lower. This initial increase in flux versus  $[\text{HNO}_3]$  is in accord with the expected trend since

Table 1—Flux and permeation of plutonium as a function of source phase nitric acid molarity

[Initial feed concentration =  $3.98 \text{ mg dm}^{-3}$  plutonium in  $\text{HNO}_3$ ; Carrier (TBP) concentration = 30% (v/v)  
TBP/dodecane; Strippant =  $0.5 \text{ mol dm}^{-3}$  ascorbic acid;  
Volume ratio of feed to strippant = 6:1]

Source phase acidity, $\text{HNO}_3$ ( $\text{mol dm}^{-3}$ )	Time elapsed (h)	Plutonium flux $J_M$ ( $\times 10^{-8} \text{ mol/m}^2/\text{s}$ )	Plutonium permeation (%)
1		—poor response—	
2	1	1.3	2.5
	3	2.9	17.4
	5	3.2	32.6
	7	3.7	52.7
	24	1.5	71.7
3	1	1.6	3.3
	3	3.6	21.8
	5	3.2	33.0
	7	3.4	48.0
	24	0.4	7.0
4	1	3.7	7.6
	3	5.4	32.7
	5	4.2	42.6
	7	3.2	46.2
	24	0.1	3.8
5	1	0.3	0.4
	3	5.4	21.6
	5	4.8	32.0
	7	3.1	28.4
	24	0.5	15.1

the flux of a cation varies with  $[\text{NO}_3^-]$  following the relationship<sup>10</sup>:

$$J_M = A (T/\eta) [\text{NO}_3^-]^{n(a)} [\text{TBP}]^{n(o)} \cdot C_{\text{Pu}}(\text{feed}) \quad \dots (1)$$

where  $T$ ,  $\eta$ ,  $[\text{TBP}]_o$ ,  $C_{\text{Pu}}(\text{feed})$  denote the absolute temp., viscosity of the membrane phase, TBP concentration in the membrane (org.) phase, and concentration of Pu in the feed, respectively. Hence there should be an increase in permeability with an increase in  $\text{HNO}_3$  concentration.  $\text{Pu}^{4+}$  ions form  $\text{Pu}(\text{NO}_3)_4 \cdot 2\text{TBP}$  type complexes upto moderate acidity but above  $2 \text{ mol dm}^{-3}$  or more,  $\text{HNO}_3$  starts reacting with TBP to form complexes of the type  $\text{TBP} \cdot \text{mHNO}_3$ <sup>11</sup>. A considerable decrease in plutonium transport at higher acidity may be attributed to the decrease in the  $[\text{TBP}]$  term in the flux equation due to formation of  $\text{TBP} \cdot \text{mHNO}_3$  species inside the membrane just adjacent to the aqueous solutions interfacing it. Moreover, at higher  $\text{HNO}_3$  molarity  $\text{Pu}^{4+}$  ions may exist in the form of  $\text{HPu}(\text{NO}_3)_5$  and  $\text{H}_2\text{Pu}(\text{NO}_3)_6$  which are unextractable by TBP causing a fall in solute flux.

As seen from Eq. (1), the value of  $D_{\text{Pu}}$  should increase with the aqueous  $[\text{NO}_3^-]$ . Therefore, the "pumping" effect in BLM study can be enhanced

by increasing the ratio of  $[\text{NO}_3^-]$  in the source phase to the  $[\text{NO}_3^-]$  in the receiving phase. To distinguish the driving force for the cation transport across the TBP membrane, experiments were performed with decreasing amounts of  $\text{HNO}_3$  mixed with  $\text{NH}_4\text{NO}_3$  maintaining the total  $[\text{NO}_3^-]$  fixed at  $2 \text{ mol dm}^{-3}$  to simulate partial neutralization of the acid waste. From the results it is clear that no significant change in plutonium transport took place by decreasing the source phase acidity while keeping  $[\text{NO}_3^-]$  constant at  $2 \text{ mol dm}^{-3}$ . This is further proof that  $\text{NO}_3^-$  anion and not the  $\text{H}^+$  ion is involved in the driving force for the plutonium transport under the present conditions. Thus the best condition of those tested for its transfer is  $\text{HNO}_3$  ( $0.5 \text{ mol dm}^{-3}$ ) +  $\text{NH}_4\text{NO}_3$  ( $1.5 \text{ mol dm}^{-3}$ ) which requires relatively lesser amounts of  $\text{HNO}_3$  to adjust  $[\text{NO}_3^-]$ .

#### *Effect of TBP (carrier) concentration on $\text{Pu}^{4+}$ transport*

The composition of the organic solution has a marked effect on the cation flux. When transport across a membrane occurs via a carrier as in facilitated-transport, the flux is generally expected to increase with increase in [carrier]. However, in carrier-mediated transport of plutonium with TBP, a more complex behaviour is seen. Table 2 summarizes data for plutonium flux versus [TBP] in the membrane. Data in Table 2 show that with increase in [carrier] in an inert diluent like dodecane, plutonium transport gradually increased reaching a maximum value at about 30% ( $1.1 \text{ mol dm}^{-3}$ ), above which the flux decreased at 40% TBP. This interesting phenomenon is apparently caused by two competing factors: (i) the concentration gradient of the plutonium complex, and (ii) the viscosity of the organic phase in the liquid membrane<sup>12</sup>. Since an increase in viscosity of TBP solution may lead to decrease in the diffusion coefficient and hence permeability of the diffusing species, these opposing effects resulted in a maximum permeation at about 30% TBP. Above this concentration, the permeation decreased with increase in [carrier].

#### *Effect of [plutonium (IV)] in feed solution*

Studying the effect of [plutonium] in the feed solution ranging from 2 to  $4 \mu\text{g/ml}$  in which the product side contained a negligible concentration of plutonium, revealed that the cation flux increased sharply with increase in [plutonium] tested up to this range. Results of the plutonium permeation through the membrane as a function of elapsed time and thus extraction of Pu(IV) into

the organic phase at various initial [plutonium] in the feed are shown in Fig. 1. Thus, the plutonium flowed down to its concentration gradient. However, as predicted by theory, plutonium will flow up its concentration gradient under appropriate conditions. The difference in permeability between experiments with varying feed acidity, carrier concentration and plutonium molarity can be understood by considering the probable expression for the rate of formation of the diffusing species at the feed interface<sup>13</sup>:

$$d [\text{Pu}(\text{NO}_3)_4 \cdot 2\text{TBP}] / dt = k^* [\text{TBP}]^2 [\text{NO}_3^-]^2 \times [\text{Pu}^{4+}] \dots (2)$$

where  $k^*$  is rate constant for the formation of the  $\text{Pu}^{4+}$ -TBP complex. This equation is based on the stoichiometry of plutonium extraction established earlier. The rate of diffusion of the metal species will thus depend upon any changes in  $\text{NO}_3^-$ , TBP and  $\text{Pu}^{4+}$  concentrations in the feed side.

#### *Membrane permeation through ILM*

Based on our findings with BLM on the plutonium transport, the ILM membranes were operated only at the optimum concentrations of feed

Table 2—Flux and permeation of plutonium as a function of carrier(TBP) concentration in the organic membrane  
Initial source phase acidity =  $2 \text{ mol dm}^{-3} \text{HNO}_3$ ; Initial [plutonium] =  $3.98 \text{ mg dm}^{-3}$ ; Strippant =  $0.5 \text{ mol dm}^{-3}$  ascorbic acid

TBP concentration in dodecane vol, %	Time elapsed (h)	Plutonium flux, $J_M$ ( $\times 10^{-8} \text{ mol/m}^2/\text{s}$ )	Plutonium permeation (%)
10	1	2.1	4.3
	3	2.9	17.8
	5	2.9	29.1
	7	2.5	34.9
	9	2.4	41.1
	24	1.0	46.6
20	1	1.6	3.3
	3	2.8	17.0
	5	2.8	28.1
	7	2.6	37.3
	9	2.5	46.3
	24	1.4	67.1
30	1	0.9	1.9
	3	2.8	17.2
	5	3.1	31.9
	7	3.6	51.9
	9	3.3	60.4
	24	1.5	71.9
40	1	1.2	2.5
	3	3.0	18.6
	5	3.1	31.9
	7	3.1	44.6
	9	2.6	44.6
	24	0.9	50.2

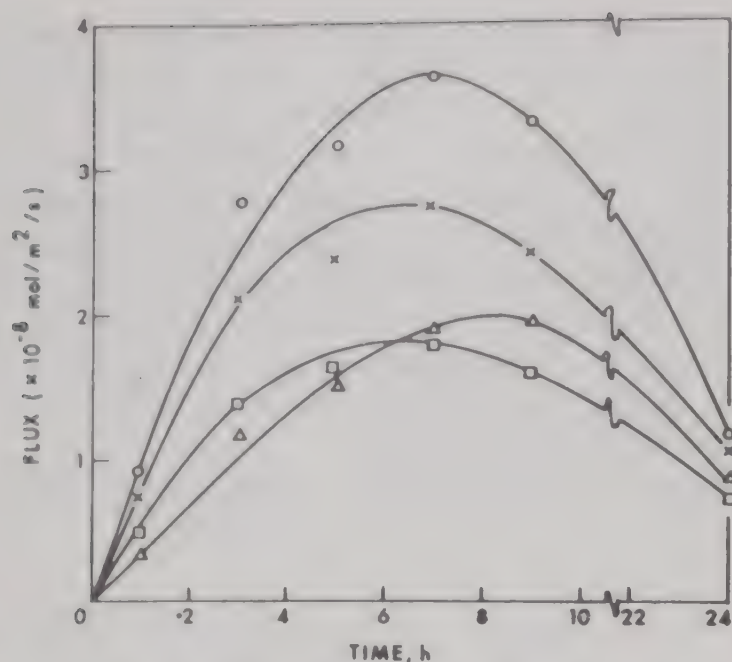


Fig. 1—Effect of initial [plutonium] in the feed solution on plutonium transport. [Membrane = 30% TBP in dodecane; feed solution =  $\text{Pu}(\text{NO}_3)_4$ ; source phase acidity =  $2 \text{ mol dm}^{-3}$ ; strippant =  $0.5 \text{ mol dm}^{-3}$  ascorbic acid. Curve —○—  $3.98 \text{ mol dm}^{-3}$ ; —X—  $3.0 \text{ mol dm}^{-3}$ ; —□—  $2.7 \text{ mol dm}^{-3}$ ; —△—  $1.99 \text{ mol dm}^{-3}$ ].

acidity ( $2 \text{ mol dm}^{-3} \text{ HNO}_3$ ), carrier concentration (30% TBP) and the strippant ( $0.5 \text{ mol dm}^{-3}$ ), ascorbic acid. Under these conditions, about 90% of plutonium could be easily recovered within 24 h employing Accurel 2E HF-PP as the membrane support and replacing the strip solution once with fresh strippant.

Experiments were performed under standardized conditions in which the feed solutions initially contained  $4.98 \mu\text{g/ml}$  plutonium. In Fig. 2, the concentrations of plutonium in acid feed and dilute ascorbic acid strip phases are represented as a function of time. It can be seen that the plutonium species are still transported in the system through this membrane against a concentration gradient. Most strikingly, plutonium ions could actually diffuse 'uphill' from the feed to the product solution even though the complexed metal in the membrane diffused downhill. The plutonium concentration of the feed solution declined to less than  $1.9 \mu\text{g/ml}$  during 7 h permeation. On changing the receiving phase after 7 h with fresh strippant, plutonium concentration in the feed solution declined to less than  $0.6 \mu\text{g/ml}$ .

The life-time of the Accurel 2E HF-PP membranes, was evaluated by periodically measuring the plutonium flux under the optimum conditions. Before performing each new flux measurement, the feed and strip solutions were replaced with fresh ones. At the end of the permeation experiment, the ILM was left in contact with the depleted feed and plutonium loaded strip solution. No

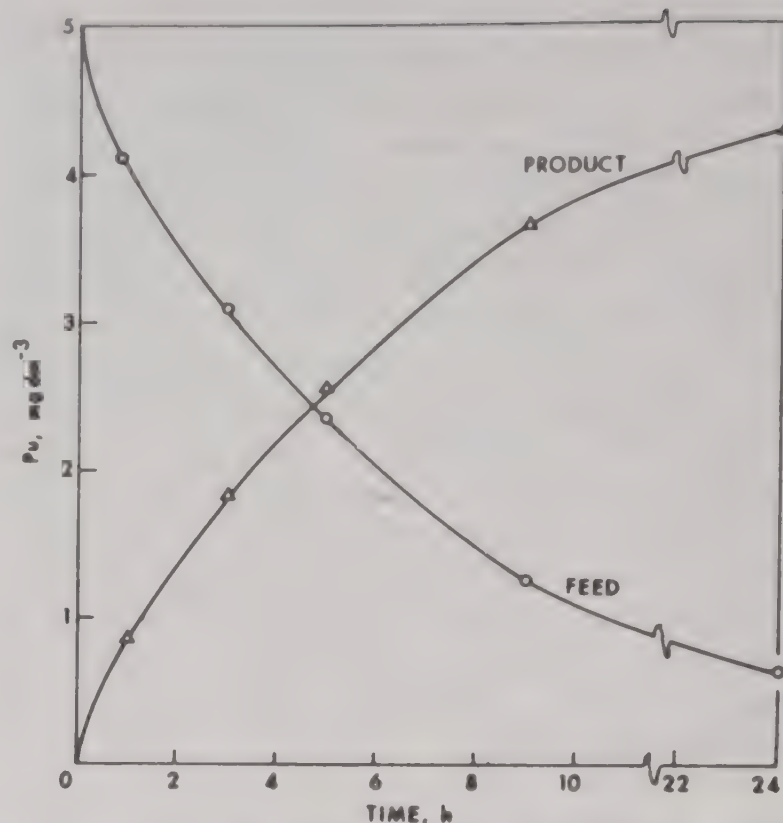


Fig. 2—Plot of [plutonium] in the feed and product solution versus time. [Feed solution =  $4.98 \mu\text{g/ml}$  plutonium, rest as in Fig. 1].

appreciable reduction of the plutonium flux was obtained when continuously operated even for seven days and thus this polymeric support can be used without any deterioration for at least a week's time.

#### Permeation of fission product through BLM and ILM

Permeation of some long-lived fission products such as Ce-144, Ru-106 and Cs-137 which often accompany plutonium was also tested. It was observed that no detectable amounts of these fission products permeated in the product side even after 24 h of operation. This was as expected since these fission products were almost inextractable by TBP/dodecane under similar conditions. Usually all fission products are trivalent metals which are not extractable in TBP. Feasibility of a moderately clean-cut separation of plutonium from some of the fission product contaminants is thus clearly established by this study.

The transport of  $\text{Pu}^{4+}$  by TBP involves the co-transport of  $\text{NO}_3^-$  anion. Maximum plutonium permeation through both the BLM and ILM membranes is attained with feed acidity of  $2 \text{ mol dm}^{-3} \text{ HNO}_3$  and 30% TBP in dodecane as the carrier. An aqueous ascorbic acid solution has been found to be the best strippant of those studied. Enrichment factors of the order of 6 or more are readily achieved by properly manipulating the feed:strip volume ratios. Applicability of both

BLM and ILM separation techniques for the processing of quite dilute ( $\mu\text{g/ml}$ ) plutonium nitrate solutions is convincingly demonstrated. Transport of several commonly associated long-lived fission product contaminants is minimal under similar conditions and hence, selective transport of  $\text{Pu}^{4+}$  is also expected.

### Acknowledgement

Thanks are due to Dr P R Natarajan, Head, Radiochemistry Div. and Dr R K Dhumwad, Head Lab. Section, F.R.D. for their keen interests in this work.

### References

- 1 Hudson M J, *Hydrometallurgy*, 9 (1982) 149.
- 2 Naylor A & Wilson P D, in *Handbook of solvent extraction*, edited by T C Lo, M H I Baird & C Hanson, (New Wiley Interscience) (1985) pp 783-798.
- 3 Danesi P R, Chiarizia R, Rickert P & Horwitz E P, *Sol Extr Ion Exch*, (1985) 3, 111.
- 4 McKibben J M, *Radiochimica Acta*, 3 (1984) 36.
- 5 Campbell D O & Burch W D, *J radiochem nucl Chem Art*, 303 (1990) 142.
- 6 Lamb J D, Bruening R L, Izatt R M, Hirashima Y, Tse P, Christensen J J, *J membr Sci*, 13 (1988) 37.
- 7 Chiarizia R, *J membr Sci*, 65 (1991) 55.
- 8 Ryan D E & Wheelright A W, *Report HW-55983*, U S Atomic Energy Comm, (1959).
- 9 Shukla J P & Misra S K, *National Symposium on Uranium Technology Bombay*, Dec 13-15 (1989).
- 10 Shukla J P & Misra S K, *J membr Sci*, 93 (1991) 64.
- 11 Korkisch J, *Modern methods for separation of rare metal ions*, (Univ of Vienna, Austria), p 144 (1969).
- 12 Babcock W C, Baker R W, Lachapelle E D & Smith K L, *J membr Sci*, 89 (1980) 7, 71.
- 13 Shukla J P, Kumar Anil & Singh R K, *Sep Sci & Tech* (in press).

## Molecular transport of binary liquid mixtures into EPDM and NBR membranes at 25°C

S B Harogoppad, T M Aminabhavi\* & R H Balundgi

Department of Chemistry, Karnatak University, Dharwad 580 003

Diffusion and sorption of several organic solvents and their binary mixtures in the whole scale of mixture composition have been studied at 25°C with NBR and EPDM rubber membranes. Diffusion results of single solvents as well as binary mixtures have been analysed to study their dependence on concentration of the probe molecules in rubber membranes.

Permselective membranes have tremendous applications in separation techniques and related areas. The molecular design of a permselective membrane is based on both sorption and diffusion phenomena. While extensive experimental and theoretical studies have been carried out on separation of gaseous mixtures<sup>1,2</sup>, relatively little has been published on separation of liquid mixtures using polymer membranes<sup>3-7</sup>. In this paper, transport data of binary solvent mixtures into NBR and EPDM membranes are presented. These membrane materials are chosen in view of their applications in several areas of science, engineering and technology wherein, they may come into contact with mixed organic liquid media. It is, therefore, useful to know how the polymer membranes would respond to the presence of such mixed solvent media. The conventional weight-gain experiments have been performed to measure sorption, diffusion and permeation of liquids through the selected membranes. However, no efforts are made to investigate the permselectivity; instead, details of molecular transport of mixed organic solvents have been considered.

### Materials and Methods

All the solvents were of reagent grade and purified before use. Binary mixtures were prepared by weighing the samples in airtight glass stoppered bottles. Refractive indices of the pure samples and their binary mixtures were measured at 25°C both before and after the sorption experiments.

NBR and EPDM samples were obtained from UTEX Industries, Weimer, Texas. The method of preparation of the polymer films and the elastomer compositions are described in our earlier papers<sup>8,9</sup>. The polymer sheets were cut into small circular pieces having a diameter of 1.94 cm with

thicknesses of 0.20-0.22 cm and weighing approximately 0.7 g. The sorption experiments were performed as per the procedures given earlier<sup>10,11</sup>.

### Results and Discussion

#### *Sorption kinetics of EPDM*

Typical sorption plots for EPDM with benzene + ethyl acetate and benzene + cyclohexane mixtures are given in Figs 1 and 2 while plots for NBR with benzene + carbon tetrachloride and benzene + methyl acetate mixtures are presented in Figs 3 and 4. As shown in Fig. 1, the sorption of benzene, ethyl acetate and their binary mixtures with EPDM increases linearly upto ~ 50% attainment of equilibrium. This is indicative of the Fickian sorption which should be expected because EPDM used is well above its glass transition temperature and thus, polymer chain segments respond almost instantaneously to the presence of penetrant molecules and their mixtures (i.e., benzene + ethyl acetate). The sorption of benzene is about eight times higher than that of ethyl acetate; however, their binary mixtures in the composition range from 0.2 to 0.8 mole fractions ( $x_1$ ) show intermediate values.

Sorption results of EPDM with benzene, cyclohexane and their mixtures are presented in Fig. 2. Here, the equilibrium sorption of cyclohexane is higher than that of benzene and this is attributed to the fast movement of the more flexible cyclohexane molecule than the more rigid, flat and sluggish movement of the benzene molecule. Surprisingly, mixtures containing 80%, 60% and 40% of cyclohexane have shown systematically higher sorption values as compared to pure cyclohexane. However, 20% cyclohexane-containing mixture

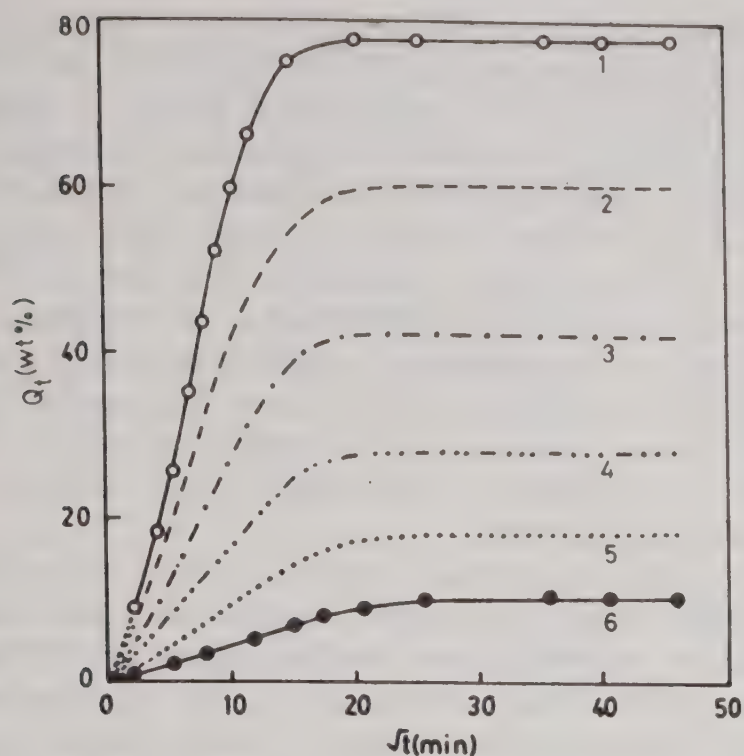


Fig. 1 - Sorption plots of EPDM with benzene + ethyl acetate mixtures at 25°C. 1, (O) Benzene; 2, (---) 80% benzene; 3, (-·-) 60% benzene; 4, (····) 40% benzene; 5, (-··) 20% benzene; 6, (●) ethyl acetate

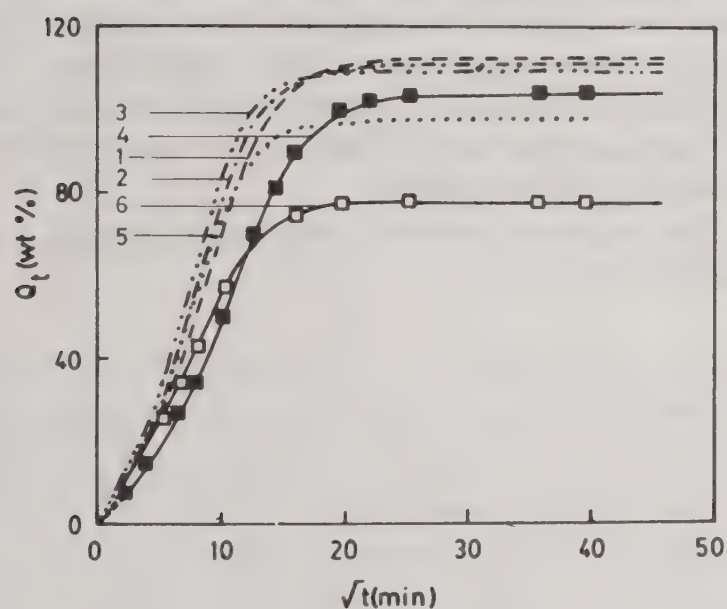


Fig. 2 - Sorption plots of EPDM with benzene + cyclohexane mixtures at 25°C. 6, (□) benzene; 4, (■) cyclohexane; 5, (····) 20% cyclohexane; 3, (-·-) 40% cyclohexane; 2, (-··) 60% cyclohexane; 1, (---) 80% cyclohexane.

exhibits an intermediate value of equilibrium sorption. The enhanced sorption rates of mixtures of cyclohexane and benzene may be attributed to the change in solvent power of the mixtures at these compositions due to specific interactions. Additionally, benzene + cyclohexane mixture exhibits a non-Fickian diffusive transport mechanism as evidenced by the slight sigmoidal shapes of the  $Q_t$  versus  $t^{1/2}$  curves.

Sorption results of EPDM with carbon tetrachloride

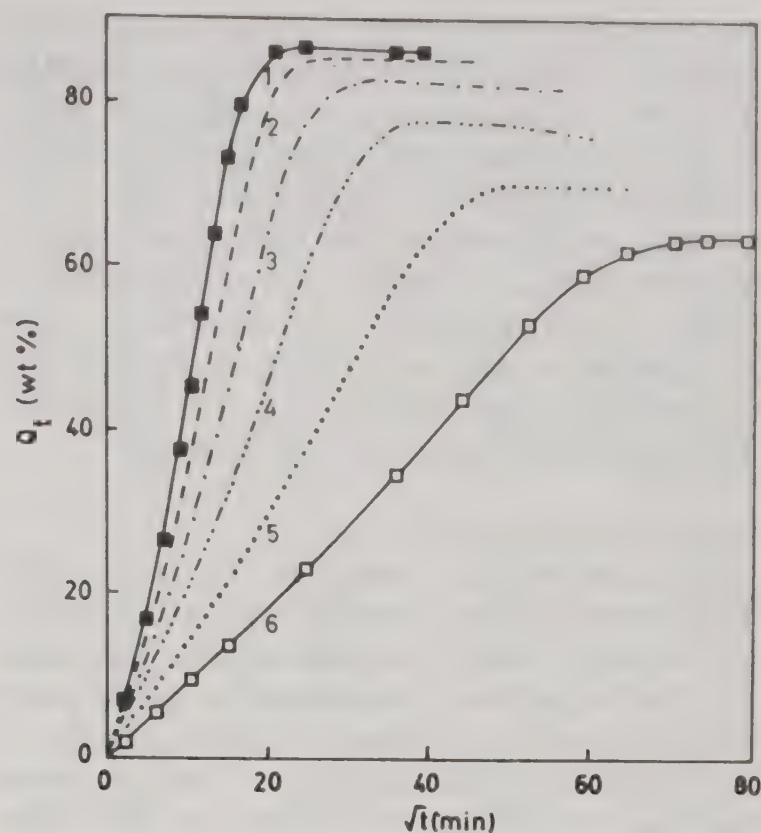


Fig. 3 - Sorption plots of NBR with benzene + carbon tetrachloride mixtures at 25°C. 1, (■) benzene; 6, (□) carbon tetrachloride; 5, (····) 20% benzene; 4, (-·-) 40% benzene; 3, (-··) 60% benzene; 2, (---) 80% benzene.

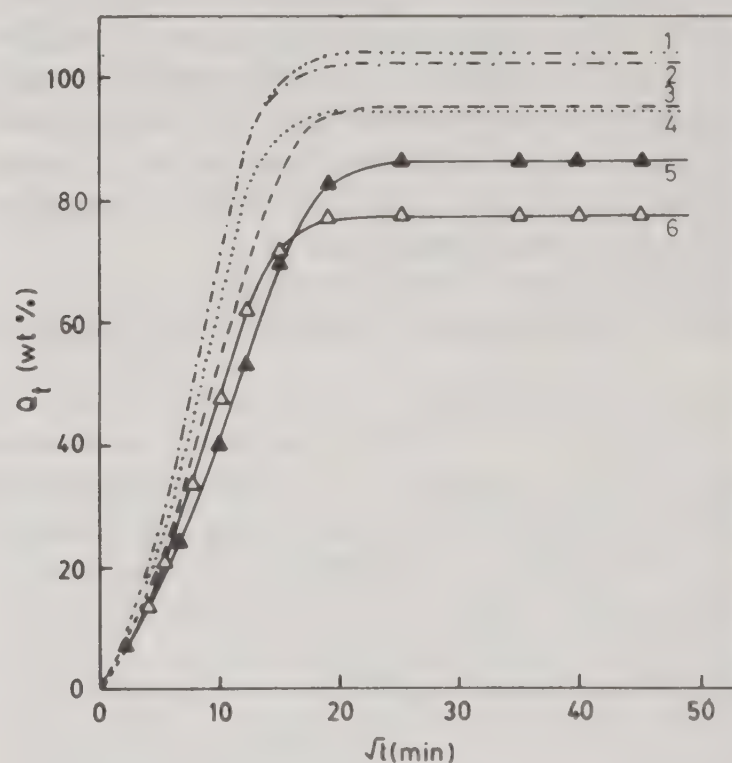


Fig. 4 - Sorption plots of NBR with benzene + methyl acetate mixtures at 25°C. 6, (Δ) Methyl acetate; 5, (▲) benzene; 4, (····) 20% benzene; 3, (-·-) 80% benzene; 2, (-··) 60% benzene; 1, (---) 40% benzene

loride, benzene and their mixtures are not presented graphically. However, it may be observed from the data given in Table 1 that sorption of carbon tetrachloride is about two times higher than that of benzene, but their binary mixtures

show sorption data which are in between pure components of the mixture as expected. The sorption results of the mixtures of carbon tetrachloride and cyclohexane are intermediate to those of their pure components; these systems show similar trends as observed in case of benzene and carbon tetrachloride mixtures. The behaviour of EPDM in the presence of mixtures of benzene + methyl acetate is identical to that of benzene + ethyl acetate mixture, but the magnitudes of the sorption data are somewhat different.

#### Sorption kinetics of NBR

The sorption data shown in Fig. 3 for NBR with benzene, carbon tetrachloride and their binary mixtures exhibit sorption kinetic behaviour typical of sorption of insignificant swelling penetrants in a rubbery polymer. A linear uptake of the penetrants as a function of  $t^{1/2}$  was observed in all cases and the sorption curves for the binary mixtures of different compositions lie in between those of pure components comprising the mixed-solvent system. The sorption process is controlled by the relaxation rate which is very slow in comparison to the rate of concurrent diffusion process. Attainment of equilibrium sorption was quicker with benzene than with carbon tetrachloride. This is ascribed to a concentration increase of benzene in the central core of the polymer membrane which might have resulted in accelerated relaxation of the chain and thereby increasing the sorption rate at longer times.

Figure 4 shows the dependence of  $Q_t$  on  $t^{1/2}$  for NBR with benzene, methyl acetate and their

mixtures. The sorptions of benzene and methyl acetate are not widely different; however, sorption of mixtures of benzene + methyl acetate is higher than either of the pure components. A similar situation exists for NBR with benzene, ethyl acetate and their binary mixtures; however, this dependence is not shown graphically. The sorption results of other binary mixtures may be explained in terms of the established solubility parameter concepts<sup>12</sup>. According to this theory, the smaller the difference between the solubility parameters of the two components, the larger is the solubility in the binary mixture.

A similar approach has also been attempted earlier<sup>13</sup>. Benzene, carbon tetrachloride and ethyl acetate are well known swelling agents for EPDM and NBR, while methyl acetate and cyclohexane act as non-solvents. In case of ethyl acetate + carbon tetrachloride mixture, a different behaviour may be expected as these solvents show mutual dipole-induced-dipole interactions on account of their respective electron donating and accepting characters<sup>14</sup>. However, in case of benzene + cyclohexane and benzene + carbon tetrachloride mixtures no specific interactions are present and hence, these might not cause deviations. The sorption coefficients  $S$ , expressed in weight percent are summarised in Table 1 for all the polymer-mixed solvent systems.

The sorption results have been further analysed<sup>10,11</sup> by Eq. (1),

$$Q_t/Q_\infty = K t^n \quad \dots (1)$$

Table 1 – Sorption ( $S$ ) data for elastomers + binary mixture systems at 25°C  
 $S$  (Wt%) for different mole fractions ( $x_1$ ) of the first named component

Binary mixtures	$x_1 = 0$	0.2	0.4	0.6	0.8	1.00
EPDM						
$C_6H_6 + C_6H_{12}$	104.13	113.14	111.22	110.30	98.14	77.54
$C_6H_6 + CCl_4$	215.11	192.44	161.57	137.93	105.68	77.75
$C_6H_6 + MeAc$	7.08	14.94	26.36	44.81	66.26	87.26 <sup>(a)</sup>
$C_6H_6 + EtAc$	10.26	18.08	28.14	42.29	59.98	77.77
$CCl_4 + C_6H_{12}$	108.34	130.33	154.55	175.97	200.42	219.77
NBR						
$C_6H_6 + CCl_4$	63.71	69.89	76.56	81.80	85.12	86.13
$C_6H_6 + MeAc$	76.82	95.02	104.30	102.58	95.83	86.60
$C_6H_6 + EtAc$	73.22	82.64	90.14	92.99	92.39	85.32

<sup>(a)</sup> refers to EPDM used in refs 8 & 9.

Table 2 – Sorption data for elastomers + binary mixtures at 25°C

Binary mixtures	Parameters	Mole fraction ( $x_1$ ) of first named component of the mixture					
		$x_1 = 0$	0.2	0.4	0.6	0.8	1.00
EPDM							
$C_6H_6 + C_6H_{12}$	$K \times 10^2$	2.09	2.74	3.36	3.55	3.43	3.14
	n	0.66	0.65	0.63	0.65	0.66	0.61
$C_6H_6 + CCl_4$	$K \times 10^2$	2.24	2.64	3.00	3.25	3.85	3.90
	n	0.66	0.65	0.64	0.64	0.61	0.63
$C_6H_6 + MeAc$	$K \times 10^2$	3.54	4.26	4.52	4.46	3.93	4.38
	n	0.51	0.52	0.55	0.54	0.59	0.59
$C_6H_6 + EtAc$	$K \times 10^2$	3.90	3.85	5.12	4.81	5.45	4.16
	n	0.52	0.56	0.52	0.55	0.53	0.61
$CCl_4 + C_6H_{12}$	$K \times 10^2$	2.21	2.27	2.25	2.35	2.28	2.34
	n	0.66	0.65	0.66	0.66	0.66	0.65
NBR							
$C_6H_6 + CCl_4$	$K \times 10^2$	1.08	1.35	2.12	2.20	2.37	2.93
	n	0.55	0.57	0.55	0.58	0.61	0.60
$C_6H_6 + MeAc$	$K \times 10^2$	3.25	3.30	3.20	3.21	2.97	2.74
	n	0.63	0.63	0.64	0.63	0.62	0.61
$C_6H_6 + EtAc$	$K \times 10^2$	2.81	2.45	2.72	2.69	2.75	2.65
	n	0.61	0.64	0.63	0.63	0.62	0.63

(a)  $K$  is expressed in  $g/g \cdot min^n$ .

where  $Q_\infty$  is equilibrium sorption coefficient. The least-squares estimations of  $K$  and  $n$  are given in Table 2. For majority of polymer-mixed solvent systems, the values of  $n$  vary in the range 0.60–0.66 suggesting the presence of anomalous diffusive transport. This enigma is also supported by the slight sigmoidal shapes of the sorption curves for these systems. In case of EPDM with benzene + ethyl acetate mixtures (Fig. 1) and for NBR with benzene + carbon tetrachloride mixture, (Fig. 3), the values of  $n$  vary from 0.50 to 0.60 suggesting that the diffusive transport in these systems closely resemble the Fickian mode. This is particularly obvious from the sorption data presented in Fig. 1 for EPDM with benzene + ethyl acetate mixtures. It is seen that the  $K$  values of Eq. (1) do not show any systematic effect on the polymer-penetrant interactions.

#### Diffusion behaviour

Diffusion coefficients were calculated from the initial linear portions of the sorption curves<sup>15</sup> as shown by Eq. (2),

$$D = \pi \left[ \frac{h\theta}{4Q_\infty} \right]^2 \quad \dots (2)$$

where  $h$  is polymer sample thickness and  $\theta$  is the slope of the linear part of  $Q_t$  versus  $t^{1/2}$  plots. These data are summarised in Table 3. The results of  $D$  and  $S$  for all the binary mixtures as a function of mole fraction are plotted in Fig. 5 (a, b, c and d) and Fig. 6(d) for EPDM and in Fig. 6 (a, b, and c) for NBR.

For EPDM with benzene + ethyl acetate mixture (Fig. 5(a)),  $D$  varies linearly with mixture compositions whereas,  $S$  varies in a slight concave manner. However, with benzene + methyl acetate mixture,  $D$  varies in a convex manner while  $S$  varies with a concave shape (Fig. 5(b)). On the other hand, mixtures of cyclohexane + carbon tetrachloride with EPDM show quite different tendencies i.e.,  $S$  varies linearly while  $D$  varies in a sinusoidal manner (Fig. 5(c)). The diffusion behaviour of benzene + cyclohexane mixture is quite different

Table 3 – Diffusivity (D) for elastomers + binary mixture systems at 25°C

D × 10<sup>7</sup> (cm<sup>2</sup>/s) for different mole fractions (x<sub>1</sub>) of the first named component

Binary mixtures	x <sub>1</sub> = 0	0.2	0.4	0.6	0.8	1.00
<b>EPDM</b>						
C <sub>6</sub> H <sub>6</sub> + C <sub>6</sub> H <sub>12</sub>	3.547	4.520	5.267	6.483	6.807	6.664
C <sub>6</sub> H <sub>6</sub> + CCl <sub>4</sub>	4.207	4.745	5.285	5.958	6.355	7.420
C <sub>6</sub> H <sub>6</sub> + MeAc	2.142	3.694	5.115	5.535	6.411	6.724
C <sub>6</sub> H <sub>6</sub> + EtAc	2.570	3.892	4.231	5.270	5.681	6.781
CCl <sub>4</sub> + C <sub>6</sub> H <sub>12</sub>	3.489	3.609	3.912	3.640	3.548	3.782
<b>NBR</b>						
C <sub>6</sub> H <sub>6</sub> + CCl <sub>4</sub>	0.315	0.661	1.207	1.866	2.692	3.521
C <sub>6</sub> H <sub>6</sub> + MeAc	5.222	5.935	6.002	5.158	4.380	3.527
C <sub>6</sub> H <sub>6</sub> + EtAc	3.745	4.271	4.198	4.250	4.207	4.135

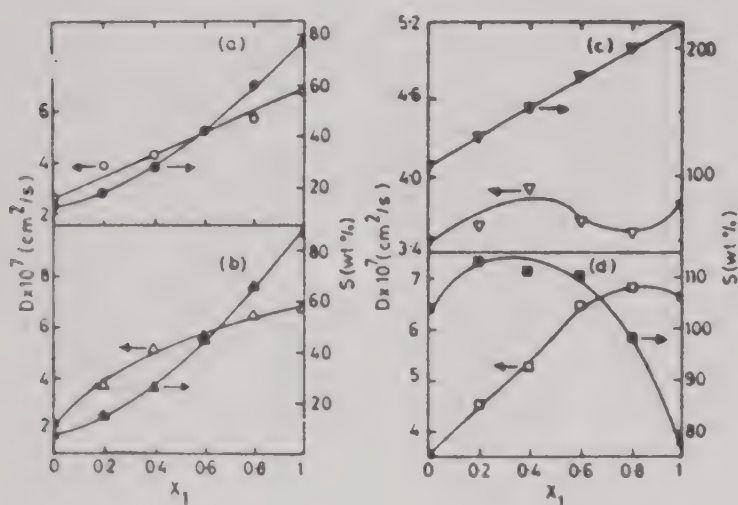


Fig. 5 – Dependence of diffusion coefficients, D, and sorption coefficients S, on mole fraction of the first component in the mixture at 25°C. (a) (○) and (●) EPDM with benzene + ethyl acetate mixtures. (b) (△) and (▲) EPDM with benzene + methyl acetate (c) (▽) and (▼) EPDM with cyclohexane + carbon tetrachloride mixtures. (d) (□) and (■) EPDM with benzene + cyclohexane mixtures.

from other systems in that both the curves (D or S versus x<sub>1</sub>) exhibit a maxima (Fig. 5(d)).

For EPDM with benzene + carbon tetrachloride mixture, the dependence of both D and S on x<sub>1</sub> is almost linear (Fig. 6(d)). Similarly, for NBR with benzene + methyl acetate mixture, we could observe pronounced maxima for both D and S around the middle of the mixture composition (Fig. 6(b)). However, this is not true in case of NBR with benzene + ethyl acetate mixtures (see Fig. 6(a)); here, S exhibits a slight maximum whereas, D is almost independent of the mixture composition. On the other hand, for NBR with benzene and carbon tetrachloride mixture, the de-

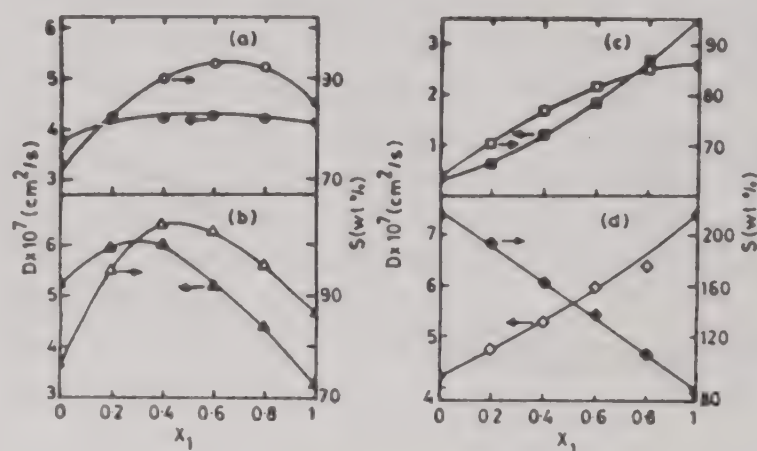


Fig. 6 – Dependence of diffusion coefficients D, and sorption coefficients S, on mole fraction of the first component in the mixture at 25°C. (a) (○) and (●) NBR with benzene + ethyl acetate mixtures. (b) (△) and (▲) NBR with benzene + methyl acetate mixtures. (c) (□) and (■) NBR with benzene + carbon tetrachloride mixtures. (d) (◇) and (◆) EPDM with benzene + carbon tetrachloride mixtures.

pendence of D and S are non-linear over the entire mole fraction range (Fig. 6(c)). While we cannot advance quantitative arguments for the shapes of curves of D or S versus x<sub>1</sub> their shapes appear to be mainly dominated by the type of specific interactions between the components of the mixtures. In each case, D initially increases with concentration, reaches a maximum, and then drops off.

To investigate details about the concentration dependence of diffusivity, we have estimated D values at different intervals from the original sorption curves by using the procedure of Joshi and Astarita<sup>16</sup>. These results are typically present-

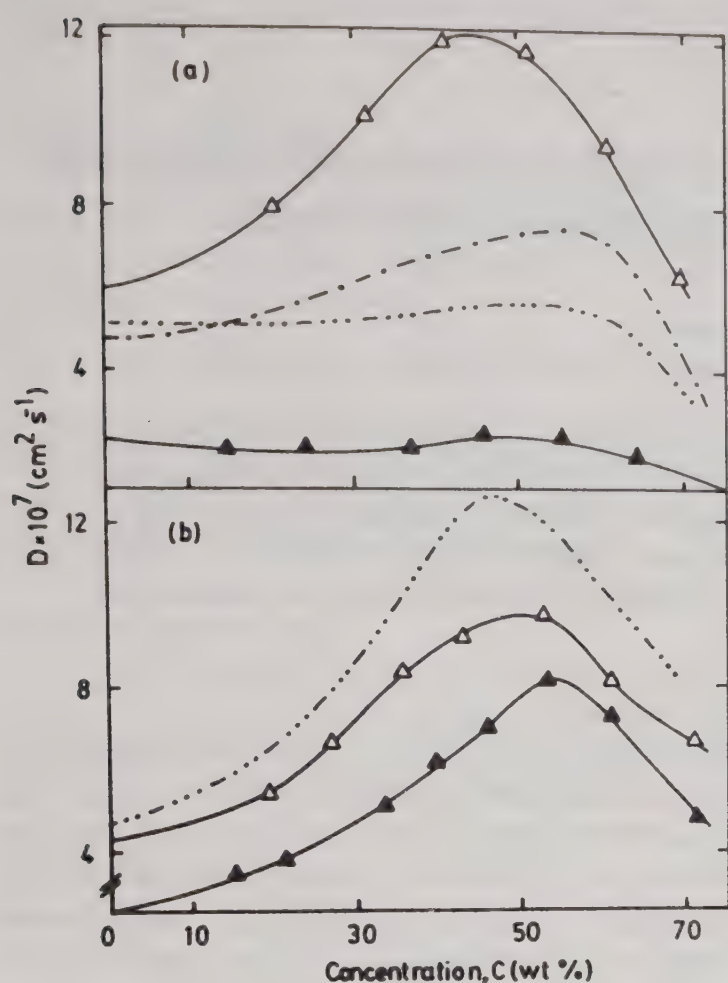


Fig. 7—Dependence of diffusion coefficient  $D$ , on concentration at 25°C. (a) EPDM with benzene+methyl acetate mixtures. Symbols: ( $\Delta$ ) benzene; ( $-\cdot-\cdot-$ ) 60% benzene; ( $-\cdots-$ ) 40% benzene; ( $\blacktriangle$ ) methyl acetate. (b) NBR with benzene+methyl acetate mixtures. Symbols: ( $\blacktriangle$ ) benzene; ( $\Delta$ ) methyl acetate; ( $-\cdots-$ ) 40% benzene.

ed for EPDM and NBR membranes with benzene+methyl acetate mixtures (Fig. 7). For EPDM+methyl acetate,  $D$  does not vary considerably because methyl acetate did not show significant swelling for EPDM. However, with benzene, we observe a sharp maximum in  $D$  versus concentration plot which tends to decrease with an increase in concentration of methyl acetate in the binary mixture. On the other hand, when NBR is considered in the presence of benzene+methyl acetate mixture (each of these liquids have considerable swelling tendencies towards NBR), a sharp maximum is observed suggesting significant concentration dependence of diffusivity for these systems. Their binary mixtures, however, show considerable dependence of  $D$  on concentration as the maximum peak for

40% benzene-containing mixture is somewhat sharper than either of the pure components, namely, benzene or methyl acetate.

In this study, it was observed that: (i) the sorption kinetics change progressively from Fickian to non-Fickian as a function of mixture composition and depends on the size of the penetrant molecule; (ii) the sorption behaviour can be explained by a consideration of the rates of diffusion and molecular relaxation processes; (iii) molecular transport of mixed solvent media follow the same pattern as those of pure components suggesting that in mixtures, the molecules move as a single unit and preferential sorption may be operative, though its effect is not really significant; (iv) perhaps other spectroscopic methods such as laser interferometry, NMR-imaging, etc., can be used in conjunction with the present gravimetric technique to study solvent diffusion rates into these polymeric systems.

## References

- 1 Aithal U S & Aminabhavi T M, *J macromol Sci Revs Macromol Chem Phys*, C31 (1991) 117.
- 2 Aithal U S, Aminabhavi T M, Balundgi R H & Shukla S S, *Polym Plastics Technol Eng*, 30 (1991) 299.
- 3 Park G S & Ruckenstein E, *J appl polym Sci*, 38 (1989) 453.
- 4 Suzuki F, Onozato K, Yaegashi H & Masuko T, *J appl polym Sci*, 34 (1987) 2197.
- 5 Suzuki F & Onozato K, *J appl polym Sci*, 27 (1982) 4229.
- 6 Barrer R M, *Proc Phys Soc*, 58 (1946) 321.
- 7 Kanamaru K & Sugiura M, *Kolloid Z Polym*, 194 (1964) 110.
- 8 Cassidy P E, Aminabhavi T M & Brunson J C, *Rubber Chem Technol*, 56 (1983) 357.
- 9 Aminabhavi T M, Manjeshwar L S & Cassidy P E, *J appl polym Sci*, 32 (1986) 3719.
- 10 Aithal U S, Aminabhavi T M & Cassidy P E, *Am chem Soc Symp, Ser No. 423, Barrier polymers and structures*, edited by W J Koros, 351 (1990), Ch. 19.
- 11 Harogoppad S B & Aminabhavi T M, *Macromolecules*, 24 (1991) 2598.
- 12 Hildebrand J H & Scott R L, *Solubility of nonelectrolytes*, 3rd Edn (Reinhold, New York), 1950.
- 13 Froehling P E, Koenhen D M, Bantjes A & Smolders C A, *Polymer*, 17 (1976) 835.
- 14 McClellan A & Pimental G, *The hydrogen bond*, (Freeman, San Francisco), 1960.
- 15 Crank J, *The mathematics of diffusion*, (Clarendon Press, Oxford), 1975.
- 16 Joshi S & Astarita G, *Polymer*, 20 (1979) 455.

## Permeability properties of polyelectrolyte complexes from carboxymethyl-cellulose and poly(2-vinyl-N-methylpyridinium iodide)

B Vishalakshi & V Kalpagam\*

Department of Inorganic and Physical Chemistry, Indian Institute of Science, Bangalore 560 012, India

Polyelectrolyte complexes between carboxymethylcellulose and poly(2-vinyl-N-methylpyridinium iodide) have been studied. The polycation of two different degrees of substitution was used to make complex precipitates that differ in the stoichiometry. The diffusive permeability of KCl and urea through the solution cast membranes of these complex precipitates has been studied. The polyelectrolyte complex membrane containing the polycation of higher degree of substitution has been found to possess good membrane properties.

Polyelectrolyte complexes formed by the ionic interaction between oppositely charged polyelectrolytes have been studied during the past three decades<sup>1-3</sup>. They possess a wide range of physical and chemical properties and have useful applications. The high permeability of these ionic hydrogels to water and other microsolutes which can be altered by controlling their charge content make these ionic hydrogels good candidates for membrane applications<sup>4</sup>. The investigations on the membrane behaviour of polyelectrolyte complexes containing polysaccharides has attracted less attention. Some of them are reported to have selective transport and controllable permeability<sup>5</sup>. In the present paper, polyelectrolyte complexes made from carboxymethylcellulose (CMC) and poly(2-vinyl-N-methylpyridinium iodide) (PC) have been studied. The effect of the degree of substitution (DS) of the polycation (PC) on the stoichiometry of the complex, preparation of the membranes and permeability of two low molecular weight solutes namely KCl and urea through these membranes have been discussed.

### Materials and Methods

Sodium carboxymethylcellulose (BDH) was used as such. The molecular weight ( $\bar{M}_v$ ) was determined<sup>6</sup> to be  $4.3 \times 10^5$ . The degree of substitution was found to be 0.73 by the acid wash method<sup>7</sup>. 2-Vinylpyridine (2VP) (Merck) was distilled twice under low pressure and was bulk polymerised at 60°C using AIBN initiator to obtain poly(2-vinylpyridine) (P2VP)<sup>8</sup>. The high molecular weight fraction was separated by fractionation using benzene-hexane solvent pair<sup>9</sup>. The molecular weight of this fraction was estimated to be  $4.86 \times 10^5$  by viscometry<sup>10</sup>. Poly(2-vinyl-N-methylpyridinium iodide) of low degree of substitution (PC-30) was prepared by reflux-

ing the solution of P2VP (1 g, 9.52 mmol) in methanol (5%, 20 ml) with methyl iodide (2 ml, 31.9 mmol) at room temperature for 24 hr. The product was recovered by vacuum evaporation from excess of the reagent and was purified by precipitation from methanol in diethylether. The pale yellow solid obtained was dried at 50°C under low pressure. The degree of quaternization was determined from Volhard's method of estimation of iodide using silver nitrate and was found to be 0.31. Poly(2-vinyl-N-methylpyridinium iodide) of high degree of substitution (PC-70) was prepared by heating the solution of P2VP (1 g, 9.52 mmol) in nitromethane (5%, 20 ml) with methyl iodide (3.6 ml, 57.6 mmol) at 50°C for 72 hr<sup>11</sup>. The product was separated by vacuum evaporation and was washed with ether. The deep yellow precipitate obtained was dried at 50°C under low pressure. The degree of quaternization was 0.71.

### Complex formation and measurements

The PEC precipitates (PEC-30 & PEC-70) were obtained by the direct addition of PC-30 and PC-70 solutions ( $0.01 \text{ mol dm}^{-3}$ ), respectively, to CMC ( $0.01 \text{ mol dm}^{-3}$ ) solution. The precipitates obtained were washed with distilled water to remove all the microions and were dissolved in formic acid. Membranes were cast from formic acid solution on glass plates and were analysed by IR spectroscopy (Hitachi 270-50). The characteristic IR bands were  $1632 \text{ cm}^{-1}$ ,  $1596 \text{ cm}^{-1}$  and  $1065 \text{ cm}^{-1}$ . The electron micrographs of gold coated PEC precipitates were recorded using the scanning electron microscope (JSM-840A).

For diffusion experiments, filter paper circles (Whatman No. 1) were coated with the formic acid solution of PEC-70 and PEC-30 and dried. They

are designated as coated PEC-70 and coated PEC-30.

#### Swelling measurements

The PEC-70 and PEC-30 membranes were equilibrated in distilled water and the equilibrium water content was calculated using Eq. (1), after blotting the surface with a filter paper.

$$\text{H}_2\text{O content (\%)} = (W_s - W_d)/W_s \times 100 \quad \dots (1)$$

where  $W_s$  = weight of the swollen sample and  $W_d$  = weight of the dry sample. Similarly, the swelling capacity of the films in KCl ( $0.09 \text{ mol dm}^{-3}$ ) and urea ( $0.9 \text{ mol dm}^{-3}$ ) was also measured.

#### Diffusion experiments

A two-chambered horizontal diffusion cell made of glass was used. The membrane holder had an inner diameter of 2.1 cm. The coated filter papers were washed with water and the swollen membranes were fixed in between the two chambers using rubber gaskets. KCl ( $0.09 \text{ mol dm}^{-3}$ ) or urea ( $0.9 \text{ mol dm}^{-3}$ ) (34 ml each) was introduced in the left hand chamber and equal amount of distilled water was taken in the right hand chamber. The cell was placed in the thermostat at  $30 \pm 0.2^\circ\text{C}$ . Efficient stirring was achieved by bubbling air through the solution. From each chamber, 0.1 ml of the solution was withdrawn and the change in concentration was measured at various time intervals. The concentration of KCl was determined by the estimation of  $\text{K}^+$  using atomic absorption spectroscopy (Perkin-Elmer-2380). Concentration of urea was measured spectroscopically by the *p*-dimethylaminobenzaldehyde method<sup>12</sup> (Hitachi U3400 UV-spectrophotometer).

#### Equilibrium sorption

The partition coefficient,  $K$ , which is defined<sup>13</sup> as the ratio of the salt concentration in the membrane,  $C_{in}$ , to that in the outer solution,  $C_{ex}$ , was determined for KCl ( $0.09 \text{ mol dm}^{-3}$ ) and urea ( $0.9 \text{ mol dm}^{-3}$ ) by desorption. The concentration of the solutes was determined as before and was expressed in ppm.

#### Results and Discussion

On addition of PC ( $0.01 \text{ mol dm}^{-3}$ ) solution to the polyanion (PA) ( $0.01 \text{ mol dm}^{-3}$ ) solution, turbidity developed which increased in intensity with the progress of the titration. At a certain point, there was sudden coagulation of the precipitate which was taken as the end point of the titration. The ratio of PA to PC at the equivalence point was found to depend on the DS of the PC. Earlier it was reported that, the stoichiometry of the complex is independ-

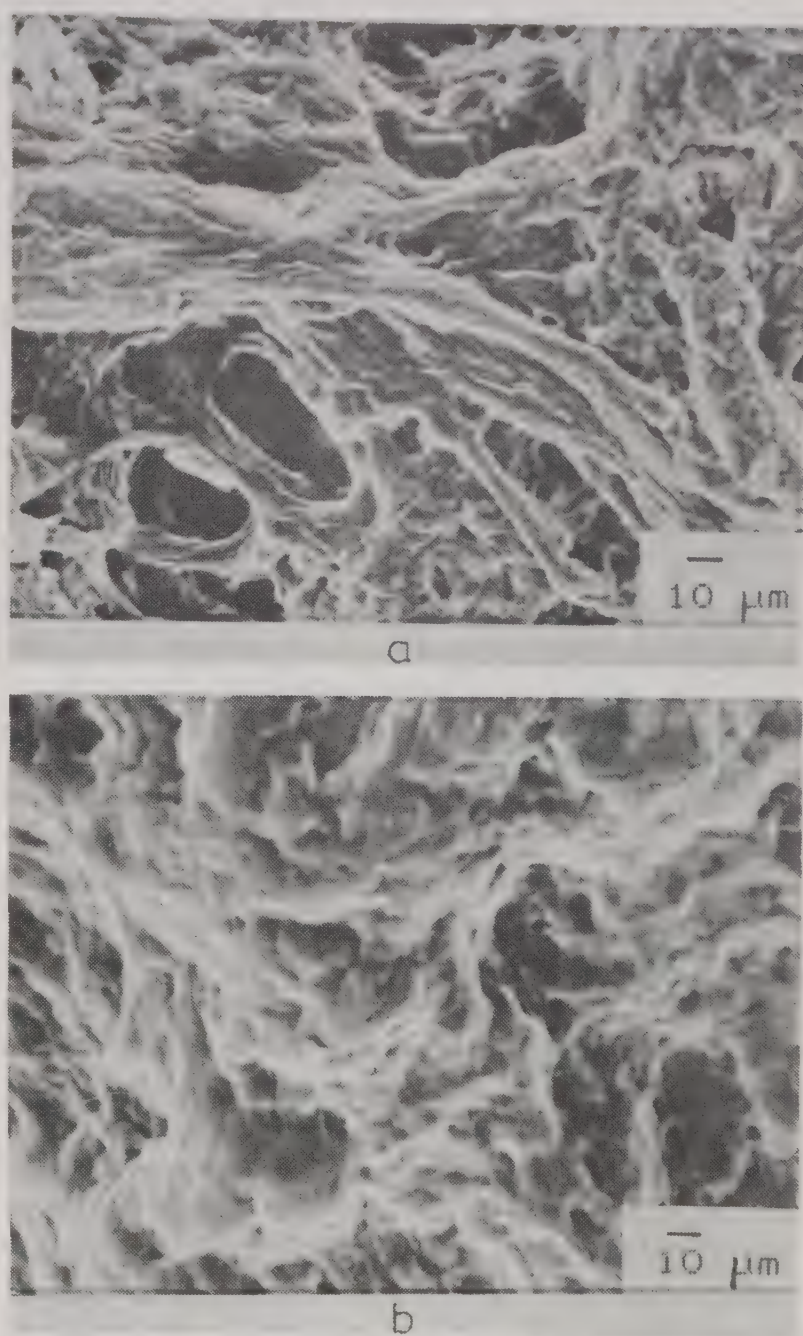


Fig. 1—Scanning electron micrographs of PEC precipitates [(a) PEC-70 ( $\times 500$ ), (b) PEC-30 ( $\times 500$ )]

ent of the DS of the PA<sup>14</sup>. We have determined the ratio of PA/PC in PEC-70 and PEC-30 to be 0.86 and 1.1 respectively. Since more than equivalent amount of PC solution is used up in making PEC-70, the precipitate and the membrane cast from it are expected to have excess positive charges in them. In a similar way, PEC-30 possesses excess negative charges on it.

The electron micrographs of the complex precipitates show that PEC-70 (Fig. 1a) is more compact in structure as compared to PEC-30 (Fig. 1b). This observation confirms the fact that in PEC-70, the neutralisation of charges takes place in a more orderly manner whereas in PEC-30, the random interchain neutralisation gives rise to a less compact structure. This difference in structure of the two PECs is expected to affect properties such as absorption of water, electrolytic behaviour and permeability.

The swelling parameters of the PEC films along with the partition coefficients are reported in Table

Table 1—Swellability ( $S$ ), partition coefficient ( $K$ ) of PEC membranes & permeability coefficients ( $P$  &  $P_s$ ) for the diffusion of KCl & urea through the PEC coated membranes

	$S$ (% w/w)		$K$		$P_s \times 10^3$ ( $\text{g cm}^{-1} \text{h}^{-1}$ )	
	PEC-70	PEC-30	PEC-70	PEC-30	PEC-70	PEC-30
Water	90.2	94.5	—	—	—	—
KCl ( $0.09 \text{ mol dm}^{-3}$ )	82.7	83.6	2.5	3.2	3.4 (19.4)	2.4 (14.4)
Urea ( $0.9 \text{ mol dm}^{-3}$ )	85.4	95	1.1	0.6	1.6 (11.0)	1.8 (37.0)

$\dagger P_s$  values are given in parenthesis.

1. The permeability coefficients,  $P$ , ( $\text{g cm}^{-1} \text{hr}^{-1}$ ) for the diffusion of KCl and urea has been calculated using the following equation derived from Fick's law of diffusion<sup>15</sup>.

$$\ln [C_0/(C_0 - 2C_t)] = 2PA_t/xV \quad \dots (2)$$

where  $C_0$  is the concentration of the solute taken initially in the left hand chamber,  $C_t$  is the concentration of the permeant in the right hand chamber at time  $t$ ,  $A$  is the area of the membrane exposed to diffusion,  $V$  is the volume of each cell and  $x$  is the amount of the polymer material deposited per unit area of the filter paper. A slight modification has been done in the original equation—instead of thickness of the membrane, the quantity  $x$  which is proportional to the thickness has been considered. This has been done due to the difficulty involved in measuring the thickness of the swollen films. The plot of  $\ln [C_0/(C_0 - 2C_t)]$  as a function of time,  $t$ , is given in Fig. 2. The values of  $P$  calculated from the slopes of the straight lines are reported in Table 1. The permeability coefficient has also been calculated considering  $x$  as the weight of the deposited polymer when swollen with the permeant per unit area of the filter paper. It has been designated as  $P_s$  and reported in Table 1, in parentheses. The former value of the permeability coefficient,  $P$ , defined in this paper is characteristic of the chemical nature of the polymer material and is independent of the change in the thickness of the membrane on swelling whereas  $P_s$  includes the effect of the change in the free volume of the material on swelling.

The swelling capacity of PEC-30 for water and the two permeant solutes studied is more than that of PEC-70 due to the less compact structure. The ionic content per repeating unit of PC-70 is more than that in PC-30. Hence the total amount of CMC units present in PEC-70 is more than that in PEC-30. PC-30, due to its low degree of substitution contains more number of uncharged pyridine units. The excess charge content in PEC-30 might be even lesser than that expected from the stoichiometry as

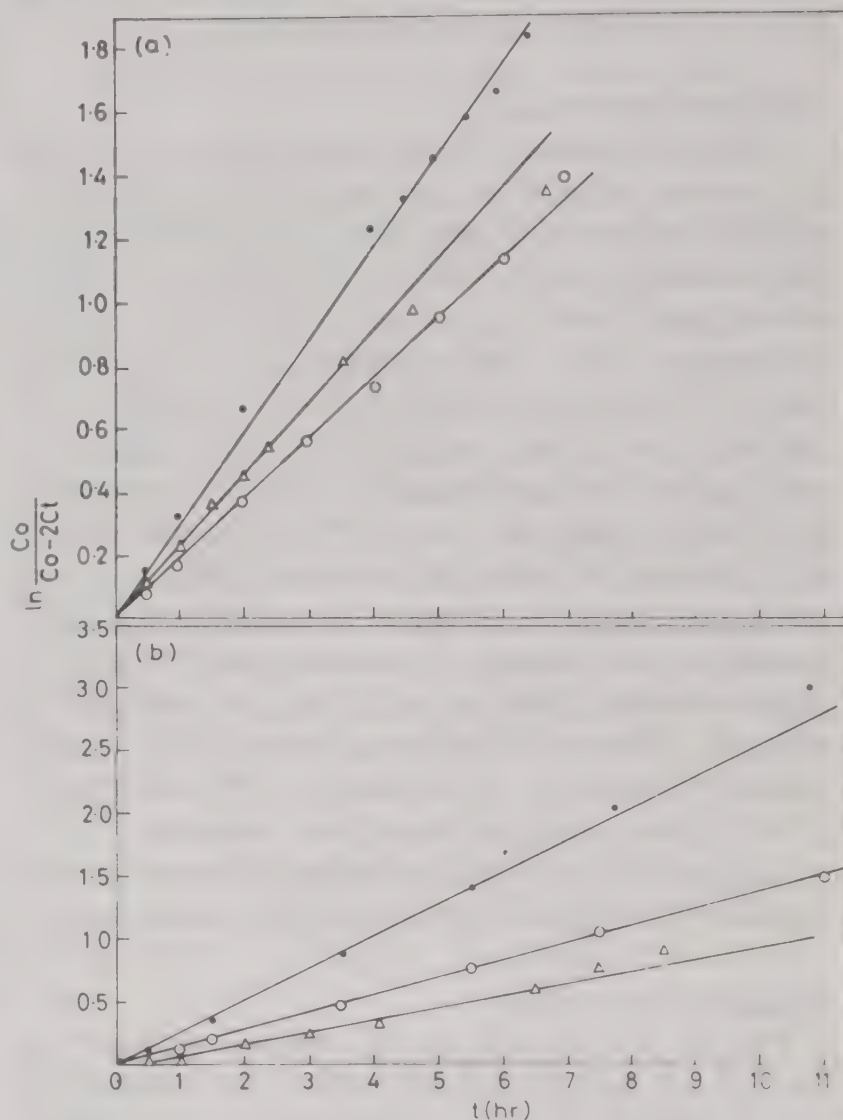


Fig. 2—Relation between  $\ln [C_0/(C_0 - 2C_t)]$  and measurement time for diffusion of (a) KCl, (b) urea [(●) Uncoated filter paper, (Δ) coated PEC-70, (○) coated PEC-30].

the excess  $-\text{COOH}$  can protonate the free pyridine units. The partition coefficients reported in Table 1 can be explained on the basis of the amount of charge and the CMC content of the PEC precipitates. KCl, an ionic solute, is less absorbed on PEC-70 as compared to PEC-30 because of the higher charge content of PEC-70. The value of  $K$  for the nonionic solute, urea is higher in PEC-70 than in PEC-30. This might be due to the higher cellulose content of PEC-70, which has an affinity for urea due to the possibility of hydrogen bond formation.

The effect of the electrostatic interaction and the contribution from the free volume on swelling to the diffusion can be seen by comparing the  $P$  and  $P_s$  values reported in Table 1. The high  $P_s$  value for urea in PEC-30 membrane shows that the permeability of a non-ionic solute is determined mainly by the free volume of the material available for diffusion which is high for PEC-30 due to its higher swelling capacity. The  $P_s$  values for KCl in the two PEC membranes is comparable as the swelling nature is not the only factor affecting its permeability. The comparison of the  $P$  values for the diffusion of KCl and urea shows that the chemical nature of the membrane contributes more towards the permeability in the case of the ionic solute due to the electrostatic interaction between the permeant and the membrane material. Diffusion of urea is little affected by the chemical nature of the membrane.

It can be concluded that the positively charged PEC-70 has better permeability for KCl and comparable permeability for urea, in spite of its compact structure. It has proved to be a better membrane material as it retains its structural stability.

Many of the polyelectrolytes made of synthetic polymers have shown good antithrombogenic character and suppress the coagulation of blood<sup>16</sup>. PECs from CMC are also reported to have good blood compatible property<sup>17</sup>. Hence, the presently studied materials involving CMC as one of the components might prove promising materials for biomedical applications such as dialysis membranes.

### Acknowledgement

Thanks are due to S. Ghosh for his kind help and valuable discussions.

### References

- 1 Bixler H J & Michaels A S, *Encycl polym sci Technol*, 10 (1969) 765 and the references cited there.
- 2 Tsuchida E & Abe K, *Adv polym Sci*, 45 (1982) 18.
- 3 Philipp B, Dautzenberg H, Linow K J, Kotz J & Dowidoff W, *Progr polym Sci*, 14 (1989) 91.
- 4 Michaels A S, *Ind eng Chem*, 57 (1965) 32.
- 5 Kikuchi Y & Kubota N, *Bull chem Soc Jap*, 61 (1988) 2943.
- 6 Brandrup J & Immergut E H, *Polymer handbook* (John Wiley & Sons, New York/London/Sydney/Toronto) (1975) IV-33.
- 7 Eyler R W, Klug E D & Diephnis F, *Anal Chem*, 19 (1947) 24.
- 8 Geuskens G, Lubikulu J C & David C, *Polymer*, 7 (1966) 63.
- 9 Brandrup J & Immergut E H, *Polymer Handbook* (John Wiley & Sons, New York/London/Sydney/Toronto) (1975) IV-192.
- 10 Arichi S, *Bull chem Soc Jap*, 30 (1966) 439.
- 11 Ladenheim H & Morawetz H, *J polym Sci*, 26 (1957) 251.
- 12 Watt G W & Chrisp J D, *Anal Chem*, 26 (1954) 452.
- 13 Yonetake K, Seo T & Iijima T, *J polym Sci: Polym Phys*, 28 (1990) 303.
- 14 Philipp B & Alsleben H, *Faserforsch Textiltech*, 21 (1970) 110.
- 15 Takigami S, Maeda Y & Nakamura Y, *J appl polym Sci*, 24 (1979) 1419.
- 16 Markley L L, Bixler H J & Cross R A, *J biomed mater Res*, 22 (1968) 145.
- 17 Ito H, Shibata T, Miyamoto T, Noishiki Y & Inagaki H, *J appl polym Sci*, 31 (1986) 2491.

## Electromembrane from polyelectrolyte complex of polyaniline and carboxymethylcellulose

Soumyadeb Ghosh & V Kalpagam\*

Department of Inorganic and Physical Chemistry, Indian Institute of Science, Bangalore 560 012, India

A composite membrane of polyaniline and carboxymethylcellulose has been prepared. The polyaniline in the membrane exists in the conducting state even at *pH* as high as 6.5, due to the Donnan effect. At high ionic strength, the polyaniline changes to the nonconducting state, but the rate is slow enough to make application of the membrane at high *pH* possible. It has been shown that the degree of protonation of polyaniline changes the permeability of the membrane. Further, we have proposed that for composites like polyaniline-carboxymethylcellulose, the permeability can be changed by changing the oxidation state of the conducting polymer, thereby changing the crosslinking between the polymer components.

Conducting polymers, a system of conjugated double bonds along the chain, have been at the forefront of research activities for the last one decade<sup>1</sup>. Among the many approaches for the improvement of the mechanical and other properties, preparation of composites of these polymers with conventional polymers and specially with polyelectrolytes, has proved to be most promising<sup>2</sup>. Conducting polymers in doped state (i.e. in conducting state) are charged and the charge is balanced by counterions termed as dopant. In the composite of such polymers with oppositely charged polyelectrolytes, the latter polymers act as the dopant, resulting in intercrosslinked polyelectrolyte complex. It has been shown that these composites, even at low level of loading of the conducting polymer (<15%), have conductivity comparable to that of the pure conducting polymer<sup>3</sup>. Further, these materials have better mechanical properties and processibility, and since the polyelectrolyte matrix swells in aqueous medium they show excellent electrochemical properties<sup>4</sup>. However, only little has been done on the polyelectrolyte nature of the conducting polymers<sup>5</sup> and their polyelectrolyte complexes<sup>6</sup>.

Polyaniline (PANi), one of the most important conducting polymers, has been used in conducting polymer polyelectrolyte composites<sup>4</sup>. This polymer has the uniqueness of undergoing 'acid doping' by protonation of the imine nitrogens present on the chain<sup>7</sup>. PANi in its most stable state, the emeraldine form, has almost equal proportion of the amine and imine nitrogens and their ratio can be changed by chemical or electrochemical redox reactions<sup>8</sup>. PANi also has fairly high solubility in organic solvents and acids in both conducting and nonconducting states<sup>9</sup>—a rare property for a conducting polymer.

Recently, we have reported that in the matrix of polyelectrolyte, PANi gets protonated to much higher extent<sup>6</sup>. In this paper results of our studies on the method of preparation and properties of a composite of PANi with carboxymethylcellulose (CMC), of different compositions, are presented and a novel concept for application of such materials as electromembranes is proposed.

### Materials and Methods

The PANi in emeraldine form was prepared by oxidative polymerisation of aniline by ammonium persulphate<sup>7</sup>. A 0.15 *M* solution of aniline in 2.3 *N* aq.HCl was cooled to  $-8^{\circ}\text{C}$  in salt-ice bath. To this, 35 ml of 0.41 *M* ammonium persulphate solution was added dropwise over a period of half an hour with constant stirring. The reaction mixture was stirred for 3 hr and then kept at low temperature (around  $5^{\circ}\text{C}$ ) for another 8 hr. The green precipitate of emeraldine form of PANi was filtered and washed with water. It was then treated with  $\text{NH}_4\text{OH}$  solution to obtain a blue coloured precipitate of PANi in the emeraldine base form. The precipitate was washed with chloroform to drain out the low molecular weight oligomers and was again dried. The compound was characterised by the comparison of its IR and UV-Visible spectra with the already reported ones<sup>9,10</sup>. PANi was then dissolved in formic acid and filtered. The concentration of the solution was found to be 0.2% by weighing, and was used for further studies.

The CMC was obtained from BDH in sodium salt form. It was found to have a degree of substitution of 0.74 and viscosity average molecular weight of  $4.3 \times 10^5$  (ref. 11). A 0.28% solution of the polymer

was prepared and from measured amount of this solution, films were cast on glass plates. After swelling the films slightly with formic acid, measured amount of the PANi-formic acid solution was added and the solvent was evaporated. Composites of different compositions, containing 1.5%, 3.7%, and 7.1% of PANi by weight respectively, were prepared. The films were kept in water for washing till constant pH value of the medium was obtained, and then the membranes were equilibrated with aqueous media of pH 6.5.

The films were observed under an optical microscope at 400 times magnification and the photographs were taken. The swellability of these membranes was determined by weighing the swollen membranes after removal of the excess water from the surface with a filter paper and calculating the weight fraction of the imbibed water in the swollen film.

The change in the UV-visible spectra of the membranes equilibrated with media of high ionic strength, was monitored with time. A PANi-CMC film of around 4  $\mu\text{m}$  thickness, cast on a quartz plate, was equilibrated with distilled water and then kept in 0.1 M KCl solution under constant stirring. It was taken out of the solution at different intervals of time and the spectra were recorded on a Hitachi U3400 spectrophotometer, in the wavelength range of 900 nm–325 nm.

## Results and Discussion

Under the optical microscope, the film of the PANi-CMC composite formed with low concentrations of PANi is found to be a homogeneous film (Fig. 1a). But at the higher concentrations of PANi, the PANi-CMC complex agglomerates (Fig. 1b). This is in accordance with the fact that in doped state of PANi, there is strong interchain interaction with formation of three dimensional metallic domains<sup>12</sup>. Hence, the composite films formed are two phase systems of PANi-CMC polyelectrolyte complex in CMC matrix. However, there seems to be intercrosslinking of the polymer all through the matrix, as the swellability of the materials is quite low even at pH 6.5. (Table 1).

The swellability of the PANi-CMC is found to decrease with the increase in its PANi content due to increase in the crosslinking. It can be noted that there is not much difference between the swellability of the 3.7% and the 7.1% loaded PANi-CMC, which shows that the swellability saturates with the percentage of loading. At the pH environment inside the film, which is lower than the external solution due to Donnan effect<sup>13</sup>, the ionisation of the

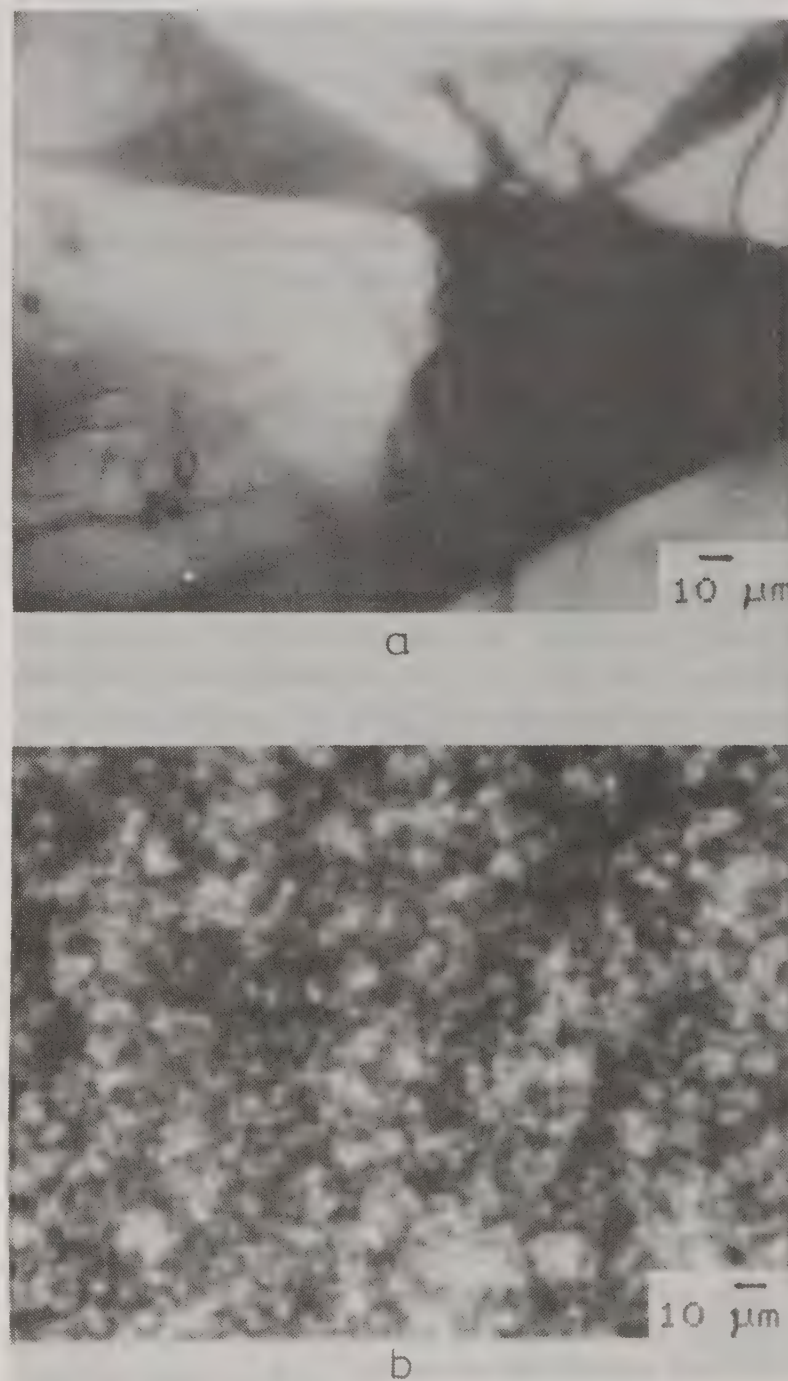


Fig. 1—Optical micrographs of PANi-CMC composite membranes of PANi [Content (wt./wt.%): (a) 1.5%, (b) 3.7%]

CMC may be low. Therefore, the excess PANi remains undoped, contributing less towards the crosslinking.

The most striking feature of these composites is the existence of PANi in the conducting state even above pH 6.5, as evident from the UV-Visible spectra (Fig. 2). It is well known that above pH 3, PANi is transformed to the nonconducting state. The protonated conducting state of the PANi has the low-energy electronic transition peak above 750 nm whereas the deprotonated, nonconducting state, has the peak around 600 nm. Therefore, in the membranes, the PANi is protonated even at much higher

Table 1—Properties of PANi-CMC composite membranes of different compositions

Composition (wt./wt.%)	Swellability (%)	$\lambda_{\max}$ (nm)	Rate of peak shift* (nm/hr)
1.5	84	809	155
3.7	55	802	100
7.1	49	774	64

\*The rate of peak shift is defined here as the average rate of change in the  $\lambda_{\max}$  value in the first one hour.

pH. This is due to the Donnan effect<sup>13</sup> as the composite contains excess of fixed negative charges. The lower value of  $\lambda_{\max}$  for the 7.1% PANi-CMC is due to the existence of the undoped PANi in the film as mentioned above. A strong polyelectrolyte may accommodate higher amount of the PANi in the conducting state, due to total ionisation of the acid groups. A composite of PANi and polystyrene sulphonate was prepared which showed existence of PANi in conducting state at much higher level of its loading. However, due to the poor mechanical properties of the material, further studies could not be done.

The existence of the PANi in conducting state at higher pH, extends the pH range for application of PANi which has applications in modified electrodes, etc. However, it must be kept in mind that the Donnan effect is applicable only for aqueous media of low ionic strength, whereas most of the electrochemical systems require quite high ionic strength to reduce the solution resistance. To check the stability of the conducting state of PANi at higher ionic strength, the change in the electronic spectrum of the PANi, equilibrated with 0.1 M KCl solution, has been observed with time. The spectra of 3.7% PANi-CMC, recorded at different times and shown in Fig. 2, shows that for considerable period of time (30 min) PANi exists in the conducting state. The rate at which the  $\lambda_{\max}$  value changes with time (Table 1), increases with the percentage loading of PANi in the composite. This is expected because at higher loading of PANi the swellability decreases, reducing the permeability of the membrane. Further, membranes showed sharp increase in the swellability when equilibrated with a high ionic strength medium. The swellability for the 3.7% loaded membrane, in 0.1 M KCl, was found to be 95%. This is due to the deprotonation of the PANi at higher ionic strength, leading to decrease in the crosslinking.

Therefore, it can be proposed that permeability can also be controlled by changing the degree of

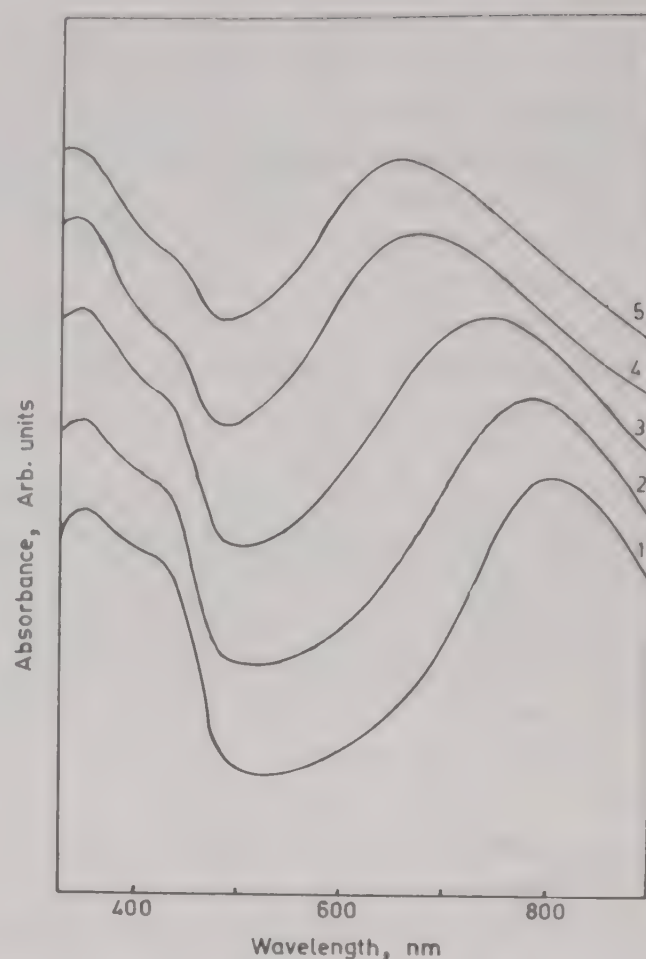


Fig. 2—UV-Visible spectra of the PANi-CMC membrane (PANi content 3.7%) kept in 0.1 M KCl solution, at different interval of time ( $t$ ) [(1)  $t = 0$  min, (2)  $t = 10$  min, (3)  $t = 35$  min, (4)  $t = 80$  min and (5)  $t = 570$  min]

protonation of the PANi chain. This can be brought about in two ways; first by changing the pH of the medium and secondly by changing the oxidation state of the PANi, i.e., by changing the proportion of the imine nitrogens. The latter method gives a very interesting and convenient method of changing the permeability of the membrane by the application of an electrical potential. These types of membranes are known as electromembranes<sup>14</sup>. However, till now electromembranes are prepared by distribution of the conducting materials in uncharged polymer matrix and the permeability of the material is controlled electrically by changing the amount of charge on it. For polyelectrolyte complexes of the conducting polymers, apart from the change in charge content of the material, the permeability is changed by the change in degree of crosslinking in the material, which is a more dominating factor for controlling permeability. Pure conducting polymers like polypyrrole have been used to make 'ion gate', where permeability of the polymer to ions has been changed by changing the oxidation state of the polymer electrochemically<sup>15</sup>. However, the films of conducting polymers have much lower permeability compared to the PANi-CMC composite making the latter a better candidate for applications.

## Conclusion

A method for preparation of PANi-CMC composites of different compositions has been standardized. The resultant materials form a two phase system where the conducting polyelectrolyte complex is distributed homogeneously in the excess of the anionic polyelectrolyte. The composite membranes, equilibrated with aqueous medium, have good swellability which is inversely dependent on the PANi content of the film and degree of protonation of PANi. The PANi in the swelled membrane remains in the conducting state even at pH as high as 6.5 due to the Donnan effect. This opens up application of the conducting PANi at higher pH. The UV-Visible spectra of the composite membrane in 0.1 M KCl solution, recorded at the different intervals of time show that the conducting state of PANi is kinetically stable upto half an hour which is large enough time period for many applications.

## Acknowledgement

The financial support for this work from CSIR, New Delhi, is gratefully acknowledged.

## References

- 1 Skotheim T A, *Handbook of conducting polymers* (Marcel Dekker, NY), 1986.
- 2 Audebert P, Bidan G, Lapkowski M & Limosin D, in *Electronic properties of conjugated polymers—Proc Int Winter School, Triol*, edited by H. Kuzmany, M. Mehring & S Roth (Springer-Verlag) 1983, 366.
- 3 Malhotra B D, Ghosh S, Chandra R, *J appl polym Sci*, 40 (1990) 1049.
- 4 Orata D, Buttry D A, *J electroanal Chem*, 257 (1988) 71.
- 5 Reiss H, *J phys Chem*, 92 (1988) 3657.
- 6 Ghosh S, Vishalakshi B & Kalpagam V, Communicated to *Synth Met*.
- 7 Chiang J C & MacDiarmid A G, *Synth Met*, 13 (1986) 193.
- 8 Focke W W, Wnek W W & Wei Y, *J phys & Chem*, 91 (1989) 5813.
- 9 Cao Y, Smith P & Heeger A J, *Synth Met*, 32 (1989) 263.
- 10 Tang J, Jing X, Wang B & Wang F, *Synth Met*, 24 (1988) 231.
- 11 Vishalakshi B, Kalpagam V, (This volume).
- 12 Ginder J M, Epstein A J, *Solid State Commun*, 63 (1987) 97.
- 13 Tanford C, *Physical chemistry of macromolecules* (John Wiley & Sons, NY), 1961.
- 14 Loh I H, Moody R A & Huang J C, *J membr Sci*, 50 (1990) 31.
- 15 Street G B, in Chap. 8 of the ref. 1.

## Studies on concentration polarisation in a membrane module

Nivedita Datta & B K Guha\*

Chemical Engineering Department, Indian Institute of Technology, New Delhi 110 016, India

The effect of flow velocity and pressure of operation is closely related in any reverse osmosis (RO) separation. Reduced separation at lower circulation velocity due to increased polarisation could only be compensated by increased pressure of operation. A mathematical model to describe the flow condition through the experimental cell has been developed to predict the mass transfer coefficients for the separation of sugar. The predicted mass transfer limitations have been confirmed by experimental findings. The flow pattern, particularly the velocity profile in cross and axial direction, controls the concentration for distribution within a RO module. Thus the effect of flow rate on the concentration build up within the modules, i.e., polarisation effect has been predicted. This has been also used to predict the separation of sugar from an aqueous solution under different operating conditions and compared with the experimental results.

### Introduction

Membrane separation processes are developing into major industrial separation systems like desalination, sugar from cane juice etc.<sup>1-3</sup>. Reverse osmosis (RO) is one of the major manifestation of such processes; it separates dissolved species from a solvent without phase change.

The mechanism of solute separation has been explained by many workers. According to the preferential sorption-capillary flow mechanism, developed by Sourirajan<sup>4</sup>, the surface of the semi-permeable membrane in contact with the separating solution has such a chemical nature that it can preferentially sorb water, which is then allowed to permeate because of the pressure gradient. The sorption of water in the membrane layer allows the formation of a preferentially sorbed pure water layer at the membrane-solution interface. The lower permeability of the solutes through the membrane prevents their passage. The movement of solution towards the permeating surface of the membrane allows a relative build-up of the solute concentration near the membrane-solution interface due to the preferential flow of solvent. The solute is mixed with the bulk flow of the liquid due to the back diffusion which is affected by the flow condition and turbulence near the surface boundary.

The build-up of solute concentration in this boundary layer region is referred to as concentration polarisation. As the solute concentration increases in the layer it exerts higher osmotic pressure and the net driving force decreases. As a re-

sult, the flow through the membrane decreases. This way the total permeate flux decreases and the rate of solute transfer through the membrane increases thereby decreasing the percent separation. Operating pressure may be increased to maintain the desired product rate. Sometimes increased concentration of solute in the boundary layer exceeds the solubility limit, and deposition of solute by precipitation may occur on the membrane surface, thereby fouling the membrane. Several workers<sup>5-8</sup> have studied concentration polarisation in different systems. The concentration polarisation may be reduced by increasing rate of back diffusion of solute from the boundary layer to the main stream flow. The back diffusion rate is a function of feed flow rate, module geometry and the solute system.

The extent of pre-enrichment of sugar solution by reverse osmosis process is limited because of the concentration polarisation effect. This can, however, be overcome by increasing either the operating pressure or the liquid circulation rate, both of which consume more energy. Therefore, an optimum balance is necessary to establish a possible degree of concentration enrichment by reverse osmosis. It is necessary to establish this optimum condition, in terms of productivity, pressure and flow rate. This analysis is possible by the study of concentration polarisation limitations of the system. In this paper a theoretical approach is being made to evaluate the limitation for the particular cell geometry and confirm the same with experimental determination.

Table 1—The compositions of membranes % (w/w)

Membrane specification	Cellulose acetate	Acetone	Acetic acid	1,4-Dioxane	Maleic acid	Methanol
M1	11	10.98	4.05	42.84	5.4	25.73
M2	11	10.98	4.05	42.84	5.4	25.73
M3	15	10.98	4.05	41.00	5.4	23.57
M4	13	10.98	4.05	41.84	5.4	24.73
M5	11	8.00	4.05	44.00	5.4	27.55

Table 2—Membrane casting conditions

Membrane specification	Casting solution temp. (°C)	Evaporation time (s)	Annealing temp. (%)
M1	20	185	85
M2	23	65	85
M3	20	185	80
M4	20	185	85
M5	30	60	60

Table 3—Characteristics of the membrane used

Membrane specification	A kg mol/m <sup>2</sup> /kPa/s × 10 <sup>8</sup>	Solute transport parameter (D <sub>AM</sub> /K δ) × 10 <sup>7</sup> m/s
M1	12.7	3.0
M2	24.1	0.71
M3	22.9	2.9
M4	27.7	1.7
M5	37.2	4.7

## Materials and Methods

The membranes used in this work were prepared from cellulose acetate (Kochlight) with acetic acid content of 55.0%. Cellulose acetate was dissolved in mixture of different solvent systems and additives. Modified membranes were cast according to Manjikian procedures<sup>9</sup>. Membranes with different porosity were obtained by varying cellulose acetate and solvents in the polymer mix, and using different casting conditions. Three different cellulose acetate contents of 11%, 13%, 15% w/w were taken for this particular study. The membrane compositions, casting conditions and characteristics are shown in Tables 1, 2 and 3 respectively. The annealing temperature used were 60°, 80° and 85°C for 10 min. The experiments were carried out in the experimental RO setup shown in Fig. 1. The membranes used in the experiment had disc shaped flat surface. The module used in the experiment was made in two halves, fastened together with high tensile bolts. The top half of the module contained the flow distribution chamber, whereas, the bottom half contained the membrane support system. An elaborate support system was used to withstand the high pressure load over the whole disc area (approximately 50 cm<sup>2</sup>). The support system consisted of a separate perforated stainless steel plate, having a thickness of 4 mm, over which two pieces of stainless steel wire mesh cloths (100 and 300 mesh size respectively) were placed. The placing of filter paper was to maintain flat surface

Test conditions maintained at 4.14 MPa at 25°C. Solute transport parameter with respect to NaCl solution had been determined.

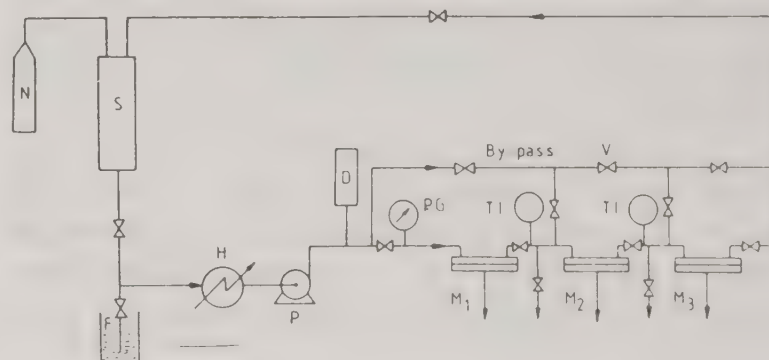


Fig. 1—Schematic diagram of reverse osmosis set-up. [N = Nitrogen cylinder, S = storage tank, H = heat exchanger, D = damper, P = pump, PG = pressure gauge, TI = temp. indicator, M<sub>1</sub>, M<sub>2</sub>, M<sub>3</sub> = modules and V = valves].

of membrane and prevent it from being stretched along the perforation walls of the wire mesh clothes. The membrane (disc shaped) was placed over the filter paper of the support assembly with its active skin layer exposed to the high pressure fluid.

The assembled membranes within the module were first subjected to a test run with pure water in order to stabilize their mechanical properties regarding compressibility and stretch characteristics. The membranes were first pressurised at 70 kg/cm<sup>2</sup> for one hour.

Fresh distilled water was then filled in the storage tank. The water was circulated through membrane modules at various pressures to determine pure water permeability [PWP]. At every

pressure setting the operation was continued for 30 min for system stabilization so that a steady-state operation could be ensured. Sampling for permeation rate determination was initiated only after this initial operation.

Sugar solutions were prepared by using laboratory grade sucrose (BDH). The required quantity (approximately 6 litres) of solution was prepared by taking the calculated quantity of sucrose and dissolving it in distilled water. The solution was then filtered and stored in the temporary storage vessel. Part of the solution (nearly 1 litre) was pumped into the RO set up and recirculated at about 5 kg/cm<sup>2</sup> pressure for rinsing purposes. The rinsing operation was continued for twenty minutes. The solution was then discarded.

Fresh sugar solution then filled the system. Back pressure was adjusted at the required level by regulating the N<sub>2</sub> flow into the storage tank. The RO system was operated for a period of thirty minutes to reach steady state. Samples of permeate and feed solution were collected simultaneously for a period of five minutes for the determination of permeation rate and separation of sugar. Two samples were collected consecutively for confirmation of the result. The system pressure was then readjusted and the experiments continued.

The collected permeate samples as well as feed samples were analysed for sugar content by means of spectrophotometer and polarometer. The sucrose content in permeate samples were analysed by the phenol-sulphuric method<sup>10</sup> using spectrophotometer.

### Theoretical model

The model is developed on the basis of flow of sugar solution between two parallel flat sheets. For this purpose the experimental test module geometry having a dome shaped (hemispherical) top section and flat plate membrane support system was presumed to be consisting of two flat sheets with one side of the sheet as impervious and the other side as semipermeable. The flow geometry is shown in Fig. 2.

The geometry was analysed based on the following assumptions:

(a) Solute removal through membrane is negligible and will not affect the general continuity equation.

(b) Solvent removal through membrane is comparatively small with respect to the total fluid in circulation.

(c) Flow is laminar.

(d) Solvent flux rate throughout the membrane is uniform and independent of longitudinal position.

Based on the above assumptions, the continuity equation of sugar separation can be written in the dimensionless form [11] as in Eq. (1)

$$\frac{\delta}{\delta L} (UC) + \frac{\delta}{\delta R} \left[ VC - \alpha_1 \left( \frac{\delta C}{\delta R} \right) \right] = 0 \quad \dots (1)$$

where

$$U = \frac{u}{\bar{u}_{(0)}}, \quad V = \frac{v}{v_{w(0)}}, \quad C = \frac{c}{c_0}$$

The dimensionless coordinates L, R represent dimensionless distances in the longitudinal and transverse directions respectively.

Boundary conditions applicable to the system are as follows:

$$\left. \begin{array}{l} \text{at } R = 0, \quad \alpha_1 \frac{\delta c}{\delta R} = VC \\ \text{at } X = 0, \quad C(O, R) = 1 \\ \text{at } R = 1, \quad \alpha_1 \frac{\delta c}{\delta R} = SVC \end{array} \right\} \quad \dots (2)$$

The velocity profile for the geometry shown in Fig. 2 can be deduced as follows:

$$u(x, R) = [\bar{u}_{(0)} - v_w x/h] \left[ 6R(1-R) + \frac{N_f}{70} \times (-28R^6 + 84R^5 - 105R^4 + 81R^2 - 32R) \right] \quad \dots (3)$$

and

$$v(R) = v_w \left[ R^2(3-2R) + \frac{N_f}{70} \times (-4R^7 + 14R^6 - 21R^5 + 27R^3 - 16R^2) \right] \quad \dots (4)$$

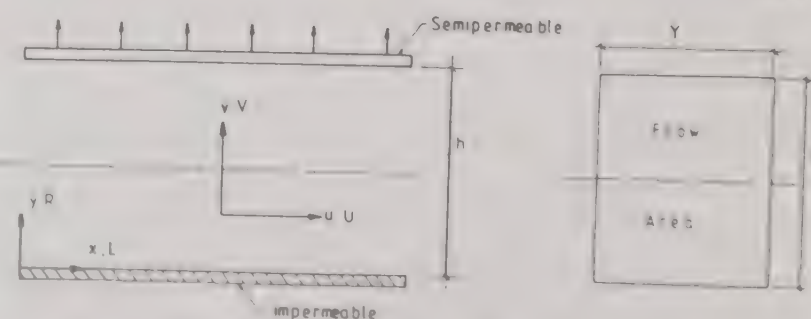


Fig. 2—Two dimensional duct (flat plate membrane).

$$\text{where, } N_f = \frac{v_w \cdot h}{\nu}$$

The Eq. (1) is solved using Eqs (2) and (4) with the boundary conditions by using finite difference method. The final solution is shown below:

$$\Gamma = 0.5 \xi + 2.85 [1 - \exp\{-(\xi/2.5)^{0.4}\}] \quad \dots (5)$$

$$\text{where } \Gamma = \frac{c_w - \bar{c}}{\bar{c}} \quad \dots (6)$$

$$\text{and } \xi = \delta_1 L / 3 \alpha_1^2 \quad \dots (7)$$

The solution of Eq. (5) is presented in Fig. 3. The experimental points, for different membranes are also indicated in Fig. 3. It is clear from Fig. 3, that theoretically predicted values are well in agreement with the experimental results.

#### Mass transfer coefficient

The general solution represented in Eq. (5), can be used to develop the equation of mass transfer coefficient, which controls the rate of back diffusion from the boundary layer to the bulk stream.

Mass balance within the boundary layer area gives,

$$v_w c + D_{AB} \frac{dc}{dy} = 0 \quad \dots (8)$$

where

$D_{AB}$  = molecular diffusion coefficient  $\text{m}^2 \text{s}^{-1}$

$v_w$  = withdrawal velocity through membrane solute,  $\text{m/s}$

$c$  = solute concentration, % (w/v)

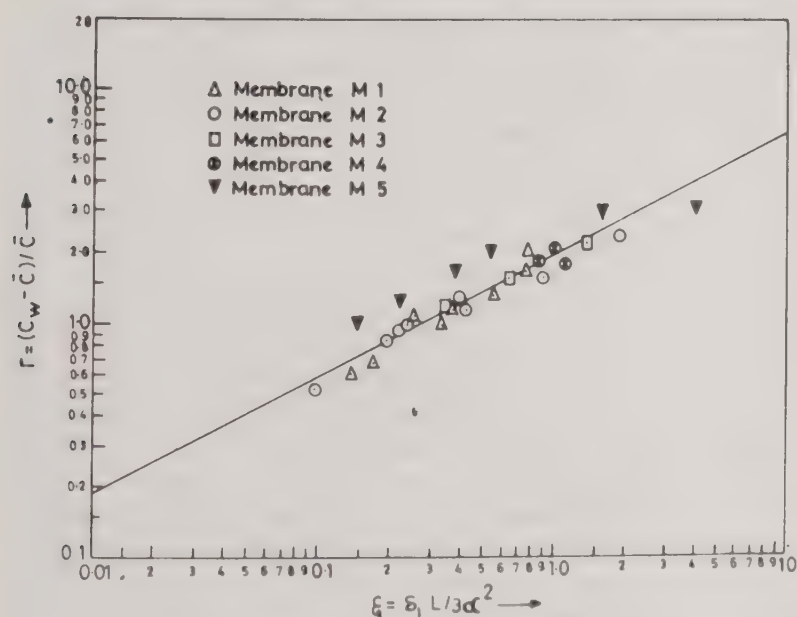


Fig. 3—General solution for laminar flow in two-dimensional duct

The Eq. (8) can be solved under the following boundary conditions

$$c = \bar{c} \text{ at } y = \delta \quad \dots (9.1)$$

$$c = c_w \text{ at } y = 0 \quad \dots (9.2)$$

where  $\bar{c}$  is the solute average concentration, % (w/v).

The general solution of the equation is given by

$$v_w = k \ln \frac{c_w}{\bar{c}} \quad \dots (10)$$

where

$$k = \frac{D_{AB}}{\delta} = \text{mass transfer coefficient, m/s}$$

Combination of Eqs (10) and (5), gives:

$$v_w = k \ln [1 + 0.5 \xi + 2.85 \{1 - \exp\{-(\xi/2.5)^{0.4}\}\}] \quad \dots (11)$$

Equation (11) can be considered as a general equation for mass transfer. The theoretical mass transfer coefficient ( $k$ ) can be predicted from the slope of the curve of  $v_w$  versus  $\ln [1 + 0.5 \xi + 2.85 \{1 - \exp\{-(\xi/2.5)^{0.4}\}\}]$  for a particular system. A typical example is shown in Fig. 4.

The corresponding experimental mass transfer coefficient values were determined using Eqs (12) and (13).

$$N_B = A[P - \{\pi(X_{A2}) - \pi(X_{A3})\}] \quad \dots (12)$$

$$N_B = k C_1 (1 - X_{A3}) \ln \left[ \frac{(X_{A2} - X_{A3})}{(X_{A1} - X_{A3})} \right] \quad \dots (13)$$

where  $A$  = pure water permeability constant,  $\text{kg mol m}^{-2} \text{kPa}^{-1} \text{s}^{-1}$ ;  $N_B$  = solvent flux,  $\text{kg mol m}^{-2} \text{s}^{-1}$ ;  $C_1$  = molar density of solution,  $\text{kg mol m}^{-3}$ ;  $\pi(X_{A2})$  = osmotic pressure at boundary layer concentration, MPa; and  $\pi(X_{A3})$  = osmotic pressure at permeate solute concentration, MPa.

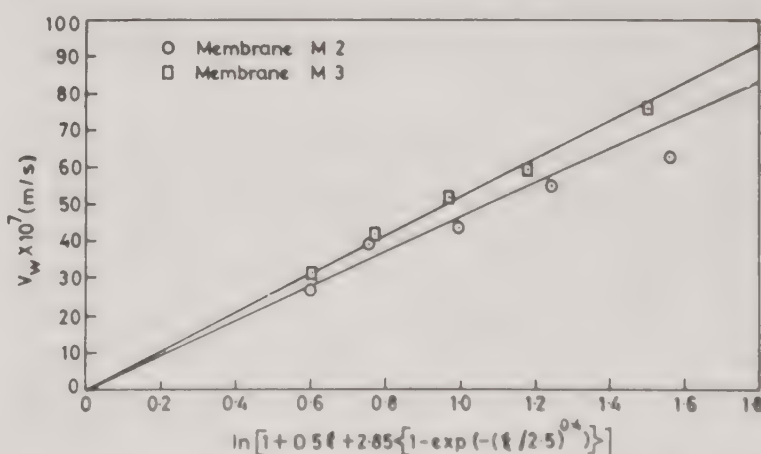


Fig. 4—Solution for predicting mass transfer coefficient in two-dimensional duct.

Table 4—Experimental and predicted values of mass transfer coefficient

Film No.	Flow Rate (cc/s)	Temp. (°C)	Value of $k$ (m/s) $\times 10^6$	
			Predicted	Exp.
M1	20.83	25.0	4.3	4.6
M2	20.83	25.0	4.3	4.6
M3	20.83	30.0	5.0	5.0
M4	12.50	25.0	4.1	4.0
M4	16.67	25.0	4.0	4.52
M4	20.83	25.0	5.0	4.97
M4	29.17	25.0	7.2	5.7
M5	20.83	25.0	6.15	5.26

The quantities  $N_B$ ,  $A$ ,  $P$  and  $X_{A3}$  are obtained from experimental data on pure water permeability [PWP], product rate [PR], solute separation, operating pressure, and membrane area. Using the above data, one can calculate  $\pi(X_{A2})$  and hence  $X_{A2}$  from Eq. (12). Using Eq. (13) one can determine experimentally mass transfer coefficient ( $k$ ). The experimental and predicted values of mass transfer coefficient ( $k$ ) are presented in Table 4.

### Results and Discussion

The results shown in Fig. 3 indicate that the experimental data obtained for various membranes operated under different conditions of temperature and pressure follow the theoretically predicted line. All the membranes show permeation and separation behaviour within close proximity of the predicted results. The exception is that for the membrane  $M_5$  where the deviations are quite high. This particular membrane is a highly porous one and hence the basic assumption of negligible solute transport and solvent flow across the membrane, compared to the bulk flow is not valid. Moreover, for a highly porous membrane the relative separation of solute and solvent is also quite low deviating further from the impermeable membrane concept.

The results on mass transfer coefficient calculations for different membranes and for varying operating flow rate conditions show good agreement between the predicted values and that estimated from the experimental observations as presented in Table 4. The results show that for a particular membrane the deviation increases with the increase in circulation flow rate. This is due to the typical flow geometry. At higher flow rates turbulence in the stream is increased and the lam-

inar flow assumption is not valid any more. Moreover, at higher flow rate the possibility of dead zone developing within the membrane surface is much more. The combination of these two effects leads to the increased deviation between experimental and predicted values of mass transfer coefficients. Thus, the results show that the mass transfer coefficient values can be predicted with reasonable accuracy for a membrane system.

### Conclusion

The separation of sugar at higher temperature using cellulose acetate membrane has considerable potential for industrial application. The existence of concentration polarisation within the boundary layer, leading to mass transfer resistance for the back diffusion of solution from membrane interface to the bulk liquid represents the major limitation in terms of operating conditions of flow rate and pressure. The mass transfer limitation has been successfully modelled for the particular cell geometry, and its applicability for different membrane systems has been confirmed. The results open up a new methodology for achieving an energy optimisation for the separation process.

### Acknowledgement

One of the authors (ND) gratefully acknowledges the CSIR, New Delhi, for the award of a Research Associateship.

### Nomenclature

$A$	= Pure water permeability constant, $\text{kg mol m}^{-2} \text{ kPa}^{-1} \text{ s}^{-1}$
$c$	= Solute concentration, % (w/v)
$\bar{c}$	= Solute average concentration, % (w/v)
$C$	= $(= c/c_0)$ Dimensionless solute concentration
$C_1$	= Molar density of solution, $\text{kg mol cm}^{-3}$
$D_{AB}$	= Molecular diffusion coefficient, $\text{m}^2 \text{ s}^{-1}$
$D_{AM}/K \delta$	= Solute transport parameter, $\text{m s}^{-1}$
$h$	= Height of flat plate module system, m
$k$	= Mass transfer coefficient, $\text{m s}^{-1}$
$L$	= $(= x/h)$ dimensionless axial position
$N_B$	= Solvent flux, $\text{gm mol m}^{-2} \text{ s}^{-1}$
$N_1$	= $(= v_w h/v)$ , dimensionless
$P$	= Operating pressure, MPa
$R$	= $(= y/h)$ dimensionless transverse position
$S$	= Fractional solute separation
$u$	= Velocity component in x-direction, $\text{m s}^{-1}$
$\bar{u}_0$	= Average fluid velocity at channel entrance, $\text{m s}^{-1}$
$U$	= $(= u/\bar{u}_0)$ , dimensionless
$v$	= Velocity component in y-direction, $\text{m s}^{-1}$
$v_w$	= Withdrawal velocity through membrane, $\text{m s}^{-1}$
$v_{w0}$	= Withdrawal velocity at channel entrance, $\text{m s}^{-1}$
$V$	= $(= v/v_{w0})$ , dimensionless
$X$	= Length of module, cm
$X_A$	= Mole fraction of solute
$Y$	= Width of module, cm

*Greek letters*

$\alpha_1$	= $(D_{AB}/v_w h)$
$\Gamma$	= $(c_w - \bar{c})/\bar{c}$
$\delta$	boundary layer thickness, m
$\delta_1$	= $(= v_w / \bar{u}_{(0)})$
$\nu$	= Kinematic viscosity $\text{cm}^2 \text{s}^{-1}$
$\xi$	= $(\delta_1 L / 3 \alpha_1^2)$
$\pi(X_A)$	= Osmotic pressure corresponding to $X_A$ , MPa
$\rho$	= Fluid density, $\text{kg cm}^{-3}$

*Subscript*

1	= Bulk solution
2	= Concentrated boundary solution
3	= Membrane-permeated product solution
o	= Channel inlet
w	= Membrane surface

**References**

- 1 *Reverse osmosis technology*, edited by Bipen S Parekh (Marcel Dekker, New York), 1988.
- 2 Kane A S, Bhalodia V O, Porecha B K, Natarajan R & Nadkanee S M, *Int Sugar J*, 89 (1987) 221-225.
- 3 Tragardh G & Gekas V, *Desalination*, 69 (1988) 9-17.
- 4 Sourirajan S, *Ind Eng Chem Fundamentals*, 2 (1963) 51-55.
- 5 Merten U, Lonsdale H K & Riley R L, *Industrial Eng Chem Fundamentals*, 3 (1964) 210-213.
- 6 Johnson A R & Acrivos A, *Ind Eng Chem Fundamentals*, 8(2) (1969) 359-361.
- 7 Srinivasan S, Chi Tien & Gill W N, *Chemical Engg Sci*, 22 (1967) 417-433.
- 8 Tiew C & Gill W N, *AIChE J*, 12(4) (1966) 722-727.
- 9 Manjikian S, *Ind Eng Chem Prod Res Dev*, 6(1) (1967) 23-32.
- 10 Dubois M, Giltes K A, Hamilton J K, Reiers J K & Smith F, *Anal Chem*, 28 (1956) 350-356.
- 11 Brian P L T., *Ind Eng Chem Fundamentals*, 4 (1965) 439-445.

## Electric power produced from two solutions of unequal salinity by reverse electrodialysis

R Audinos

Ecole Nationale Supérieure de Chimie  
118 route de Narbonne  
F 31 400 TOULOUSE  
France

The present study shows that it is possible to convert the energy of mixing of two solutions of different salinities into electric power by reverse electrodialysis. The laboratory electrodialyzer used was fitted in turn with two different pairs of permselective membranes, AMV-CMV and ARP-CRP. Solutions of  $\text{ZnSO}_4$  (216/18.8, 201/34.6, 110/40.2 and 127/14.2 g/l) and of NaCl (245/13 and 250/1 g/l) were used in batch recirculation process. Only NaCl solutions (294/1, 295/1 and 150/1 g/l) were used in continuous flow operation. Results show the influence of the type of membrane, composition and concentration of solutions, and type of electrode used on the process of conversion. The maximum power obtained is 400 mW/m<sup>2</sup>.

### Introduction

When a continuous potential is fed to the electrodes of a usual electrodialysis stack, ions move from the diluting compartment(d) to the concentration compartment(b) by migration: cations pass mainly through cationic membranes(c) and anion through anionic membranes(a) (Fig. 1).

In the case of a solution containing only one salt, the current density,  $i$ , results from the flux of the two kind of ions through the membrane involved<sup>1</sup>:

$$i = z_1 J_1 F + z_2 J_2 F \quad \dots (1)$$

Every flux density  $J_j$  is associated to the driving forces  $X_j$  by the classical relationship<sup>2</sup>:

$$J_j = \sum_f L_{jf} X_f \quad \dots (2)$$

In the case of electrodialysis, these driving forces result<sup>3</sup> from real gradients acting upon ions, such as a difference in electric potential,  $\Delta\phi$ , in chemical potentials,  $\Delta \ln a_j$ , in pressure,  $\Delta p$ , in temperature,  $\Delta T$ .

$$X = -zF\Delta\phi - RT\Delta \ln a - v\Delta p + s\Delta T \quad \dots (3)$$

When no electric field is applied from the outside to the stack, components of solutions move by *reverse electrodialysis* from one compartment to the other. So, a difference in potential ( $\Delta\phi$ ) appears between the two sides of the membrane due to all the driving forces:

$$\Delta\phi = \frac{RT}{F} \sum_k T_k \Delta \ln a_k - \Delta p \sum_k T_k v_k + \Delta T \sum_k T_k s_k \quad \dots (4)$$

Where  $T_k$  is the transference number of the species  $k$  (ion or molecule) for the membrane involved (anionic or cationic)<sup>4</sup>.

In the case of a stack, if the relationship (4) is applied to two concentrating compartments  $b_1$  and  $b_2$ , separated by a diluting compartment  $d$ , limited by an anionic membrane  $a$  and a cationic membrane  $c$ , the difference in potential is the following:

$$\begin{aligned} \phi_{b2} - \phi_{b1} = & -\frac{RT}{F} \sum_k (T_{ak} - T_{ck}) \ln \frac{a_{bk}}{a_{dk}} \\ & - \sum_k (T_{ak} - T_{ck}) (v_{bk} p_b - v_{dk} p_d) \\ & + \sum_k (T_{ak} - T_{ck}) (s_{bk} T_b - s_{dk} T_d) \quad \dots (5) \end{aligned}$$

Using operating conditions such that only the first term of relationship (5) remains, one obtains:

$$\Delta\phi = \sum_k (T_{ak} - T_{ck}) \Delta E \quad \dots (6)$$

where  $\Delta E$  represents the term  $-(RT/F) \ln(a_{bk}/a_{dk})$ .

When the stack has  $N$  unit cells, all of the same type, the difference in potential between the two concentrating compartments  $b$  of the extremities is:

$$\Delta V = N \Delta\phi \quad \dots (7)$$

as the electric potential of the concentration cells due to solutions of different concentrations in the alternating diluting and the concentrating compartments vanishes.

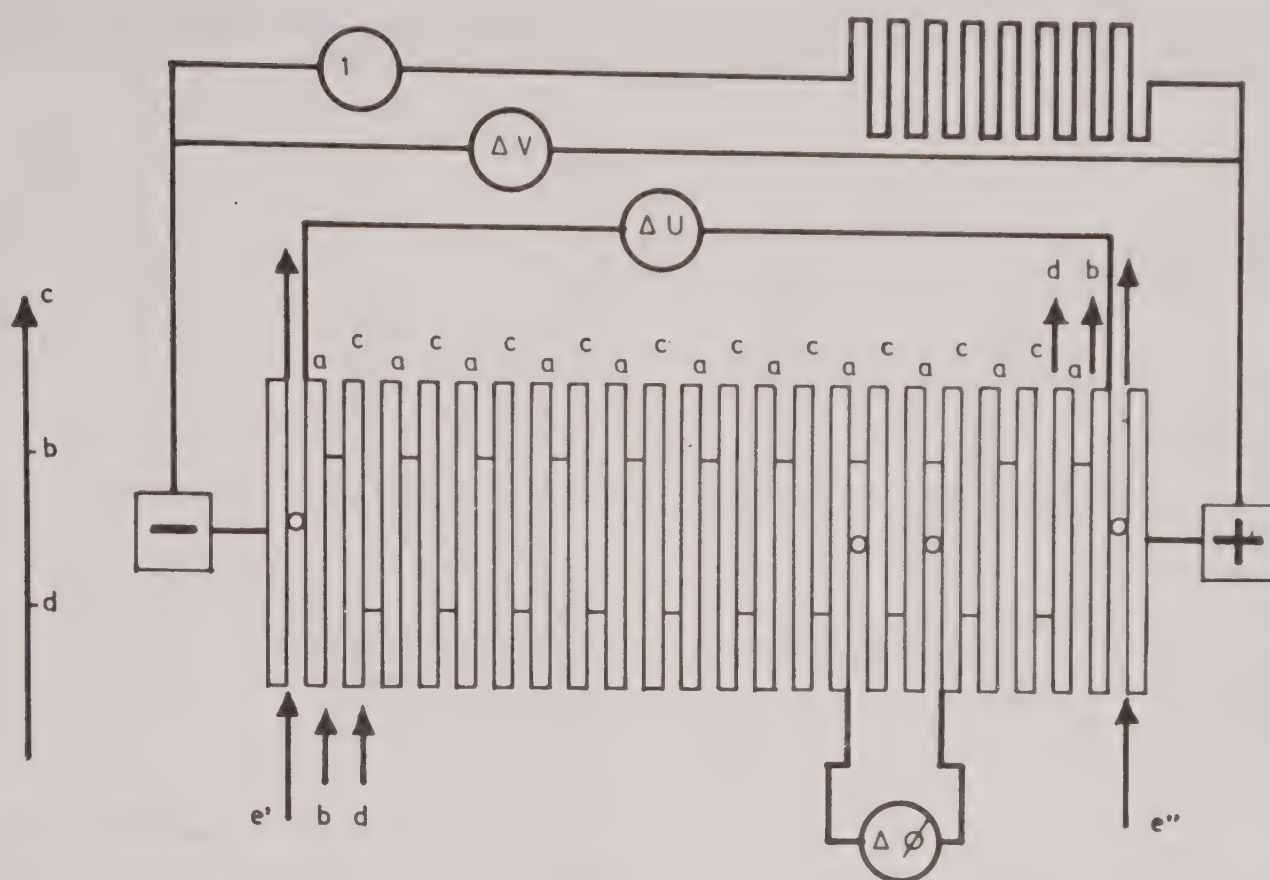


Fig. 1—Reverse electrodialysis: principle. [a: anion exchange membrane, b: concentrating solution, c: cation exchange membrane, d: diluting solution, e' & e'': washing solutions of electrodes, C: concentration,  $I$ : electric current,  $\Delta U$ : difference of potential on the wires of the stack,  $\Delta V$ : difference of potential between the membranes of the extremities of the stack and  $\Delta\phi$ : difference of potential for a unit cell ( $\phi_2 - \phi_1$ )].

In practice, the difference in potential arising in the wire of the electrodes of the stack is:

$$\Delta U = \Delta V - \eta - rI \quad \dots (8)$$

where  $\eta$  is the sum of the overpotentials on the electrodes,  $r$  the internal resistance and  $I$  the electric current.

### Thermodynamical considerations

When substances pass from one compartment to another, there is a variation in the internal energy for each of the subsystem b and d. When these transfers of matter occur in the same direction as the electric field, under reversible conditions, the electric energy  $W_{er}$  is given by the following<sup>5</sup> equation:

$$W_{er} = - \int_{inlet}^{outlet} \left[ \sum_k \partial \mu_k dn_k \right]_d^b = - \left[ \sum_k \Delta \mu_k dn_k \right]_d^b \quad \dots (9)$$

By permutation of the sums, with a view to putting together terms arising from the different components of the solutions, salt S and water W, this relationship can be written as:

$$-W_{er} = \Delta G_S + \Delta G_W \quad \dots (10)$$

where:

$$\Delta G_S = (\mu_{bS}^{outlet} - \mu_{bS}^{inlet}) dn_{bS} - (\mu_{dS}^{outlet} - \mu_{dS}^{inlet}) dn_{dS} \quad \dots (11)$$

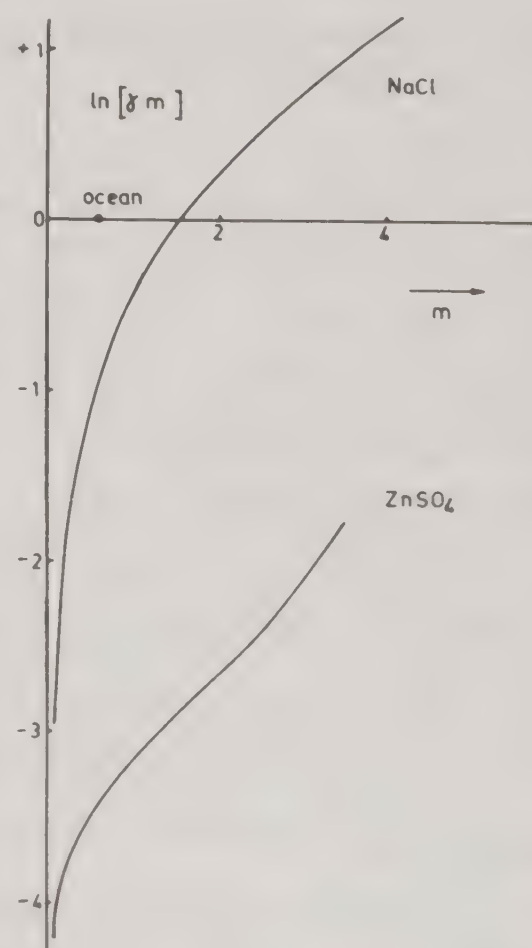


Fig. 2—Variations of  $\ln(\gamma m)$  as a function of the molality ( $m$ ) for two typical solutions

Table 1—Comparison of Rhône Poulenc (RP) and Asahi Glass (MV) membranes and NaCl and ZnSO<sub>4</sub> solutions in the case of a total recirculation process

Run	1	2	3	4	5	6
Electrolyte	NaCl		ZnSO <sub>4</sub>			
Concentrations (g/l)						
of the concentrate						
-initial	245	250	216	201	110	127
-final	205	190	213.6	209.9	108.6	122.6
of the diluate						
-initial	13	1	18.8	34.6	40.2	14.3
-final	21	14	17.0	38.3	39.0	33.3
Membranes	AMV-CMV	ARP-CRP	AMV-CMV	ARP-CRP	AMV-CMV	ARP-CRP
Potentials and transference						
$\Delta E$ (calculated) (mV)	-135	-172	-29.3	-22.0	-14.2	-15.9
$\Delta V$ (determined) (mV)	1178	782.6	254.9	149.6	129.2	120.8
$\Delta V$ (measured) (mV)	970	918.5	151.4	234.6	230.0	263.8
$\Sigma(T_{ck} - T_{dk})$ resulting	0.718	0.534	0.516	1.066	1.619	1.659

and

$$\Delta G_W = (\mu_{bw}^{\text{outlet}} - \mu_{bw}^{\text{inlet}})dn_{bw} - (\mu_{dw}^{\text{outlet}} - \mu_{dw}^{\text{inlet}})dn_{dw} \quad \dots (12)$$

On the other hand, the Lavoisier's law shows that:

$$dn_{bs} = dn_{ds} \quad \dots (13)$$

and

$$\dots (14)$$

Moreover, if the chemical potentials ( $\mu_k$ ) are expressed in the form given by Gibbs,

$$\mu_k = \mu_k^0 + RT \ln a_k \quad \dots (15)$$

It is clear that  $W_{er}$ , the energy reversibly exchanged, is a function of terms such as  $RT \ln (a_k^{\text{outlet}} / a_k^{\text{inlet}})$  for every phase, b and d.

Figure 2 shows that  $W_{er}$  is so important that the differences between terms  $\ln a_k = \ln (\gamma_k m_k)$  are high, when the differences in molality  $m_k$  are high.

Scan from the sole point of view of the useable work, it is best to operate with a solution of low molality as diluate. But in this case, the internal resistance  $r$  of the stack increases. Weinstein and Leitz<sup>6</sup> have calculated the optimal concentration of the diluate for the apparatus used by them. Their calculations show that the dilute solution should contain 1.5 g of NaCl per liter when the concentrated solution is sea water with 33.3 g of NaCl per liter. Clampitt and Kiviat<sup>7</sup> found an optimal concentration of 2.3 g of NaCl per liter.

However, it cannot be denied that for increase in potential difference it is much more important that values of activities of diluate and concentrate be far apart rather than the difference in molalities.

On the other hand, it is possible to make a choice regarding the the nature of the salt. Curves given on Figure 2, using data from the literature<sup>8</sup>, show that for the same difference in molality, NaCl solutions give a difference in potential and energy higher than those for the ZnSO<sub>4</sub> solutions.

Generally, it is possible to say that 1:1 electrolytes give higher energy than 2:2 electrolytes.

### Materials and Methods

The classical stack of electrodialysis<sup>4</sup> used here is fitted with 11 anionic and 10 cationic membranes, giving 10 diluting and 10 concentrating compartments, and then 10 unit cells (Figure 1). Gaskets are 3 mm thick, with a transfer area of 42 cm<sup>2</sup>, solutions flowing in a tortuous path. Depending upon the solution used, NaCl or ZnSO<sub>4</sub>, electrodes were sheets of Ag-AgCl or zinc.

Both solutions flow in co-current successively in each unit cell: this leads to a difference in potential for each unit cell, between the inlet and the outlet. the two electrodes are washed by two solutions of different compositions, one dilute and the other concentrated, containing the same salt as that used in the unit cells.

Experiments were carried at room temperature. Intensity, quantity of electricity, differences in potential between the outer membranes and between the two electrode and pH of the solutions were continuously measured; the refraction index was measured every 15 min with a view to knowing the concentration of solutions. Runs were stopped after 210 minutes.

The couples of anionic and cationic exchange membranes used are different. The first ones are

Table 2—Comparison of the energy obtained as a function of the composition and the concentration of the solutions for Asahi Glass membranes (runs 1, 3, 5) and the Rhône Poulenc membranes (runs 2, 4, 6, 8) in the case of a total recirculation

Run	1	2	3	4	5	6
Electrolyte	NaCl		ZnSO <sub>4</sub>			
Potentials, current and energy						
$\Delta U$ (measured)(mV)	387	374	179	77	118	114
$\eta/I-r$ (ohm)	52	24	51	114	11	7
$i$ (A/m <sup>2</sup> )	3.82	4.61	0.37	0.15	0.25	0.24
$W$ (mW)	5.92	6.24	0.26	0.05	0.12	0.11
$\omega$ (mW/m <sup>2</sup> )	148.0	156.0	6.50	1.25	3.00	2.75

homogeneous membranes Selemion AMV and CMV, made by Asahi Glass Co (Japan) by copolymerisation of styrene and butadiene, reinforced with a polyvinylchloride fabric. The second are heterogeneous membranes ARP and CRP, made by Rhône Poulenc (France), including ion exchange resins in polyvinylchloride, reinforced with a polyester fabric.

Transference numbers under the experimental conditions were determined by measuring the membrane potentials at 25°C.

The values so obtained and those given in the literature<sup>9,10</sup> were used (Table 1) to calculate  $\Delta V$ (determined).

## Results

### Total recirculation

The first step of the present work was to investigate the importance of the composition of the solutions, their nature and concentration, and that of the kind of membrane. The solutions were continuously recycled, so, in time, the concentration of diluate and that of concentrate change. Figure 3 shows that the variations in concentration are greater for NaCl solutions than those for ZnSO<sub>4</sub> solutions. Table 1 indicates that the difference in potential is greater in the case of NaCl solutions than in the case of ZnSO<sub>4</sub> solutions.

In this table, values of  $\Delta E$  were calculated with the mean experimental concentrations, using activity coefficients reported in the literature<sup>8</sup>:

$$\Delta E = \frac{1}{2} \frac{2RT}{F} \left[ \left( \ln \frac{a_b}{a_d} \right)_{\text{inlet}} - \left( \ln \frac{a_b}{a_d} \right)_{\text{outlet}} \right] \quad \dots (16)$$

With  $\Delta E$  so calculated and with the values of the transference numbers measured for ions, assuming zero for that of water, the difference of potential between the concentrating compartments b of the extremities of the stack was determined according to relations 6 and 7:

$$\Delta V(\text{determined}) = N \sum_{\text{ions}} (T_{aj} - T_{cj}) \Delta E \quad \dots (17)$$

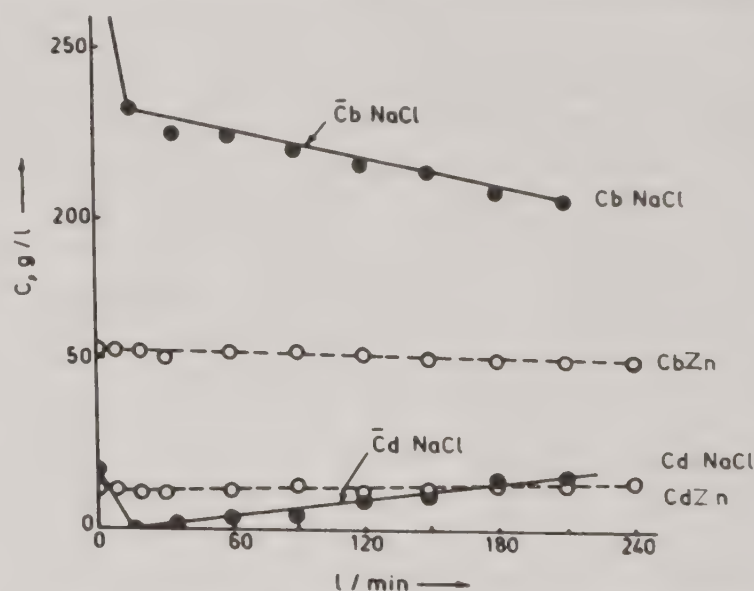


Fig. 3—Variations of the concentrations in the case of a total recirculation for a solution of NaCl (run 2) and a solution of ZnSO<sub>4</sub> (run 6). [ $C_b$ : concentration of the concentrating solution (g/l),  $C_d$ : concentration of the diluting solution,  $\bar{C}_b$ ,  $\bar{C}_d$ : mean values and  $t$ : time (min)]

The values of  $\Delta V$ (determined) are compared to the mean of those measured between two probes of silver or of gold, located on the external faces of the extreme anionic membranes of the stack, in the concentrating compartments b of the extremities.

It appears that  $\Delta V$ (determined) is smaller than the mean of  $\Delta V$ (measured): this can be explained by the fact that the two means used are not for the same time of the run.

However, the values of  $\Delta V$ (measured) for NaCl solutions are higher than those for ZnSO<sub>4</sub> solutions.

From the values of  $\Delta E$  and  $\Delta V$ (measured) it is possible to calculate the term  $\Sigma (T_{aj} - T_{cj})$ : this term is greater for the ARP-CRP membranes than that for the AMV-CMV membranes in the case of ZnSO<sub>4</sub> solutions, but contrary is the case for NaCl solutions. In this case the values of  $\Sigma (T_{aj} - T_{cj})$  so determined are close to those obtained with the values of the transference number directly measured.

In Table 2, the importance of the nature of the solution is indicated by the fact that the difference in potential measured on the wires of the stack,  $\Delta U$ ,

Table 3—Differences of potential for NaCl solutions in the case of Rhône Poulenc membranes without recirculation

Run	7	8b	9b
Time (min)	120	210	210
Concentrations of the concentrate (g/l)			
-initial	294	295	150
-final	285.5	288.25	145
Concentrations of the diluate (g/l)			
-initial	1	1	1
-final	4	3	4
<i>Potentials and transference</i>			
$\Delta E$ entrance (calculated) (mV)	284	285	238
$\Delta E$ entrance (calculated) (mV)	218	242	172
$\Delta E$ mean (calculated) (mV)	251	263.5	205
$\Delta V$ determined (mV)	1310	1375.4	932.7
$\Delta V$ (measured) (mV)	1064	770.0	638.6
$\Sigma(T_{ck} - T_{ak})$ resulting	0.424	0.292	0.311
$\Sigma(T_{ck} - T_{ak})$ measured	0.522	0.522	0.455

Table 4—Values of the energies obtained for NaCl solutions in the case of Rhône Poulenc membranes without recirculation

Run	7	8a	8b	9a	9b
Time (min)	120	120	210	120	210
<i>Potentials, current and energy</i>					
$\Delta U$ (measured) (mV)	650.6	676.8	675.8	584.7	582.6
$\eta/I-r$ (ohm)	26.37	—	30.76	—	16.99
$i$ (A/m <sup>2</sup> )	6.14	5.93	5.91	5.55	5.15
$W$ (mW)	16.265	16.076	15.993	12.988	12.002
$\omega$ (mW/m <sup>2</sup> )	406.6	401.9	399.8	324.7	300.0
$\rho$ (%) (with $\Delta U$ )	7.13		21.69		7.31

the current density,  $i$ , and the power  $W$  are greater for NaCl solutions than those for ZnSO<sub>4</sub> solutions.

From the electrical point of view, both kind of membranes are similar, but the term involving the internal resistance and the overpotential is not the same:

$$\eta - r = \frac{\Delta V - \Delta U}{I} \quad \dots (18)$$

In the case of NaCl solutions, the ratio of the electric energy so obtained, to the reversible electric energy  $W_{er}$ , is calculated.

$$P = q \cdot \Delta U (\text{mean}) \quad \dots (19)$$

The ratio  $100.P/W_{er}$  is then equal to 7.9% for AMV-CMV membranes, and to 4.2% for ARP-CRP membranes. One of the main factors involved in this ratio is the overpotential on the electrodes: only about 40% of the difference in potential measured on the outer membranes is present on the wires. When the ratio is recalculated by using,  $\Delta V$  (measured) instead of  $\Delta U$  (measured) in equation (19), the previ-

ous values are changed into 21.1% and 10.3% respectively.

#### Continuous circulation

The previous experiments indicate clearly that NaCl solutions give better results than ZnSO<sub>4</sub> solutions. So we used such solutions in continuous runs, in a stack fitted with ARP-CRP membranes.

In these runs, concentrations are less modified than in the case when the solutions are recirculated, but the differences in potential are quite the same. The differences between the values of run 7 and 8a are due to the fact that the electric and hydraulic circuits were reversed: the anode of run 7 being the cathode of run 8a, and the diluting circuit being the concentrating one, and vice versa. So, the silver chloride produced on the anode during run 7 is used as the cathode during run 8a.

The difference in potential measured on the wires,  $\Delta U$  (measured), and calculated,  $\Delta E$  (calculated), vary in the same manner during runs 7 and 8a (Tables 3 and 4).

For these runs, the electric current has almost the

Table 5—Increase of the energy per unit area between 1954 and 1980

Year	e mm	s cm <sup>2</sup>	$\Delta U/N$ mV	N	$\omega$ mW/cm <sup>2</sup>	$C_d^0$ g/l	$C_b^0$ g/l
1954 <sup>(11)</sup>	1	8	67.4	46	0.41	0?	29.2
1955 <sup>(12)</sup>	0.7	8	148	44	0.85	0?	29.2
1976 <sup>(6)</sup>	1	232	—	30	337.6	1.51	33.3
1980 <sup>(14)</sup>	3	40	67.5	10	399.8	1	295
1980 <sup>(17)</sup>	1	—	50	—	6000	5.9	234

e: thickness of each frame

s: active area of each membrane

same value, being higher than that for runs where solutions are recirculated (Tables 2 and 4).

As a consequence, the electric power obtained per unit area of active surface is about 2.5 times greater (Table 4). It is thus clear that, from an electrical point of view, a continuous operation is better than a batch process.

Moreover, taking into account the fact that the theoretical difference of potential decreases slightly from the entrance unit cell to the outlet one ( $\Delta E^{\text{entrance}}$  and  $\Delta E^{\text{outlet}}$  in Table 3), a continuous flow with compartments fed in parallel should give a higher value of  $\Delta U$ .

### Discussion

From the point of view of the yield and the difference in potential on the wires,  $\Delta U$ , it is better to use a concentrate with a high salt content (run 8b) than a concentrate with a low salt content (run 9b), as the energy theoretically suitable,  $W_{\text{er}}$ , should be greater in the former case. In the case of concentrates with the same salt content (runs 7 and 8b) it is better to have enrichment of the diluate. Some authors<sup>6,7</sup> have demonstrated that the concentration of the diluate can be optimized.

The power resulting from a reverse electrodialysis is then a function of the mechanical configuration of the stack and of the membranes<sup>11,12,13</sup>. Table 4 indicates that, on 20 years, the power per unit area of elementary surface,  $\omega$ , increases around 4000: the highest values being those for our runs 7 and 8, 400 mW/m<sup>2</sup> (ref. 14) which are ten times lower than those of Lacey<sup>15</sup>. This can partially be explained by the fact that membranes he used are better than those used in our experiments. The increase in energy per unit area between 1954 and 1980 is given in Table 5.

These high values of the power per unit area of runs 7 and 8 are obtained with heterogeneous membranes. However, for NaCl solutions, homogeneous membranes used in the case of a total recirculation give almost the same values. This indicates that it

shall be interesting to develop special membranes for reverse electrodialysis, with surfacic resistance of the order of 0.5 ohm.cm<sup>2</sup> (ref. 16) and transference numbers near one.

However, the energy so supplied is only about one-tenth of the total energy available. Particularly, the part of energy so obtained,  $P/W_{\text{er}}$ , depends on the overpotentials of the electrodes,  $\eta$ , and on the internal resistance of the stack,  $r$ . The value of the overpotentials  $\eta$  becomes negligible in front of  $\Delta V$  in a real stack, where a great number ( $N$ ) of unit cells partly diminish the overpotential, as indicated by relationships [7] and [8]. In the same time, the power  $w$  per unit area of elementary surface increases as the internal resistance  $r$  decreases, for example when the thickness of the stack is lowered, or when the temperature is raised<sup>17</sup>.

### Conclusion

Reverse electrodialysis transforms directly into electricity a non-negligible part of the energy produced when two solutions of different salinities are mixed together.

Experiments carried out with two kinds of membranes show that aqueous NaCl solutions are better than ZnSO<sub>4</sub> solutions. The ratio of the energy obtained to the theoretical energy is still low, 7 or 21%. However, the power per unit area of elementary surface, 400 mW/cm<sup>2</sup> and the difference in potential per unit cell, 60 to 67 mV/unit cell, could be increased by using ion exchange membranes specially devoted to reverse electrodialysis, in a stack fitted with low overpotential electrodes.

### Nomenclature

$a$	= activity
$E$	= potential (volt)
$F$	= Faraday constant (96,418 coulombs/g equiv)
$G$	= free enthalpy (joule)
$i$	= current density (A/m <sup>2</sup> )
$I$	= current (ampere)
$J$	= flux density (mol/s m <sup>2</sup> )

$L_{ii}$	=	phenomenological coefficient
$m_k$	=	molality of k (mol/kg of water)
$n$	=	number of ions, of mol
$N$	=	number of elementary cells
$p$	=	pressure (pascal)
$P$	=	energy produced (joule)
$q$	=	quantity of electricity (coulomb)
$r$	=	internal resistance (ohm)
$R$	=	gas constant (8,314 joule/mol.kelvin)
$T$	=	temperature (kelvin)
$t_k$	=	transference number of k
$U$	=	potential (volt)
$v$	=	molar volume ( $m^3/mol$ )
$V$	=	potential (volt)
$W$	=	energy (joule)
$w$	=	power (watt)
$X_i$	=	driving force
$z$	=	charge number of an ion (g equiv:mol)

#### Greek letters

$\gamma$	=	activity coefficient
$\eta$	=	overpotential (volt)
$\mu$	=	chemical potential (joule/mol)
$\rho$	=	yield (%)
$\phi$	=	potential (volt)
$\omega$	=	power per unit area ( $W/m^2$ )

#### Subscripts

a	=	anionic, i.e. of an anion exchange membrane
b	=	of the concentrate
c	=	cationic, i.e. of a cation exchange membrane
d	=	of the diluate
er	=	reversibly exchanged

f	=	of the force f
j	=	of the ion j
k	=	of the ion or the molecule k
S	=	of the salt
W	=	of the water

#### References

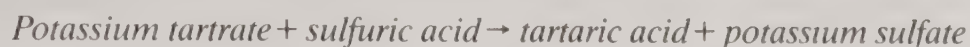
- 1 Audinos R, *Electrodialysis*, Ch 10 in *Water, waste water and sudge filtration*, edited by S Wigneswaran & R Ben Aim, (CRC Press, Boca Raton) 1989.
- 2 Lakshminarayanaiah N, *Transport phenomena in membranes* (Academic Press, New York) 1969.
- 3 Audinos R, Paci S & Beringuier H, *Chim Phys*, 87 (1990) 127-174.
- 4 Spiegler K, *Principles of desalination* (Academic Press, New York) 1966.
- 5 Audinos R, *Electrodialyse inverse Journal of power sources*, 10 (1983) 203-217.
- 6 Weinstein J & Leitz B, *Science*, 191 (1976) 557.
- 7 Clampitt B & Kiviat F, *Science*, 194 (1976) 719.
- 8 Robinson R & Stokes R, *Electrolyte solutions* (Butterworths, London) 1959.
- 9 Asahi Glass C<sup>o</sup>, *Technical note*
- 10 Rhône Poulenc, *Technical note*
- 11 Pattle R, *Nature*, London, 174 (1954) 660.
- 12 Pattle R, *Chem Process Eng*, 36 (1955) 351.
- 13 Mehta G, *J memb Sci*, 1 (1982) 107.
- 14 Audinos R, *C.R. Acad Sci Paris, Sci C*, 296 (1980) 413.
- 15 Lacey R, *U.S. Dept of Energy*, Contract E G 77 C 05 5544.
- 16 Forgacs C & O'Brien R, *Utility load smoothing by a reverse electrodialysis system*, 156th meeting, The Electrochemical Society, Los Angeles, 14-19 October 1979.
- 17 Lacey R, *Ocean Eng*, 7 (1980) 1.

## Direct production of pure concentrated tartaric acid from its salts by electromembrane processes

R Audinos\* & S Paci

Ecole Nationale Supérieure de Chimie, 118 route de Narbonne, F31 400, Toulouse

A concentrated tartaric acid solution is directly produced from oenological wastes by a double decomposition in electrochemical reactors fitted with ion exchange membranes. In the classical route of production of tartaric acid, a first set of neutralization-separations is used with a view to precipitating calcium tartrate. Then, the acid is produced by metathesis with an aqueous solution of sulfuric acid. The final solution obtained is generally a diluted mixture of tartaric and sulfuric acids which must be separated. In the first step of the process described here, the wasted tartaric salts are treated with a base, in such a way that a soluble neutral salt is formed in an aqueous solution. Then, the solution is fed into an electromembrane reactor where the metathesis of the neutral salt gives tartaric acid, and the corresponding salt or the neutralizing base according to the type of reaction used. In the case of an electrometathesis reactor, the reaction involved can be written as:



In the case of an electrolysis reactor, the reaction is:



In each case, the use of an electromembrane reactor allows one to obtain a pure solution of each of the products, tartaric acid, potassium sulfate or potassium hydroxide.

For each kind of stack assembly involved, the influence of the DC voltage applied to the outer electrodes, the concentration of the feeding solutions to each of the four cells and the velocity of the four streams have been studied. The results obtained allow the process to be modelised. According to the operating conditions, a more or less concentrated tartaric acid solution is produced in the concentrating cells.

### Introduction

Tartaric acid,  $\text{C}_4\text{H}_4\text{O}_6\text{H}_2$ , is encountered in juices of many plants, particularly in grape juice. This diacid-dialcohol,  $\text{COOH-CHOH-CHOH-COOH}$ , is at once an organic acid, a buffer, a reducing compound and a complexing compound of metallic ions.

It is mainly obtained from co-products of wine production and less than one-tenth of its production is based on synthesis from petroleum derivatives. The worldwide production is about 100,000 metric ton a year<sup>1</sup>.

Tartaric acid is a product of common use. Its acidic properties are used in biscuit, candies or sweets fabrications, in fruit juice or beverage production; in jam manufacture to catalyze the hydrolysis of sucrose; and in oenology, for acidification of too mellow grape.

As a buffer, tartaric acid is used whenever it is necessary to keep a constant pH; for example in pharmaceutical products, in some chemical reactions and in galvanoplasty.

As a reducing agent, it is used in photographic developers, in silvering of mirrors, in dyeing with me-

als. As a complexing compound, it is used in concrete or plaster with a view to reduce setting time.

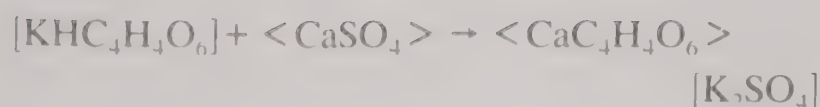
The production of tartaric acid by traditional routes is inadequate. So, three alternatives are possible: to use another acid, such as citric acid; to produce tartaric acid by synthetic methods from maleic acid issued in petrochemistry; or to improve the yields of the usual routes.

### *The classical route of producing tartaric acid*

Tartaric acid is mainly obtained from hydrogenotartrate of potassium,  $\text{KHC}_4\text{H}_4\text{O}_6$ , known as custard tart, and from precipitates containing calcium tartrate.

According to the process described in Fig. 1, hydrogenotartrate of potassium contained in vinasses, a residue of wine production, is treated with calcium carbonate to obtain the insoluble calcium tartrate salt,  $\text{CaC}_4\text{H}_4\text{O}_6$ .

In the second step, addition of calcium sulfate,  $\text{CaSO}_4$ , is necessary to change the remaining soluble potassium tartrate into the insoluble calcium salt.



After these two reactions, the tartrate anion is present only as the calcium tartrate salt,  $\text{CaC}_4\text{H}_4\text{O}_6$ , which is not soluble. Then the tartaric acid is produced from its calcium salt by adding a stronger acid, generally sulfuric acid.

All these reactions are based on the fact that some salts of tartaric acid can precipitate easily. Such a route is common in the classical chemistry.

However, the increase in intermediary steps requires control of many fluxes of matter, with various compositions. As a consequence, the operating processes, although being safe, are complicated by a great multiplicity of operations.

#### *Production of tartaric acid by an electrometathesis reaction*

The use of calcium compounds allows one to obtain precipitates, but leads to the formation of calcium sulfate as by-product. Generally, this by-product cannot be reused and is wasted.

On the other hand, it is well known that the neutral potassium salt of tartaric acid is very soluble, whereas the acidic salt is only slightly soluble<sup>2</sup>. For example, this acidic salt contributes to the formation of a precipitate in wine bottles.

Based on the use of soluble tartrates, the process consists of dissolving the tartaric ions in a neutral salt, by reaction with potash:



Then, tartaric acid is directly produced from the potassium salt by a metathesis reaction with sulfuric acid. The double decomposition reaction is as follows:

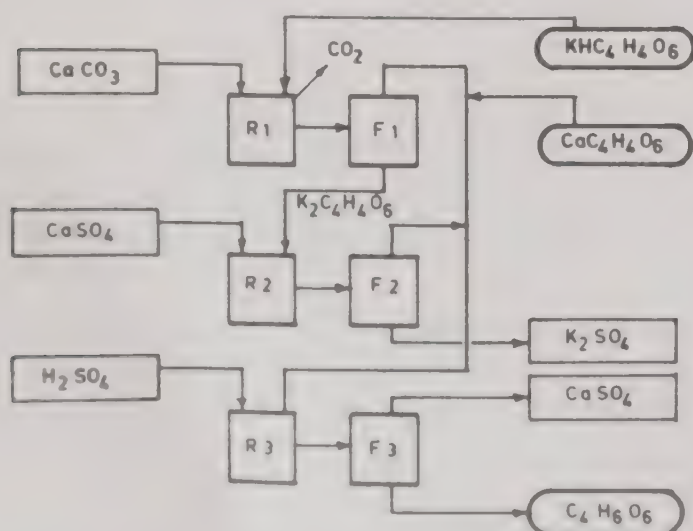
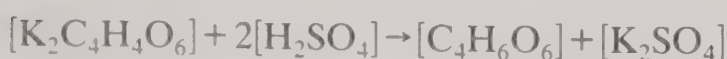


Fig. 1—Classical route for the production of tartaric acid [R1, R2, R3 = reacting vessels; F1, F2, F3 = dead end filters].

In the traditional method, tartaric acid and potassium sulfate are mixed together in the same aqueous solution. The separation of these products by a classical procedure is not easy at all. On the other hand, if the reaction occurs in a membrane reactor, using the selective means of electrodialysis the two products are created in separate volumes: it is one of the advantage of an electrometathesis reaction with membranes<sup>3</sup>.

Such a method is indicated in Fig. 2. It clearly appears that this route is less complicated than a traditional process, like that indicated in Fig. 1.

#### **Materials and Methods**

Use of a selective permeability artificial membrane technique (SPAMT) involves optimisation of a method and a process<sup>4</sup>.

The method consists of optimising theoretical conditions for a separation based on properties of membranes, considerations of energy and of substances<sup>5</sup>. This is indicated in Fig. 3.

**Membranes**—As the metathesis reaction involved is a reaction between ions, membranes capable of distinguishing ions are needed. In the study described here, only heterogeneous ion exchange

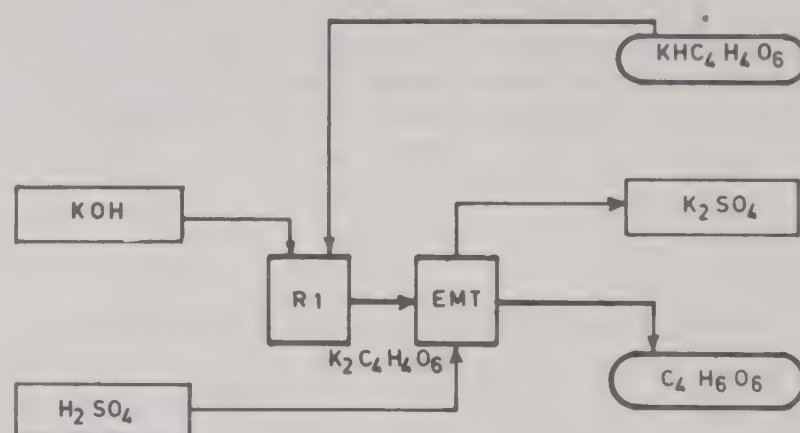


Fig. 2—Production of tartaric acid from hydrogenopotassium tartrate by an electrometathesis with sulfuric acid [R1 = neutralization tank; EMT = electrometathesis stack].

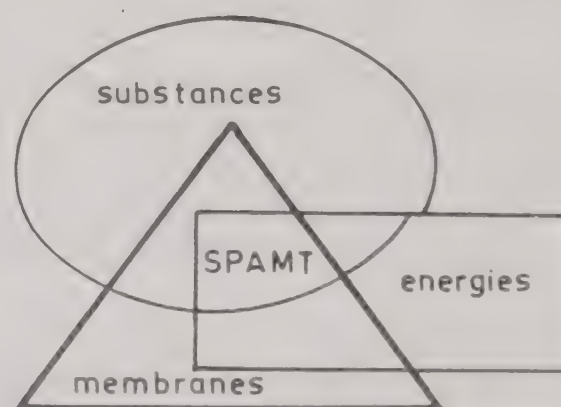


Fig. 3—Membrane technique at the intercept of membranes-energies-substances [SPAMT = semi-permeable artificial membranes technique].

membranes from the French company, Rhône Poulenc were used.

**Energy**—It is also clear that ions can easily be moved by an electric field. So, the driving force is the one created by the gradient of the difference of an electrical continuous potential. In this study, the electric field is always oriented in the same direction, perpendicular to the surface of the flat membranes, as in an electrodialysis stack.

**Substances**—In the present case, electrometathesis needs the substances to be soluble, and to be ionized. This aspect demands that the physicochemical properties of the medium be well known.

Now, the practical fitting involves 4 channels for the solutions, apart from the 2 channels necessary to wash the electrodes.

The study of the process aims at optimising conditions regarding the elementary cell<sup>6</sup>, the stack, the insertion in the production mode, and the technoeconomic analysis<sup>7</sup>.

## Results and Discussion

### The electrometathesis reaction

The electrometathesis reaction was carried out in an apparatus similar to a classical electrodialysis stack, but it included 2 diluting and 2 concentrating streams, in addition to the 2 needed by the electrodes, as indicated in Fig. 4.

Reactants were introduced as liquids in this membrane reactor by means of separated aqueous solutions of dipotassium tartrate and sulfuric acid (channels d and g, in Fig. 4).

Products obtained were tartaric acid,  $C_4H_4O_6H_2$ , and hydrogenopotassium sulfate,  $KHSO_4$  (channels b and f, Fig. 4).

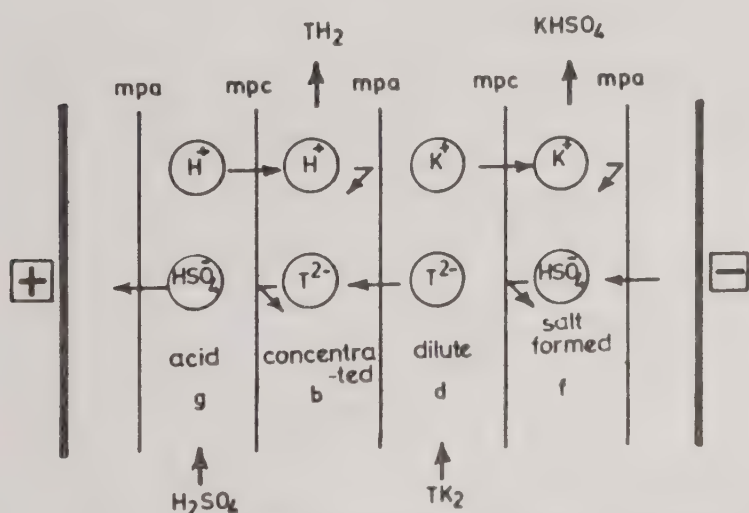
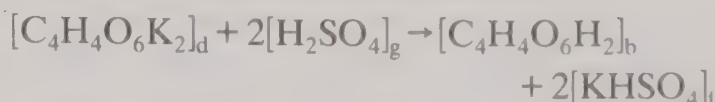


Fig. 4—Electrometathesis of dipotassium tartrate with sulfuric acid in a four channel stack [b = stream of the tartaric acid produced  $TH_2$ ; d = diluting stream of dipotassium tartrate  $TK_2$ ; f = stream of the hydrogenopotassium sulfate produced; g = auxiliary stream of sulfuric acid; mpa = anion exchange membrane, and mpc = cation exchange membrane].

The reaction may be written as:



This way of production offers two main advantages in comparison to the one used in classical reactors:

(1) Each compartment being separated, substances are never in direct contact. As opposed to a traditional reactor, there is never mixing of reactants and consequently of products. So, the difficult problem of separation of the products is avoided.

(2) As products are created in different vessels, it is possible to use a volume appropriate to the desired concentration for each of them. In a traditional reactor, this operating mode is not possible as all the substances are in the same reacting vessel.

### The elementary cell

The unit cell is already described by the method used. In practice, the separating frames used in this study make a tortuous path for the solution. The channels of rectangular cross section of 3 mm × 10 mm are (7 times × 6) 42 cm long. Ion exchange membranes are heterogeneous ARP and CRP membranes described in another publication.

Under the electric field, ions migrate and create concentration polarization layers near each of the 4 membranes of the unit cell, as indicated in Fig. 5.

If the electric current is too high, the departure of ions from the exporting channels can split water into ions, near the membranes<sup>8</sup>. As an elementary cell includes the 2 diluting compartments d and g, 2 possibilities arise. So, each case was studied separately, whereas in the other compartment the circulating solution had a concentration high enough to avoid any ionolysis of water.

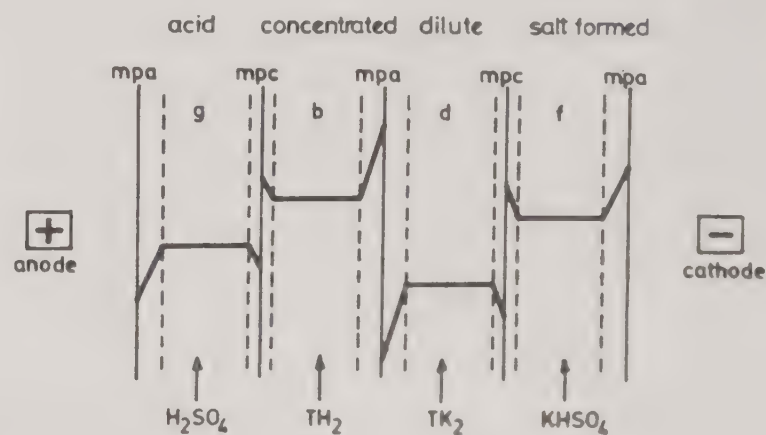


Fig. 5—Concentration polarization layers in a four channel unit cell [b = stream of the tartaric acid produced  $TH_2$ ; d = diluting stream of dipotassium tartrate  $TK_2$ ; f = stream of the hydrogenopotassium sulfate produced; g = auxiliary stream of sulfuric acid; mpa = anion exchange membrane, and mpc = cation exchange membrane].

The critical current is indicated by the measurements of current density,  $j$ , of conductivity  $\sigma$  and of pH of the diluting solution, as a function of the difference in potential,  $\Delta U$ , applied to the stack<sup>9</sup>. The results obtained are reported in Fig. 6. They show that the critical current varies linearly with the initial concentration of dipotassium tartrate or with the initial concentration of sulfuric acid, according to the case under study<sup>10</sup>.

It appears that for the same molar concentration, the critical current is first reached in the compartment where the dipotassium tartrate flows. As a practical consequence, it is then sufficient to use an aqueous sulfuric acid solution of a concentration not less than that of the dipotassium tartrate.

Then, from the water splitting point of view, it is possible to ignore the sulfuric acid solution.

### The stack

In order to reduce investment costs, it is always necessary to transfer the maximum of matter in minimum time. So, it is necessary to increase the electric current as far as possible without reaching its critical value. It is clear that this value is first reached at the outlet of the channel.

The straight line representing the critical current,  $J_{crit}$ , is related to the concentration by the relation:

$$j_{crit} = \frac{K}{\partial} [\text{salt}]_{outlet}$$

where  $K$  depends only on the transport number of anions in the membrane and on the equivalent conductivity of these ions<sup>10</sup>. On the other hand, the concentration at the outlet equals the concentration at the inlet, minus the quantity of salt transferred along the channel:

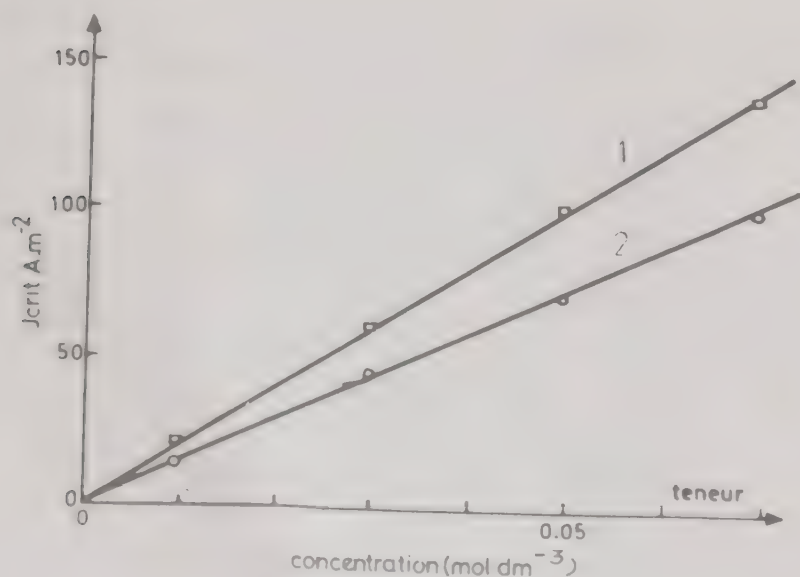


Fig. 6—Values of the critical current,  $j_{crit}$  due to each reactant in the electrometathesis stack, as a function of the concentration [1,  $H_2SO_4$  (acid g); 2, dipotassium tartrate ( $TK_2$ ) (diluted)].

$$[\text{salt}]_{outlet} = [\text{salt}]_{inlet} - \frac{n}{\|z\| F Y} \frac{Z_c}{v} j_{crit \text{ salt}}$$

By eliminating the value of the concentration of the salt at the outlet from the two previous equations we get the following relationship for the critical current:

$$j_{crit \text{ salt}} = \frac{[\text{salt}]_{inlet}}{\frac{\partial}{K} + \frac{n}{\|z\| F Y} \frac{Z_c}{v}}$$

So, it is possible to increase the value of the critical current either by reducing  $Z_c$ , the length of the

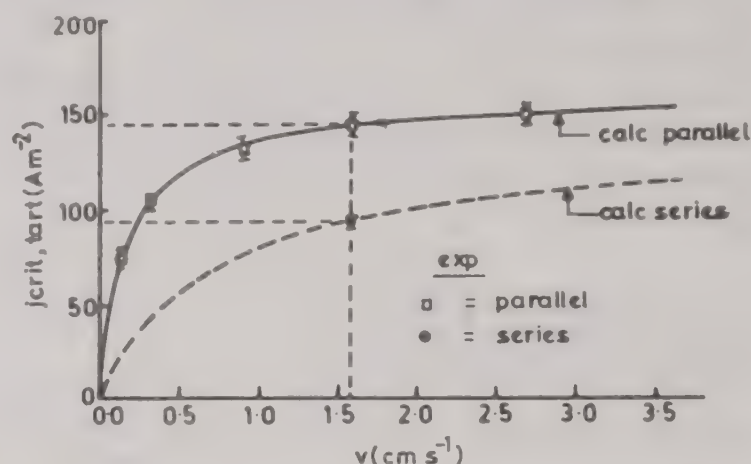


Fig. 7—Influence of tangential velocity on the critical current,  $j_{crit}$ , in series and parallel flows.

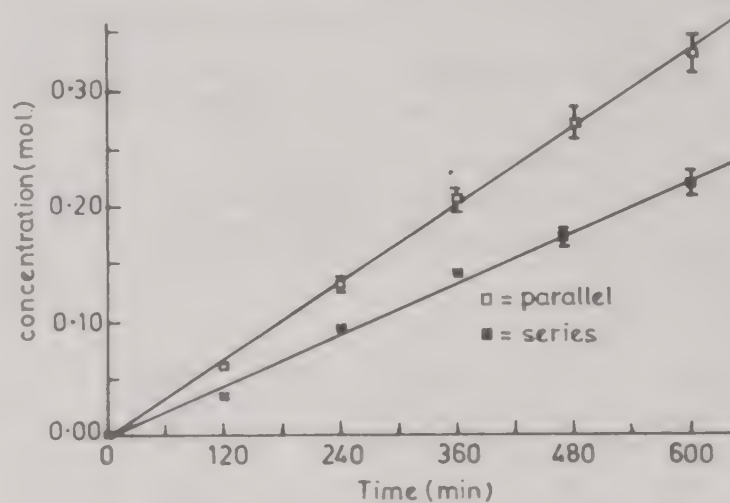


Fig. 8—Comparison in the transport of tartrate ions in parallel or series flow as a function of time.

Table 1—Initial operating conditions [number of runs = 15, Temp. = 298K,  $\Delta U = 10V$ ,  $v = 1.6 \text{ cm.s}^{-1}$ ]

Stream	Solution	Initial volume	Initial conc.
Acid used	$H_2SO_4$	not recirculated	$0.1 \text{ mol.l}^{-1}$
Concentrate	$TK_2$	75 ml	$5.10^{-4} \text{ mol.l}^{-1}$
Diluate treated	$TK_2$	10 liter	$15 \text{ g.l}^{-1}$
Resulting salt	$KHSO_4$	500 ml	$5.10^{-4} \text{ mol.l}^{-1}$

channel, or by increasing the tangential velocity  $v$  in the channel.

For a constant transfer area, the best way to proceed is to use a high tangential velocity in a stack with compartments fed in parallel as shown in Fig. 7.

Practically, the interest in using a parallel feeding centres on the quantity of matter transferred from the diluting stream to the concentrating one. So, for identical operating conditions, the quantity of moles of tartaric ion transported from the diluate to the concentrate, is greater for a parallel flow than that for a serial flow, as indicated in Fig. 8.

#### *Inclusion in the production mode*

Using the operating conditions described before, some production of tartaric acid from dipotassium tartrate was carried out. The starting volumes and concentrations are indicated in Table 1.

For example, if we start with an initial volume of the diluate as 10 litres and dissolve 15 g of  $C_4H_4O_6K_2$  per litre, the final concentration of the concentrate is about  $125 \pm 5$  g of tartaric acid per litre.

However, as indicated in Fig. 9, the concentration of the concentrated tartaric acid solution does not always increases with time. The weakening is attributed to the water transport.

Even if the water flux is only about  $13 \text{ mol.s}^{-1}.\text{m}^{-2}$ , i.e. 3000 time less than that of tartrate ion, which is about  $44,000 \text{ mol.s}^{-1}.\text{m}^{-2}$ , it is sufficient to check the increase in the concentration with time.

Moreover, it is interesting to notice that for a serial flow, the value of the final concentration is 1.5 times lower.

#### *Electrohydrolysis reaction with bipolar membranes. The method*

The electrometathesis reaction permits to produce concentrated tartaric acid from dilute solu-

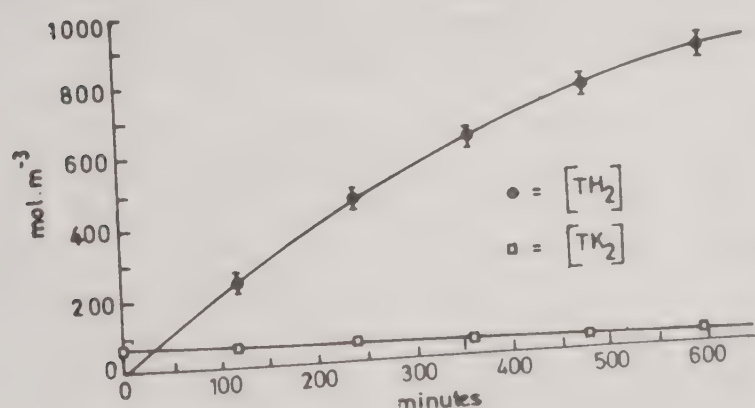


Fig. 9—Variation in concentrations (in  $\text{mol.m}^{-3}$ ) of dipotassium tartrate,  $TK_2$ , and of tartaric acid,  $TH_2$ , with time (in min) in the electrometathesis reaction.

tions of dipotassium tartrate. However, it gives potassium sulfate as waste. In the present case, this potassium sulfate can be used to fertilize the wine yard. Potassium is then recycled in byproducts of wine making.

This cycle can be shortened, and transportation avoided, by direct production of potash, from dipotassium tartrate, by using an electrohydrolysis reaction with membranes.

As a matter of fact, among the acidic anions that are suitable for displacing the tartaric acid from its salts, the hydroxyl anion,  $OH^-$ , is an interesting electron donor. For example, the oxyhydril ion can be produced by splitting water into its ions.

Then, the electrohydrolysis reaction with membranes involves a metathesis reaction with membranes and the ionolysis of water, as indicated by the following equation:



In such a reaction, a bipolar membrane, bip, substitutes the sulfuric acid compartment g, as indicated in Fig. 10, and gives directly the protons and the hydroxyl ions.

As noted earlier, the advantages of the electrometathesis reaction with membranes include production of pure products in solution, and obtaining concentrated solutions of tartaric acid, starting from a diluted solution of dipotassium tartrate.

Moreover, the co-product formed is a potash solution, which can be directly reused to dissolve the hydrogenopotassium tartrate on the plant itself.

#### *The process*

The stack used is similar to that fitted for the electrometathesis reaction with membranes, but every compartment, g, where the stream of aqueous sulfuric acid solution flows, is now substituted by a bipolar membrane, bip. But, in order to obtain a suffi-

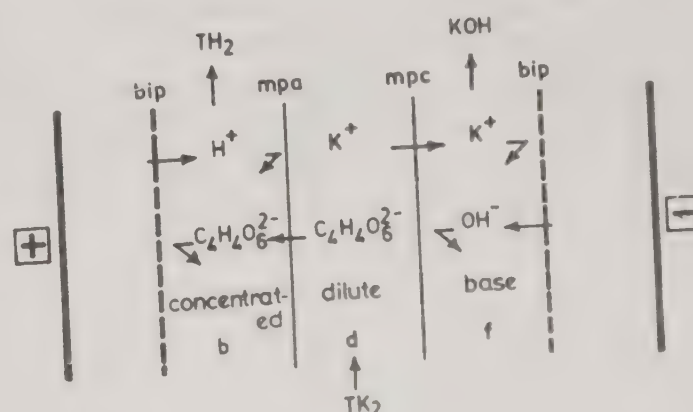


Fig. 10—Elementary cell for electrohydrolysis of potassium tartrate with a bipolar membrane [b = stream of tartaric acid produced  $TH_2$ ; d = diluting stream of dipotassium tartrate  $TK_2$ ; f = stream of hydrogenopotassium sulfate produced; mpa = anion exchange membrane; mpb = bipolar membrane; mpc = cation exchange membrane].

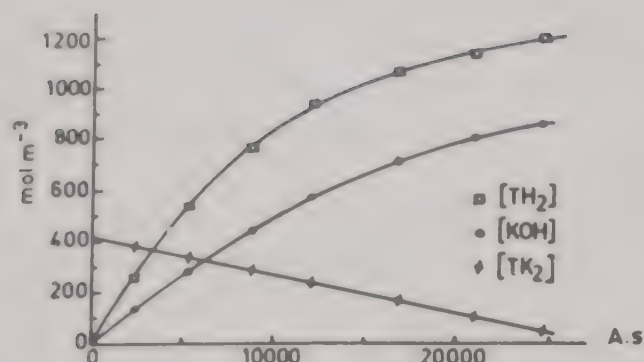


Fig. 11—Variation of concentration (in mol.m<sup>-3</sup>) of dipotassium tartrate, TK<sub>2</sub>, and tartaric acid, TH<sub>2</sub>, with electric charge (in coulombs (A.S)), used during the electrohydrolysis with bipolar membranes.

cient quantity of OH<sup>-</sup> ions from a bipolar membrane, it is necessary to have the current density high enough. Therefore, the critical current is first obtained in the diluting compartment (d) where the aqueous solution of dipotassium tartrate flows. So, it is sufficient to increase the content of dipotassium tartrate of the feeding solution. In fact, the increase in C<sub>4</sub>H<sub>4</sub>O<sub>6</sub>K<sub>2</sub> is economically favourable.

As an example, starting with 1.21 litre of diluate d containing 100 g of TK<sub>2</sub> per litre, the final concentration of concentrate b rises to 180 g of TH<sub>2</sub> per litre, as indicated in Fig. 11.

At the same time, the potash solution produced overstates 0.8 mol per litre. Then, it can be reused to neutralize the hydrogenopotassium tartrate incoming to the plant.

As indicated in Fig. 12, the whole process is now very short.

## Conclusion

Either by an electrometathesis reaction with membranes, or by an electrohydrolysis reaction with membranes, an aqueous solution of pure tartaric acid is obtained. In the first case this solution contains more than 100 g of tartaric acid per litre, and in the second case a solution with 180 g of tartaric acid per litre is easily produced from a solution of hydrogenopotassium tartrate. This salt, of low solubility, is collected as a waste in wine making.

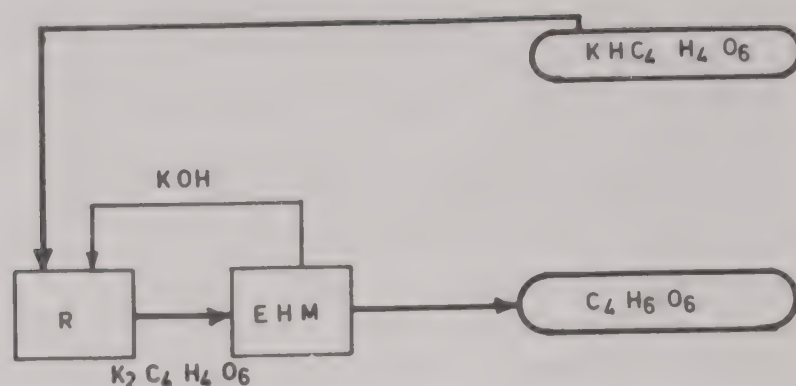


Fig. 12—Production of tartaric acid from hydrogenotartarate by an electrohydrolysis with bipolar membranes [EHM = electrohydrolysis stack with bipolar membranes; R = neutralization tank].

Such concentrations of tartaric acid are compatible with the final evaporation, which gives the crystals. In both routes, potassium appears as a co-product, either in the sulfate form, or as potash. It can be reused. But, the electrohydrolysis reaction with membranes has the advantage of recycling this potassium inside the process itself, on the plant.

## References

- 1 Mourgues J, Conte T & Roussel J, *Récupération des sels de l'acide tartrique*, *Revue des oenologues et des techniques viticoles et oenologiques*, 42 (1979) 17-20.
- 2 Landolt-Bornstein, *Numerical data and functional relationship in science and technology* (Springer Verlag, Berlin) 1975.
- 3 Wilson J R, *Demineralization by electrodialysis* (Butterworth, London) 1960.
- 4 Audinos R, *Membrane techniques in the chemical industry*, *Chemie Ingenieur Technik*, 53 (1981) 215.
- 5 Lakshminarayanaiah N, *Transport phenomena in membranes* (Academic Press, New York) 1969.
- 6 Audinos R, *Electrodialysis*, Ch 10 in *Water, waste water and sludge filtration*, edited by S Winneswaran & R Ben Aim (CRC Press, Boca Raton) 1989.
- 7 Audinos R, *Etude technico-économique des procédés à membranes*, Ch 10 in *Energetique des procédés*, Coordonateur P Le Goff (Lavoisier, paris) 1989.
- 8 Lacey R E & Loeb S, *Industrial processing with membranes* (Wiley Interscience, New York) 1972.
- 9 Audinos R, *Détermination du courant limite d'électrodialyse par conductivité*, *Electrochimica Acta*, 25 (1980) 405-410.
- 10 Paci S, titre, *Dr. Thesis*, Toulouse III University, 1989.

## Removal of phenol from refinery waste waters using liquid surfactant membranes in a continuous column contactor

A N Goswami\*, S K Sharma, Anshu Sharma & T C S M Gupta  
Indian Institute of Petroleum, Dehra Dun 248 005

The novel separation technique of liquid surfactant membrane permeation has been used for the removal of phenol from refinery waste waters. Experimental data are presented on continuous scale extraction of phenol, which is a typical toxic pollutant present in refinery waste waters, using liquid surfactant membranes in counter current Oldshue Rushton type stirred column. Experimental data have been generated under a range of operating parameters like flow rates, phase ratios and measurements include mass transfer, drop sizes and dispersed phase holdup. The effects of these parameters on extraction of phenol have been analyzed.

Phenols are among the more refractory and hard-to-treat pollutants in petroleum refinery waste waters<sup>1</sup>. Typical concentrations of phenolics in oily and process waters range from 12 to 30 ppm and in caustic wash effluents from 50 to 200 ppm<sup>1</sup>. At present, biological treatment (trickling filters, activated sludge process, oxidation ponds, aerated lagoons) is being used in several Indian refineries to bring down the level of pollutants like phenols to meet MINAS specifications<sup>1</sup> (for phenol, MINAS specification limit concentrations to < 1 ppm). Biological treatment procedures require large land area, have attendant problems of sludge disposal and are often prone to failure from shock loadings.

The novel separation process based on liquid surfactant membrane permeation has recently emerged as a versatile technique with proven potential in several fields. These membranes which may be of two types, "oil" or "aqueous", are formed when water-in-oil (W/O) emulsion or oil-in-water (O/W) emulsion is dispersed as drops in an external aqueous or oil phase respectively. Aqueous liquid membranes are used for the separation of hydrocarbons<sup>2,3</sup> while oil liquid membranes are used for waste water cleanup<sup>4</sup>, metal winning operations<sup>5</sup> and biochemical/biomedical separations<sup>6</sup> in general.

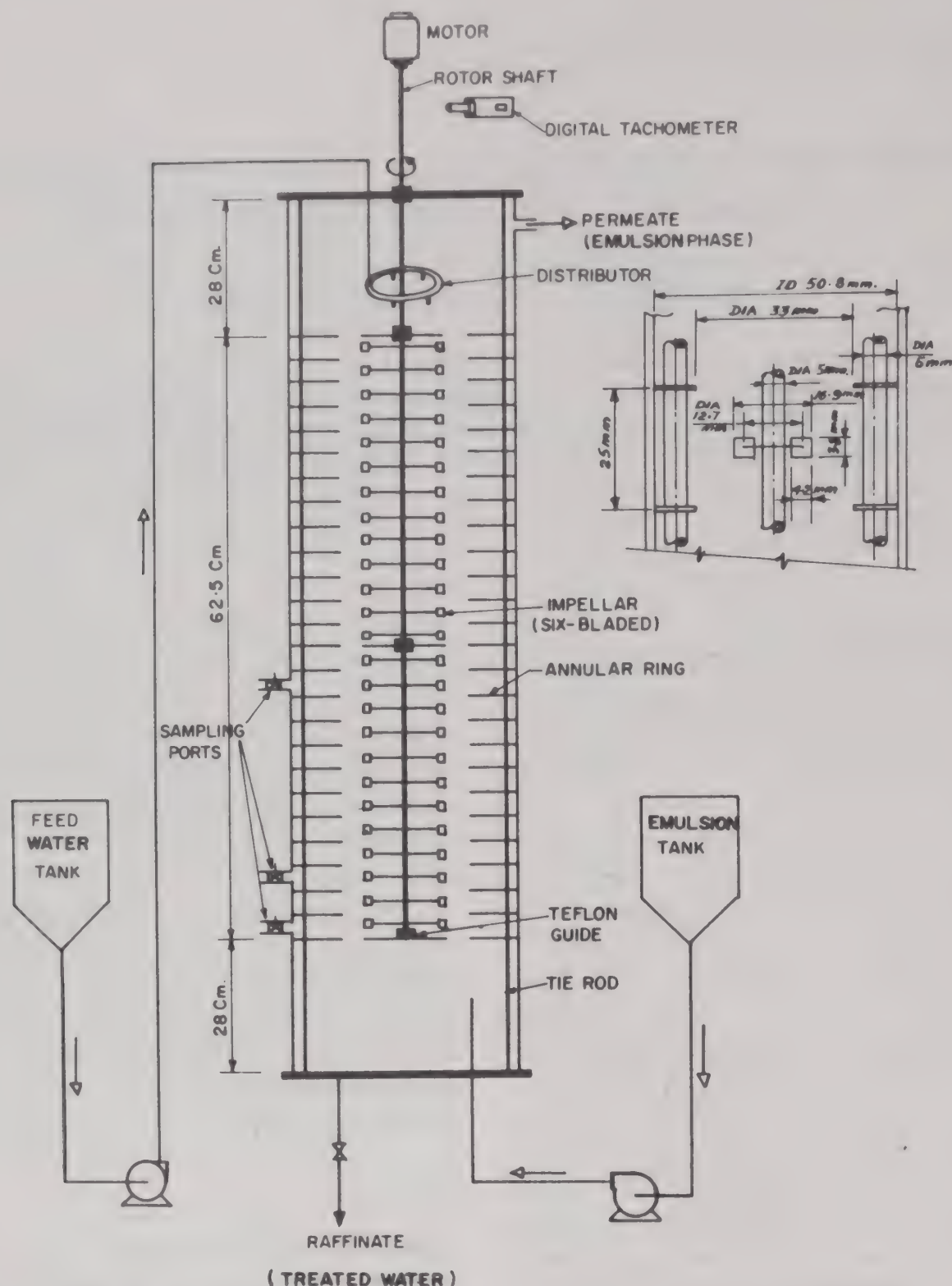
At present two industrial scale plants on the liquid surfactant membrane process are in operation<sup>7,8</sup>. The process is more economical than solvent extraction or biological treatment for phenol removal from aqueous wastes<sup>9</sup>.

Several groups have reported experimental data on batch extraction of phenolics from waste waters using liquid surfactants membranes<sup>4,10,11,15,16</sup>. The present authors have recently shown how a shape factor correction can be applied for effective

diffusivity estimation in a simulation model developed for predicting batch extraction rates in these systems<sup>12</sup>. However, an industrial scale separation based on this process will use continuous contacting equipment. Though the available information on industrial scale liquid surfactant membrane plants indicates that the continuous contactor used is basically a stirred counter current column typically used in liquid-liquid extraction operations, to date there have been very limited experimental data reported on continuous scale liquid surfactant membrane separations in such type of equipment<sup>13,14</sup>. The present paper reports results of an experimental study on the removal of phenol from waste water using liquid surfactant membrane in a continuous scale Oldshue Rushton type contactor.

### Materials and Methods

The continuous scale experiments have been carried out using an Oldshue Rushton column contactor (52 mm i.d.). This contactor is basically a compartmented stirred column (Fig.1). In a typical experiment, a water-in-oil emulsion of aqueous NaOH emulsified in kerosene containing 5% DIATROLITE SMO 80 (Dai Ichi Karkaria, Bombay) was introduced into the column at the bottom through a nozzle distributor while the phenolic feed water entered the column at the top. Metering pumps (M/s V K Pump Industries, Bombay) were used to deliver the emulsion and phenolic feed water phases to the contactor from the respective reservoirs. The stirring action of the turbine impellers in each of the 25 compartments of the column breakup the emulsion into globules (100 to 300  $\mu\text{m}$  diam.) as they rise through the contactor in counter current flow to the phenolic aqueous phase. It is the interstitial kerosene phase between the tiny microdroplets (1 to 10  $\mu\text{m}$ ) of



measured by instantaneous shut down of all entry and exit valves followed by measurement of volume of excess coalesced emulsion phase collected.

### Results and Discussion

The experiments have been carried out at ambient temperatures (30-33 °C) over a range of parameters like emulsion flow rate ( $Q_E$ , 20 to 50 ml/min), phenolic feed water flow rate ( $Q_W$ , 50 to 110 ml/min), phenol concentration in the feed water (200, 1000 ppm), sodium hydroxide concentration ( $C_N^\circ$ , 0.2, 0.5, 1.0 wt%) and microdrop holdup in the emulsion (0.2 to 0.5). The effect of variation of these parameters on fractional extraction of phenol from feed water, average drop size of emulsion globules and holdup of dispersed phase ( $\phi_2$ ) in the contactor are reported in Table 1 and Figs 3-5.

#### Effect of emulsion flow rate

As flow rate of emulsion is increased, data reported in Table 1 show that both dispersed phase holdup as well as emulsion macrodrop diameter in the column increase. The specific interfacial area per unit volume

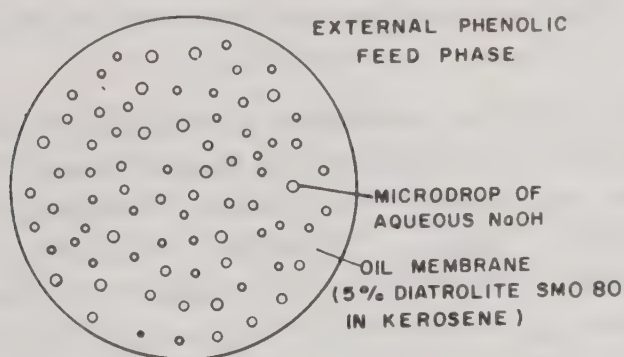


Fig. 2—Diagram of liquid surfactant membrane emulsion macrodrop

in the column is  $[6\phi_2/d_{32}]$  and as shown in Table 1 this increases with emulsion flow rate. The increase in dispersed phase holdup with emulsion flow rate will also increase the average residence time of the emulsion globule in the column. Both factors will increase extraction efficiency. However, leakage of internal phase has also to be considered. This leakage may lead to a decrease in extraction efficiency and is expected to be more when internal phase contains higher concentration of NaOH. Phenol extraction data reported in Fig. 3 shows that whereas extraction efficiency increases, with phenol concentration in

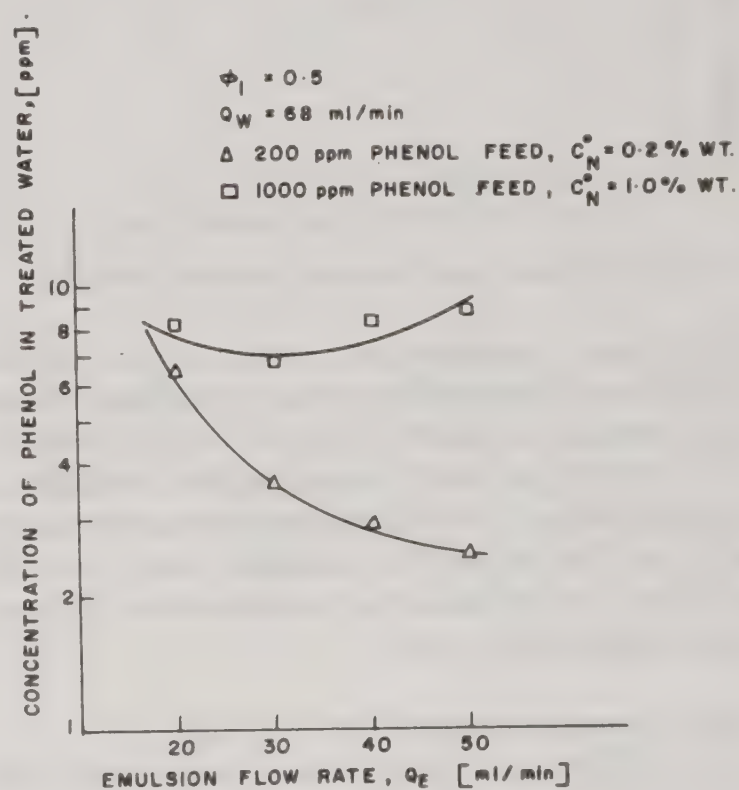


Fig. 3—Effect of emulsion flow rate on phenol extraction

Table 1—Experimental data on continuous scale extraction of phenol from waste water using liquid surfactant membranes  
[Phenol concentration in feed water : 200 ppm; membrane phase : 5% Diatrolite SMO 80 in kerosene; RPM : 500]

Sl.No.	Volumetric flow rate emulsion ( $Q_E$ ) (ml/min)	Volumetric flow rate water ( $Q_W$ ) (ml/min)	Microdrop holdup in emulsion $\phi_1$	Dispersed phase holdup $\phi_2$	Macrodrop diameter ( $d_{32}$ ) ( $\mu\text{m}$ )	Phenol conc. treated water (ppm)	Specific interfac. area ( $\text{m}^2/\text{m}^3$ )
1	20	68	0.5	0.104	182	6.5	3428
2	30	68	0.5	0.150	234	3.5	3846
3	40	68	0.5	0.210	230	2.5	5478
4	50	68	0.5	0.260	282	2.5	5531
5	30	50	0.5	0.160	242	3.4	3966
6	30	90	0.5	0.150	182	2.4	4945
7	30	110	0.5	0.150	188	2.2	4787
8	30	68	0.2	0.310	159	36.0	11698
9	30	68	0.3	0.220	150	23.0	8800
10	30	68	0.4	0.260	159	13.0	9811
11	30	68	0.5	0.260	160	12.5	9750

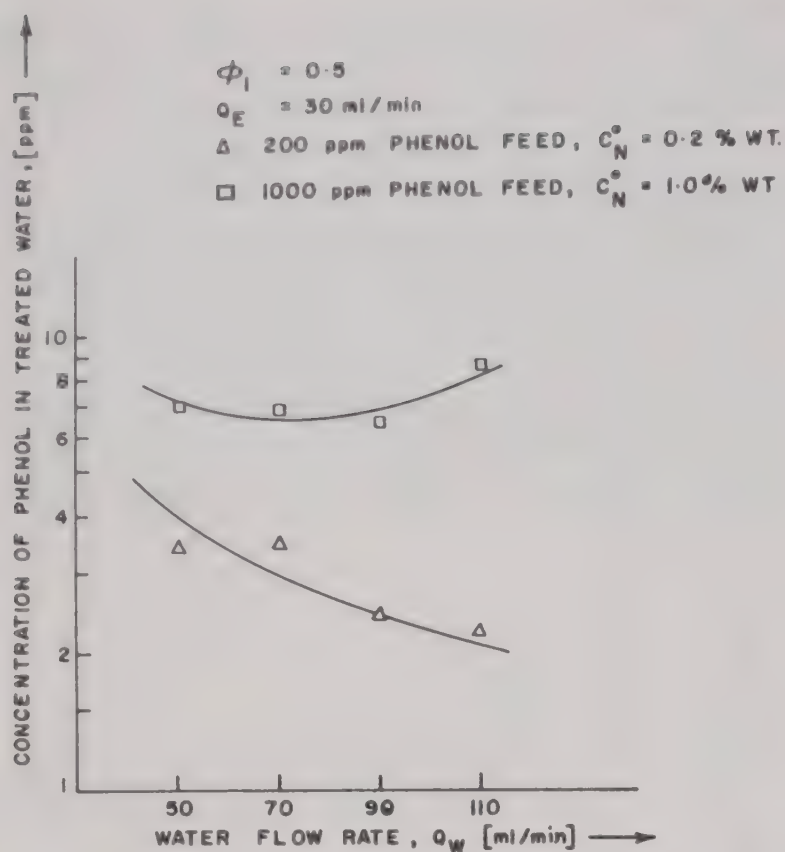


Fig. 4—Effect of water flow rate on phenol extraction

treated water decreasing with emulsion flow rate for the 200 ppm phenolic feed, which employed a lower concentration of NaOH (0.2wt%) in the emulsion, for the 1000 ppm feed, leakage effects dominate as the emulsions used contain a higher concentration (1 wt%) of NaOH in the internal phase so that concentration of phenol in treated water increases with emulsion flow rate.

#### Effect of aqueous phenol feed flow rate

As the flow rate of the phenolic feed, which is the continuous phase in the column, increases, data reported in Table 1 show that the dispersed phase holdup in the column remains practically constant while the average drop diameter of the emulsion macrodrops diameter in the column decrease. The specific interfacial area increases and extraction efficiency should, therefore, increase with increase in water flow rate so that phenolic content in treated water will decrease. This is borne out by the extraction data shown in Fig. 4 for both 200 as well as 1000 ppm phenol feeds. However, for the 1000 ppm feed, which used a higher concentration of NaOH (1 wt%) in the internal phase, the extraction efficiency decreased at high flow rates due to leakage effects so that phenol concentration in treated water increased at flow rates above 90 ml/min.

#### Effect of internal microdrop holdup in the emulsion

Experimental data reported in Table 1 show that as internal microdrop holdup ( $\phi_1$ ) in the emulsion is increased from 0.2 to 0.5, there is no significant

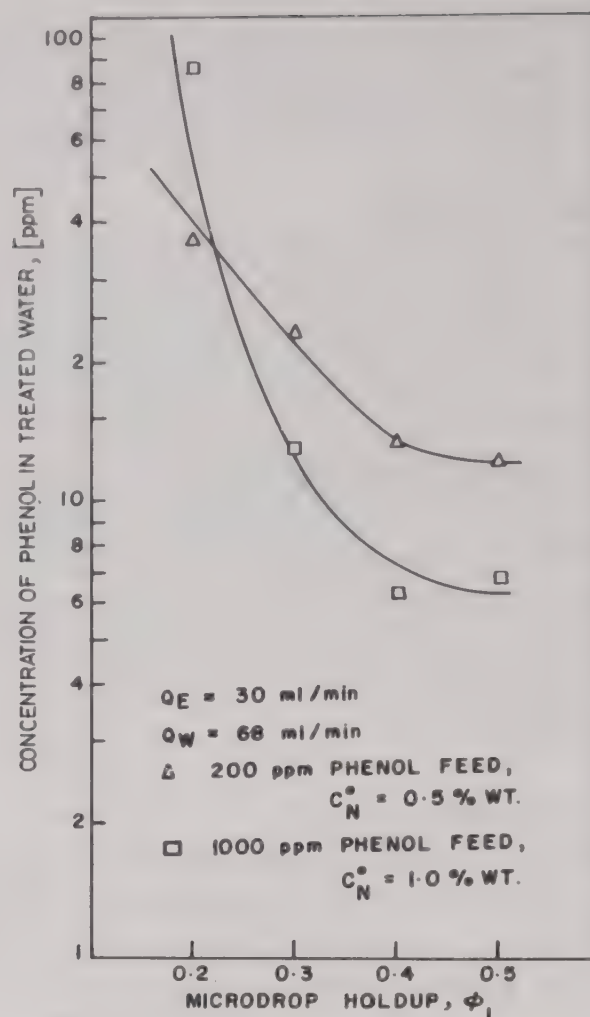


Fig. 5—Effect of microdrop holdup in emulsion on phenol extraction

change in the emulsion macrodrop average diameters, but the dispersed phase holdup in the column decreases. The specific interfacial area, therefore, decreases. However, extraction data reported in Fig. 5 show that extent of extraction increases sharply for both 200 as well as 1000 ppm phenolic feeds with phenol concentration in treated water decreasing sharply with increase in microdrop holdup. This can be rationalized on the basis of models like Jefferson-Witzell-Sibbitt<sup>10</sup> or Russell<sup>4</sup> for effective diffusivity of solutes (phenol) in the composite emulsion macrodrop. These models predict an increase in effective diffusivity of solute with increase in microdrop holdup due to decrease in diffusional path length across the liquid membrane phase so that extraction rates will increase.

Thus, the present experimental data on extraction of phenol from waste water using liquid surfactant membrane show that extraction efficiencies increase with flow rates of emulsion and phenolic feed water phase as well as with increase in emulsion microdrop holdup, but leakage effects dominate when concentration of NaOH is high in the internal phase.

#### References

1. Minimal National Standards Oil Refineries (Central Board for the Prevention and Control of Water Pollution, New Delhi) Comprehensive Industry Document Series, 1981-82 (COIN DS 4 1981-82).

- 2 Goswami A N & Rawat B S, *J memb Sci*, 24 (1985) 145.
- 3 Sharma A, Goswami A N, Rawat B S & Krishna R, *Jmemb Sci*, 32 (1987) 19.
- 4 Kataoka T, Nishiki T & Kimura S, *Jmemb Sci*, 41 (1989) 197.
- 5 Ruppert M, Draxler J & Marr R, *Sep Sci & Tech*, 23 (1988) 1659.
- 6 Thein M P, Hatton T A & Wang D I, *Bio Tech & Bio Eng*, 32 (1988) 604.
- 7 Furst W, Draxler J & Marr R, *World Congr Chem Eng III, Tokyo*, 3 (1986) 331.
- 8 Xiujuan Z & Jianghong L, in *Separation technology*, edited by N N Li & H Strathman (Eng Found, New York) 1988.
- 9 Li N N & Frankenfeld J, in *Liquid membranes, Encyclopedia of Chem Proc & Design*, edited by J J McKetta (Marcel Dekker Inc, New York).
- 10 Ho W S, Hatton T A, Lightfoot E N & Li N N, *AIChEJ*, 28 (1982) 662.
- 11 Teramoto M, Takihana H, Shibutani M, Yuasa T & Hara N, *Sept Sci & Tech*, 18 (1983) 397.
- 12 Goswami A N, Sharma A & Sharma S K, *J memb Sci* (in press).
- 13 Rautenbach R & Machhammer. O, *J membs Sci*, 36 (1988) 425.
- 14 Wang C & Bunge A L, *Paper presented at 21a, AIChE Summer National Meeting, Denver, Aug.21-24 (1988)*.
- 15 Boyadzhiev L, Beuzensheh E & Lazarovs L, *J memb Sci*, 21 (1984) 137.
- 16 Borwanker R P, Chan C C, Wasan D T, Kurzeja R N, Gu Z M & Li N N, *AIChEJ*, 34 (1988) 753.
- 17 *Manual on Disposal of Refinery Wastes API Method 716-57, Determination of Phenolic Materials, 4-Aminoantipyrine Method* (American Petroleum Institute, New York).

## Transport of water through cellulose derivatives used as the cover of osmotic systems for drug release

A L Iordanskii, A Ya Polishchuk & L P Razumovskii

Institute of Chemical Physics of the USSR Academy of Sciences, 4-Kosygin Street, Moscow 117 334, USSR

A reliable method to predict the mechanism and velocity of drug release has been developed based on the sorption and diffusion properties of water for transport through polymer membranes such as cellulose diacetate (CDA), CDA with cellulose acetyl propyl (CAP), cellulose acetyl fluorate (CAF) and its blend with cellulose triacetate (CTA).

The study of physicochemical parameters of water sorption and diffusion is attracting the attention of researchers in connection with the evaluation of polymer systems for controlled drug release<sup>1-3</sup>. This is due to the direct relation between transport characteristics of water and working features of covers of the osmotic drug systems. The main aim of the present study is to develop a reliable method of prediction of the mechanism and velocity of drug release based on the sorption and diffusion properties of water for transport through polymer membrane.

### Theoretical

#### *Diffusion-convective model of solvent transport and drug release out of osmotic polymer system*

The therapeutic system in question is the so-called "reservoir type" system. Due to the existence of the special hole in the coating of pill drug release occurs not only through the mechanism of diffusion but also the convection one. Generally, the diffusion-kinetic process includes solvent transport and drug core release which could be described by the following equations:

$$\frac{\partial C_w}{\partial t} = r^{-2} \cdot \frac{\partial}{\partial r} \left( D \cdot r^2 \cdot \frac{\partial C_w}{\partial r} \right) \quad R < r < R + l$$

$$C_{w0} = C_0(1 - \exp(-k_w t)) \quad r = R \quad \dots (1)$$

$$C_{w1} = \int_0^t C_1(C_d) \exp(-k_d(t - \tau)) d\tau \quad r = R + l$$

$$C_d = \exp \left( \sigma / \rho V_0 \int_0^t j_w d\tau \right) \int_0^t v_s(\tau) d\tau$$

$$j_d = j_w C_d / \rho$$

$$v_d = j_d \sigma$$

where  $C_w$  is the solvent concentration in polymer ( $C_{w0}$  and  $C_{w1}$  are its boundary concentrations on the border with liquid solvent and saturated solution of pill, respectively),  $D$  is the diffusion coefficient of solvent,  $C_0$  and  $C_1$  are the equilibrium values of  $C_{w0}$  and  $C_{w1}$  which corresponds to the solvent activity in a liquid state or saturated solution.  $C_d$  is the concentration of saturated solution of drug,  $k_w$ ,  $k_d$  are the rate constants of the process of boundary relaxation,  $j_w$ ,  $j_d$  are the water and drug fluxes respectively,  $v_s$  is the velocity of drug core dissolution,  $\rho$  is the solvent density,  $\sigma$  is the area of hole,  $v_d$  is the velocity of drug release,  $R$  is the radius of pill,  $l$  is the thickness of coating, and  $V_0$  is the pill volume. As a first approximation, we consider the pill to be a sphere, but after slight modification the model is able to take into account different geometries of systems in question.

### Experimental

Non-oriented cellulose diacetate (CDA), blends of CDA with cellulose acetyl propyl (CAP), cellulose acetyl fluorate (CAF) and its blend with cellulose triacetate (CTA) films were studied. Sorption measurements were carried out using a McBain balance, the sensitivity of the quartz spiral being 1.27 mg/mm and the weight of polymer sample in the range 60-110 mg. The dependence of the diffusion coefficient on the sorbate concentration was studied by the method of intervals<sup>4,5</sup>.

Diffusion coefficients were calculated using Eq. (2)

$$\frac{\Delta M_t}{\Delta M_\infty} = 1 - \frac{8}{\pi^2} \exp \left( - \frac{\pi^2 D t}{l^2} \right), \quad \dots (2)$$

where  $\Delta M_t$  and  $\Delta M_\infty$  are the changes in the film weight at instant  $t$  and in the state of sorption equilibrium, respectively.

### Results and discussion

The equilibrium values of water sorption (%) from liquid phase are 14, 10, 9 and 7 for polymers CDA, CDA+CAP, CAF and CAF+CTA respectively which show that all polymers are moderately hydrophilic polymers.

Sorption isotherms of CDA and CDA+CAP (Fig. 1) are typical for this kind of polymer. The de-

pendence of diffusion coefficients of water in these polymers on its concentration were observed to be the same (Fig. 2) and can be described by Eq. (3)

$$D_1 = 3.5 \times 10^{-8} \exp(-27 \cdot \bar{c}_w) \quad \dots (3)$$

where  $\bar{c}_w$  is the average concentration of water in CDA (or CDA+CAP), and  $D_1$  its diffusion coefficient.

In contrast, the study of transport properties of water in CAF and CAF+CTA showed that in spite of lower equilibrium water content, these polymers have some unusual features which could be used for improving working parameters of system in question. Sorption isotherms of water (Fig. 3) indicated slight plastification of CAF and CAF+CTA. Moreover, the isotherm for the case of blend (2) is linear. Deviation from Henry's law is observed for CFA at values of activity more than 0.8 which corresponds

to bi-modal distribution of water in matrix with number of water molecules in cluster equal to 10 (ref. 6). These isotherms lead to different features of transport of water in CFA and CFA+CTA in comparison with those of CDA and CDA+CAP.

Figure 4 illustrates the concentration dependence of diffusion coefficients of water in films of CFA (1) and its blend with CTA (2). The main feature is the increase in transport parameters of water as its concentration in polymers increases. The expressions of these dependencies are as follows:

$$\left. \begin{aligned} D_2 &= 8 \times 10^{-10} + 1.1 \times 10^{-7} \cdot \bar{c}_w \\ D_3 &= 5.6 \times 10^{-9} + 3.3 \times 10^{-7} \cdot \bar{c}_w \end{aligned} \right\} \quad \dots (4)$$

where  $D_2$  and  $D_3$  are the diffusion coefficients of water in CFA and CFA+CTA, respectively. The linear character of this dependence could be explained by intermediate properties of moderately hydrophilic polymers, and by two opposite effects which are swelling of polymer matrix causing the ac-

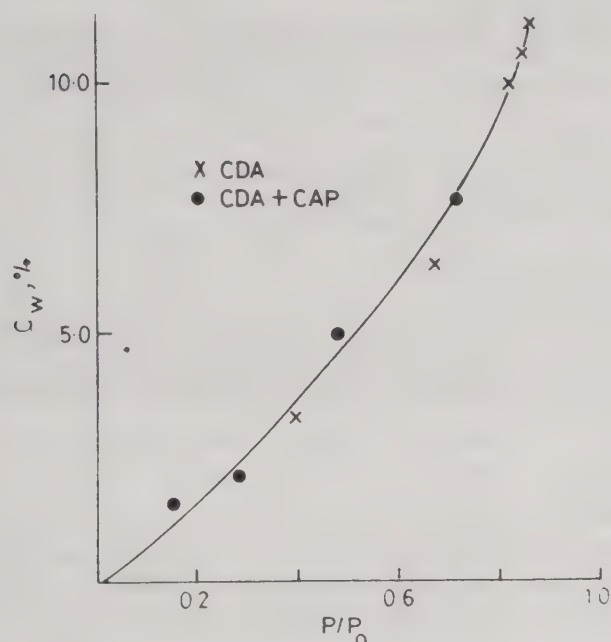


Fig. 1—Water sorption isotherms by films of CDA and CDA+CAP

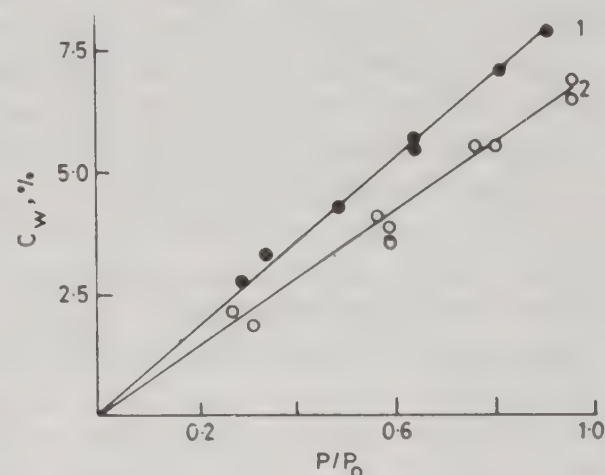


Fig. 3—Water sorption isotherms for films of CAF(1) and CAF+CTA(2)

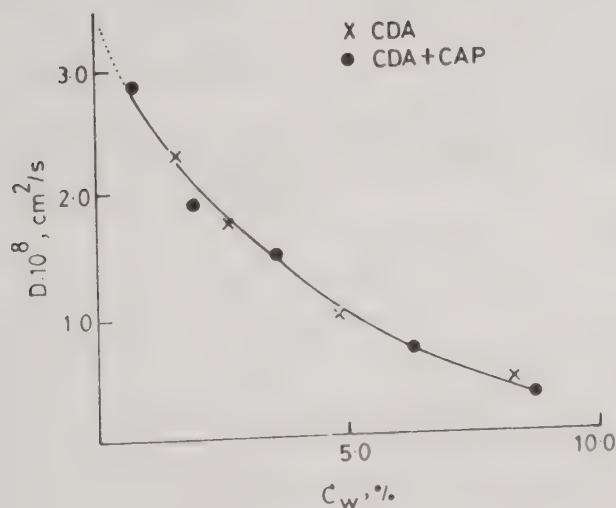


Fig. 2—Dependence of water diffusion coefficient in CDA and CDA+CAP on water contained in polymers

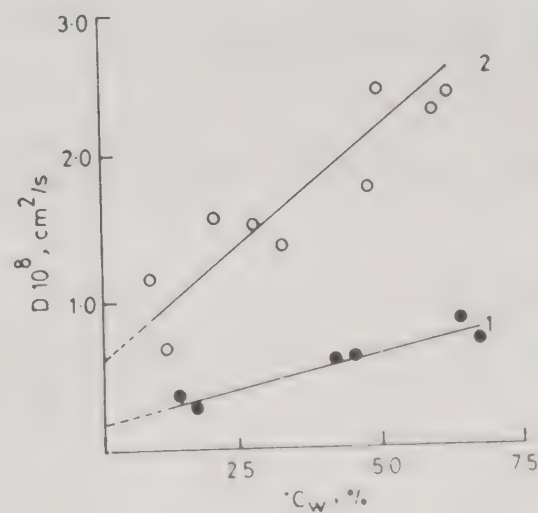


Fig. 4—Dependence of water diffusion coefficient in CAF(1) and CAF+CTA(2)

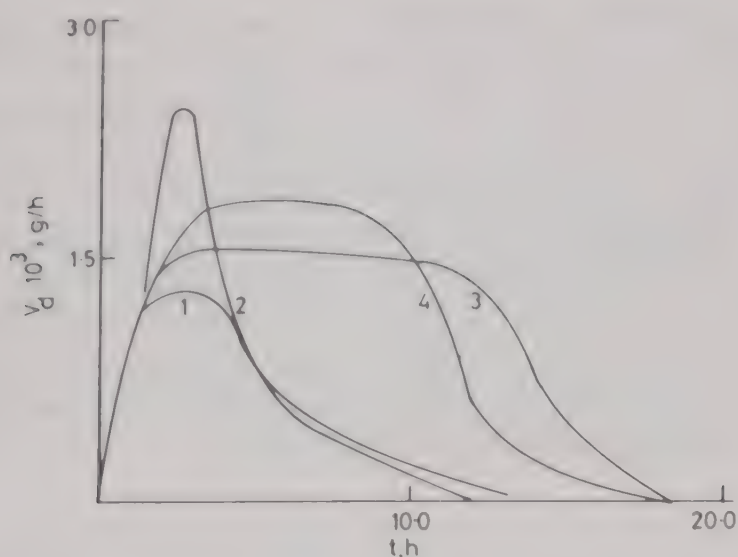


Fig. 5—The profiles of release velocity for sulbutamol sulphate, 37°C. [1—theoretical curve for  $D_w = \text{const} = 10^{-8} \text{ cm}^2/\text{s}$ ; 2—CDA; 3—CFA; 4—CFA + CTA]

celeration of transport of water and formation of clusters slowing it down.

The mathematical model of controlled drug release took into account diffusive and sorption features of polymers, namely, the dependencies 3 and 4, and the constant diffusion coefficient was the initial point of modelling of transport processes in system as a whole. The result of modelling are represented in Fig. 5. The kinetic curve of release obtained for the case of constant  $D$  shows the general features of drug release, of which the main are:

- (i) An increase in drug concentration in the solution of pill followed by acceleration of release.
- (ii) The steady-state or maximum release due to the end of processes of relaxation and the formation of saturated solution.
- (iii) Decrease in the velocity of release followed by the tendency of activities of water in liquid phase and saturated solution to be the same, which is caused by dissolution of the core of pill.

Curve 2 (Fig. 5) illustrates the case of the exponential decrease of diffusion coefficient as concentration of water in polymer increases. For this case, the deceleration of flux of solvent follows the increase in activity of water in saturated solution. Because of equality of fluxes of water and dissolved drug this means that the velocity of drug release will decrease

with passage of time. For this reason, the polymer coating which is characterized by such concentration dependence of diffusion coefficient does not provide steady-state release. This result can be seen in Fig. 5 (curve 2).

On the other hand, it is obvious that steady-state flux of solution of drug could be reached when the velocities of dissolution of pill and transport of water through polymer coating are in opposite directions. Curves 3 and 4 in Fig. 5 show the modelling of such a system for which we used experimental dependencies (3, 4). It is shown that the time interval of steady-state part of drug release is defined by constants involved in expression for  $D$ . For example, it should be expected that the coating of CAF + CTA will provide steady-state release for longer time than that by CAF. At the same time, the velocity of steady-state release will be higher for CAF due to the higher value of water solubility in this polymer.

As a whole, the proposed model enables one to predict the behaviour of controlled drug release system of reservoir type with different polymer coatings, and to predict the mechanism and the velocity of release which are required.

### Acknowledgement

The authors are grateful to Dr. A. P. Maslyukov for samples of various cellulose derivatives and their blends.

### References

- 1 Hariharan D & Peppas N A in *Proceeding 18th International Symp on Controlled release of bioactive materials* edited by I W Kellaway, (Amsterdam The Netherlands), 1991, p. 138-139.
- 2 Langer R & Peppas N A, *J macromol Sci Rev Macromol*, C23 (1983) p. 61-126.
- 3 Iordanskii A L, Polishchuk A Ya & Yu Kosenko R, *J chem biochem Kinet*, (1991) p. 19-30.
- 4 Kokes R J, Long F A & Hoard J L, *J chem Phys*, 20 (1952) p. 1711-1715.
- 5 Reitlinger S A, *Permeability of polymers* (Russ) (Moscow, Khimia), 1974, 269p.
- 6 Polishchuk A Ya, Iordanskii A L & Zaikov G E, *Plastic materials* (Plastmassy—Russ) (1988) p. 38-40.

## Permselectivity of acetate ion to nitrate ion in electrodialysis of aqueous solutions†

P R Shah, G Y Khan & A A Khan\*

Indian Institute of Chemical Technology,  
Hyderabad 500 007, India

Estimation of permselectivity,  $\tau$ , of the electrodialysis (ED) membranes with respect to acetate and nitrate ions shows that  $\tau$  decreases as the current density increases until it attains a constant value which corresponds to its value at limiting current density. Increase in flow velocity of diluate solution results in a corresponding increase in the  $\tau$  values, while the ratio of concentrations of acetate ions to nitrate ions seems to influence  $\tau$  in a similar fashion. It is thus possible to operate ED stacks to achieve a predetermined degree of separation of acetate and nitrate ions by selecting the experimental parameters.

The design of electrodialysis stacks provides for alternate diluate and concentrate compartments. Process streams flowing through these cells respectively get depleted or enriched with respect to the charged ions depending upon a number of parameters including flow rates and compositions of process streams, current density, hydrodynamic conditions within each compartment, and characteristics of the membrane as well as the relative rate of transport of the various charged species present<sup>1-5</sup>. It is the latter phenomenon, which has also been termed 'ion fractionation by permselective membranes'<sup>6</sup>, that has attracted the attention of several investigators in the past. Factors affecting the electro-diffusion of ions in systems consisting of glycine and sodium chloride<sup>6</sup> and calcium and potassium chlorides<sup>7</sup> have been studied in view of specific industrial applications. Similarly, the separation of isotopes and sweetening of citrus juices by selective removal of acids<sup>8</sup> have also been investigated.

In the present work a system consisting of two monovalent anions, acetate and nitrate; has been selected. This is encountered in the purification of raw glyoxal solutions in some of the commercial plants<sup>9</sup>. In these plants, controlled partial oxidation of acetaldehyde (in the aqueous phase) with nitric acid produces a mixture of glyoxal and acetic acid as the main products with some nitric acid.

While removal of the acetate ions does not present serious problems, nitrate ions are more difficult to handle; a combination of several factors is responsible for this difficulty, mainly because nitric acid is nonvolatile and highly oxidising. It is, therefore, necessary to resort to preferential and total removal of nitrate ions before the raw solutions can be further processed. Electrodialysis appears to be the most appropriate technique for this system as it offers removal of both anions without affecting the quality and concentration of the glyoxal product. The present investigation was, therefore, aimed at evaluation of fundamental data to characterise the system and investigate the influence of operating parameters on the transfer processes encountered in electrodialysis.

### Theoretical

A general equation describing the transport of two monovalent anions sharing the same cation has been derived by Benedetto and Lightfoot<sup>10</sup>, and Wills and Lightfoot<sup>11</sup> which demonstrates that the selective transport is proportional to ion mobility ratio in the solution phase. It is also possible to conclude from the above studies that at high current densities, the membrane loses its selectivity. Huang and Tsai<sup>12</sup> showed that if the transport processes within the membrane are mainly governed by electrical migration with negligible bulk flow and diffusion, a simplified version of the Nernst-Planck equation as applied to the membrane phase can be obtained (Eq. 1).

$$N_i = Z_i U_i F C_i \Delta E \quad \dots (1)$$

In view of the above, the general definition of permselectivity of the ion exchange membrane for ion 1 relative to ion 2,  $\tau_1^2$ , is given by Eq. (2).

$$\tau_1^2 = \frac{N_{1(i)}/N_{2(i)}}{C_{2,0}^0/C_{1,0}^0} \quad \dots (2)$$

A practical procedure of determining  $\tau_1^2$ , by measuring the relative concentration of the two species with respect to time, was also suggested<sup>7</sup> wherein

$$\ln \frac{C_{2,0}^0}{C_{2,\theta}^0} = \tau_1^2 \ln \frac{C_{1,0}^0}{C_{1,\theta}^0} \quad \dots (3)$$

†IICT Communication No. S-1685.

## Experimental

Selecion CMV and AMV ion exchange membranes (Asahi Glass Co. Ltd., Japan) were used in the electrodialysis (ED) stack. The characteristics of the membranes are shown in Table 1. Nitric acid, acetic acid and bisodium sulphate used were of chemically pure grade.

The electrodialysis unit was fabricated and assembled at IICT, Hyderabad. The unit consists of three storage tanks, made of stainless steel, connected to centrifugal pumps. All wetted parts of the pumps were made of glass filled polypropylene. The pumps (Syp Engineering, India) were magnetically coupled to the drives in order to avoid leakage of circulating fluids. Control valves and differential pressure manometer were provided in the manifolds (Fig. 1). DC voltage was provided through a regulated DC power supply from a thyristor type rectifier (ITL make), with a 30 V, 10 A stepless variable output. A control panel with suitable instruments was mounted on the frame housing the storage tanks, pump assemblies and the ED stack<sup>13</sup>.

The stack was made of Bakelite filter press frames at either end in which titanium plate electrodes were installed. Cation exchange and anion exchange membranes were placed alternately between the filter press frames with high density polyethylene (HDPE) spacers (1 mm) between the membranes. Polytetrafluoroethylene (PTFE) gaskets (0.5 mm) were used between the spacers and the membrane. Turbulence promoters made of flexible polyvinylchloride (PVC) wire mesh were used to keep the membranes flat and to decrease the thickness of boundary layers between the membranes. The ion exchange membranes, AMV (anionic) and CMV (cationic) (15 cm × 15 cm), with an effective area of 136.89 cm<sup>2</sup> each were used. The stack was made up with six diluate and five concentrate compartments.

Table 1 – Type and properties of selecion membranes

Property	CMV	AMV
	strongly acidic cation-permeable membranes (Na <sup>+</sup> type)	strongly basic anion-permeable membranes (Cl <sup>-</sup> type)
Thickness, mm	0.11-0.15	0.11-0.15
Bursting strength, kg/cm <sup>2</sup>	3-5	3-5
Specific resistance, Ω-cm <sup>2</sup>	180-240	170-230
Resistance per area, Ω-cm <sup>2</sup>	2.0-3.5	2.0-3.5
Transport number T <sub>Na<sup>+</sup></sub>	Over 0.91	—

Feed solution (diluate) containing nitric acid and acetic acid was taken in Storage Tank ST-102. Concentrate solution consisting of slightly acidified distilled water was taken in Storage Tank ST-104. Storage Tank ST-103 was used for the electrode rinse solution (2.75% bisodium sulphate, w/w).

All the three solutions were pumped through the ED stack at controlled flow rates. Adjustment of control valves ensured almost equal pressure (as indicated by the manometer) and approximately equal flow rates in diluate and concentrate compartments. After stabilising the differential pressure, an electric potential was applied across the stack to attain a specific current density for a desired period. Samples of diluate as well as concentrate were drawn at regular intervals to determine the concentrations of nitric acid and acetic acid by standard titrimetric methods.

## Results and discussion

The rate of transfer of the anions was monitored at current densities of 7.3, 14.6, 21.9, 29.2 mA/cm<sup>2</sup> for an initial concentration ratio of nitric acid to acetic acid of 1:10 (% by weight) in the feed (diluate) and a flow rate of 40 cm<sup>3</sup>/sec. The volumetric flow rate of the feed solution was used

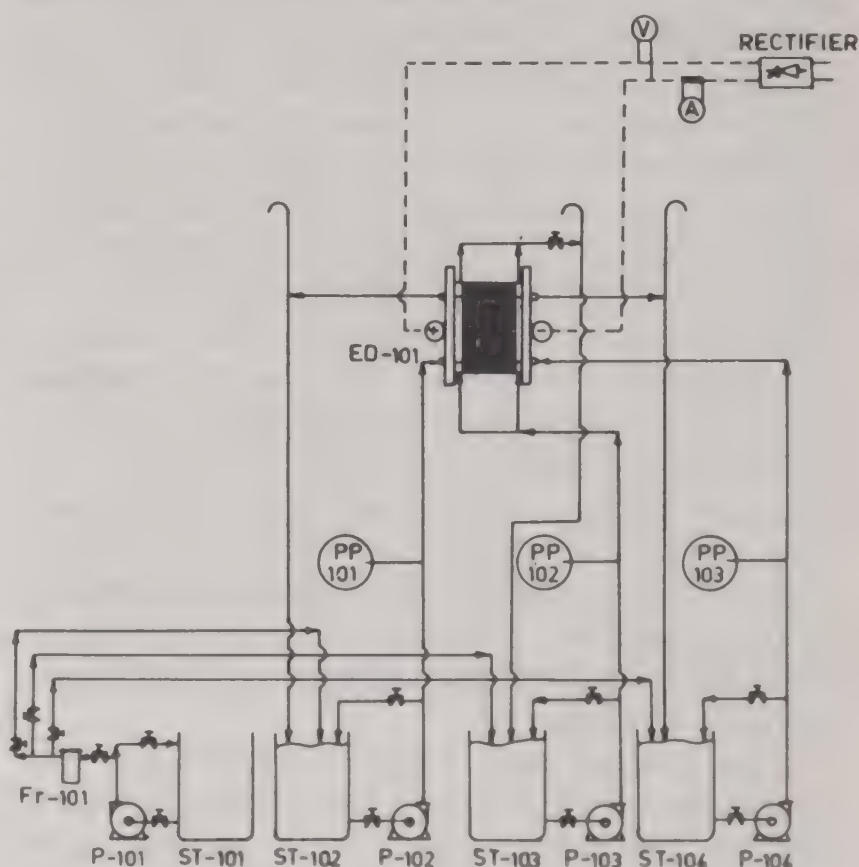


Fig. 1 – Schematic flow chart of electrodialysis unit [ED-101:electrodialyzer, Fi-101:filter, P-101:raw liquid pump, P-102:diluate pump, P-103:electrode rinse pump, P-104:concentrate pump, ST-101:raw liquid tank, ST-102:diluate tank, ST-103:electrode rinse tank, ST-104:concentrate tank, A:ammeter, V:voltmeter, and PP:pressure point (to monometer)]

to compute the linear velocity,  $V$ , by taking into consideration the total cross-sectional area available through the stack, i.e., number of cell pairs multiplied by cross-sectional flow area of each. The total concentration of acids in feed was 11% (w/w). The permselectivity,  $\tau$ , was calculated from the slopes of the linear plots of  $\ln[C_0^0/C_\theta^0]_{\text{NO}_3^-}$  versus  $\ln[C_0^0/C_\theta^0]_{\text{CH}_3\text{COO}^-}$  (Fig. 2). From this data the effect of variation of current density on permselectivity was plotted (Fig. 3). It is observed that permselectivity steadily decreases with increasing current density until it attains a limiting value. Higher current densities do not seem to further reduce the value of  $\tau$ .

For studying the effect of flow rates on permselectivity, variation of  $\tau$  was obtained at a feed (dilute) concentration ratio of nitric acid to acetic acid of 1:10 and total acid concentration of 11% (w/w) at a predetermined current density of 14.6 mA/cm<sup>2</sup>. The feed flow rates studied were 30 cm<sup>3</sup>/sec, 40 cm<sup>3</sup>/sec and 50 cm<sup>3</sup>/sec (i.e. corresponding to flow velocities of approximately 2, 3 and 3.5 cm/sec). A plot of  $\tau$  versus flow velocity  $V$ , showed a linear relationship between the two parameters.

The influence of concentration ratio,  $R$ , of acetate ions to nitrate ions in feed (dilute) solution on permselectivity was investigated by taking solutions with different concentration ratios such as 3:1; 4:1; 5:1 and 10:1 of acetic acid to nitric acid. The pattern of separation of anions was studied at a feed flow rate of 40 cm<sup>3</sup>/sec and a current density of 14.6 mA/cm<sup>2</sup>. The plot between

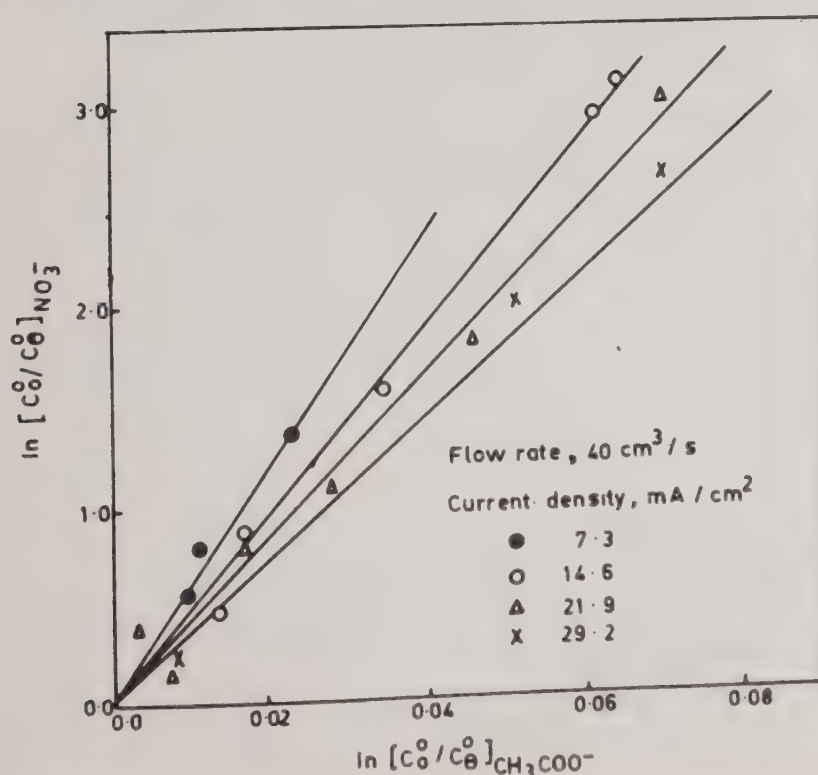


Fig. 2 – Relation between  $\ln[C_0^0/C_\theta^0]_{\text{NO}_3^-}$  and  $\ln[C_0^0/C_\theta^0]_{\text{CH}_3\text{COO}^-}$

permselectivity,  $\tau$ , and concentration ratio,  $R$ , (Fig. 4) shows that  $\tau$  remains practically constant.

From the above results it is seen that for a range of current density of 7.3–29.3 mA/cm<sup>2</sup>, feed flow rate of 30–50 cm<sup>3</sup>/sec, and ratio of concentration of anions of approximately 3 to 10, permselectivity of acetate to nitrate ion,  $\tau_{\text{CH}_3\text{COO}^-}^{\text{NO}_3^-}$ , decreases with increase in current density and increases linearly with increase in flow rate of feed solution. With respect to the concentration ratio, 'R', the value of  $\tau_{\text{CH}_3\text{COO}^-}^{\text{NO}_3^-}$  is observed to fall slightly and then remain more or less constant with increase in 'R'. The variation of permselectivity,

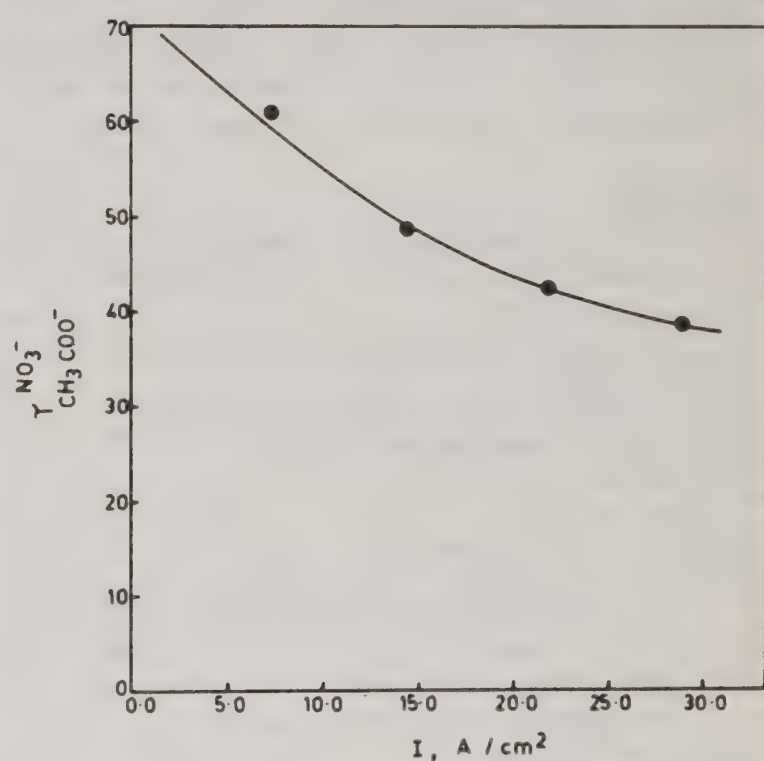


Fig. 3 – Effect of current density on permselectivity

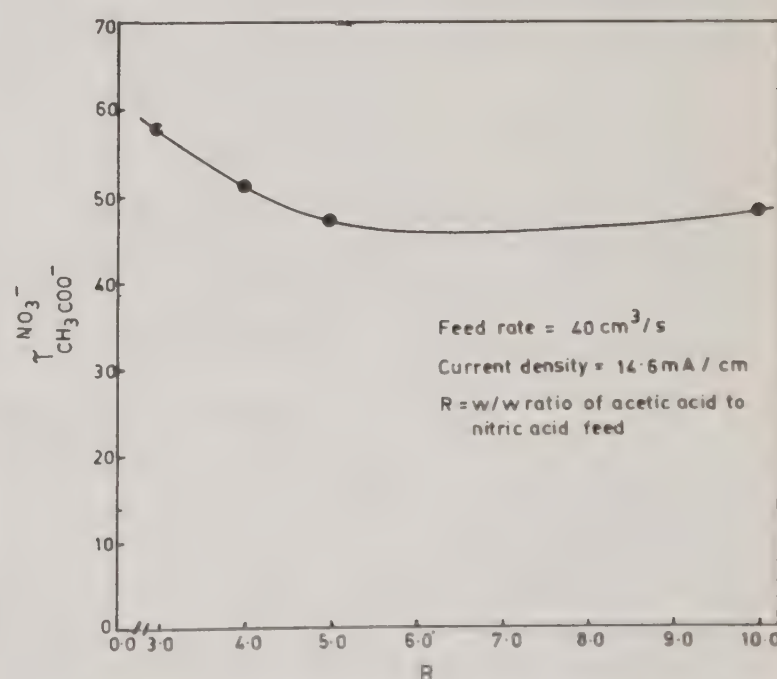


Fig. 4 – Effect of concentration ratio of acetic acid to nitric acid on permselectivity

$\tau_{\text{CH}_3\text{COO}^-}^{\text{NO}_3^-}$ , with respect to current density, flow rate, and concentration ratios of acetate ions to nitrate ions is in agreement with reported literature trends<sup>7,11</sup>.

Dimensional analysis leads to a correlation of type  $\tau_i^2 = a\text{St}^b R^c$  where  $\text{St} = I/FC_iV$ , is the Stanton Number and  $R$  is the ratio of concentration of the two anions. Experimental results are well represented by the following equation with a regression coefficient of 0.9964 and standard deviation of 0.0076.

$$\tau = 0.02762 \text{St}^{-0.4365} R^{-0.3647}$$

This equation predicts the dependence of  $\tau$  on initial total concentration of anions, current density, feed flow rate, as well as the concentration ratios of acetate ions to nitrate ions in the feed solution.

#### Nomenclature

$C_i$	: concentration of species $i$ in the membrane, g mol/lit
$C_{i,0}^0$	: initial concentration of ionic species in bulk solution, g mol/lit
$C_{i,0}^0$	: concentration of bulk solution after a lapse of time, g mol/lit
$C_i$	: total concentration of ionic species, g mol/lit
$E, \Delta E$	: electrical potential gradient, volts
$F$	: Faraday's constant
$i$	: ion species
$I$	: current density, mA/cm <sup>2</sup>
$N_{1i}, N_{2i}$	: flux of ionic species 1 and 2 respectively at the interface of diffusion layer and membrane, g mol/lit.cm <sup>2</sup>
$R$	: ratio of concentrations of acetate ions to nitrate ion
$\text{St}$	: Stanton Number $I/FC_iV$
$U_i$	: ionic mobility in bulk solution, cm <sup>2</sup> /Es
$V$	: flow velocity, cm/s
$Z_i$	: charge of the ion
$\tau$	: permselectivity

#### Subscripts

0	: initial condition
$\theta$	: after a lapse of time
1, 2	: ionic species 1 and 2
$i$	: ionic species $i$ or value at interface

#### Superscripts

0	: bulk solution
---	-----------------

#### References

- 1 Burton H Sandessage & Edgardo H Pairi, *Symposium on the less common means of separation, Inst Chem Engrs*, (1963) 16.
- 2 Donald A Cowan & Jerry H Brown, *Ind Eng Chem*, 51(12)(1959) 1445.
- 3 *Industrial processing with membranes*, Edited by Lacey E Robert and Sydney Loeb, (Wiley-Interscience, New York), 1972.
- 4 Lynn E Applegate, *Chem Eng*, 91(12)(1984) 64.
- 5 H Strathmann, *J memb Sci*, 9 (1981) 121.
- 6 DiBenedetto A T & Lightfoot E N, *Ind Eng Chem*, 50(4) (1958) 691.
- 7 Huang Ting-Chia & Yu Tsu-Ming, *Chem Engg J*, 26 (1983) 119.
- 8 Voss H, *J memb Sci*, 27 (1986) 165.
- 9 Ullman *Encykl Tech Chem*, 4 Aufl, 12, (1976) 377 (Ger.).
- 10 DiBenedetto A T & Lightfoot E N, *Amer Inst chem Eng J*, 8(1), (1962) 79.
- 11 Wills G B & Lightfoot E N, *Amer Inst chem Eng J*, 7(2) (1961) 273.
- 12 Huang Ting-Chia & Fuan Nar Tsai, *Proceedings of the National Science Council of China*, Number 8, Part 3, (May 1975) 247.
- 13 Raghava Rao J, Prasad B G S, Narsimhan V, Ramasami T, Shah P R & Khan A A, *J memb Sci*, 46 (1989) 215.

## Macrocycle-facilitated transport of uranyl ions across supported liquid membranes using dicyclohexano-18-Crown-6 as mobile carrier

Anil Kumar\*, R K Singh, J P Shukla†,  
D D Bajpai & M K T Nair

PREFRE Plant, BARC, Tarapur 401 502

Transport of uranyl ions from aqueous nitric acid solutions across DC18C6/toluene by supported liquid membrane has been investigated using thin flat-sheet polypropylene membrane films as solid supports. More than 95% of uranium can be transported through 0.4 M DC18C6/toluene into dilute aqueous nitric acid strip-pant in about 3-4 hr. Stability of the flat sheet membranes has also been tested.

Interest in the development of new and improved techniques for the separation of ions and molecules has increased in recent years. Of late, much attention has been drawn towards possible uses of artificial membranes in specific separation procedures of industrial and analytical importance<sup>1,2</sup>. Carrier-mediated supported liquid membrane (SLM) is expected to be one of the most efficient membranes for separation processes as facilitated transport is more effective than passive transport. Also, they have a great potential for low cost and energy savings. Both high permeability and improved selectivity are easily attained through enhanced selective transport of carrier species across the membrane soaked in permeant fluid<sup>3-5</sup>. Novel practical applications of such membranes have also been envisaged for the recovery of metals from leach solutions generated in the hydrometallurgical operations; plutonium, americium removal from aqueous nitric acid waste streams generated during plutonium recovery operations in the PUREX process<sup>6-9</sup> etc. Likewise, transport of uranyl ions through SLM consisting of TBP in kerosene supported in Celgard 2400 polypropylene microporous film has been recently reported<sup>10</sup>.

In view of these considerations, a comprehensive work programme has been initiated by us to explore the potential applications of liquid membranes particularly for treating dilute uranium solutions employing a macrocyclic carrier, namely dicyclohexano-18-Crown-6 (DC18C6), which was found to be

highly selective and efficient for uranium extraction into toluene medium<sup>11</sup>. In the present study, DC18C6 dissolved in toluene, was thus selected as the mobile carrier in the facilitated transport of U(VI) across an organic SLM. Effects of important parameters that affect cation flux in liquid membranes such as feed acidity, carrier (DC18C6) concentration in the organic membrane phase, chemical stability of the flat-sheet polypropylene membrane, nature and type of strippant in receiving phase were systematically evaluated. 'Enka' Accurel polypropylene (PP) films were tested as the flat polymeric solid supports for SLM studies.

### Experimental

All the chemical used were of A.R or G.R grade unless specified otherwise. dicyclohexano-18-Crown-6 (DC18C6) (Aldrich Chemicals, U.S.A) was used as supplied. U-233 radio-tracer ( $6.5 \text{ mg dm}^{-3}$ ) was used throughout this study. Details of glass SLM transport cells were discussed elsewhere<sup>12</sup>. Single-stage SLM measurements were carried out with simple two compartment permeation cell which consisted of a feed solution ( $3 \text{ cm}^3$ ) separated by a product solution chamber ( $3 \text{ cm}^3$ ) by a supported liquid membrane having an effective membrane area of  $1.13 \text{ cm}^2$ . The feed and product samples were mechanically stirred well at room temperature to avoid concentration polarization between the membrane interfaces and bulk of solution. Membrane permeabilities were determined by monitoring the uranium concentration radiometrically in both the phases as a function of time. Uranium flux,  $J_M$  was computed using Eq. (1)

$$J_M = C_{U, \text{receiving}} \times V / (A \times t) \quad \dots (1)$$

where  $C_{U, \text{receiving}}$  = initial uranium concentration in the receiving phase,  $\text{mol/dm}^3$ ;  $V$  = volume of receiving phase,  $\text{dm}^3$ ;  $A$  = effective area of the membrane,  $\text{m}^2$ ; and  $t$  = time elapsed.

### Results and discussion

#### Permeation through SLM

Uranium(VI) is appreciably extractable by DC18C6/toluene from nitric acid media and therefore permeated easily across a supported liquid membrane. Of the different aqueous strippants such as dilute nitric acid, oxalic acid, perchloric acid tested, more than 95% of uranium could be recovered only with 0.3 M nitric acid. With rest of the strip-

†Radiochemistry Division, BARC.

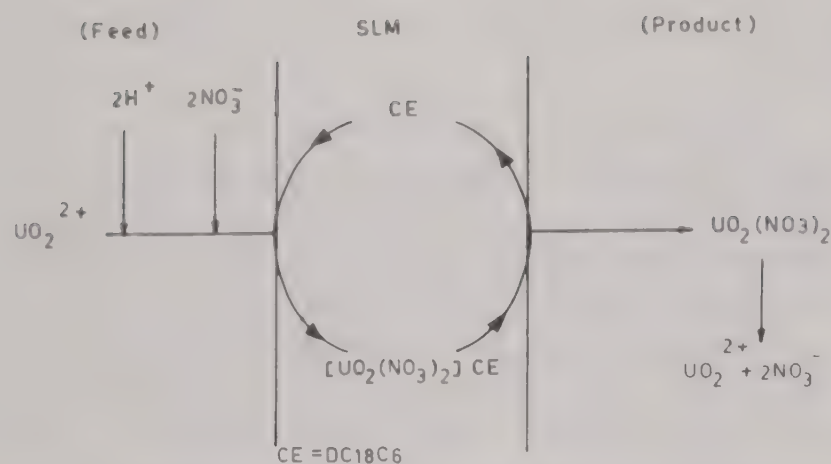


Fig. 1—Possible scheme for uranium(VI) transport from concentrated  $\text{HNO}_3$  solution to dilute  $\text{HNO}_3$  through DC18C6/toluene based supported liquid membrane.

Table 1—Flux and permeation of uranium as a function of carrier (DC18C6) concentration in the organic membrane

Initial source phase acidity: 7  $\text{MHNO}_3$ ; initial uranium concentration:  $6.5 \text{ mg dm}^{-3}$ ; strippant: 0.3  $\text{MHNO}_3$

	Carrier concentration, $\text{MDC18C6}$					
	0.05	0.1	0.2	0.3	0.4	0.5
Rate of transfer <sup>a</sup>						
1 hr	1.0	1.5	1.6	1.7	2.9	1.7
3 hr	0.9	1.0	1.1	1.0	1.5	1.0
Uranium permeation (%)						
1 hr	25.2	56.9	60.2	68.2	84.4	64.7
3 hr	38.2	68.9	88.2	92.5	97.9	92.2
<sup>a</sup> $\times 10^{-7} \text{ mol/m}^2/\text{s}$						

pant, maximum recovery achieved never exceeded 60%. Possible mechanism for U(VI) transport from the source phase to an aqueous receiving phase through DC18C6/toluene based SLM is shown in Fig. 1.

Composition of the organic solution has a marked effect on a cation flux. When transport across a membrane occurs via a carrier, as in facilitated transport, the flux is generally expected to increase with increase in carrier concentration. However, in macrocyclic mediated transport of uranium with DC18C6 a more complex behavior is seen. Table 1 summarizes data of flux versus DC18C6 concentration in the organic membrane. Increasing carrier concentration in diluent like toluene, uranium transport gradually increased reaching a maximum at about 0.4  $\text{M}$  DC18C6 and thereafter decreased significantly for the higher concentrations of carrier. Increase in viscosity of DC18C6/toluene solution may lead to decrease of the diffusion coefficients and hence decrease in permeability of the diffusing species.

Table 2—Flux and permeation of uranium as a function of source phase nitric acid molarity

Initial Feed Concentration:  $6.5 \text{ mg dm}^{-3}$  uranium in  $\text{HNO}_3$ ; carrier concentration: 0.5  $\text{MDC18C6/toluene}$ ; strippant: 0.3  $\text{MHNO}_3$

	Source phase acidity, $\text{MHNO}_3$								
	1	2	3	4	5	6	7	8	9
Rate of transfer <sup>a</sup>									
1 hr	—	0.1	1.4	1.5	1.9	2.6	2.9	2.1	1.7
3 hr	—	0.2	1.7	1.3	1.8	1.6	1.5	1.4	1.2
Uranium permeation (%)									
1 hr	Nil	7.9	27.1	36.2	48.6	60	84.4	73	38
3 hr	Nil	18.5	64.8	70.2	80.9	90.3	97.9	95	70.1
<sup>a</sup> $\times 10^{-7} \text{ mol/m}^2/\text{s}$									

Table 3—Stability and life time of a flat-sheet polypropylene membrane

Initial source phase acidity: 7  $\text{MHNO}_3$ ; Initial uranium concentration:  $6.5 \text{ mg dm}^{-3}$ ; strippant: 0.3  $\text{MHNO}_3$ ; carrier concentration: 0.3  $\text{MDC18C6}$

	Days elapsed <sup>b</sup>					
	1	2	3	4	5	6
Rate of transfer <sup>a</sup>						
1 hr	1.7	1.8	1.6	1.7	1.8	1.6
3 hr	1.0	0.9	1.1	1.0	0.9	1.1
Uranium permeation (%)						
1 hr	70.7	72.5	67.8	70.7	72.4	67.8
3 hr	92.5	93.6	90.1	92.5	93.6	90.1
<sup>a</sup> $\times 10^{-7} \text{ mol/m}^2/\text{s}$ ; <sup>b</sup> membrane was soaked in 0.3 $\text{M}$ DC18C6/toluene in each run						

Results for the single-ion transport of nearly  $6.5 \text{ mg U dm}^{-3}$  from an aqueous feed adjusted to different nitric acid molarities through a DC18C6/toluene SLM membrane into a dilute nitric acid strip solution are summarized in Table 2. The maximum uranium recovery nearly over 95% and maximum flux reaching  $2.9 \times 10^{-7} \text{ mol/m}^2/\text{s}$  after about 1 hr of transport process took place from relatively higher feed acidity up to 7  $\text{MHNO}_3$  in 0.4  $\text{M}$  DC18C6 while its enhanced acidity to about 9  $\text{M}$  adversely affected the uranium transport and plummeted to as low as 70% or even less. The probable reason for decreasing uranium permeability beyond 7  $\text{MHNO}_3$  is because of complexation of DC18C6(CE)

with nitric acid yielding a complex species of type  $\text{CE.mHNO}_3$  ( $m = 1, 2$ ). The difference in the transfer rates of metal ion observed with varying feed acidity and carrier concentrations can be explained by considering the probable expression for the rate of formation of the diffusing species at the feed interface (Eq. 2).

$$d[\text{UO}_2(\text{NO}_3)_2.\text{CE}]/dt = k^*[\text{CE}][\text{NO}_3^-]^2[\text{UO}_2^{2+}] \dots (2)$$

where  $k^*$  is rate constant for the formation of the  $\text{UO}_2^{2+}$ -CE complex, the stoichiometry of which has already been determined as 1:1 (ref. 11).

#### *Chemical stability, regeneration and life time of the membrane*

The chemical stability of the Accurel HF-PP membrane was found to be excellent against concentrated nitric acid and solvent toluene. It was not attacked by either, as uranium flux was found to be almost the same after 2-3 repeated runs using the same membrane already soaked into DC18C6/toluene (Table 3). Experiments were also conducted to observe the regeneration of the membrane. Uranium permeability was evaluated periodically by measuring the uranium flux under the optimum conditions. Before performing each new flux measurement, the feed and strip solutions were replaced with fresh ones. At the end of the permeation experiment, the SLM was left in contact with the depleted feed and uranium loaded strip solution. Loss of carrier was only observed after about 12 hr of continuous use since uranium flux dropped significantly.

#### **Acknowledgement**

The authors wish to thank Shri A.N. Prasad, Director, Fuel Reprocessing and Nuclear Waste Management Group for all the encouragement given during the course of this work. Thanks are also due to Dr. P.R. Natarajan, Head, Radiochemistry division, and Shri A.K. Venugopalan, PREFRE for their keen interests in this work.

#### **References**

- 1 Lonsdale H K, *J membr Sci*, 10 (1982) 81.
- 2 Way J D, Noble R D, Flynn T M & Sloan E D, *J membr Sci*, 12, (1982) 239.
- 3 Dubpernell, in *Modern electroplating*, (edited by F.A. Lowenheim,) 1984, p. 94.
- 4 Loiacono O & Drioli E, "Processi di separazione in idrometallurgia con membrane liquide", *Chim Oggi*, (1985) p. 11.
- 5 Smith K L, Babcock W C, Baker R W & Conrod M G. "Coupled transport membranes for removal of chromium from electroplating rinse solutions", in *Chemistry in water reuse*, (edited by J. Cooper), Vol. 1 Ann Arbor Science, (Ann Arbor Michigan) (1981) p. 311.
- 6 Danesi P R, *Sep Sci and Tech*, 19 (1984-85) 857.
- 7 Danesi P R, Chiarizia R, Rickert P & Horwitz E P, *Sol Ext Ion Exch*, 3, (1985) 111.
- 8 Muscatello A C, Navratil J D & Price M Y, in *Liquid membranes: Theory and applications*, edited by R D Noble and J D Way, ACS Sym Series No. 347, Washington (1987).
- 9 Noble R D, Koval C A & Pellegrino J J, *Chem Engg Progr*, 58 (1989).
- 10 Chaudry M A, Islam N & Mohammad D, *J radioanal nucl Chem*, 109 (1987) 11.
- 11 Shukla J P, Singh R K & Anil Kumar, *Radiochimica Acta*, 54 (1991) 73.
- 12 Shukla J P & Mishra S K, *J membr Sci* (in press).

## Studies on ultrafiltration membrane systems based on cellulosic and polysulfone polymers

K C Thomas, V Ramachandhran, B M Misra & M P S Ramani\*  
Desalination Division, Bhabha Atomic Research Centre,  
Bombay 400 085

Ultrafiltration (UF) membranes have been prepared from aromatic polysulfone and cellulose acetate polymers using the appropriate polymer, solvent and additive composition. The membranes have been characterized in terms of pure water permeability (PWP), membrane constant (A), solute transport parameter  $(D_{AM}/K\delta)_{NaCl}$  and average pore size on the skin surface. The UF performance has been evaluated in terms of water permeation velocity and solute separation using polyethylene glycol solute (PEG-6000). Characterization data and UF performance data have also been discussed.

The reverse osmosis (RO) technology developed at BARC has been employed for desalination as well as for effluent treatment applications during the last few years. We have also recently installed and successfully tested a reverse osmosis plant for treatment of low level radioactive liquid effluents containing different types of radionuclides. The studies indicated achievement of a 20-fold decontamination of activity as well as a 20-fold volume reduction of the effluents. The decontamination of uranium-bearing-effluents has also been tried in plate module based RO units utilising cellulose acetate membranes. It was observed that relatively more porous CA membranes are suitable for rejection of large sized radionuclides and at the same time offer higher permeate output at lower pressures. Recently there has been a renewed interest in ultrafiltration (UF) processes<sup>1-3</sup>. In view of this, a programme was undertaken in our laboratory to develop ultrafiltration and nanofiltration membranes based on cellulosic and non-cellulosic polymers for processing of nuclear streams.

Cellulosic, polyamide and polysulfone membranes were prepared using appropriate additives, solvents and casting conditions. The cellulosic and polysulfone membranes showed better reproducibility and stability. Hence, these membranes were taken up for detailed study. Some aspects like membrane preparation, characterization and performance are reported in this note.

Several factors including the nature of the synthetic polymer, composition of the membrane casting solution, parameters involved in phase inversion technique and post fabrication treatments can significantly affect the ultimate UF membrane properties<sup>4</sup>. Characterization of UF membrane systems is generally attempted in terms of transport analysis using basic transport equations<sup>5</sup> developed for reverse osmosis systems or pore size determination by various techniques<sup>6,7</sup>.

In the present work, the membranes are characterized in terms of pure water permeability (PWP), membrane constant (A) and solute transport parameter  $(D_{AM}/K\delta)_{NaCl}$  using Kimura-Sourirajan transport analysis developed for RO systems. The separation characteristics of the membranes have been evaluated using sodium chloride and polyethylene glycol (PEG) solutes. An attempt has been made to evaluate the average pore radius on membrane surface using modified Hagen-Poiseuille equation<sup>8</sup>.

### Experimental

#### *Preparation of membranes*

(a) *Cellulosic*: Cellulose triacetate (acetyl content 43.2%) and cellulose secondary acetate (acetyl content 39.4%) were obtained from M/s Mysore Acetate and Chemicals, India. Other solutes were used as such without further purification. A mixed solvent system of dioxane and acetone was used to dissolve the cellulose triacetate and cellulose secondary acetate blend polymers. N-methylpyrrolidone was selected as additive. The membrane was cast by spreading a clear solution onto a clean glassplate allowing the solvents to evaporate for a definite period in ambient conditions and gelling the nascent film in service water maintained at a selected temperature. The membranes were used without thermal annealing. Details of casting solution composition, thickness, solvent evaporation time and gelling temperature, etc. are given elsewhere<sup>9</sup>.

(b) *Polysulfone*: Polysulfone (PS) was obtained from Aldrich Chemical Co., Inc., USA. Solvent and additives were LR grade and used without purification. Dimethyl acetamide was used as the solvent. The casting solution was spread on nylon cloth support, solvent evaporated and the nascent film gelled in ambient temperature water containing additives. The composition of casting solution and

Table 1—Composition of polysulfone membranes  
Concentration, % weight

	PS-2	PS-8	PS-13
Polymer, %	18	20	20
DMAc	78	80	80
Gelation bath	Ambient service water containing 10% DMAc	Ambient service water containing 5% DMAc	Ambient service water containing 15% DMAc

Table 2—Membrane characterization data

Membrane No.	PWP ( $\times 10^3$ ) (kg/h)	A ( $\times 10^6$ ) (gmol H <sub>2</sub> O/m <sup>2</sup> .skPag)	(D <sub>AM</sub> /K $\delta$ ) <sub>NaCl</sub> ( $\times 10^7$ ) (m/s)
AT-9	270	3.95	379.6
AT-11	259.9	3.81	332.7
PS-8	20.6	0.209	155.8
PS-13	23.3	0.236	—
PS-2	58.3	0.589	109.5

Effective membrane area:  $15.04 \times 10^{-4} \text{ m}^2$

the amount of additive in the gelation bath are given in Table 1.

### Membrane characterization

The membranes were tested using a specially fabricated test cell similar to the one used in RO experiments. NaCl, mixed electrolyte and polyethylene glycol 6000 (PEG-6000) were used as feed solutes for studying the membrane performance. The membrane performance was evaluated in terms of water permeation velocity and per cent solute separation. The characterization data of the membranes in terms of pure water permeability (PWP), membrane constant (A) and solute transport parameter ( $D_{AM}/K\delta$ ) were obtained from experimentally obtained data on permeability of pure water, product rate and solute separation data using a set of transport equations derived for RO systems<sup>5</sup>. In UF also, the basic transport equations governing solute and solvent transport through the membrane are treated as applicable<sup>3</sup> as long as water is preferentially sorbed at the membrane solution interface and there is no solute accumulation in the membrane pores.

### Results and discussion

The pure water permeability (PWP), membrane constant (A) and solute transport parameter ( $D_{AM}/K\delta$ ) for cellulosic and polysulfone membranes are given in Table 2. It can be seen that mixed cellulose

Table 3—Performance data for aqueous sodium chloride  
Membrane No. Operating pressure (KPa) Water permeation velocity (cms/day) % Separation

AT-9	1368	602.9	17.2
AT-11	2027	627.5	17.0
PS-2	2027	116.4	9.8
	4054	186.3	13.7
PS-8	2027	51.2	5.9
	4054	130.4	2.0

Effective membrane area:  $15.04 \times 10^{-4} \text{ m}^2$

Feed: 5000 ppm sodium chloride

Table 4—Performance data for aqueous PEG-6000

Membrane No.	Operating pressure (KPa)	Water permeation velocity (cms/day)	% Separation
AT-9	709	232.8	64.6
AT-11	709	214.2	61.2
PS-8	1014	21.7	73.0
PS-13	1014	24.5	58.3
PS-2	1014	55.9	24.2

Effective membrane area:  $15.04 \times 10^{-4} \text{ m}^2$

Feed:  $4.87 \times 10^{-3}$  gmoles/litre

acetate membranes have higher values of PWP, A and ( $D_{AM}/K\delta$ )<sub>NaCl</sub> in contrast to polysulfone membranes. This is due to the incorporation of high boiling additive, viz., N-methylpyrrolidone, in the casting solution. Two sets of membranes, viz., AT-9 and AT-11, with comparable UF performance are included mainly to show that similar membranes could be obtained by adopting either higher solvent evaporation and lower gelation temperature or lower solvent evaporation and higher gelation temperature.

In the case of polysulfone membranes, higher PWP and A values were obtained for PS-2 membranes as compared to PS-8 membrane system, due to lower polymer concentration. Higher concentration of DMAc in gelling medium further improves the A and PWP values though the effect is not as drastic as that observed by lowering polymer concentration. It can be seen that PWP, A and ( $D_{AM}/K\delta$ ) values vary significantly for different membrane systems.

The performance data obtained for the two membrane systems with respect to 5000 ppm NaCl solution are given in Table 3. The NaCl rejection by these membranes are around 5 to 10% while the permeate flux ranges from 100 to 200 gfd. These data are comparable with the standard data for UF membranes reported in literature<sup>4</sup>. These values may

therefore be taken as representative for the performance characterization of the UF membranes.

The separation characteristics of these membranes with respect to PEG-6000 solute were evaluated and the results are given in Table 4. Data show that PEG-6000 solute is rejected moderately by these membranes. It can be seen that mixed cellulose acetate membranes offer a much higher water flux for similar separation of PEG-6000 solute in comparison to polysulfone membranes. The comparable solute separation in both the membrane systems indicate the possible existence of similar pore size in the membrane surface though the number of pores on polysulfone membranes may be smaller compared to cellulosic membranes. This could be due to the absence of any additive in the polysulfone casting solution. The lower water flux in the case of polysulfone membranes could also be accounted for by the less hydrophilic nature of the base polymer compared to cellulose acetates. The lower separation of PEG solute and higher water flux obtained in the case of PS-2 membranes indicate the possibility of larger size pores on membrane surface.

#### Pore size determination

In addition to transport analysis (of UF membrane systems) using organic and inorganic solutes, UF membranes are generally characterized in terms of molecular weight cut off (MWCO) and average pore size and pore size distribution. Several techniques such as permoporometry, bubble point technique, solute passage and electron microscopy have been reported. We have evaluated the average pore radius of our membranes using a modified Hagen-Poiseuille equation expressed in a suitable form using the hydraulic flow measurements through membrane and thickness of membrane. The data obtained are presented in Table 5. Eventhough the existence of asymmetric structure in these membranes has been ascertained by permeability measurements (obtained by reversing the membrane surface facing the feed), the total thickness has been used in computation because of difficulty in ascertaining the exact skin thickness. The data presented in Table 5 indicate that higher pore radius was obtained by flow

Table 5—Average pore radius of ultrafiltration membranes

Mem-brane No.	Membrane thickness ( $\times 10^2$ cms)	Hydraulic water flow (ml/cm <sup>2</sup> .s)	Hydrostatic pressure gradient (dynes/cm <sup>2</sup> )	Void content	Pore radius (nm)
AT-9	2	$4.65 \times 10^{-5}$	$4.42 \times 10^4$	0.70	15.5
AT-11	1.7	$6.6 \times 10^{-5}$	$4.42 \times 10^4$	0.69	17.17
PS-2	1.2	$1.05 \times 10^{-3}$	$4.42 \times 10^4$	0.63	60.2

measurements for cellulose acetate membranes than the reported values<sup>6</sup> for similar membranes. This could be due to the use of total thickness instead of actual skin thickness. The higher values obtained for PS-2 membranes compared to AT-9 and AT-11 explains the lower separation with PEG-6000 solutes obtained in the former case. However, the values obtained in the case of AT-9 and AT-11 are not far off the reported values. This indicates the lack of formation of a precise dense skin at the membrane surface and the thickness of the barrier layer is indeed a significant portion of total thickness.

Ultrafiltration membranes in sheet form based on cellulosic as well as non-cellulosic polymers have been successfully prepared and the separation of NaCl and PEG by these membranes has been calculated from solute passage experiments. The membranes are presently under evaluation test under varying conditions of pH, temperature and radiations. These membranes have a good potential for the treatment of various industrial effluents containing macromolecules and also for uranium-bearing nuclear streams.

#### References

- 1 Quinn R M, *Desalination*, 46 (1983) 113-123.
- 2 Fontyn M *et al.*, *J membr Sci*, 36 (1987) 141-145.
- 3 Oldani M & Schock G, *J membr Sci*, 43 (1989) 243-258.
- 4 Wijmans J G *et al.*, *J membr Sci*, 14 (1983) 263.
- 5 Sourirajan S & Takeshi Maturra, *Reverse osmosis/ultrafiltration process principles* (NRCC Publication, Ottawa, Canada), 1985.
- 6 *Ultrafiltration membranes and applications*, edited by A R Cooper (Plenum Press, New York), (1980).
- 7 Abaticchio P *et al.*, *Desalination*, 78 (1990) 235.
- 8 Pusch W & Walch A, *J membr Sci*, 10 (1982) 325.
- 9 Thomas K C *et al.*, *J membr Sci* (Communicated).

# Pertraction of copper(II) in the presence of cobalt(II), nickel(II), manganese(II) and iron(II) using supported liquid membrane

K Sarangi\*

Central Salt & Marine Chemicals Research Institute,  
Bhavnagar 364 002

and

P V R Bhaskar Sarma

Regional Research Laboratory, Bhubaneswar 751 013

Pertraction of Cu(II) in the presence of several bivalent cations such as Co(II), Ni(II), Mn(II) and Fe(II) using D2EHPA(di-2-ethyl hexyl phosphoric acid)-kerosene supported liquid membrane is reported. The standard parameters used for the study are [Cu(II)] in feed  $7.869 \text{ mol m}^{-3}$ , [D2EHPA] in membrane phase  $400 \text{ mol m}^{-3}$ ,  $[\text{H}_2\text{SO}_4]$  in strip solution  $1800 \text{ mol m}^{-3}$ , pH 4.5 and temperature 303 K. The rate constants  $k_1$ , membrane diffusion coefficient  $\bar{D}$ , aqueous film diffusion coefficient  $k_w$  have been estimated from different approximated limiting conditions. Membrane diffusion coefficient  $\bar{D}$  for copper-D2EHPA complex has been determined by dialysis experiment as  $1.2 \times 10^{-12} \text{ m}^2 \text{ s}^{-1}$ . Co(II), Ni(II) and Fe(II) copermeate along with Cu(II) to a small extent while Mn(II) copermeates significantly and it has been found that  $J_{\text{Mn}}$  is more than  $J_{\text{Cu}}$ . Separation factors are calculated and reported.

To minimise the cost of conventional liquid-liquid extraction, and to make easier and simple operating units, a new technique namely liquid membrane (LM) has been exploited for extraction/separation purposes, particularly for the treatment of dilute leach solutions, effluents, waste waters etc. Two major steps i.e. extraction and stripping associated with a conventional solvent extraction process are reduced to one in LM technique<sup>1</sup>. The leach liquors of multi metal minerals (nickel-ferrous laterites, ocean nodules, complex sulphides etc.) contain various metals due to non selective dissolution and for the extraction of different metal ions, di-2-ethylhexyl phosphoric acid (D2EHPA) is being used commercially<sup>2</sup>. These led us to investigate the pertraction of Cu(II) ion in the presence of Co(II), Ni(II), Mn(II) and Fe(II) across a supported liquid membrane (SLM) with D2EHPA as the carrier and kerosene as the membrane solvent.

## Experimental

The commercial reagent, D2EHPA (K & K, USA) was diluted with distilled kerosene (b.p. 170-220°C) and used as the carrier. Feed solution was prepared by dissolving  $\text{CuSO}_4 \cdot 5\text{H}_2\text{O}$  (BDH, Anal-ar) in deionised water.  $\text{H}_2\text{SO}_4$  ( $1800 \text{ mol m}^{-3}$ ) was used as strip solution. The pH of the feed and strip solution were measured with a systronics 335 pH meter with a glass and a calomel electrode and were adjusted to desired pH using dilute  $\text{H}_2\text{SO}_4/\text{NaOH}$ .

Celgard 2400 (Questar Inc., USA), a hydrophobic microporous polypropylene film with thickness 0.025 mm, porosity 38% and an average poresize of  $0.02 \mu$  was used as the solid support for the liquid membrane. The microporous film was impregnated with the carrier and the excess carrier was washed with distilled water<sup>3</sup>.

The membrane was then clamped in between two stainless steel half cells (Fig. 1) forming two compartments. PVC sheets and gaskets were used to prevent leakage. The membrane area was  $27.5 \text{ cm}^2$  with effective membrane area of  $10.45 \text{ cm}^2$  (effective membrane area = membrane area  $\times$  porosity). Compartment-I and Compartment-II were filled with feed and strip solution ( $100 \text{ cm}^3$  each in all experiments) respectively. Equimolar ( $7.869 \text{ mol m}^{-3}$ ) concentrations of Cu(II), Co(II), Ni(II), Fe(II) and Mn(II) were taken in feed solution. Both the aqueous solutions in compartment-I and compartment-II were stirred by mechanical stirrers (Remi

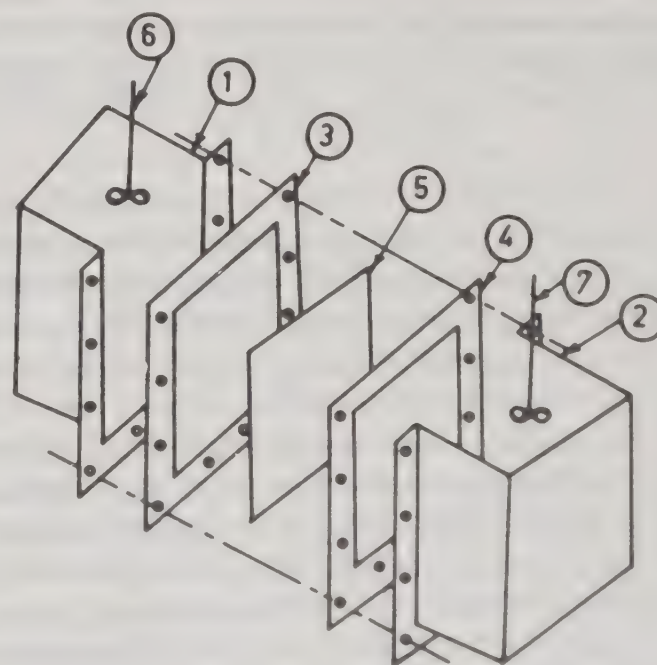


Fig. 1—Exploded view of an apparatus used for the experiment. (1) = Compartment I. (2) = Compartment II. (3) & (4) = PVC sheets with gaskets. (5) = supported liquid membrane. (6) & (7) = mechanical stirrers

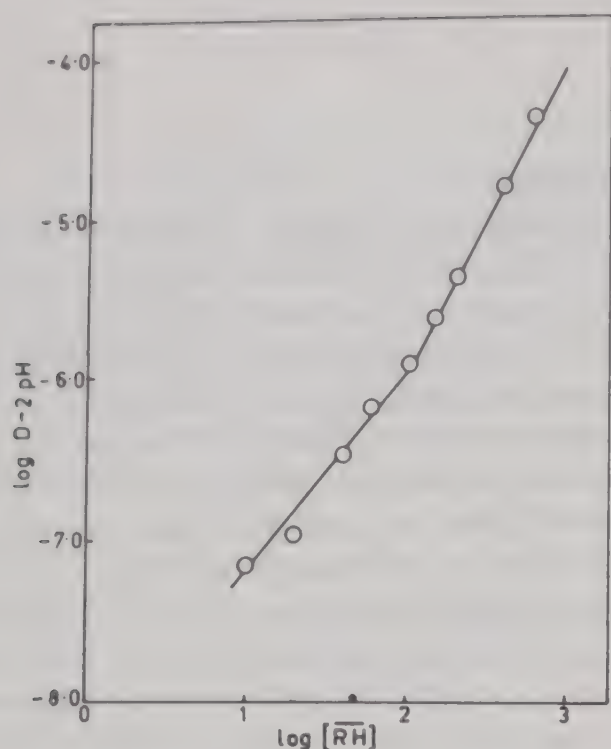


Fig. 2—Effect of D2EHPA concentration on the extraction of Cu(II), (Aqueous phase:  $[\text{Cu(II)}] = 7.869 \text{ mol m}^{-3}$ , organic phase: variable D2EHPA concentration)

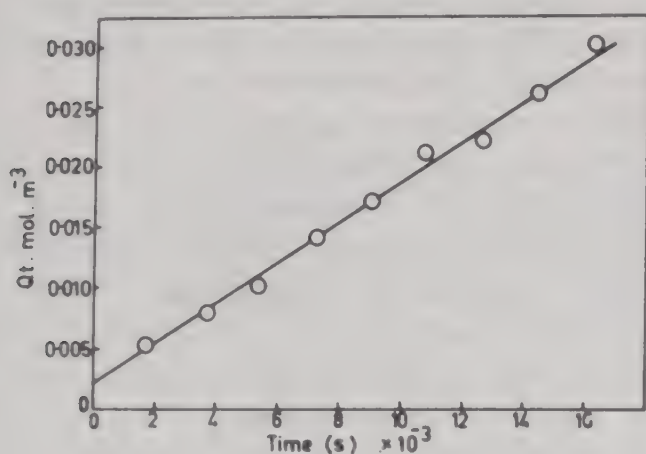


Fig. 3—Enrichment of Cu(II) in strip solution in dialysis experiment (Feed solution:  $[\text{Cu(II)}] = 39.34 \text{ mol m}^{-3}$ , pH 4.5, strip solution:  $[\text{H}_2\text{SO}_4] = 1800 \text{ mol m}^{-3}$ , membrane  $[\text{D2EHPA}] = 400 \text{ mol m}^{-3}$ )

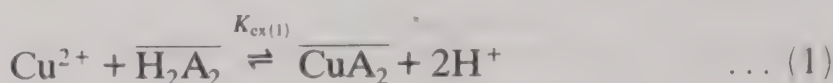
Motor, Type LT-58.1 HP/Watts 1/20 with maximum RPM of 4000) fitted with glass impeller. The impellers consist of two blades with dimensions of thickness 2 mm, width 10 mm and length 10 mm. Stirring speeds were measured by using a digital tachometer (Electron Digital Tachometer Type No DT 20001A) and were maintained at  $200 \text{ min}^{-1}$ . Samples of 1 ml were collected from both the compartments at desired time interval by pipette and analysed using atomic absorption spectrophotometer (Perkin Elmer Model 272). For temperature control, the transport cell was kept in a constant temperature bath which was controlled by a Jumo type thermometer having an accuracy of  $\pm 1^\circ\text{C}$ .

For equilibrium studies, equal volume (25 ml) of Cu(II) solution and D2EHPA in kerosene were

shaken in separatory funnels for 5 min, till complete extraction. After equilibrium the phases were separated and the aqueous phase was analysed for copper. The pH of the aqueous phase was measured, before and at the end of extraction.

## Results and Discussion

The possible types of reactions of D2EHPA with divalent copper can be represented as



$$K_{\text{ex}(1)} = \frac{[\overline{\text{CuA}_2}][\text{H}^+]^2}{[\text{Cu}^{2+}][\overline{\text{H}_2\text{A}_2}]} = D_1 \frac{[\text{H}^+]^2}{[\overline{\text{H}_2\text{A}_2}]} \quad \dots (3)$$

$$K_{\text{ex}(2)} = \frac{[\overline{\text{CuA}_2 \cdot \text{H}_2\text{A}_2}][\text{H}^+]^2}{[\text{Cu}^{2+}][\overline{\text{H}_2\text{A}_2}]^2} = D_2 \frac{[\text{H}^+]^2}{[\overline{\text{H}_2\text{A}_2}]^2} \quad \dots (4)$$

where  $K_{\text{ex}(1)}$  and  $K_{\text{ex}(2)}$  are extraction constants,  $\text{H}_2\text{A}_2$  is used for dimeric D2EHPA and  $D_1$  and  $D_2$  are equal to  $[\overline{\text{CuA}_2}]/[\text{Cu}^{2+}]$  and  $[\overline{\text{CuA}_2 \cdot \text{H}_2\text{A}_2}]/[\text{Cu}^{2+}]$  respectively.

The mass action plot of  $\log D - 2 \text{ pH}$  versus  $\log [\overline{\text{H}_2\text{A}_2}]$  (Fig. 2) was obtained from the results of contacting solutions containing  $[\text{Cu(II)}] 7.869 \text{ mol m}^{-3}$  at pH 4.5 varying D2EHPA concentration from 10 to  $1000 \text{ mol m}^{-3}$ . The slope of this plot is 1.2 at low concentration of D2EHPA and increases to 2.0 at higher concentration of D2EHPA. The change of slope takes place at the mole ratio  $> 12.74$  of  $[\text{D2EHPA}]$  to  $[\text{Cu(II)}]$ . The values of  $K_{\text{ex}(1)}$  and  $K_{\text{ex}(2)}$  were calculated to be  $4.4 \times 10^{-8}$  and  $4.5 \times 10^{-10}$  respectively. The value of  $K_{\text{ex}(2)}$  is used for calculation of  $k_1$ ,  $k_w$  and  $\bar{D}$  as higher concentration of D2EHPA is used in kinetic studies.

The amount of metal ion permeated per unit area  $(V/A)[\text{M(II)}]$  was plotted against time  $t$ . The permeation rates per unit area or flux  $J = (V/A) \{[\text{M(II)}]/dt\}$  were calculated from the initial slopes of the  $(V/A)[\text{M(II)}]$  versus time plots (Fig. 3), where  $V$  is the volume of the aqueous feed solution,  $A$  is the effective membrane area,  $[\text{M(II)}]$  is concentration of metal ion and  $J$  is the flux of the metal ion.

Permeation rate for the metal ion through D2EHPA-kerosene SLM can be expressed<sup>4</sup> as

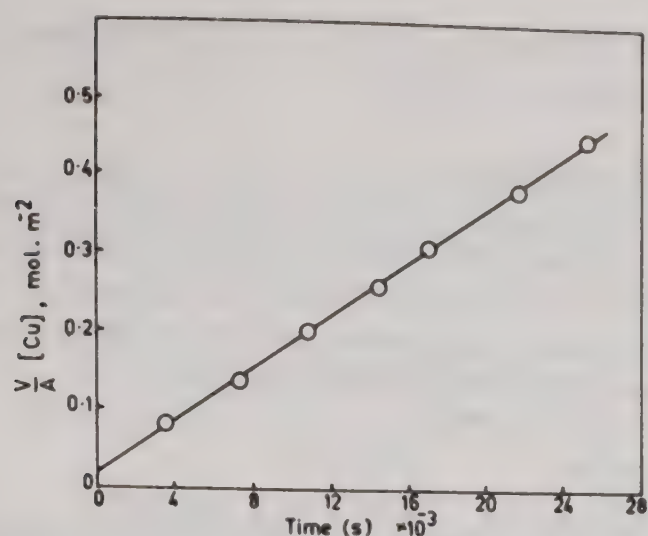


Fig. 4—Variation of the concentration of the copper-D2EHPA complex with time in diffusion dialysis experiment. (Feed solution: copper-D2EHPA complex, strip solution: kerosene, membrane: kerosene)

$$J = \frac{k_1 [Cu^{2+}] [\overline{H_2A_2}]}{[H^+] + k_1 k_w^{-1} [\overline{H_2A_2}] + k_{-1} \left( \frac{\delta_0}{\overline{D}} \right) [H^+]^2} \quad \dots (5)$$

Where  $k_1$  is the forward reaction rate constant,  $k_{-1}$  is the backward reaction rate constant,  $k_w$  is the aqueous film diffusion coefficient,  $\overline{D}$  is the membrane diffusion coefficient and  $\delta_0$  is the membrane thickness.

Copper fluxes for the three limiting cases are as follows:

(1) Diffusion of copper in the aqueous film is rate controlling

$$J = k_w [Cu^{2+}] \quad \dots (6)$$

(2) Forward chelating reaction is rate controlling

$$J = k_1 [Cu^{2+}] [\overline{H_2A_2}] / [H^+] \quad \dots (7)$$

(3) Diffusion of the complex in the membrane is rate controlling

$$J = \left( \frac{\delta_0}{\overline{D}} \right) K_{ex} [Cu^{2+}] [\overline{H_2A_2}]^2 / [H^+]^2 \quad \dots (8)$$

For the determination of diffusivity the time dependent concentration of the copper-D2EHPA complex of the dialysis experiment<sup>5</sup> was plotted against time  $t$  (Fig. 4). From the slope of the linear plot the diffusion coefficient of the copper-D2EHPA complex in the membrane phase was calculated to be  $1.2 \times 10^{-12} \text{ m}^2 \text{ s}^{-1}$ .

The effect of  $pH$  of the feed solution on copper flux was studied between  $pH$  0.5 to 4.5 (Fig. 5) keeping the metal ion concentration of the feed, acid

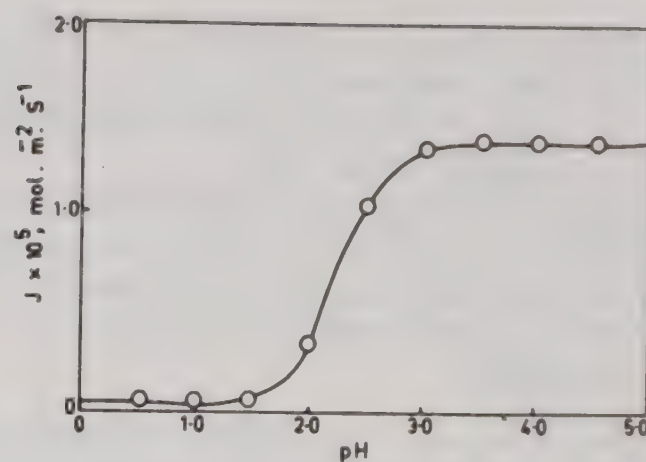


Fig. 5—Effect of  $pH$  on copper flux. (Feed solution:  $[Cu(II)] = 7.869 \text{ mol m}^{-3}$ , variable  $pH$ , strip solution:  $[H_2SO_4] = 1800 \text{ mol m}^{-3}$ , membrane:  $[D2EHPA] = 400 \text{ mol m}^{-3}$ )

Table 1—Pertraction of Cu(II), Co(II), Ni(II), Mn(II) and Fe(II) through D2EHPA kerosene SLM at 303 K

{ $pH = 4.5$ ; [Metal] in feed =  $7.869 \text{ mol m}^{-3}$ ;  $[H_2SO_4]$  in strip solution =  $1800 \text{ mol m}^{-3}$ }

	$J_{Cu} \times 10^{-6}$ $\text{mol m}^{-2} \text{ s}^{-1}$	$J_M \times 10^{-6}$ $\text{mol m}^{-2} \text{ s}^{-1}$	Separation factor $J_{Cu}/J_M$
Cu(II)	14		
Cu(II)-Co(II)	11	2	5.95
Cu(II)-Ni(II)	14	1.8	7.78
Cu(II)-Mn(II)	5	15.0	0.33
Cu(II)-Fe(II)	5	2.8	1.79

where  $M = \text{Mn/Fe/Co/Ni}$  for a binary system.

concentration of the strip solution, temperature and carrier concentration in membrane phase fixed. At low  $pH$  between 0.5 to 1.5, Cu(II) permeation was negligible and it started from  $pH$  2.0 onwards and increased with increase in  $pH$  upto 4.5. Teramoto *et al.*<sup>6</sup> assumed that in the region of low  $pH$  the rate of copper-SME529 complex formation of the feed/membrane interface is slow and this step is rate determining. On the other hand, at low  $[H^+]$ , the flux is high and  $H^+$  affected the rate marginally. In this region of  $pH$ , diffusion through the peripheral oil layer and the internal diffusion limit the transport rate. It seems most likely that at  $pH$  2.0 to 3.0, the forward reaction is rate determining and by using Eq. (7) the forward reaction rate constant  $k_1$  is calculated to be  $(2 \pm 0.1) \times 10^{-8} \text{ m s}^{-1}$ . In the  $pH$  region 3.0 to 4.5 (Fig. 5) the copper flux was found to be independent of  $[H^+]$  and it was assumed that in this  $pH$  region the permeation rate is controlled by the aqueous film diffusion and membrane diffusion. The membrane diffusion coefficient was calculated to be  $9.93 \times 10^{-11} \text{ m}^2 \text{ s}^{-1}$  (using Eq. 8) by neglecting

aqueous film diffusion and aqueous film diffusion coefficient was calculated (using Eq. 6) to be  $1.78 \times 10^{-6} \text{ m s}^{-1}$  by assuming the membrane diffusion to be negligible respectively.

The effect of temperature was studied in the range of 283 to 323 K. The activation energies were calculated from the slopes of the Arrhenius plots at pH 4.5 and 2.0 and found to be 14.5 and 39.1 kJ mol<sup>-1</sup> respectively.

Pertraction of copper was studied in the presence of different bivalent metal ions such as Co(II), Ni(II), Mn(II) and Fe(II). It was found that D2EHPA-kerosene liquid membrane is more selective for Cu(II) than Co(II), Ni(II) and Fe(II). These metal ions co-permeate alongwith Cu(II) to a small extent. But in the presence of Mn(II), this liquid membrane is more selective for Mn(II) than Cu(II). Fluxes for different metal ions and separation factors,  $J_{\text{Cu}}/J_{\text{M}}$ , (where  $J_{\text{Cu}}$  is the copper flux and  $J_{\text{M}}$  is the flux of

other metal ion.  $M = \text{Mn/Fe/Co/Ni}$  for a binary system) are given in Table 1.

### Acknowledgement

The authors express their thanks to the Director, RRL, Bhubaneswar and Dr R P Das for permission to carry out the work. One of the authors (K S) is grateful to the Department of Ocean Development for awarding a research fellowship.

### References

- 1 Akiba K & Kanno T, *Sep Sci Tech*, 18 (1983) 831.
- 2 Ritcey G M & Ashbrook A W, *Solvent extraction, principles and application to process metallurgy*, Vol I (Elsevier, Amsterdam), 1984.
- 3 Lee K H, Evans D F & Cussler E L, *AIChE J*, 24 (1978) 860.
- 4 Sarangi K, *Extraction of metals using liquid membrans*, Ph.D. Thesis, Uktal University, 1989.
- 5 Imato T, Ogawa H, Morooka S & Kato Y, *J chem Eng, Japan*, 14 (1981) 289.
- 6 Teramoto M & Tanimoto H, *Sep Sci Tech*, 18 (1983) 871.

## Transport of alkali metal cations through liquid membrane using non-cyclic synthetic ionophores

Neena Mahadevan & (Mrs) Uma Sharma\*

School of Studies in Chemistry, Vikram University,  
Ujjain (M.P.)

Furan and acetaldehyde have been condensed in ethanol in the presence of conc. HCl to get linear oligomers possessing tetrahydrofuran units. A series of synthetic ionophores is synthesized with the introduction of different end groups at the terminal positions of tetraethylene glycol. For the transport of  $\text{Na}^+$  and  $\text{K}^+$ , **3**, **4** exhibit selectivity for  $\text{Na}^+$  over  $\text{K}^+$ , while **1**, **2** and **5**, **6** show greater transport ability with no selectivity through liquid membrane. From the results of ion transport study, relationship between the structure and transport ability is discussed.

Alkali metal cations ( $\text{Na}^+$ ,  $\text{K}^+$ ) play vital role in bio-systems. Some of the natural ionophores, e.g., actins, nigericin and monensin possess tetrahydrofuran units and have potential ability for carrying an ion across a biological membrane. Recently, appreciable interactions between oxyethylene units and alkali metal ions have been shown by the complex formation of synthetic acyclic oligoethylene glycols and their derivatives with alkali metal salts<sup>1</sup>.

In this study, the synthetic acyclic ionophore tetraethylene glycol and its derivatives having acetoacetate, ethyl benzoate and quinolyl end groups and tetrahydrofuran units (Fig. 1, **1-6**) have been synthesized. They have been used as the carriers and their abilities for selective ion transportation examined.

### Experimental

Alkali metal picrates were prepared as reported earlier<sup>2</sup>. Ionophores **1** and **3** were obtained from Fluka. Ionophores **2**, **4**, **5** and **6** were synthesized<sup>3,4</sup> according to Schemes 1-3.

*Preparation of tetraethylene glycol bis(acetoacetate) (2) and tetraethylene glycol bis(ethylbenzoate) (3)*

A mixture of ethyl acetoacetate (2.0 ml) and tetraethylene glycol (0.66 mol) was stirred and heated slowly over a period of 3 hr to  $180^\circ\text{C}$  at atmospheric pressure. During this period 68 ml of ethanol was

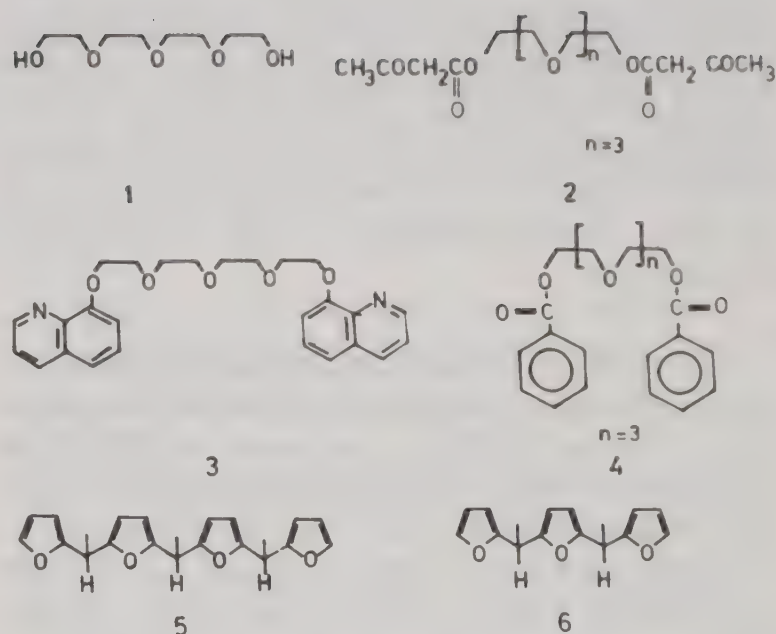
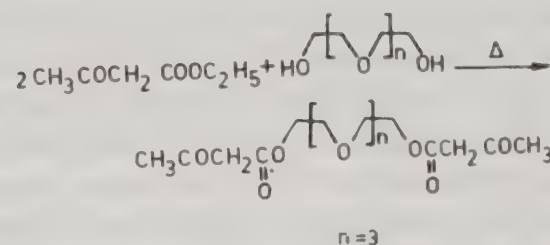
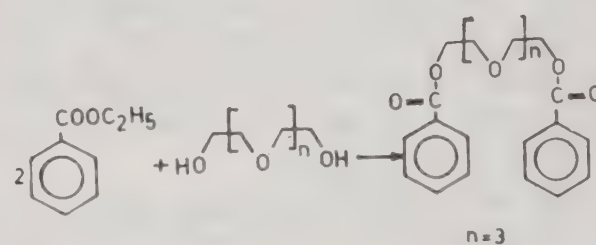


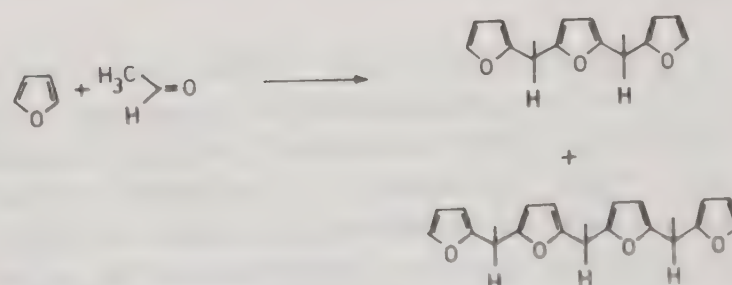
Fig. 1—Ionophores **1-6** used in the present study.



Scheme -1



Scheme -2



Scheme -3

collected. Once ethanol ceased to distil off, distillation was continued at 20 mm, leading to the collection of excess ethyl acetoacetate. The oily residue in the distillation pot was nearly pure (**2**) (87% yield); its  $^1\text{H}$  NMR spectrum showed signals at  $\delta$  2.25 (s,  $6\text{CH}_3$ ), 3.42 (s,  $4\text{CH}_2$ ), 3.59 (s,  $8\text{OCH}_2$ ), 3.64 (m,  $4\text{OCH}_2$ ) and 4.24 (m, 4 ester  $\text{OCH}_2$ ). Because of decomposition of **2** at elevated temperature, no exact mass spectral molecular weight determination was possible.

For (**3**), ethyl benzoate (2.0 mol) and tetraethylene glycol (0.66 mol) were stirred and heated over a period of 3 hr to  $210^\circ\text{C}$  at atm pressure. After removing excess ethyl benzoate under reduced pressure, the residue in pot was characterised. Its  $^1\text{H}$  NMR spectrum showed signals at  $\delta$  4.07 ( $-\text{COOPh}$ ), 3.59 (s,  $9\text{OCH}_2$ ) and 1.48 (s,  $\text{C}_6\text{H}_5$ ). No exact mass spectral analysis was possible.

*Preparation of 1,1-ethylidene bis-5-(methylfurfuryl)furan (**5**) and 2,5-bis-(methylfurfuryl)furan (**6**)*

To an ice-cooled mixture of 68 g (1.0 mol) of furan, 30 ml of ethanol and 20 ml of 35% hydrochloric acid, 22 g (0.5 mol) of acetaldehyde was added with stirring. The addition required 30 min and the reaction was continued for 20 hr at room temperature. The resulting dark green solution was diluted with ether, washed with sodium carbonate and dried. After evaporation of solvents and unreacted furan, a mixture of **5** and **6** was fractionally distilled.

[**6**]-b.p.  $114-116^\circ\text{C}$  (0.1 mm), yield 20.1 g.  $^1\text{H}$  NMR ( $\text{CDCl}_3$ ):  $\delta$  1.54 (d, 6H), 4.15 (q, 2H), 5.90 (d, 2H). Mass spectrum  $m/z$  (%) 250 (100), 242 (30), 241 (190), 161 (68), 141 (30), 113 (23), 105 (58), 95 (66), 81 (57), 77 (34).

[**5**]-b.p.  $165-168^\circ\text{C}$  (0.03 mm) yield 8.0 g.  $^1\text{H}$  NMR ( $\text{CDCl}_3$ ):  $\delta$  1.52 (d, 3H), 1.54 (d, 6H), 4.11 (q, 1H), 4.16 (q, 2H), 5.99 (d, 2H, inside  $\beta$ -H of terminal furan), 6.25 (d, 2H outside  $\beta$ -H of terminal furan) and 7.28 (d, 2H,  $\alpha$ -H). Mass spectrum  $m/z$  (%) 35 (100), 350 (450), 336 (140), 335 (130), 189 (170).

The transportation study of alkali metal cations was carried out using three sets of apparatus<sup>5</sup> identical with that shown schematically in Fig. 2. In addition, a blank experiment was performed for each salt in which the membrane contained no carrier. No detectable amount of cation across the chloroform membrane was found in blank experiments.

A chloroform solution (350 ml) containing  $1.0 \times 10^{-3} \text{ M}$  carrier was located at the bottom of a

Table 1—Amount of  $\text{Na}^+$  and  $\text{K}^+$  cation transported using metal picrates with ionophores **1-6** through  $\text{CHCl}_3$  membrane after 24 hr

[S.P.: metal picrate ( $1.0 \times 10^{-2} \text{ M}$ ), R.P.: distilled water, membrane phase:  $1.0 \times 10^{-3} \text{ M}$  ionophore in  $\text{CHCl}_3$ ]

Ionophore	Transported cation (%)		Total (%)	Selectivity $\text{Na}^+/\text{K}^+$
	$\text{Na}^+$	$\text{K}^+$		
<b>1</b>	90	40	130	2.25
<b>2</b>	20	6.0	26	3.3
<b>3</b>	28	2.0	30	14.5
<b>4</b>	25	3.0	28	8.3
<b>5</b>	44	34	78	1.2
<b>6</b>	32	17	49	1.8
Control	0	0	0	

Reproducibility:  $\pm 7\%$

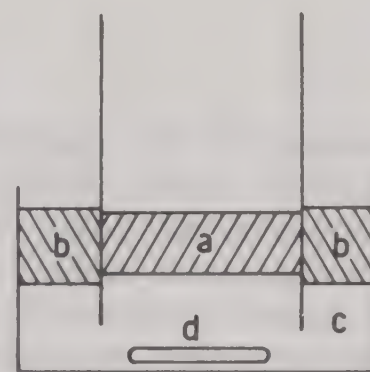


Fig. 2—The liquid membrane cell used for the transportation study. [(a) source phase, (b) receiving phase, (c) membrane phase and (d) magnetic stirrer].

120  $\times$  65 mm glass beaker. Atop this layer there were two water phases separated by a glass cylinder open at both ends and fixed with the help of rubber sole. The inner phase comprised alkali metal picrate solution 42 ml ( $1.0 \times 10^{-2} \text{ M}$ ) serving as a cation source and outer phase comprised doubly distilled water (168 ml) serving as receiving phase. The three phases were agitated constantly by a magnetic stirrer which provided constant and reproducible stirring. The system was sealed to minimize evaporation. The vessels were maintained at  $25 \pm 1^\circ\text{C}$  in a copper bath, in which water at  $25^\circ\text{C}$  was circulated continuously from a thermostat. Samples were withdrawn from the outer receiving phase by a syringe after 24 hr and analysed for cation content using a Perkin Elmer model 2380 atomic absorption spectrophotometer.

## Results and discussion

Amounts of cation transported by various synthetic ionophores **1-6** after 24 hr are listed in Table 1. Na<sup>+</sup> selective ion transport was observed with ionophores **3** and **4** while **1**, **2**, **5** and **6** exhibited more transport ability but less selectivity. Presence of hydrophobic tetrahydrofuran units in **5**, **6** and aromatic donor end groups in **3** and **4** decreases their solubilities in the aqueous medium and reduces the flexibility of the oxyethylene chain. In addition, the pseudocyclic conformation of ligand and stability of complexes are greatly enhanced by the  $\pi$  electrons of the aromatic donor end groups<sup>6</sup> in ionophores **3**, **4**; ionophore **3** adopts pseudocyclic conformation as was reported in case of its RbI complex<sup>7</sup>. The inner cavity size (dia. 2.9 Å) of **3** was estimated to be of the order of ionic radius of K<sup>+</sup> (1.33 Å) while Na<sup>+</sup> ion is smaller in size, forms less stable complex and is transported more efficiently and selectively by **3**. Highest transport ability was observed with simple glycols and linear oligomers of tetrahydrofuran units, as these ionophores can

adopt more easily according to the size of both cations and thus selectivity is lost.

These results indicate that the nature of end group and flexibility of ionophore are very important factors for the ion transportation ability and selectivity. We can design an effective and selective carrier by altering end groups for the efficient separation of certain cation species.

## References

- 1 (a) Poonia N S & Bajaj A V, *Chem Rev*, 79 (1979) 389.  
(b) Hiratani K, Nozakawa I, Nakagawa T & Yamada S, *J membr Sci*, 12 (1982) 207.
- 2 Bhagwat V W, Poonia N S & Sarad K, *Inorg nucl Chem Lett*, 13 (1977) 227.
- 3 Kellogg R M, Van Bergen T J, Herk Van Doren, Hedstrand D, Kooi J, Kruizinga W H & Traaoswijk C B, *J org Chem*, 45 (1980) 2854.
- 4 Kobuke Y, Hanji K, Horiguchi K, Asada M, Nakayama Y & Furkawa J, *J Am chem Soc*, 98 (1976) 7414.
- 5 Lamb J D, Christensen J J, Izatt S R, Bedkē K, Astin M S & Izatt R M, *J Am chem Soc*, 102 (1980) 838.
- 6 Moody J J, Saad B B, Thomas J D R, *Analyst*, 113 (1988) 1295.
- 7 Saenger W & Brand H, *Acta Crystallogr*, 35 (1979) 838.

## New cation exchanger of poly(N-substituted phenylmaleimide) type

Chetan G Patel, Dinesh K Patel, Jayant S Parmar\*

Department of Chemistry, Sardar Patel University,  
Vallabh Vidyanagar 388 120

Four gel type cation exchange resins have been prepared from the condensation product of maleic anhydride and *p*-aminobenzoic acid, i.e., 4-(2,5-dioxopyrrolin-1-yl) benzoic acid (DPBA): homopolymer of DPBA (A), copolymer with styrene (B), cross-linked polymer with divinyl benzene (DVB, 10wt%) (C) and condensation product of 4-aminobenzoic acid with poly(maleic anhydride-co-styrene) (D). The adsorption behaviour of these polymers has been investigated with different cations under various experimental conditions.

Ion exchangers are widely used in analytical chemistry, hydrometallurgy, antibiotic purification, and separation of radioisotopes, and finds large scale applications in water treatment and pollution control<sup>1,2</sup>. Various commercial exchangers have a polymeric base (styrene, acrylic acid, phenol-formaldehyde, etc.) with cationic or anionic units as the site of exchange. In view of rising costs of the polymers, the need exists for either preparing new, cheaper exchangers or finding an efficient substitute that can atleast partly replace the polymeric content of commercial ion exchangers without affecting properties like thermal stability and ion exchange capacity. The present work is an attempt in this direction.

Little attention seems to have been paid to the preparation of ion-exchange resins containing various ion-exchangeable groups on poly(N-

phenylmaleimide) base. In an earlier publication<sup>3</sup>, we had reported the synthesis and characterization of the cation-exchange resins having  $-\text{COOH}$  as functional group on poly(N-phenylmaleimide) matrix. The present work describes detailed ion-exchange study of the synthesized polymers (A-D) with transition metal ions.

### Experimental

The polymers, viz. poly (DPBA) (A), poly (DPBA-co-styrene) (B), poly(DPBA-co-DVB) (C) and poly(DPBA-co-styrene-co-maleic anhydride) (D) were prepared as reported earlier<sup>3</sup>. A batch type equilibration procedure was used to determine the metal uptake from aqueous solution by the resin. The dried resin was ground to 100-150 mesh size powder and stirred with aqueous metal ion solution for a specified period of time under various conditions. The amount of metal ions in the supernatant was subtracted from the amount initially added to give the amount of metal ion adsorbed by the resin<sup>4</sup>.

### Results and discussion

Table 1 summarizes the properties of various polymers. These polymers, containing  $-\text{COOH}$  as a functional group, were prepared by various routes. Polymers (A, B & D) are soluble in solvents like DMF, DMSO and aq. alkali, etc. To impart chemical stability, polymerization was carried out using DVB as cross-linking agent. The polymer with 10% DVB content was only found to be hydrolytically stable, and so it was studied in detail along with others.

#### Optimum pH of metal ion uptake

The effect of pH on the capacities of polymers (A-D) for the transition metal ions is shown in Fig.

Table 1—Properties of polymers (A-D)

Polymer	Colour	N (%) [Expt.]	Softening point (°C)	Solubility	$\eta$ , (DMF, 0.1 M NaNO <sub>3</sub> ) dl.g <sup>-1</sup> (30°C)
A	Cream	6.3	300	DMF, DMSO, dioxane, aq. alkali	0.02
B	Cream	3.99	230-240	DMF, DMSO, aq. alkali	0.20
C	Cream	3.79	300	Swells in DMF, aq. alkali	—
D	Light brown	4.9	191-210	DMF, cyclo- hexanone, aq. alkali	0.415

(1a-d). A mixture of polymer (50 mg), 40 ml of an electrolyte solution (1.0 M,  $\text{NaNO}_3$ ) and 2 ml metal ion (0.1 M) solution was equilibrated for 24 hr at room temperature. The pH of the test solutions was adjusted prior to equilibration with the resin sample by adding dil.  $\text{HNO}_3$  or  $\text{NaOH}$ . After equilibration and filtration, concentration of metal ion remaining in solution was determined by chelatometric titration<sup>5</sup>.

From Fig. (1a-d), it can be seen that the adsorption of metal ion on the resin increases with the in-

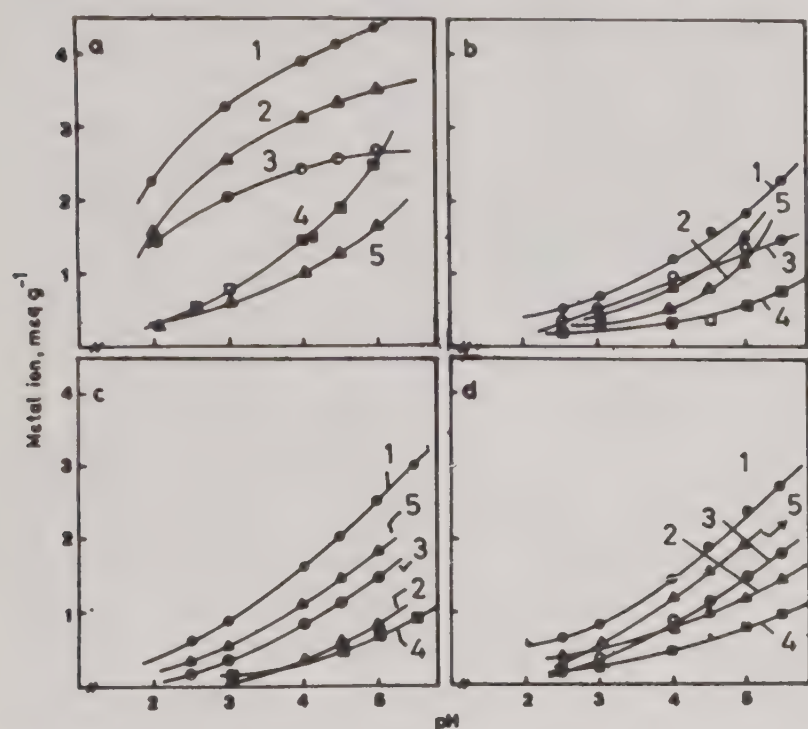


Fig. 1—Effect of pH on the capacities of the polymers for the heavy metal ions: (a), polymer A; (b), polymer B; (c) polymer C; and (d), polymer D [1, ●,  $\text{Cd}^{2+}$ ; 2, Δ,  $\text{Cu}^{2+}$ ; 3, ○,  $\text{Ni}^{2+}$ ; 4, □,  $\text{Zn}^{2+}$ ; 5, ▲,  $\text{Pb}^{2+}$ ].

crease in pH of the solution with maxima in the pH range, 4-5. Under the experimental conditions, the selective adsorption of the various metal ions on polymers (A-D) at the pH 4.5 is in the following order:

A:  $\text{Cd}^{2+} > \text{Cu}^{2+} > \text{Ni}^{2+} > \text{Zn}^{2+} > \text{Pb}^{2+}$

B:  $\text{Cd}^{2+} > \text{Ni}^{2+} > \text{Cu}^{2+} > \text{Pb}^{2+} > \text{Zn}^{2+}$

C:  $\text{Cd}^{2+} > \text{Pb}^{2+} > \text{Ni}^{2+} > \text{Cu}^{2+} > \text{Zn}^{2+}$

D:  $\text{Cd}^{2+} > \text{Pb}^{2+} > \text{Ni}^{2+} > \text{Cu}^{2+} > \text{Zn}^{2+}$

The above trend suggests that all the polymers (A-D) selectively adsorb  $\text{Cd}^{2+}$  ion over other metal ions and polymer A has the highest metal exchange capacity. The resins B and C are more brittle and harder than resins A and D, since both contain higher content of benzene units in the backbone chain. As a result, resins B and C undergo lesser swelling in aqueous solution as compared to resins A and D, and thus possess lower metal adsorption capacity. This clearly suggests that adsorption capacity of metal ions is not only affected by the ion exchange capacity of the resins but also by the extent of swelling in aqueous media.

#### *Influence of contact time on adsorption*

A mixture of polymer (50 mg), 40 ml of an electrolyte solution (1.0 M  $\text{NaNO}_3$ ) and metal ion (2 ml, 0.1 M) was equilibrated for different periods of time and then capacity was determined in each case. The metal ion adsorbed was calculated in % against the time, (hr) for all the metal ions under study. It is seen that the time needed for almost complete saturation

Table 2—Comparison of the rates of cation uptake by polymer A-B<sup>a</sup>

Time, hr	Polymer	Metal ion adsorbed <sup>b</sup> , %					
		$\text{Ni}^{2+}$	$\text{Cu}^{2+}$	$\text{Zn}^{2+}$	$\text{Pb}^{2+}$	$\text{Cd}^{2+}$	$\text{Fe}^{3+}$
0.5	A	16	7	15	56	29	47
	(B)	(23)	(29)	(9)	(35)	(20)	(58.5)
1	A	23	14	22	72	36	56
	(B)	(29)	(37)	(14)	(59)	(34)	(70.2)
2	A	31	29.5	55	81	80	80
	(B)	(46)	(53)	(37)	(73)	(52)	(87.2)
3	A	46	41	72	90	87	97
	(B)	(69)	(59)	(54)	(83)	(69)	(100)
5	A	79	70	89	97	98	100
	(B)	(78)	(69)	(73)	(97)	(86)	—
7	A	100	90	100	100	100	—
	(B)	(88)	(83)	(100)	(100)	(98)	—
9	A	100	100	100	100	100	—
	(B)	(99)	(95)	(100)	(100)	(100)	—

<sup>a</sup> $\text{Me}(\text{NO}_3)_2 = 0.1 \text{ mol/l}$ , 2 ml;  $\text{NaNO}_3 = 1 \text{ mol/lit}$ , 40 ml; pH = 2.5 for  $\text{Fe}^{3+}$  and pH = 4.5 for all other cations.

<sup>b</sup>Related to the amount of metal ions in the state of equilibrium, 24 hr (100%).

Table 3—Comparison of the rates of cation uptake by polymer C-D<sup>a</sup>

Time, hr	Polymer	Metal ion adsorbed <sup>b</sup> , %					
		Ni <sup>2+</sup>	Cu <sup>2+</sup>	Zn <sup>2+</sup>	Pb <sup>2+</sup>	Cd <sup>2+</sup>	Fe <sup>3+</sup>
0.5	C	9.4	23	8.3	53.5	21.5	29.3
	(D)	(20.5)	(29.5)	(14.5)	(55.3)	(22.1)	(35.2)
1.0	C	20.0	36.7	13.7	73.0	54.0	40.2
	(D)	(37.0)	(37.5)	(35.1)	(69.5)	(45.6)	(62.8)
2.0	C	37.1	53.5	22.1	94.8	73.0	61.2
	(D)	(52.9)	(55.3)	(69.5)	(90.0)	(69.5)	(78.2)
3.0	C	56.5	72.2	55.3	98.0	86.0	100
	(D)	(72.2)	(83.8)	(86.5)	(98.0)	(86.8)	(98.9)
5.0	C	79.9	88.0	83.1	100	95.0	—
	(D)	(88.5)	(98.5)	(100)	(100)	(99.0)	—
7.0	C	97.0	90.1	97.7	100	100	—
	(D)	(98.0)	(100)	(100)	(100)	(100)	—

<sup>a</sup>Me(NO<sub>3</sub>)<sub>2</sub> = 0.1 mol/lit, 2 ml; NaNO<sub>3</sub> = 1 mol/lit, 40 ml; pH = 2.5 for Fe<sup>3+</sup> and pH = 4.5 for all other cations

<sup>b</sup>Related to the amount of metal ions in the state of equilibrium, 24 hr (100%).

Table 4—Distribution ratio (D) of metal ions as a function of pH for polymer-C.

pH	Distribution ratio, D (ml g <sup>-1</sup> )			
	Ca <sup>2+</sup>	Ni <sup>2+</sup>	Pb <sup>2+</sup>	Cd <sup>2+</sup>
3.0	19.8	89.9	62.2	107.2
4.0	60.6	137.9	152.2	205.4
4.5	71.1	166.7	200.0	279.3
5.0	81.0	211.8	225.6	305.1

of the capacity of the polymer for metal ions is about 5-7 hr (Tables 2 and 3).

#### Distribution ratio of metal ions

The distribution of each metal ion, between polymer phase and aqueous phase, was determined at various pH and in presence of 1.0 M NaNO<sub>3</sub> solution at 30°C. The experiments were carried out as described earlier. Adsorbability of a metal ion on the resin can be expressed in terms of the distribution ratio, D, which is defined as:

$$D = \frac{\text{meq. of metal on the resin}}{\text{meq. of metal in the solution}} \times \frac{\text{volume of solution (ml)}}{\text{weight of resin (g)}}$$

Adsorption of cations generally increased with increasing pH studied upto pH 3.5 for Fe<sup>3+</sup> and 5.5 for other metal ions to avoid hydroxide formation. This study is useful in selecting the optimum pH for selective adsorption of a particular metal ion from a mixture of metal ions. For example, from Table 4 it could be seen that at pH 4.5 the Pb<sup>2+</sup> ions (D = 200) can be selectively separated from mixture with Ca<sup>2+</sup> ion (D = 71.1).

Table 5—Separation of metal ions, using polymer-C

Pb <sup>2+</sup> :Ca <sup>2+</sup>	Amount of metal ions adsorbed, (mg)	
	Pb <sup>2+</sup>	Ca <sup>2+</sup>
0 : 10	—	20.1
4 : 6	52.1	16.5
5 : 5	89.1	10.1
6 : 4	120.2	5.4
10 : 0	160.1	—

Polymer = 300 mg, metal ion solution = 50 ml, Conc. of total metal ions = 1.2 mmol

It is reported that<sup>6</sup> using standard procedures, Pb<sup>2+</sup> and Ca<sup>2+</sup> ions could be separated from their mixture. Following this procedure the separation of Ca<sup>2+</sup> ions from a mixture of Ca<sup>2+</sup>-Pb<sup>2+</sup> was carried out (Table 5). The results indicate that at about equal proportions of the two ions, Pb<sup>2+</sup> gets adsorbed nine times as much as Ca<sup>2+</sup> ions.

#### Acknowledgement

One of the authors (CGP) is highly grateful to CSIR, New Delhi for providing financial assistance (SRF).

#### References

- 1 Helfferich F, *Ion exchange*, (McGraw Hill, New York), 1962.
- 2 Kunin R, *Ion exchange resins*, 3rd Edn, (Wiley, New York) 1958.
- 3 Patel C G, Patel D K & Parmar J S, *High performance polymers*, 3(2) (1991) 89.
- 4 Reilley C N, Schmid R W & Sadak F S, *J chem Educ*, 36, (1959) 555.
- 5 Vogel A I, *Textbook of quantitative inorganic analysis*, 4th Edn, (1978) 177.
- 6 Vogel A I, *Textbook of quantitative inorganic analysis*, 4th Edn, (1978) 329.

## Separation of Co(II)-Zn(II), Co(II)-Mn(II) and Zn(II)-Mn(II) systems from their binary solutions through supported liquid membrane containing organophosphorus acid as extractant

R Mohapatra, S B Kanungo\* & P V R B Sarma

Regional Research Laboratory, Bhubaneswar 751 013

The separation of Co(II)-Zn(II), Co(II)-Mn(II) and Zn(II)-Mn(II) systems has been carried out from their aqueous sulphate solutions through supported liquid membrane (SLM) containing organophosphorus acid in kerosene as extractant. The implications of these data in hydrometallurgy are briefly discussed.

Liquid membrane containing a carrier or extractant dissolved in an organic solvent and supported on microporous polymer film is fast emerging as a new technique for the concentration and separation of metal ions from waste water, industrial effluent and dilute leach liquor obtained from hydrometallurgical processing of lean ores. The main advantages of this process are, (a) low consumption of extractant, (b) low capital and operating cost, (c) low energy requirement and (d) possibility of achieving high separation factor<sup>1</sup>.

The technique of impregnating a porous film support with a dilute solution of extractant was first demonstrated by Bloach<sup>2</sup> and Cussler<sup>3</sup>. In later years, the SLM was used not only for the separation of metals ions<sup>4-8</sup> but also for the removal of other materials such as acids from waste water.

The separation of Co(II) from Ni(II) through SLM containing solution of Cyanex-272 in a mixture of decalin and isopropyl benzene has been studied by Danesi and Rickert<sup>9</sup>. Sarangi *et al.*<sup>10</sup> have reported the results of separation of several binary metal ions through liquid membrane containing LIX64N or D2EHPA or both in kerosene solution as carriers. Though many works have been reported during the last several years on the use of SLM as a technique of separation, none of these workers have used kerosene as a diluent, though it is widely used in the solvent extraction of metals. In this note we report the separation of Co(II)-Zn(II), Co(II)-Mn(II) and Zn(II)-Mn(II) binary systems through SLM containing D2EHPA or Cyanex-272 diluted in kerosene.

## Experimental

Di(2-ethylhexyl) phosphoric acid (D2EHPA) supplied by K and K, USA and bis(2,4,4-trimethyl pentyl) phosphinic acid (Cyanex-272) supplied by Cyanamide, USA were used as extractants; they were diluted in re-distilled kerosene (b.pt. 170°-200°C).

The feed solutions were prepared by dissolving MnSO<sub>4</sub>.H<sub>2</sub>O, CoSO<sub>4</sub>.7H<sub>2</sub>O and ZnSO<sub>4</sub>.7H<sub>2</sub>O (BDH, Analar) in deionised water. Acetate buffer was used for maintaining pH of the feed solution. Ionic strength was adjusted with the help of 0.1M Na<sub>2</sub>SO<sub>4</sub> solution.

The microporous polypropylene film Celgard 2500 was used as solid support for the liquid membrane. The film was impregnated with the extractant solution under moderate vacuum (10<sup>-2</sup> Torr). The film has a thickness of 0.025 mm and 45% nominal porosity with an average pore size of 0.04 µm.

## Method

The cell used for the experiment has been described earlier<sup>1</sup>. The compartment I of the cell was filled with 100 cm<sup>3</sup> of feed solution and the compartment II was filled with the same volume of stripping solution, i.e., sulphuric acid of 900 mol m<sup>-3</sup>. Both the phases were agitated by mechanical stirrers. Samples were collected from both the compartments at suitable intervals of time and the metal ions were analysed using a Perkin Elmer (Model 337) atomic absorption spectrophotometer.

## Results and discussion

The M(II) flux across the membrane was calculated from the slope of linear plot of M(II) concentration in the compartment II against time. The flux is given by

$$J = \frac{V}{A} \frac{d[M(II)]}{dt} \text{ mol m}^{-2} \text{ s}^{-1}$$

where, V is the volume of solution (m<sup>3</sup>) and A is the effective membrane area (m<sup>2</sup>).

The following metal ion solution-organic carrier systems have been studied:

### (1) Co(II)-Zn(II)-D2EHPA system

The aqueous feed solution contains Co(II) and Zn(II) concentration of 2.54 and 3.02 mol m<sup>-3</sup> re-

Table 1—Separation factors for some binary metal ion systems under different experimental conditions

Metal ion	pH	Extractant sol.	Metal ion flux mol m <sup>-2</sup> s <sup>-1</sup>	Separation factors (s)
Co(II)-Zn(II)	3.35	D2EHPA-Kerosene	J <sub>Zn</sub> = 4.2 × 10 <sup>-6</sup> J <sub>Co</sub> = 0.81 × 10 <sup>-6</sup>	J <sub>Zn</sub> /J <sub>Co</sub> = 5.2
	4.5	-do-	J <sub>Zn</sub> = 6.15 × 10 <sup>-6</sup> J <sub>Co</sub> = 1.20 × 10 <sup>-6</sup>	J <sub>Zn</sub> /J <sub>Co</sub> = 5.1
Co(II)-Mn(II)	3.5	-do-	J <sub>Mn</sub> = 0.93 × 10 <sup>-6</sup> J <sub>Co</sub> = 0.25 × 10 <sup>-6</sup>	J <sub>Mn</sub> /J <sub>Co</sub> = 3.7
	4.5	-do-	J <sub>Mn</sub> = 1.49 × 10 <sup>-6</sup> J <sub>Co</sub> = 0.405 × 10 <sup>-6</sup>	J <sub>Mn</sub> /J <sub>Co</sub> = 3.6
Zn(II)-Mn(II)	3.5	-do-	J <sub>Mn</sub> = 10.0 × 10 <sup>-6</sup> J <sub>Zn</sub> = 3.4 × 10 <sup>-6</sup>	J <sub>Mn</sub> /J <sub>Zn</sub> = 3.1
	4.5	-do-	J <sub>Mn</sub> = 12.9 × 10 <sup>-6</sup> J <sub>Zn</sub> = 4.1 × 10 <sup>-6</sup>	J <sub>Mn</sub> /J <sub>Zn</sub> = 2.9
Zn(II)-Mn(II)	3.5	Cyanex-272 Kerosene	J <sub>Zn</sub> = 4.21 × 10 <sup>-6</sup> J <sub>Mn</sub> = 1.05 × 10 <sup>-6</sup>	J <sub>Zn</sub> /J <sub>Mn</sub> = 4.0
	4.5	-do-	J <sub>Zn</sub> = 6.20 × 10 <sup>-6</sup> J <sub>Mn</sub> = 1.35 × 10 <sup>-6</sup>	J <sub>Zn</sub> /J <sub>Mn</sub> = 4.6

spectively. Metal ion fluxes ( $J_{Co}$  and  $J_{Zn}$ ) were determined at pH 3.35 and 4.50 and D2EHPA concentration of 400 mol m<sup>-3</sup>. It is observed that both  $J_{Co}$  and  $J_{Zn}$  vary in a similar manner with pH so that the ratio of  $J_{Zn}/J_{Co}$  which is considered as a separation factor, is almost same.

#### (2) Co(II)-Mn(II)-D2EHPA system

In this system the concentrations of Co(II) and Mn(II) in aqueous feed solution are 2.54 and 2.73 mol m<sup>-3</sup> respectively and the membrane has D2EHPA concentration of 80 mol m<sup>-3</sup>. Metal flux values are found to vary with pH in the same manner as in (1) so that no difference in the separation factor is observed at different pH values.

#### (3) Zn(II)-Mn(II)-D2EHPA system

The initial concentrations of Zn(II) and Mn(II) in the aqueous feed solution are 3.06 and 3.64 mol m<sup>-3</sup> respectively and the other conditions are same as in (1). Table 1 shows that separation factor is poor as both the metals exhibit good transport through such as system.

#### (4) Zn(II)-Mn(II)-Cyanex 272 system

The initial concentrations of Zn(II) and Mn(II) in the feed solution are same as in (3). The flux values are also measured at the same pH values. The separation factor shows some improvement over system (3) when Cyanex-272 is used as an extractant instead of D2EHPA.

Although the results presented in Table 1 are of preliminary nature, they suggest that by choosing

suitable extractant and experimental conditions, it is possible to achieve more selective separation of metal ions. Further work in this direction is being pursued in this laboratory.

#### Acknowledgement

The authors wish to thank Dr R P Das, Head of Hydro & Electrometallurgy Divn., for his interest and support. Thanks are also due to Director, RRL, Bhubaneswar for his permission to publish this note. One of the authors (R M) is grateful to the Department of Ocean Development, Govt. of India, for awarding a fellowship.

#### References

- 1 Danesi P R, *Sep Sci Technol*, 19 (1984) 857.
- 2 Bloach R, *Hydrometallurgical separations by solvent membranes in Membrane science and technology*, edited by J E Flinn (Plenum Press, New York), 1970, 187.
- 3 Cussler E L, *AIChE*, 17 (1971) 1300.
- 4 Baker R W, Tuttle M R & Lonsdale H K, *J membr Sci*, 2 (1977) 213.
- 5 Babcock W C, Baker R W, Lachapelle E D & Smith K L, *J membr Sci*, 7 (1980) 71, 89.
- 6 Pearson D, *Ion exchange membranes*, edited by D S Flett (Society of Chemical Industry, London) 1883, 55-73.
- 7 Nishiki T & Bautista R G, *AIChE*, 31 (1985) 2093.
- 8 Chaudry M A, Malik M T & Hussain K, *Sep Sci Technol*, 24 (1989-90) 1293.
- 9 Danesi P R & Rickert P, *Solv Extr Ion Exchange*, 4 (1986) 149.
- 10 Sarangi K, Acharya S, Sarma P V R B & Das R P, *International conference on base metals technology* (Jamshedpur, 8-10 Feb) 1989, pp 235-238.
- 11 Mohapatra R, Kanungo S B & Sarma P V R B, *Sep Sci Technol*, 27 (1992) 765.

## BOOK REVIEW

**Basic principles of membrane technology**, by M. Mulder (Kulwer, Dordrecht), pp. 372, Price £ 24.0 (Paperback), 1991, ISBN 0-7923-0979-0.

The present book, essentially written as a text-book for students, attempts at presenting the various aspects of membrane technology beginning with the properties of membrane polymers to the ultimate uses of the membranes and process design.

The introductory chapter deals with the history of development of the membranes, membrane processes and the theoretical aspects. The second chapter on membrane materials and their properties is brief and sketchy. It covers porous membranes for UF and MF on one extreme and non-porous membranes for gas separations and pervaporation on the other. The material choice for RO separations, particularly polar and nonpolar membrane materials for organic and inorganic solutes in aqueous media, is not discussed. The relevance of LC (liquid chromatographic) data in the appropriate selection of the membrane materials could also have been mentioned.

The overview of various membrane preparation techniques (chapter III) includes a detailed discussion on phase inversion techniques in terms of thermodynamics of polymer solutions and its demixing. The surface characterizations of nonporous membranes (chapter IV) by plasma etching, ESCA, XPS, SMIS and AES are of interest. But use of density gradient column and wide angle X-ray scattering (WAXS) are techniques more useful for characterisation of polymers than for membranes. The transport through porous and nonporous membranes (chapter V) is discussed in terms of phenomenological approach using non-equilibrium thermodynamics and mechanistic models such as pore flow and the solution diffusion models. The chapter is, however, not balanced. The author does not consider at all the preferential sorption capillary flow mechanism, which was first evolved for explaining reverse osmosis separation and is presently extended to explain all the membrane processes. It is also surprising that there is no reference to the work of Sourirajan at all. The solution diffusion mechanism has been indicated, particularly in the context of pervaporation and gaseous separations. Discussions on the various mechanisms along with their range of applicabilities could also have been included.

The treatment of concentration polarisation in chapter VII could also have been improved. Flux

decline with time is not due to concentration polarisation. Concentration poolarisation is a negative driving force which should appear on the numerator of equation (VII-1) and not a positive resistance in the denominator of the equation. Hence, the concept of concentration polarisation as given by the author is wrong. In equation (VII-3) on page 284 the second term on the RHS should have a negative sign. The author is dealing with the mass transfer coefficient 'K'. Concentration polarisation or equivalent boundary layer phenomenon is of concern in the engineering of membrane separation plants. Sourirajan gives an excellent development of concentration polarisation and solute transport through the membranes as engineering parameters. The concept 'K' is borrowed from that. But sadly there is no mention of the reference or the Kimura-Sourirajan equations.

The last chapter dealing with module & process design is too general and even the limited information presented is too superficial to be of any significance. The process calculations indicated for the single stage sea water desalination by reverse osmosis is too innocent. The use of membrane performance at 15 bar pressure for 1500 ppm sodium chloride solution to evaluate 'A' as well as the projection of the performance for sea water feed at 50 bar pressure is not consistent with established design procedures. The author does not take into account concentration polarisation in the computations. The concept and determination of pure water permeability as proposed by Sourirajan would have been more appropriate as it avoids experimental errors due to concentration polarisation.

Overall, the book is of average worth on the basis of the first six chapters including the introduction. The last two chapters dealing with engineering aspects considerably diminish the worth of the book. A book should have precision and clarity of concepts in order to serve as an authoritative source of information to the reader particularly students.

There are also too many printing and possibly grammatical errors. The reference to tables and figures in the text have been wrongly made in many places. For instance on page 339 Table VIII-6 is referred to under sea water reverse osmosis. But the Table actually gives data on ultrafiltration.

M P S Ramani  
Desalination Division  
Bhaba Atomic Research Centre  
Bombay 400 085

## Errata

Paper entitled, "Syntheses of polystyrene chelating resin containing the schiff base derived from 3-formylsalicylic acid and *o*-hydroxybenzylamine and its copper(II), nickel(II), iron(II), zinc(II), cadmium(II), zirconium(IV), molybdenum (V and VI), and uranium(VI) complexes by A Syamal and M M Singh, *Indian J Chem*, 31A (1992) 110-115.

The sub-headings in the right hand column of page 111 should read as:

"Synthesis of PS-LMoOCl.DMF" instead of "Synthesis of PS-LMoO<sub>2</sub>.DMF".

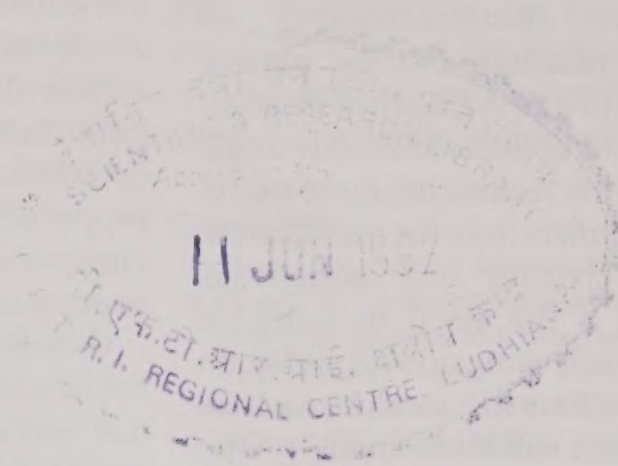
"Synthesis of PS-LMoO<sub>2</sub>.DMF" instead of "Synthesis of PS-LFeCl.2DMF".

"Synthesis of PS-LFeCl.2DMF" instead of "Synthesis of PS-LZr(OH)<sub>2</sub>.2DMF".

Paper entitled, "Solvent behaviour of cupric chloride in non-aqueous solvents" by Prem P Singh, Manjula Soni and S. Maken, *Indian J Chem*, 31A (1992) 227-231.

Due to an inadvertant mistake at the printing stage, references 13 to 20 were missed. The following references should be included after reference 12 on page 231.

- 13 Andrew A W, Armitage D A, Broadbank R W C, Morcom K W & Muju B L, *Trans Faraday Soc*, 67 (1971) 128.
- 14 Hefley J D & Amis E S, *J phys Chem*, 69 (1965) 2082.
- 15 Harned H S & Owen B B, *The physical chemistry of electrolytic solutions* (Reinhold, New York) 1967, (a) p. 556; (b) p. 66 (c) p. 560 (b) p. 164.
- 16 Glasstone S, *An introduction to electrochemistry* 4th Edn (Van Nostrand, East-West, New Delhi) 1974, p. 250.
- 17 Bose K, Das A K & Kundu K K, *Trans Faraday Soc*, 71 (1975) 1838.
- 18 Roy R N, Vernon W & Bothwell A L M, *Electrochim Acta*, 17 (1972) 5.
- 19 Born M, *Z Phys*, 21 (1920) 45.
- 20 Cotton F A & Wilkinson G, *Advanced inorganic chemistry* (Interscience Publishers, New York) 1962, pp 48, 662.



CSIR GOLDEN JUBILEE SERIES

# BODY'S BATTLES

**WAR** makes rattling good history", said Oscar Wilde referring to the struggles of nations to capture new and to retain old territories. But other battles not visible to the naked eye are equally fascinating. An account of the miniscule wars found within the confines of the human body is breathtaking if only for the fact that these are being fought every single living moment. The human body is continually besieged and attacked by a multitude of microbial enemies of great cunning and guile. However, nature has endowed the human body with an unique built-in defence organization that can be envy of the most modern technologically advanced nation.

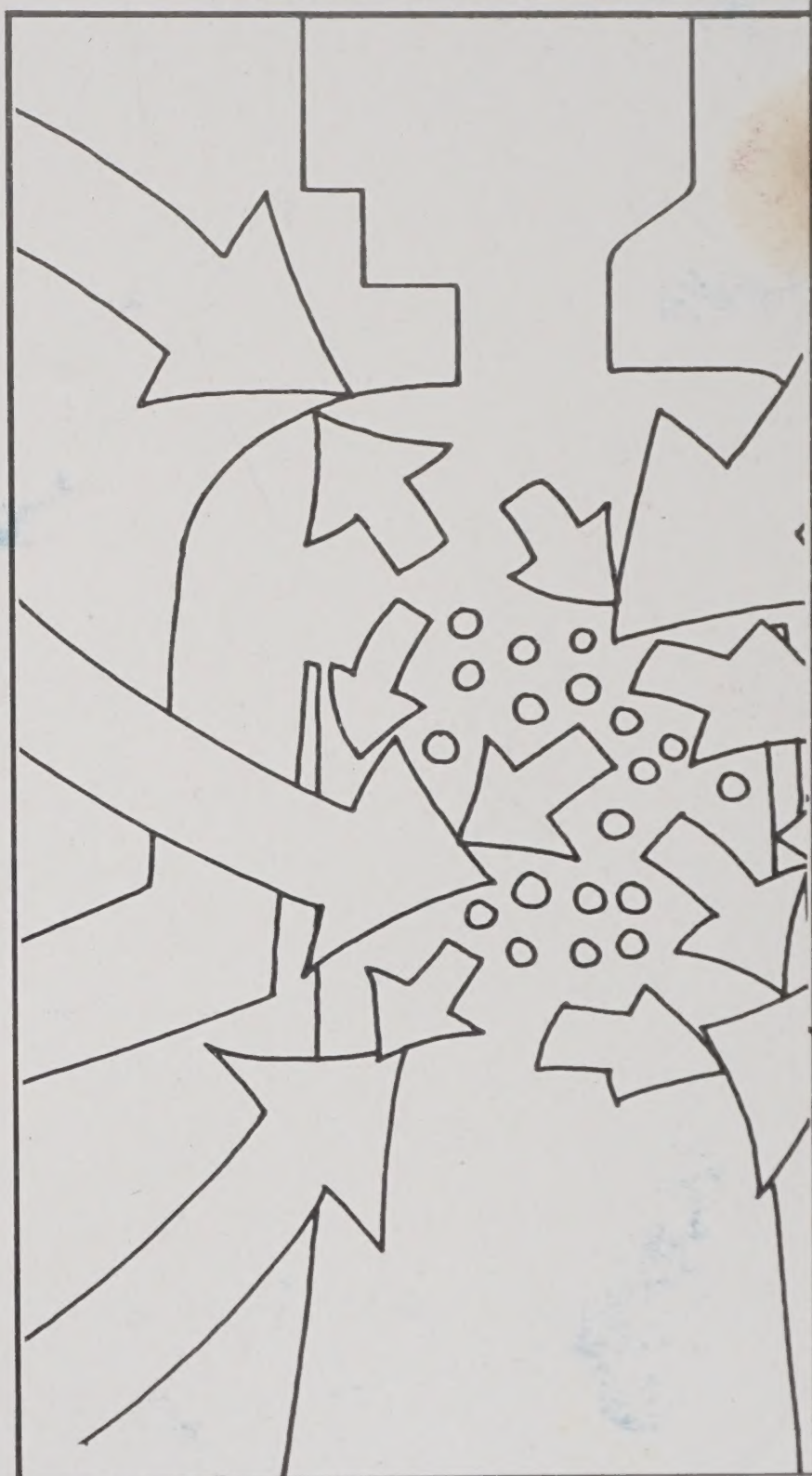
This attractive and lavishly illustrated book, written especially for the non-specialist, unfolds the dramatic story of this inner defence organization, the diversity and specificity of its armament, and the methodical way in which it maintains a round the clock vigil to meet squarely every imaginable threat to the human body and also how it wins the body's battles most of the time.

Price : Rs.9/- Paper back  
:Rs.18/- Hard Bound

Orders should be accompanied by money order or Demand Draft made payable to PUBLICATIONS & INFORMATION DIRECTORATE, NEW DELHI and sent to:

The Senior Sales & Distributions Officer,  
Publications & Information Directorate, CSIR  
Dr K.S. Krishnan Marg,  
New Delhi - 110 012

**BAL PHONDKE**



# BRING THE WORLD UNDER YOUR FEET.



TITANIC

# action

THE ONLY OFFICIAL  
WORLD CUP INDIAN SHOES

DL-18023/92  
RN 7090/63